Visible Light Communication System

Ahmed Taha Hussein

Submitted in accordance with the requirements for the degree of Doctor of Philosophy

University of Leeds

School of Electronic and Electrical Engineering

December 2016

The candidate confirms that the work submitted is his own, except where work which has formed part of jointly authored publications has been included. The contribution of the candidate and the other authors to this work has been explicitly indicated below. The candidate confirms that appropriate credit has been given within the thesis where reference has been made to the work of others.

The work in Chapter 2 of the thesis has appeared in publications as follows:

1. A. T. Hussein, and J.M.H. Elmirghani, “A survey of optical and terahertz (THz) wireless communication systems,” IEEE Communications Surveys and Tutorials, (to be submitted), 2016.

My contribution: literature review that covered most optical wireless (OW) systems and summarised new areas of research in OW and THz systems that deserve further investigations and produced the paper.

Professor Elmirghani: Helped with the preparation of paper.

The work in Chapter 4 of the thesis has appeared in publications as follows:

2. A. T. Hussein, and J.M.H. Elmirghani, “Mobile Multi-gigabit Visible Light Communication System in Realistic Indoor Environment,” Journal of Lightwave Technology, vol.33, no.15, pp.3293-3307, August 2015. **[Best paper award, Carter prize, University of Leeds, 2016].**

My contribution: literature review, developed the new idea of RGB laser diodes (LD) in indoor visible light communication (VLC) systems and designed imaging

receiver with 50 pixels and simulated system at low data rate (30 Mb/s), and high data rate (5 Gb/s) produced results of the proposed systems in Matlab.

Professor Elmirghani: Originator of the idea of laser diodes for visible light communication and helped with the preparation of paper.

3. A. T. Hussein, and J.M.H. Elmirghani, “High-Speed Indoor Visible Light Communication System Employing Laser Diodes and Angle Diversity Receivers,” The 17th International Conference in Transparent Optical Networks (ICTON), pp.1-6, July 2015.

My contribution: literature review, developed the idea of RGB-LD for VLC system and designed three branched angle diversity receiver (ADR), optimised the azimuth, elevation and field of view (FOV) for each branch in ADR. The simulation results built in Matlab and compared with basic VLC system.

Professor Elmirghani: developed the idea of RGB-LD with the new ADR in VLC system and helped with the preparation of paper.

The work in Chapter 5 of the thesis has appeared in publications as follows:

A. T. Hussein, and J.M.H. Elmirghani, “Mobile Multi-gigabit Visible Light Communication System in Realistic Indoor Environment,” Journal of Lightwave Technology, vol.33, no.15, pp.3293-3307, August 2015.

My contribution: literature review, introduced the idea of delay adaptation with imaging receiver (50 pixels) at high data rate (10 Gb/s) in realistic indoor environment and enabled the system with full mobility, simulation of the proposed idea in Matlab and produced results and compared them with traditional VLC systems (non-adaptive systems).

Professor Elmirghani: Originator of the idea delay adaptation technique developed the receiver design and helped with the preparation of paper.

4. A. T. Hussein, and J.M.H. Elmirghani, “Performance Evaluation of Multi-gigabit Indoor Visible Light Communication System,” The 20th European Conference on Network and Optical Communications, (NOC), pp.1-6, June 2015.

My contribution: literature review, enhanced and extended the ideas of RGB-LD and delay adaptation with seven branches ADR in order to operate at high data rate (5 Gb/s) in a realistic indoor environment.

Professor Elmirghani: Developed and enhanced the idea of delay adaptation technique with seven branched angle diversity receivers, helped with development of system models and the preparation of paper.

The work in Chapter 6 of the thesis has appeared in publications as follows:

5. A. T. Hussein, and J.M.H. Elmirghani, “10 Gbps Mobile Visible Light Communication System Employing Angle Diversity, Imaging Receivers and Relay Nodes,” Journal of Optical Communications and Networking, vol.7, issue 8, pp.718–735, August 2015.

My contribution: literature review, developed the new idea of relay node for VLC system. Produced three novel VLC systems that operate at 10 Gb/s with full mobility in realistic environment. Different room sizes were also considered to examine the performance of the proposed systems. Produced the results in Matlab and compared them when all systems employed delay adaptation.

Professor Elmirghani: Originator of the idea of relay nodes, developed the new algorithms and helped with the preparation of paper.

The work in Chapter 7 of the thesis has appeared in publications as follows:

6. A. T. Hussein, M. T. Alresheedi, and J. M. H. Elmirghani, “20 Gb/s Mobile Indoor Visible Light Communication System Employing Beam Steering and Computer Generated Holograms,” Journal of Lightwave Technology, vol. 33, no. 24, pp.5242-5260, December 2015.

My contribution: literature review, developed the new ideas of beam steering for VLC system and computer generated holograms (CGHs) with imaging receivers to enhance system performance and enable VLC systems to operate at high data rate (20 Gb/s). Produced results and compared them with previous VLC systems.

Dr. M. T. Alresheedi (Academic collaborator with the Department of Electrical Engineering, King Saud University, Riyadh, Saudi Arabia): helped with the development of the idea of CGHs and the preparation of paper.

Professor Elmirghani: Originator of the ideas of computer generated holograms and beam steering, developed the system models and helped with the preparation of the paper.

The work in Chapter 8 of the thesis has appeared in publications as follows:

7. A. T. Hussein, M. T. Alresheedi, and J. M. H. Elmirghani, “Fast and Efficient Adaptation Techniques for Visible Light Communication Systems,” Journal of Optical Communications and Networking, vol.8, issue 6, pp.382-397, 2016.

My contribution: literature review, devolved new search algorithm based on D&C in order to reduce the time needed to select the best pre-calculated hologram also to enhance the system performance and enable VLC systems to operate at high data rate (25 Gb/s). Produced results and compared them with previous VLC systems.

Dr. M. T. Alresheedi (Academic collaborator with the Department of Electrical Engineering, King Saud University, Riyadh, Saudi Arabia): helped with the development of the idea of fast CGHs and the preparation of paper.

Professor Elmirghani: Originator of the idea of fast computer generated holograms, developed the system models and helped with the preparation of the paper.

8. A. T. Hussein, M. T. Alresheedi, and J. M. H. Elmirghani, "25 Gbps Mobile Visible Light Communication Employing Fast and Efficient Adaptation Techniques'', 18th International Conference in Transparent Optical Networks (ICTON), pp.1-7, July 2016.

My contribution: literature review, devolved new search algorithm based on D&C in order to reduce the time needed to select the best pre-calculated hologram combined with an imaging receiver. Produced results and compared them with previous VLC systems.

Dr. M. T. Alresheedi (Academic collaborator with the Department of Electrical Engineering, King Saud University, Riyadh, Saudi Arabia): helped with the development of the idea of fast CGHs with imaging receiver and the preparation of the paper.

Professor Elmirghani: Originator of the idea of fast computer generated holograms, developed the system models and helped with the preparation of the paper.

The work in Chapter 9 of the thesis has appeared in publications as follows:

9. A. T. Hussein, M. T. Alresheedi, and J. M. H. Elmirghani, “High Data Rate Backup Systems for Visible Light Communication’’, IET Communications, to be submitted, 2016.

My contribution: literature review, devolved four new IR systems (HDIR with wide FOV, HDIR with imaging, BSIR and CDIR) in order to provide multi Gb/s data rates when the VLC system is off. Produced results, compared systems’ performance and wrote the paper.

Dr. M. T. Alresheedi (Academic collaborator with the Department of Electrical Engineering, King Saud University, Riyadh, Saudi Arabia): helped with the development of the idea of backup systems and the preparation of the paper.

Professor Elmirghani: Originator of the idea of backup systems developed the system models and helped with the preparation of paper.

The work in Chapter 10 of the thesis has appeared in publications as follows:

10. A. T. Hussein, M. T. Alresheedi, and J. M. H. Elmirghani, “Collaborative VLC/IROW Systems’’, IET communications, to be submitted, 2016.

My contribution: literature review, devolved the concept of collaborative VLC/IROW system and investigated the impact of partial dimming on VLC system performance. Proposed adaptive rate technique (ART) to mitigate the impact of light dimming and introduced cluster distributed IR system with beam steering to collaborate with VLC system to maintain the target data rate in the case of partial dimming. Produced results and wrote the paper.

Dr. M. T. Alresheedi (Academic collaborator with the Department of Electrical Engineering, King Saud University, Riyadh, Saudi Arabia): helped with the development the idea of collaborative VLC/IROW system and the preparation of the paper.

Professor Elmirghani: Originator of the idea of collaborative VLC/IROW system, developed the system models and helped with the preparation of the paper.

My parents, brother, sister, my wife and my children (Mohammed and Mustafa), this work is dedicated to you.

Acknowledgements

First and foremost, all praise to Almighty Allah, for endowing me with health, patience, and knowledge to complete this work. I would like to acknowledge my supervisor, Professor Jaafar Elmirghani for his guidance and patience through my PhD journey. I am very grateful for his teaching and friendship. He has offered me invaluable opportunities and continuously kept faith in me. I feel very honoured to have had the chance to work with him.

I am very grateful and thankful to the Higher Committee for Education Development (HCED) in Iraq for fully funding my PhD. I also thank the University of Mosul in Iraq for their financial support.

Many thanks go to my colleagues in the Communication Systems and Networks group in the School of Electronic and Electronic Engineering at University of Leeds. Also, I send my special thanks to Dr. Mohamed Musa and Dr. Mohammed Alhartomi. It was a privilege to have known them. I thank them for their company, reassurance and fruitful discussions.

I would like to express my appreciation to my beloved family back home, my mother, sister and brother. I don’t have enough words to thank them for supporting me in all possible ways. They are the reason behind my life achievements and have always shown me by example that everything is doable. I hope I made them proud.

Finally, I am very grateful and thankful to my young family. My children, little Mohammed and baby Mustafa. Their smiles and innocent gazes have changed the definition of life for me. I thank them for making my life so fulfilled and rewarding and for making every day so special. I dedicate my final acknowledgements to the love of my life, my dear wife Marwa, without her

kindness, sacrifices, and patience I would not have been able to pursue my dreams. I truly appreciate her standing by my side and thank her for her love, support and attention.

Abstract

Visible light communication (VLC) systems have become promising candidates to complement conventional radio frequency (RF) systems due to the increasingly saturated RF band and the potentially high data rates that can be achieved by VLC systems. Over the last decade, significant research effort has been directed towards the development of VLC systems due to their numerous advantages over RF systems, such as the availability of simple transmitters (light emitting diodes, LEDs) and receivers (silicon photo detectors), better security at the physical layer, improved energy efficiency due to the dual functionally (i.e., illumination and communication) and hundreds of THz of license-free bandwidth. However, there are several challenges facing VLC systems to achieve high data rates (multi gigabits per second). These challenges include the low modulation bandwidth of the LEDs, co-channel interference (CCI), inter symbol interference (ISI) due to multipath propagation and the light unit (i.e., VLC transmitter) should be ‘‘ON’’ all the time to ensure continuous communication.

This thesis investigates a number of techniques to overcome these challenges to design a robust high-speed indoor VLC system with full mobility. A RGB laser diode (LD) is proposed for communication as well as illumination. The main goal of using LD is to enable the VLC system to achieve multi-gigabits data rates when employing a simple modulation technique (such as on-off keying (OOK)), thus adding simplicity to the VLC system. A delay adaptation technique (DAT) is proposed to reduce the delay spread and enable the system to operate at higher data rates (10 Gb/s in our case). The thesis proposes employing angle diversity receivers (ADR) and imaging diversity receivers to mitigate the impact of ISI, CCI, reduce the delay spread (increase the channel bandwidth) and increase the signal to noise ratio (SNR) when the VLC system

operates at high data rates (5 Gb/s and 10 Gb/s) under the effects of mobility and multipath dispersion.

Moreover, the work introduces and designs three new VLC systems, an ADR relay assisted LD-VLC (ADRR-LD), an imaging relay assisted LD-VLC (IMGR-LD) and a select-the-best imaging relay assisted LD-VLC (SBIMGR-LD), which are modelled and their performance is compared at 10 Gb/s in two VLC room sizes (5m × 5m × 3m and 4m × 8m × 3m). As well as modelling in two different room scenarios: an empty room and a realistic environment were considered.

The work also introduces and designs a high-speed fully adaptive VLC system that employs beam steering and computer generated holograms (CGHs), which has the ability to achieve 20 Gb/s with full receiver mobility in a realistic indoor environment. Furthermore, a new high-speed fast adaptive VLC system based on a divide-and-conquer methodology is proposed and integrated with the system to reduce the time required to identify the optimum hologram. The new system has the ability to achieve 25 Gb/s in the worst case scenario.

This thesis also proposes four new infrared (IR) systems to support VLC systems when the light is totally turned off. In addition, it introduces the concept of a collaborative VLC/IR optical wireless (OW) system and investigates the impact of partial dimming on the VLC system performance. An adaptive rate technique (ART) is proposed to mitigate the impact of light dimming. Finally, an IROW system (cluster distributed with beam steering) is introduced to collaborate with a VLC system to maintain the target data rate in the case of partial dimming.

Contents

List of Figures

List of Tables

List of Abbreviations

ADC	Analogue to Digital Convertor
ADR	Angle Diversity Receiver
ART	Adaptive Rate Technique
ADRR-LD	ADR Relay Assisted LD-VLC
ALE	Artistic Licence Engineering
AM	Amplitude Modulation
APD	Avalanche Photodiode
BAM	Bit Angle Modulation
BCM	Beam Clustering Method
BPSK	Binary Phase Shift Keying
BPF	Band Pass Filter
BJT	Bipolar-Junction Transistor
BER	Bit Error Rate
BSR	Beam steering
BSIR	Beam Steering Infrared
BN	Background Noise
CAP	Carrier-less Amplitude and Phase
CCI	Co-Channel Interference
CDIR	Cluster Distributed Infrared
CDBSIR	Cluster Distributed Beam Steering Infrared
CS	Communication Setup
CF	Cost function
CSMA	Carrier Sense Multiple Access
CP	Communication Plane
CPC	Compound Parabolic Concentrator
CGH	Computer Generated Hologram
CSK	Colour Shift Keying
CQI	Channel Quality Indicator

CDS	Conventional Diffuse System
DAT	Delay Adaptation Technique
DAC	Digital to Analogue Convertor
DPPM	Differential Pulse-Position Modulation
DSP	Digital Signal Processor
DMT	Discrete Multi-tone Modulation
D&C	Divide and Conquer
EGC	Equal Gain Combining
FCGHs	Fast Computer Generated Holograms
FSO	Free Space Optical Communication
FET	Field Effect Transistor
FEC	Forward Error Correction
FAI	Fully Adaptive Imaging
FOV	Field of View
GSI	Geospatial Information Authority
hps	Half Power Semi-angle
HPF	High pass filter
HDIR	Hybrid Distributed Infrared
IR	Infrared
IrDA	Infrared Data Association
IM/DD	Intensity Modulation and Direct Detection
IMGR-LD	Imaging Relay Assisted LD-VLC
ISI	Inter Symbol Interference
IROW	Infrared Optical Wireless
JEITA	Japanese Electronics and Information Technology Industries Association
LD	Laser Diodes
Li-Fi	Light Fidelity
LEDs	Light Emitting Diodes
LEA	Location Estimation Algorithm

LOS	Line of Sight
LSMS	Line Strip Multi-spot diffusing System
LMS	Least Mean Square
LPF	Low Pass Filter
LSB	Least Significant Bit
MRC	Maximum Ratio Combining
MAC	Medium Access Control
MRI	Magnetic Resonance Imaging
MSB	Most Significant Bit
MFTP	Maximum Flickering Time Period
MIMO	Multiple input multiple output
NSF	National Science Foundation
NRZ	Non Return to Zero
NLOS	Non-Line of Sight
OMEGA	hOME Gigabit Access network
OOK	On-Off Keying
OFDM	Orthogonal Frequency Division Multiplexing
OW	Optical Wireless
PAR	Peak to Average Power Ratio
PHY	Physical Layer
PD	Photodetector
PWM	Pulse Width Modulation
PIN	Positive Intrinsic Negative
PPM	Pulse Position Modulation
QoS	Quality of Service
QAM	Quadrature Amplitude Modulation
QPSK	Quadrature Phase Shift Keying
RF	Radio Frequency
RZ	Return to Zero
rms	Root Mean Square

RLS	Recursive Least Squares
STB	Select the Best
SBIMGR	Select-the-Best Imaging Relay Assisted LD-VLC
SC	Selection Combining
SCM	subcarrier modulation
SSL	Solid State Lighting
SNR	Signal to Noise Ratio
THz	Terahertz
TCA	Trans-conductance Amplifier
TIA	Trans-impedance Amplifier
uFSO	Under Water Communication
UVC	Ultra Violet Communication
UWB	Ultra-wideband Wireless System
VLC	Visible Light Communication
Wi-Fi	Wireless fidelity
WDM	Wavelength Division Multiplexing
WiGig	Wireless Gigabit Alliance
ZF	Zero Forcing

List of Symbols

α	Incidence angle with respect to the transmitter's normal
α_1	Angle between the first reflected ray *R2* and the normal of the reflective element 1
α_2	Angle between the second reflected ray *R3* and the normal of the reflective element 2
A	Photodetctor area
$A_{eff}(\delta)$	Effective signal-collection area
Az	Azimuth angle
β	Angle between the incident ray from the transmitter and the reflective element's 1 normal
β_1	Angle between the first reflecting ray *R2* and the normal of the reflective element 2
c	Speed of light
D	Root mean square delay spread
dA	Reflection surface element area
δ	Angle of incidence with respect to the receiver normal
Δt	Differential delays between VLC beams
d_y	The horizontal distance separating the transmitter's normal and the diffusing spot alongside the y-axis
El	Elevation angle
η	Quantum efficiency of the device
$f"(x$, y)	The normalised desired object energy
γ	Angle between the normal of the reflective element 1 and the reflected ray
$g(\delta)$	Concentrator gain

h	Reception area height
$h(t)$	Impulse response
h_p	Planck's constant
$I(t, Az, El\ )$	Received photocurrent at the output of the detector at a certain point in time, and at a given azimuth and elevation of the photodetector
λ	Wavelength
M_t	The total number of reflecting elements
μ	Mean delay
N	Internal refractive index
n	Mode number that determines the shape of the radiated beam
$\hat{n}_1$	Normal of the reflective element 1
$\hat{n}_2$	Normal of the reflective element 2
$\hat{n}_r$	Normal of the receiver
$\hat{n}_t$	Normal of the transmitter
P_{LOS}	Direct received power
P_e	Probability of error
P_{FST}	Received powers from the first reflecting elements
P_{SEC}	Received powers from the second reflecting elements
P_s	Average transmitted optical power
P_{s0}	The power associated with logic 0
P_{s1}	The power associated with logic 1
ψ_c	Concentrator's FOV (semi-angle)
$\emptyset$	Reception angle for any detector in the ADR
P_r	The total received optical power at the receiver
q	Electronic charge

Q	Gaussian function
R	Photodetector responsivity
R_d	Direct link distance between the receiver and the transmitter
R_1	Distance between the reflective element 1 and the transmitter
R_2	Distance between the receiver and the reflective element 1
R_3	Distance between the receiver and the reflective element 2
R_{e1}	Position vector of the reflective element 1
R_{e2}	Position vector of the reflective element 2
R_r	Position vector of the receiver
R_t	Position vector of the transmitter
ρ_1	Reflection coefficient of the first order reflective elements
ρ_2	Reflection coefficient of the second order reflective elements
σ_{shot}	Background shot noise component
$\sigma_{preamplifier}$	Preamplifier shot noise component
σ_{signal}	Signal noise
t	Absolute time
t_i	Time delay associated with the received optical power P_{r_i}
$T_c(\delta)$	Transmission factor of concentrator
TP	Pulse width of bit
Tb	Duration of the bit
w_i	The weight of every branch/pixel
Xr	Distance between the receiver and the y-z wall
$x(t)$	Transmitted instantaneous optical power
Yr	Distance between the receiver x-z wall

1 Introduction

Using light as a means of communication is not a new idea. In fact, optical wireless (OW) communication is more than three centuries old. Techniques such as ship flags, semaphore and fire beacons were the earliest stages of OW. The reflection of sunlight by mirrors is another early method of optical communication. A good example of such a system is the heliograph shown in Figure 1.1, in which mirror movement produces light flashes that can be used to send Morse code [1]. In the 19th century, this system was a very effective instrument for optical communication over a distance of 50 miles or more. The major uses of this device were in surveys, forest protection work and by the military. It was in use until 1935 [1].

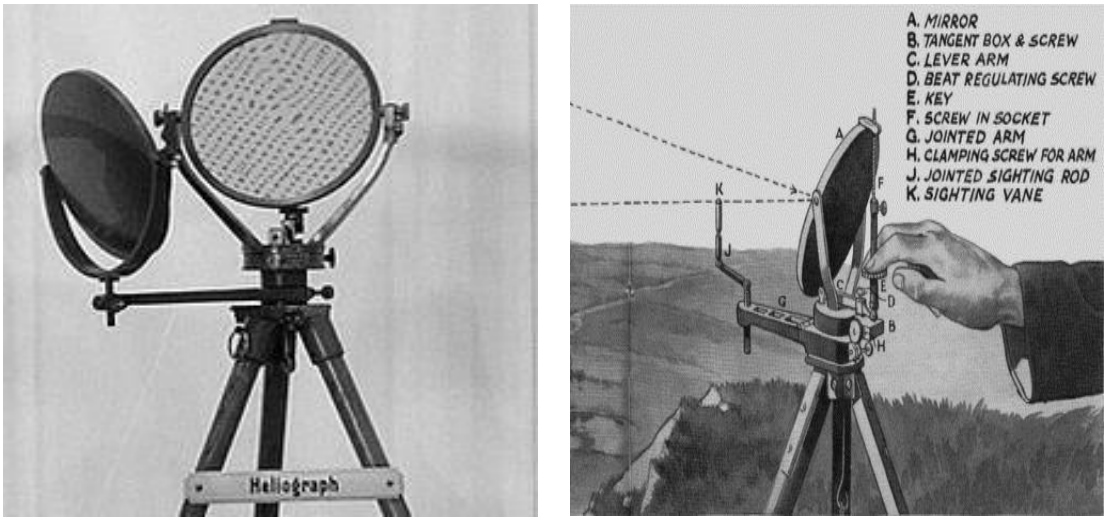

(a) (b)

Figure 1.1: The heliograpgh, (a) the British army version (Mance Mark V), (b) schematic structure and assembly [1].

In 1880, Alexander Graham Bell and Sumner Trainer invented and developed the photophone, which is a light-based free space communication system. The device was used to transmit sound on a beam of light [2]. Figure 1.2 shows the photophone. The device was based on electronic detection, and the receiver

consists of a selenium crystal, which converts the optical signal into an electrical current. Bell's photophone used the conductivity of selenium crystals, where the electrical conductivity depends on the intensity of the light it is exposed to [2]. The photophone has been recognised as the primogenitor of modern fibre optics that today transport over 80% of the world's telecommunications traffic. Nowadays, optical communication systems exhibit much higher data rates with better quality of service (QoS) compared to the old methods [3].

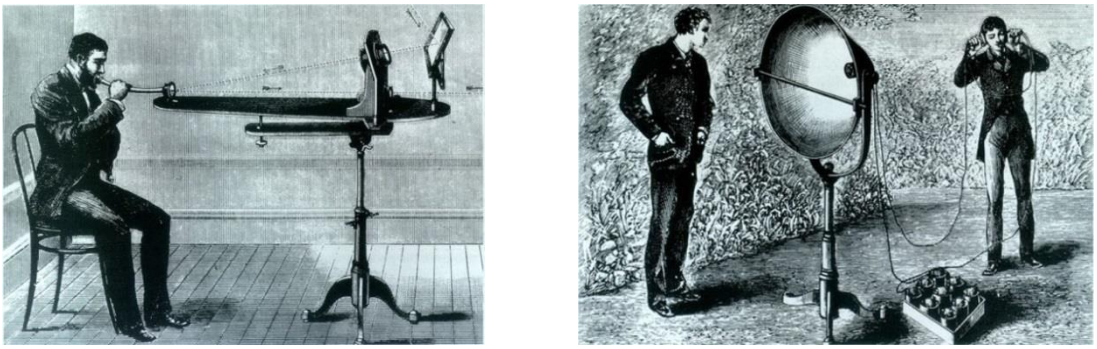

(a) (b)

Figure 1.2: The photophone, (a) transmitter, (b) receiver [2].

Modern telecommunications has experienced exponential growth in applications and research over the past decades. Wired physical connections have been established to convey information between different devices. However, physical connections introduce difficulties in installation, re-wiring and maintenance. An alternative method that can achieve the same performance for such systems is wireless communication based on radio frequency (RF) transmission. The RF band is the basis of most currently used wireless communication systems. Unfortunately, the growth in demand for more frequencies, high data rate services, better QoS and lower cost components have reduced the available RF spectrum. These demands have forced researchers to find other options. Figure 1.3 shows the electromagnetic spectrum.

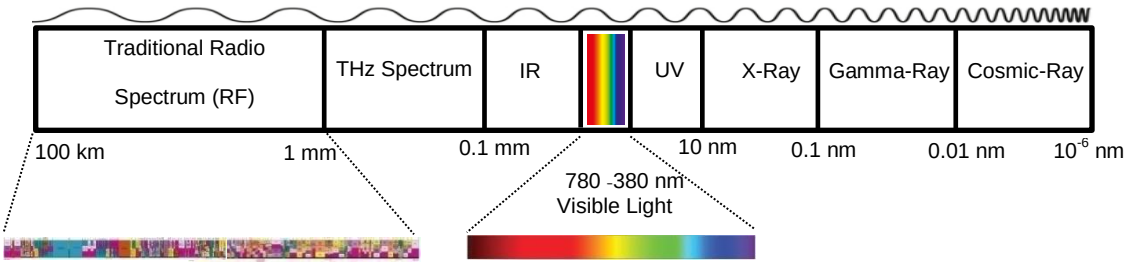

Figure 1.3: The electromagnetic spectrum.

Achieving very high data rates (multi gigabits per second) using the relatively narrow bandwidth of RF systems is challenging [4]. According to a GreenTouch research study, mobile Internet traffic over this decade (2010-2020) is expected to increase by 150 times [5]. Given this expectation of dramatically growing demand for data rates, the quest is already underway for alternative spectrum bands beyond microwaves and millimetre waves (RF spectrum). Different technology candidates have entered the race to provide ultra-fast wireless communication systems for users, such as OW systems for indoor and outdoor use [6]-[8], ultra-wideband wireless system (UWB) [9], 60 GHz band for local wireless multimedia access [10] and terahertz (THz), which has been studied as a new alternative in this race [11]-[14].

Modern OW communication systems coincided with the invention of the first laser in 1960 [15]. However, this technology was not deployed until the 1990s when the transmitter and the receiver components became available at low cost [16]. OW communication systems include outdoor systems, such as free-space-optical (FSO), ultra violet communication (UVC) and underwater communications (uFSO), while indoor systems are those such as infrared data association (IrDA), infrared optical wireless communication (IROW) and visible light communication (VLC) systems [3].

The term ‘visible light communication’ refers to the use of light waves in free-space propagation in the visible band as a transmission medium for

communication (see Figure 1.3). The visible signal is electromagnetic radiation whose wavelengths are located between those of IR and UV. Visible radiation has wavelengths between 380 nm and 780 nm [4].

Along with radio, the term wireless is also applicable to systems which utilise other regions of the electromagnetic spectrum, such as infrared. It has been more than three decades since OW systems were introduced [6]. OW offers a number of advantages over its radio frequency counterpart, such as abundance of unregulated bandwidth, no multipath fading and cost effective at rates near 100 Mb/s [4]. To an extent, RF and OW may be viewed as complementary rather than competitive media. For example, if a wireless LAN is required to cover a large area, where users can roam freely and remain connected to the network at all times, then radio is the only cost-effective medium which can achieve this. If, however, a wireless LAN is required to cover a more modest area, but deliver advanced high bandwidth multimedia network services such as video conferencing and video on demand, then OW is the only medium which truly has the bandwidth available to deliver this [3]. The comparison between the properties of RF and OW is shown in Table 1.1

So far, commercially available OW systems have not come close to delivering the high data rates which are potentially available from the OW spectrum, the reasons for this are more to do with the limited range, difficultly to operate outdoor, high power requirement and cost constraints rather than any fundamental limitations of the core technology [4].

OW is a challenging medium and there are numerous considerations which must be taken into account when designing high speed indoor OW links. Non-directed LOS and diffuse links incur a high optical path loss and must also contend with multipath propagation. Whilst multipath propagation does not result in multipath fading in indoor OW systems, since detector sizes are huge in comparison with the wavelength, it does give rise to inter symbol interference

(ISI), which is one of the primary impairments to achieving high speed communication [4]. In addition, OW links must be capable of operating in environments where intense ambient light levels exist, which degrades link performance in two ways. Firstly, the average power of the background radiation generates shot noise in the receiver, which is independent of the transmitted signal, and secondly, artificial sources of ambient light generate a periodic interference signal, which can contain harmonics into the MHz region for fluorescent lamps driven by electronic ballasts [6].

Table 1.1: Properties of RF and OW

Property	RF	OW
Bandwidth regulated	Yes	No
Multipath fading?	Yes	No
Multipath dispersion	Yes	Yes
Dominant noise	Other users	Background light
Average power proportional to	$\int \|f(t)\|^2 \, dt$	$\int \|f(t)\| \, dt$

1.1 Motivation and Research Objectives

Significant research effort is being directed towards the development of VLC systems due to their numerous advantages over RF systems, such as:

- The nature of light gives the VLC system immunity against interference caused by adjacent channels with the possibility of frequency reuse in different parts of the same building, which means abundant capacity.
- The VLC system also offers better security at the physical layer.
- The availability of simple front-end devices at low cost.
- VLC helps realise energy efficient systems.
- Hundreds of terahertz of license-free bandwidth.
- Harmless for humans and other electronic devices.
- Easy to integrate into the existing lighting infrastructure.

There are however several challenges hindering the development of VLC systems, and these challenges include:

- The low modulation bandwidth of light emitting diodes (LEDs).
- Multipath propagation, which may cause inter-symbol-interference (ISI).
- Multiple transmitters, which may cause co-channel interference (CCI).

The primary objectives of this work were to:

1- Propose and evaluate new techniques to enhance the performance of VLC systems under the influence of multipath dispersion and mobility.
2- Design and model indoor mobile VLC systems that operate at higher data rates (i.e., 5, 10, 20 Gb/s and beyond) in a realistic indoor environment.
3- To investigate the benefits of using angle diversity receivers and imaging receivers in VLC system.
4- To investigate the use of delay adaptation to increase the signal to noise ratio (SNR), 3 dB channel bandwidth and reduce the delay spread.
5- To investigate the use of relay nodes in VLC systems to improve VLC links.
6- To investigate additional adaptation methods that can improve the VLC system's performance, such as beam steering and computer generated holograms.
7- To investigate fast and efficient adaptation algorithms for VLC systems.
8- To propose and evaluate new IROW systems to support VLC.
9- To investigate the impact of partial dimming on VLC systems performance.

1.2 Research Contributions

The author has:

1- Designed, investigated and evaluated the use of RGB laser diodes (LD) for communication as well as illumination in VLC systems instead of light emitting diodes (LED). The main goal of using RGB-LD is to enable the VLC system to achieve multi-gigabit/s data rates when employing a simple modulation technique, such as on-off keying (OOK), thus adding simplicity to the VLC system. Based on the new VLC transmitter, the author has designed and evaluated different VLC systems:

   A. RGB-LD system in conjunction with three branch angle diversity receivers (ADR).
   B. RGB-LD system coupled with an imaging receiver.

   The author optimised the azimuth, elevation and filed of view (FOV) of each detector in the ADR to achieve the best SNR and to minimise the delay spread. He also introduced a custom imaging receiver with 50 pixels (detectors). These detectors enable the system to reduce the impact of ISI and CCI. The reduction in the delay spread and improvement in 3 dB channel bandwidth and SNR enable the new systems to operate at a high bit rate of 5 Gb/s.

2- Introduced a novel delay adaptation technique (DAT) for indoor VLC systems. The main goal was to reduce the impact of ISI and enhance the SNR, thus enabling the system to achieve mobility while operating at high bit rates of 5Gb/s and 10 Gb/s. Based on the DAT, the author has designed and evaluated different VLC systems:

   A. DAT LD-VLC system combined with seven branch ADR.
   B. DAT LD-VLC system coupled with an imaging receiver.

   The author has also evaluated the performance of both systems in a realistic indoor environment where physical partitions introduce shadowing and signal blockage, windows cause signal loss and

bookshelves, chairs and cabinets are present and cause additional reflections.

3- Introduced novel mobile VLC systems that employ relay nodes, angle diversity and imaging receivers. The author has also designed and introduced two novel algorithms for relay node systems. In addition, he has proposed and evaluated different VLC systems:

   A. An ADR relay assisted LD-VLC (ADRR-LD).
   B. An imaging relay assisted LD-VLC (IMGR-LD).
   C. A select-the-best imaging relay assisted LD-VLC (SBIMGR-LD).

   The author has also evaluated and compared the performance of the proposed systems at 10 Gb/s in two room sizes (5m × 5m × 3m and 4m × 8m × 3m). In addition, two different room scenarios were considered: an empty room and a realistic environment room.

4- Proposed for the first time a VLC system that employs a beam steering technique and a new location estimation algorithm (LEA). The LEA was used to estimate the receiver location so that part of the white light can be directed towards a desired target (receiver) using beam steering to improve the SNR and channel bandwidth. The increase in channel bandwidth and SNR were used to achieve a high data rate (20 Gb/s), where previous VLC systems used to operate at 5 and 10 Gb/s. The data rate achieved is a world record data rate with a single modulation format and without colour multiplexing. The system's robustness against signal blockage and shadowing was also considered.

5- Proposed and designed a fully adaptive high speed 25 Gb/s mobile VLC system that employs fast computer generated holograms (FCGHs) and DAT coupled with an ADR and an imaging receiver. The FCGHs were based on a divide-and-conquer (D&C) method. The new, fast and efficient fully adaptive VLC system improved the receiver SNR and reduced the time required to estimate the position of the VLC receiver. It

was also able to adapt to environmental changes, providing a robust link against signal blockage and shadowing. It should be noted that the data rates achieved by the proposed system (i.e., 25 Gb/s for a stationary user and 22.2 Gb/s for a mobile user) are the highest data rates to date for an indoor VLC system with a simple modulation format (OOK) and without the use of relatively complex wavelength division multiplexing approaches.

6- Proposed, designed and evaluated high data rate (1.25 Gb/s and 2.5 Gb/s) backup communication systems. Four new IR systems (hybrid diffuse IR with wide field of view receiver, hybrid diffuse IR with imaging receiver, beam steering IR with imaging receiver and cluster distributed IR with imaging receiver) were introduced to support the VLC system when the light is totally turned off.

7- Introduced and implemented the concept of a collaborative VLC/IROW system. The author has also investigated the impact of partial dimming on the VLC system performance and proposed an adaptive rate technique (ART) to mitigate the impact of light dimming. In addition, a new IROW system (cluster distributed with beam steering) has been proposed to collaborate with the VLC system to maintain the target data rate in the case of partial dimming.

1.3 Publications

The original contributions are supported by the following publications:

Journals

1. A. T. Hussein, and J.M.H. Elmirghani, “Mobile Multi-gigabit Visible Light Communication System in Realistic Indoor Environment,” Journal of Lightwave Technology, vol.33, no.15, pp.3293-3307, August 2015. **[Best paper award, Carter prize, University of Leeds, 2016].**

2. A. T. Hussein, and J.M.H. Elmirghani, “10 Gbps Mobile Visible Light Communication System Employing Angle Diversity, Imaging Receivers and Relay Nodes,” Journal of Optical Communications and Networking, vol.7, issue 8, pp.718–735, August 2015.
3. A. T. Hussein, M. T. Alresheedi, and J. M. H. Elmirghani, “20 Gb/s Mobile Indoor Visible Light Communication System Employing Beam Steering and Computer Generated Holograms,” Journal of Lightwave Technology, vol.33, no.24, pp.5242-5260, December 2015.
4. A. T. Hussein, M. T. Alresheedi, and J. M. H. Elmirghani, “Fast and Efficient Adaptation Techniques for Visible Light Communication Systems,” Journal of Optical Communications and Networking, vol.8, issue 6, pp.382-397, 2016.
5. A. T. Hussein, M. T. Alresheedi, and J. M. H. Elmirghani, “High data rate Backup Systems for Visible Light Communication,” IET Communications, (to be submitted), 2016.
6. A. T. Hussein, M. T. Alresheedi, and J. M. H. Elmirghani, “Collaborative VLC/IROW Systems,” IET Communications, (to be submitted), 2016.
7. A. T. Hussein, and J. M. H. Elmirghani, “A Survey of Optical and Terahertz (THz) Wireless Communication Systems,” IEEE Communications Surveys & Tutorials, (to be submitted), 2016.

Conferences

8. A. T. Hussein, and J.M.H. Elmirghani, “Performance Evaluation of Multi-gigabit Indoor Visible Light Communication System,” The 20th European Conference on Network and Optical Communications, (NOC), pp.1-6, June 2015.
9. A. T. Hussein, and J.M.H. Elmirghani, “High-Speed Indoor Visible Light Communication System Employing Laser Diodes and Angle Diversity

Receivers," The 17th International Conference in Transparent Optical Networks (ICTON), pp.1-6, July 2015.

10. A. T. Hussein, M. T. Alresheedi, and J. M. H. Elmirghani, "25 Gbps Mobile Visible Light Communication Employing Fast and Efficient Adaptation Techniques'', The 18th International Conference in Transparent Optical Networks (ICTON), pp.1-7, July 2016.

1.4 Overview of the Thesis

The next chapter provides a general review of indoor visible light communication systems. Comparison between VLC and RF systems is presented. It also presents VLC systems structure, including transmitter and receiver components and VLC link configurations. In addition, the chapter outlines the design challenges of indoor VLC systems and signal modulation techniques.

Chapter 3 presents the VLC channel model used in all the systems designed and presented in this work. It also provides an analysis of the impulse response, delay spread and SNR of a single detector receiver with various fields of view.

Chapter 4 introduces a novel VLC transmitter an RGB-LD light unit whose design is described. The new VLC transmitter is coupled with angle diversity receiver. In addition, a custom design imaging receiver is introduced for this VLC system in this chapter. The results show significant improvements in terms of data rate.

Chapter 5 presents a novel delay adaptation technique for VLC systems. The VLC systems introduced in Chapter 4 are developed in this chapter. The results show that the use of DAT with RGB-LD and an imaging receiver enable the new VLC system to achieve BER of 10^{-5} while operating at high bit rates (10 Gb/s) in

a realistic indoor environment. The chapter focuses on designing a high-speed indoor VLC system with full mobility, based on a combination of these techniques.

Chapter 6 introduces a 10 Gb/s mobile VLC system that employs relay nodes, ADR and imaging receivers. It also introduces two novel algorithms to create optimum transmitter-relay and relay-receiver communication links. The proposed systems are examined in two different room scenarios: an empty room and a realistic room. In addition two room sizes (5m × 5m × 3m and 4m × 8m × 3m) were considered. It demonstrates that the performance of the proposed systems is better in the small office compared to the large office due to the shorter distance between the transmitters and receiver, which led to reduced path loss and delay spread and to increased SNR. It also demonstrates that the BER achieved by the new VLC system is better than 10^{-7} at 10 Gb/s in the worst case scenario.

Chapter 7 proposes a 20 Gb/s Mobile VLC system employing beam steering and computer generated holograms (CGHs). The work in this chapter also investigates the effect of beam steering on room illumination. The results indicate significant enhancements in channel bandwidth and SNR, compared to previous systems. Robustness to shadowing and signal blockage is also considered, and the results show that the proposed system can typically maintain line of sight (LOS) links at any location in the room, and this gives immunity against shadowing and mobility.

Chapter 8 introduces a 25 Gb/s fully adaptive mobile VLC system based on fast and efficient adaptation algorithms. A fast computer generated holograms (FCGHs) method based on a divide and conquer approach is proposed to improve the SNR and reduce the required time to estimate the position of the VLC receiver. The performance and system complexity of the new VLC system is studied and is compared to previous VLC systems.

Chapter 9 Proposes four IR backup systems to support the VLC system when the light units are turned off. The proposed systems are able to maintain high data rate service (1.25 Gb/s and 2.5 Gb/s) when the VLC system is disabled. The simulation results show that the proposed systems have the ability to achieve high data rates (1.25 Gb/s and 2.5 Gb/s) with BER of 10^{-9} in the presence of multipath dispersion, receiver noise and mobility.

Chapter 10 Introduces the concept of collaborative VLC/IROW system. The impact of partial dimming on the VLC system performance is investigated. An adaptive rate technique (ART) is proposed to mitigate the impact of light dimming. In addition, new IROW systems (distributed cluster and distributed clusters with beam steering) are introduced to collaborate with a VLC system to maintain the target data rate in the case of partial dimming.

Chapter 11 summarises the contributions of the work and outlines possible directions of future work.

2 Review of Visible Light Communication Systems

2.1 Introduction

Traditional radio and microwave communication systems suffer from limited channel capacity due to the limited radio spectrum available. Concurrently, the data rates requested by users continue to increase exponentially. Nowadays, many people carry more than one wireless device at any time, for instance, a smart phone, smart watch, tablet and smart glasses. By 2017, it is expected that more than 11 Exabytes of data will have to be transferred through mobile networks every month [17]. Different technology candidates have proposed to provide high data rate services for users. Recently, the wireless gigabit alliance (WiGig) has proposed the utilisation of the unlicensed 60 GHz frequency band to enable a 7 Gb/s short range wireless link. However, tracking algorithms and sophisticated digital beam forming are required for application in mobile wireless networks due to the high path loss of radio waves in this spectrum range (i.e., 60 GHz) [18].

Since the RF spectrum is expensive and limited, new and complementary wireless transmission techniques are required to relieve the RF spectrum. There is a potential band of the electromagnetic spectrum (i.e., the optical band) available that is able to provide tens of gigabits per second for users in the near future [19], especially for indoor users. It has been more than three decades since the first OW systems were proposed as an alternative technology to RF systems to support high data rates [6]. Since then, a large and growing body of research in this area has emerged, and in the last ten years OW communication has gone from strength to strength as a potential high

speed method for local area networks [6], [20]-[27]. OW systems are candidates for high data rates in the last mile of network access. One of the most promising OW systems for realising ubiquitous wireless networks is a VLC system based on white LEDs, because LEDs can be simultaneously used for illumination and data communications [28]. The dual functionality of a VLC system, i.e., illumination and communication, makes it a very attractive technology for many indoor and outdoor applications, such as car-to-car communication via LEDs, lighting infrastructures in buildings for high speed data communication and high data rate communication in airplane cabins.

The main factor that has helped the development of VLC systems is the recent development of solid state lighting (SSL), which will provide high brightness LEDs of about 100 lx and 200 lx in the near future [29], [30], with a longer lifetime (about six years) in comparison to conventional artificial light sources, such as incandescent light bulbs (lifetime is about four months). In addition, SSL has a high response (speed), smaller size, low power consumption and no health hazards. Figure 2.1 shows the practical luminous efficacy of different available light sources.

There are two different approaches generally used to generate white light from LEDs. The first method is white light generated using a phosphor layer (yellow light is emitted) that is coated on blue LEDs. The light emitted by blue LEDs ($\lambda \approx 470$ nm) is absorbed by the phosphor layer, and the blue wavelength excites the phosphor causing it to glow white, and then the phosphor emits light at longer wavelengths. The second method is by using RGB LEDs. With the correct mixing of three colours (red, green and blue) white light can be created, such as in colour TV. The lower cost and lower complexity of the first method makes it more popular. However, the modulation bandwidth is limited to tens of MHz's due to the slow response of the phosphor, and this puts a limitation on the communication data rate. Both techniques have been demonstrated in

conjunction with VLC systems [31], [32]. Figure 2.2 depicts the methods of generating white light from the LEDs.

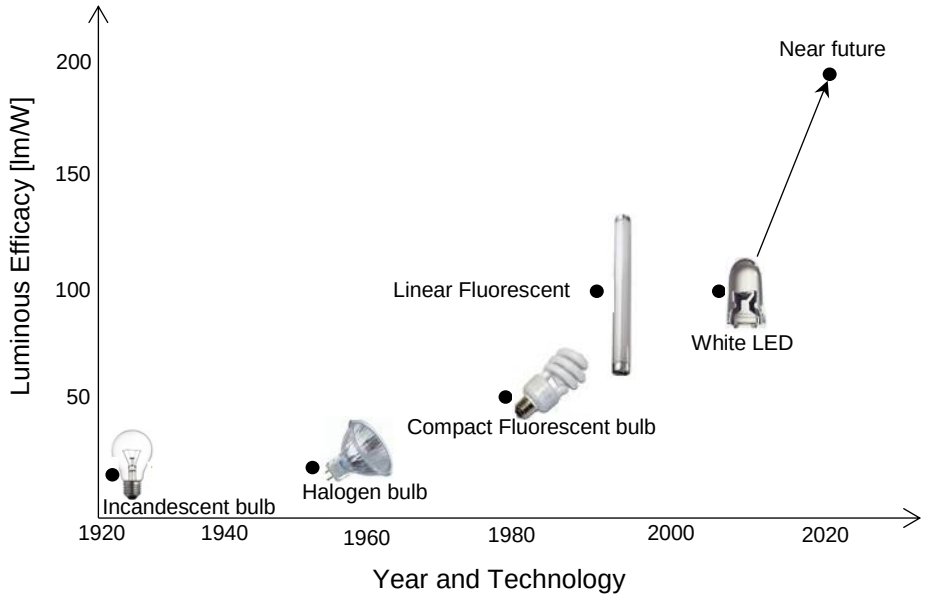

Figure 2.1: Comparison of different light sources in terms of luminous efficacy.

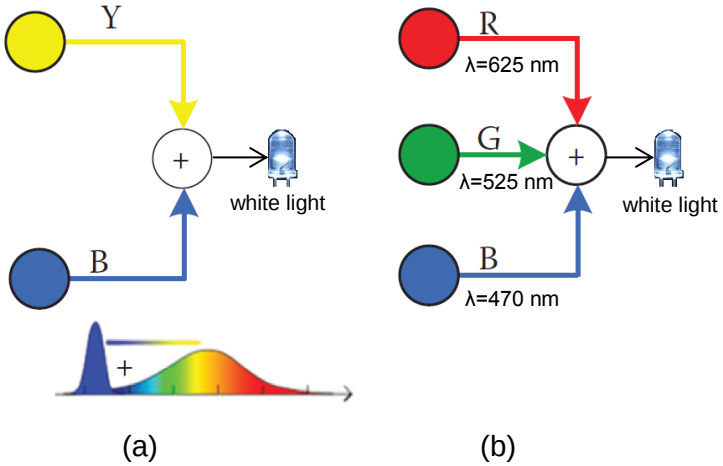

(a) (b)

Figure 2.2: Two white emissions approaches from LEDs, (a) phosphor LED method, (b) RGB method.

Following this introduction, this chapter is organised as follows. The indoor VLC system structure is described in Section 2.3. Design challenges in indoor VLC systems, such as ISI, multipath dispersion and photodetector high capacitance, are discussed in Section 2.4. Next, signal modulation techniques and VLC

standards are presented in Sections 2.5 and 2.6, respectively. The chapter concludes by describing current indoor VLC systems.

2.2 Comparison between Visible Light Communication and Radio Frequency

VLC and RF systems have advantages and limitations that need to be carefully studied. VLC and RF systems are complementary transmission techniques, with different applications favouring the use of one medium over the other. For example, RF is favoured in applications where transmission over long distance or through walls is desired and user mobility must be maximised. On the other hand, VLC is favoured in short to medium link applications where aggregate system capacity must be maximised at minimal cost or receiver signal-processing complexity must be minimised.

RF is the basis of most of the current wireless communication systems. However, the growth in demand for more frequencies, lower cost components, higher data rates and better QoS, have forced researchers to look deeply into other options, such as VLC. VLC offers several significant advantages over RF. For example, rapid deployment, low start-up operational costs and high bandwidth similar to fibre optic. The VLC spectral region offers virtually unlimited bandwidth (380~780 nm) that is an unregulated worldwide spectrum, and this leads to reduced system cost. The nature of light gives the VLC system immunity against interference caused by adjacent channels with the possibility of frequency reuse in different parts of the same building, which means abundant capacity. The VLC system also offers better security at the physical layer, and this is due to the fact that light does not penetrate through opaque barriers, which means that eavesdropping is not possible as with radio systems. The availability of simple front-end devices at low cost, the provision of energy efficiency, hundreds of terahertz of license-free bandwidth, being harmless for humans and other electronic devices and being easy to integrate into the

existing lighting infrastructure are also benefits. The detector (photodiode) is very large in size, typically tens of thousands of wavelengths, hence VLC systems are free from fading [23], [26], [33], [34], and the freedom from fading can greatly simplify the design of VLC systems.

A VLC system is not without drawbacks. VLC access points that are interconnected via a wired backbone will need to be installed because the light cannot penetrate through walls from one room to another. In addition, the spread in the received pulse due to multipath dispersion degrades the SNR. Multipath dispersion is attributed to reflective surfaces, such as walls, windows, doors and ceilings. Since these reflective elements act as small emitters that diffuse the signal in the form of a Lambertian pattern, the transmitted data arrives at the receiver from multiple different paths, which makes the transmitted pulses spread [26]. Furthermore, the received signal at the receiver includes shot noise induced by intense ambient light sources (sunlight and other light sources), and this leads to signal corruption by background noise [35], [36]. Moreover, the available current modulation bandwidth of the transmitters (LEDs) is very low compared with the VLC spectrum, which means transmission bandwidth is limited by the LED bandwidth. In addition, using white LEDs for communication is naturally a one direction communication (downlink), useful for applications such as background music transmission, therefore, providing an uplink to a portable transmitter structure can be a big challenge.

A VLC system requires a photodetector with a large photosensitive area to achieve an acceptable performance. However, the photodetector capacitance is directly proportional to its area, i.e., a large photosensitive area results in large capacitance, and consequently the available bandwidth in the receiver will decrease [37]. Table 2.1 summarises the comparison between VLC and RF systems.

Table 2.1: Comparison between VLC and RF systems in indoor wireless communications.

	VLC systems	RF systems
Advantages	• Bandwidth is unregulated. • No interference between links operating in different rooms. • High security. • No multipath fading. • Inexpensive technology.	• Transmission through walls and other objects is possible. • High flexibility and mobility for users.
Disadvantages	• Multiple transmitters lead to CCI. • Sensitive to ambient light (Background noise). • ISI induced due to multipath dispersion. • Low modulation bandwidth of transmitters (LEDs). • Dynamic range. • High path loss. • Installation of access points for communication between rooms.	• Interference from other users and systems. • Regulated bandwidth. • Low security. • Multipath fading.

2.3 Indoor VLC System Structure

A block diagram of an indoor VLC system is shown in Figure 2.3. The VLC system consists of (1) a transmitter that uses white LEDs or visible LD, (2) a VLC channel (VLC links design) and (3) a receiver that employs a photodetector (PD).

Digital and analogue components are used in the transmitter and receiver structure. The data stream, baseband modulator and digital to analogue convertor (DAC) are the digital components in the transmitter. Similarly, the digital components in the receiver are the analogue to digital convertor (ADC), demodulator and data sink. The trans-conductance amplifier (TCA), bias Tee and LED/LD are the analogue components in the transmitter. The receiver includes the PD, trans-impedance amplifier (TIA) and band pass filter (BPF). The AC signal in the transmitter is added onto the DC current by a bias Tee (a device used to inject DC power into a high frequency transmission line). Since LEDs work in a linear region with unipolar driving currents, the absolute driving current (AC+DC) has to be larger than zero. The total current is fed to the LEDs to emit the modulated output power. The power received by the PD is converted into a current (I-PD), and this current consists of two components: the AC and DC parts. The AC component is amplified and then filtered using TIA and BPF respectively. Finally, the digital signal is demodulated after conversion with ADC [4].

2.3.1 Transmission of VLC data

The main function of the VLC transmitter is to convert an electrical signal into an optical form and then launch the resulting optical signal into the free space link. LEDs are currently used for VLC transmission [38]. White LEDs are available at low cost and they are considered eye-safe, even at relatively high powers. This is due to their sufficiently large surface area emitting light over a relatively wide spectral range [38]. Commercial white LEDs emit light into semi-angles in the range of 12^{o} to 70^{o} [39].They are also more affordable and reliable compared to incandescent light bulbs. Therefore LEDs are a preferable source of light for indoor applications. Inspite of LEDs having several advantages, they also have some drawbacks, including:

- Low modulation bandwidth (typically tens of MHz).

- Low electro-optic power conversion efficiency (typically 10 to 40%).
- Non linearity [40].

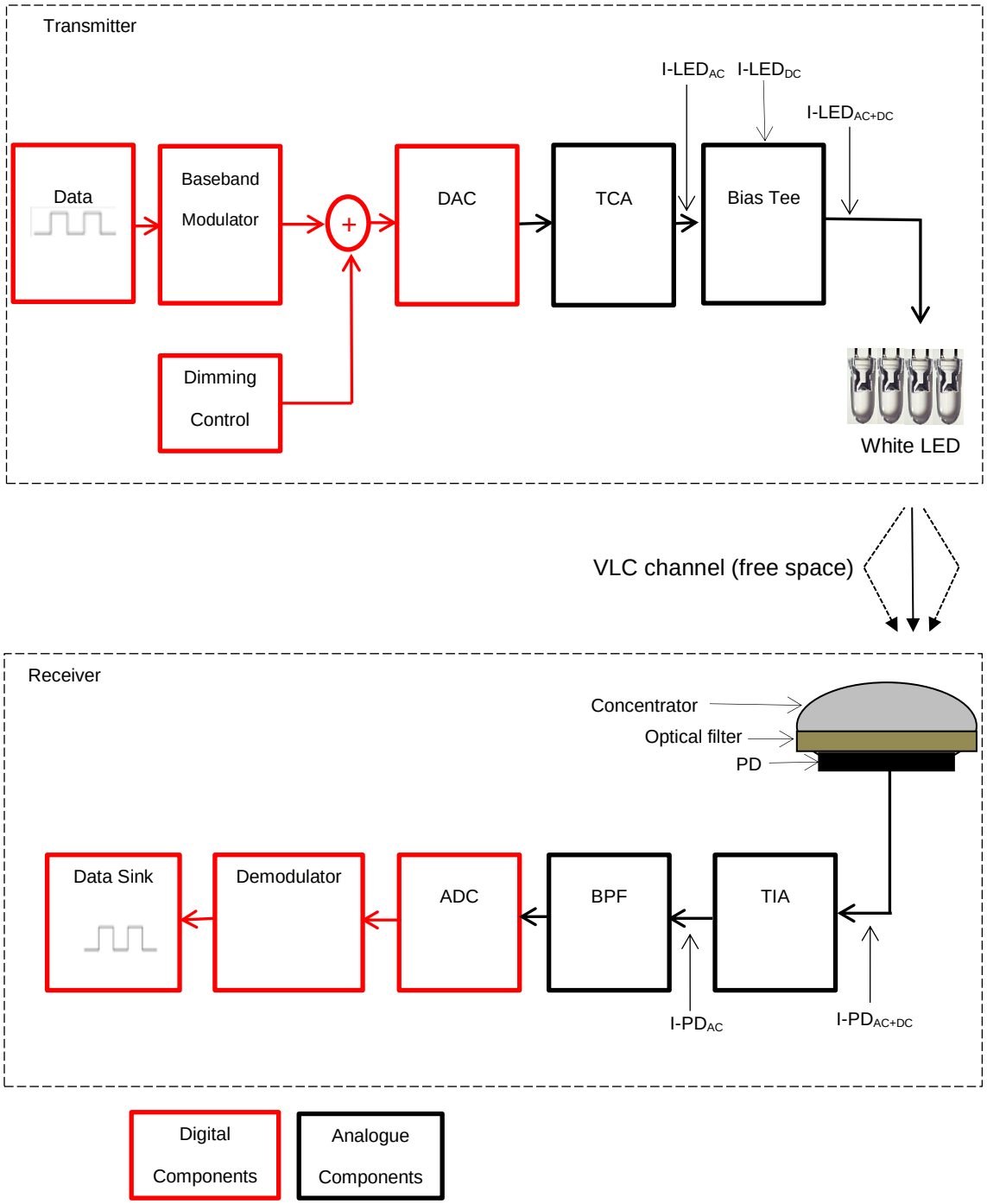

Figure 2.3: Block diagram of VLC system.

On the other hand, white LD may be considered as alternatives to LEDs in VLC systems due to their numerous advantages, which include:

- Wide modulation bandwidth (typically hundreds of MHz to more than 10 GHz).
- High electro-optic power conversion efficiency (typically 30 to 70%).
- Linear electrical to optical signal conversion characteristics [26].

However, LD are more expensive than LEDs as well as requiring a more complex drive circuit.

2.3.2 VLC transmission link design

There are two criteria to classify VLC links: (i) the degree of directionality between the transmitter and the receiver and (ii) the existence of a direct path between the transmitter and the receiver. These classifications are based on the radiation pattern of the transmitter and field of view (FOV) of the receiver. The link classification schemes are illustrated in Figure 2.4.

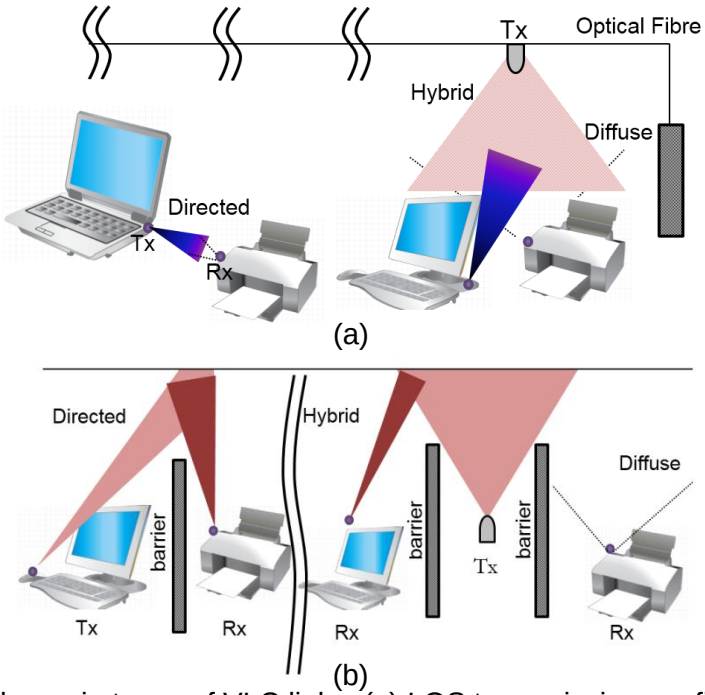

Figure 2.4: The main types of VLC links, (a) LOS transmission configurations, (b) NLOS transmission configurations.

Line of sight (LOS) and non LOS (NLOS) transmission configurations represent the two main types of indoor VLC links [34], [41], [42]. LOS links provide a direct path between the transmitter and receiver, minimise multipath dispersion and enhance the power efficiency of the VLC communication system. However, LOS links suffer from shadowing. On the other hand, NLOS links rely on reflections from the walls, ceiling and other objects. The NLOS links offer robust links and protection against shadowing and signal blockage, but they are severely affected by multipath dispersion, which results in ISI and pulse spread [34]. The effects of multipath dispersion can be mitigated through the use of equalisation and/or diversity. In a VLC system, LOS can be achieved with many light units on the ceiling. However, the optical path differences between the light units results in ISI. In this work, both LOS and NLOS links are considered.

LOS and NLOS systems can further be classified into directed, hybrid and diffuse according to the orientation of the transmitter and receiver [43], [44]. In directed links both the transmitter and receiver are directed (i.e., have narrow beam/FOV). A hybrid link can be formed either by a transmitter with a narrow radiation beam and a receiver that is non-directed, or vice versa. In the diffuse scenario, the transmitter uses a wide radiation beam and the receiver employs a wide FOV detector. The three classifications of LOS and NLOS configurations are shown in Figure 2.4 (a) and (b).

2.3.3 Receiver components

A VLC receiver converts the received optical signal into an electrical signal. It comprises a photodetector and a pre-amplifier circuit that are placed behind a front end. The front end consists of a concentrator and an optical filter (see Figure 2.3). The concentrator increases the amount of received signal power at the receiver [45]-[48]. The optical filter reduces the amount of ambient light captured by removing the captured light outside the signal optical spectral band [49]-[53]. A key component in a VLC receiver is the photodetector where the

optical signal that is represented as ‘’1’’ and ‘’0’’ bits is converted directly into an electric current. The next process is the amplification of the electrical current, therefore, the photodetector is followed by a preamplifier. The main components of a VLC receiver are discussed next.

2.3.3.1 Concentrators

Increasing the active area of the photodiode leads to an improvement in the received optical power. However, this would increase the capacitance, hence reducing the receiver bandwidth and restricting the transmission rates [54]-[56]. An optical concentrator can be used to increase the collected signal power by increasing the effective collecting area. The main function of optical concentrators is to guide light rays incident over a large area into light rays that emerge from a smaller area.

There are two types of concentrators: imaging and non-imaging. Imaging concentrators can be found in long range systems such as FSO. In general, most indoor OW links, including VLC, typically consider the use of non-imaging concentrators. The effective signal-collection area can be written as [26]:

$$A_{eff}(\delta) = \begin{cases} A\cos(\delta), & 0 \le \delta \le \pi/2 \\ 0 & \delta > \pi/2 \end{cases} \tag{2.1}$$

where δ is the angle of incidence with respect to the receiver normal and A is the physical area of the detector. An idealised non-imaging concentrator has a relationship between the FOV and gain. The maximum achievable concentrator gain is as follows [33], [57]-[59]:

$$g(\delta) = \begin{cases} \frac{N^2}{\sin^2 \psi_c}, & 0 \le \delta \le \psi_c \\ 0 & \delta > \psi_c \end{cases} \tag{2.2}$$

where N is an internal refractive index and ψ_c is the semi-angle FOV of the concentrator (usually $\psi_c \le 90^o$). The above formula shows an inverse relation

between the gain and FOV of the receiver. If the receiver's FOV is reduced, the gain is increased.

In this section, two types of optical concentrators are introduced. The non-directional hemispherical lens and compound parabolic concentrator (CPC). A hemispherical concentrator has an acceptance semi-angle of 90^{o}, therefore $g(\delta) = N^2$. A hemisphere-based receiver has an effective area of:

$$A_{eff}(\delta) = AN^2 \cos(\delta) \tag{2.3}$$

Figure 2.5 shows a non-directional hemispherical lens that employs a planar filter.

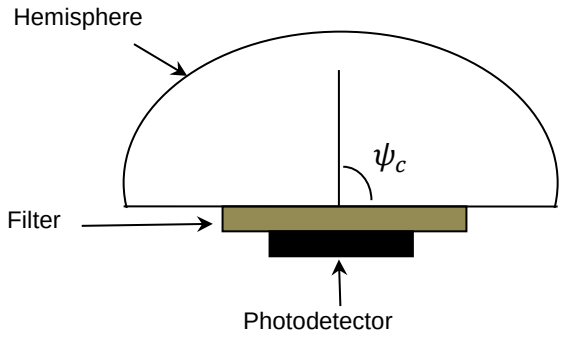

Figure 2.5: Non-directional hemispherical lens that employs a planar filter.

The CPC is an angle transforming device that can collect and concentrate the light from a large input area down into a smaller detector area. A CPC can achieve a much higher gain than a hemispherical concentrator, but this is at the cost of a narrow FOV (ψ_c). This makes a CPC more appropriate for LOS links. An array of CPC elements can be used with an ADR to reduce the multipath dispersion effect and hence improve the performance of the system [60], [61]. A CPC can be coupled with an optical filter on the front surface, as shown in Figure 2.6.

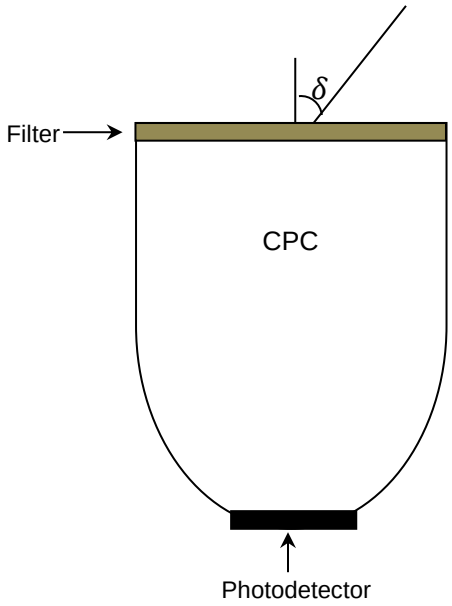

Figure 2.6: Compound parabolic concentrator.

2.3.3.2 Optical filters

OW systems are vulnerable to ambient light and sunlight. Therefore, to reduce the effect of unwanted noise components in the received electrical signal, an optical filter can be used prior to detection by the photodetector [62]. Figure 2.7 illustrates the relative spectral power densities of the three common ambient light sources. A high pass filter (HPF) and a BPF are generally used in OW systems. A HPF passes light at wavelengths higher than the cut off wavelength, and they are usually made of colour glass or plastic and their transmission characteristics are substantially independent of the angle of incidence [26]. A BPF is the other alternative that can be used to minimise the ambient light in OW receivers. A BPF can have very narrow bandwidths (typically 1 nm), and can be fabricated using multiple thin dielectrics with varying indices of refraction and relies upon optical interference in the created Fabry-Perot cavities [63]. The transmission characteristics of such BPFs vary greatly depending on the angle of incidence. Therefore, they should be used with an adequate concentrator to be suitable for diffuse systems, such as a hemispherical concentrator [26]. The

modulation bandwidth available in the transmitters (LEDs) is typically less than the VLC channel bandwidth, which means that the former limits the transmission rates. A blue optical filter at the receiver is used to filter the slow response yellowish component, and this technique is considered to be the simplest and most cost effective approach to increase data rates [64]-[66].

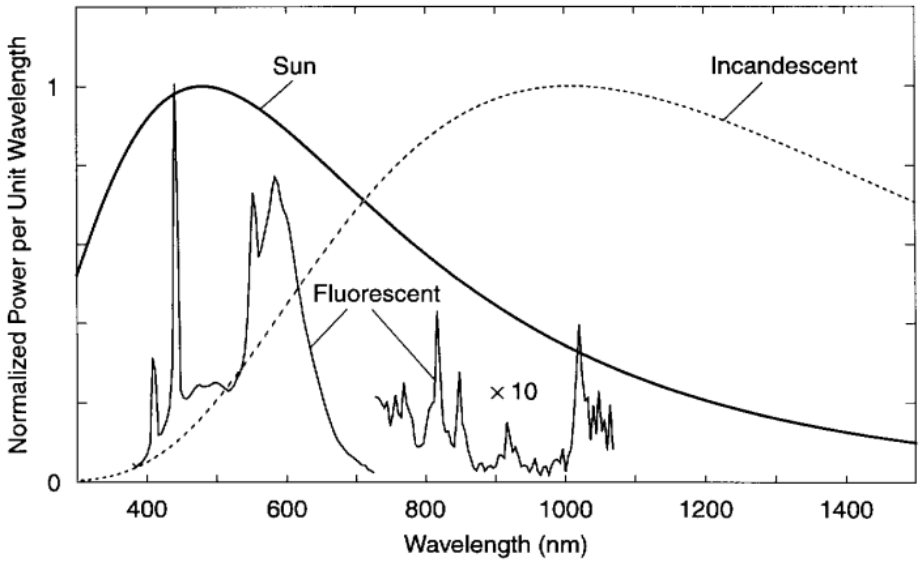

Figure 2.7: Relative spectral power densities of the three common ambient light sources [26].

2.3.3.3 Photodetectors

A photodetector is an optoelectronic transducer that generates an electrical signal that is proportional to the incident light. Since, the received light in an OW system is generally weak, the photodetector must therefore meet important performance specifications, such as:

- High sensitivity at the operating frequency.
- High conversion efficiency within its operational range of wavelengths.
- High response speed.
- High reliability, low cost and small size.
- Low noise level.

- Low bias voltage required in portable devices together with tolerance to temperature fluctuations.

Two types are commonly used in OW systems: PIN photodiodes and the avalanche photodiodes (APDs). PIN photodiodes require less complex biasing than APDs and are cheaper and simpler to manufacture. However, PIN photodiodes are less sensitive than APDs. APDs are usually 10 to 15 dB more sensitive than PINs [26]. APDs provide an inherent current gain through an ionisation process, hence improving the SNR and reducing the effect of front-end noise [67]. APDs are the preferred choice when the ambient induced shot noise is weak and the pre-amplifier noise is the major source of noise. Shot noise due to the ambient light is present in OW systems, and therefore a PIN photodiode is considered to be the better option [68].

A photodiode should have a large bandwidth and a high responsivity (PIN photodiodes are capable of operating at high bit rates [69]). The bandwidth of the photodiode is limited by the transit time of the carriers through the PN junction. Responsivity is a key parameter in photodiode models and is measured at the central optical frequency of operation. Responsivities of silicon photodiodes operating in the 430nm-655nm wavelength bands, are in the range of 0.21 A/W to 0.46 A/W [70]. The responsivity of the photodiode can be expressed as [63]:

$$R = \frac{\eta q \lambda}{h_p c} \tag{2.4}$$

where q is the electronic charge, η is the quantum efficiency of the device, λ and c are the wavelength and the speed of light respectively and h_p is the Planck constant. The internal quantum efficiency (η) is the probability of the incident photon producing an electron-hole pair (typically in range of 0.7 to 0.9).

2.3.3.4 Preamplifiers

The preamplifiers that are used in the photo-receivers can be categorised into three types: low impedance, high impedance and trans-impedance preamplifiers. The low impedance preamplifier offers a large bandwidth but has high noise and hence low receiver sensitivity. On the other hand, the high impedance preamplifier provides high sensitivity but an equaliser must be used to mitigate the limitations imposed on the frequency response by the front end RC time constant. In addition, due to their high input load resistance they also have a limited dynamic range [3], [68]. In contrast, a trans-impedance preamplifier provides a large dynamic range and avoids the need for an equaliser. Therefore, it is suitable in most OW link applications. However, it has lower sensitivity (high noise level) compared to a high impedance amplifier. Sensitivity can be improved when a field-effect transistor (FET) is used as a front-end device instead of a bipolar junction transistor (BJT). However, in terms of power consumption, a BJT can provide better performance [68], [71]. In this work, both FET and BJT are considered and used.

2.4 Design Challenges of Indoor VLC Systems

VLC systems have become promising candidates to complement conventional RF systems due to the increasingly saturated RF band and the potential high data rates that can be achieved by VLC systems [4]. Over the last decade, significant research effort has been directed towards the development of VLC systems due to their numerous advantages over RF systems, such as the availability of simple transmitters (i.e., LED) and receivers (silicon photo detectors). However, there are several challenges facing VLC systems to achieve high data rates (multi gigabits per second). These challenges include the low modulation bandwidth of the LEDs (VLC transmitters), provision of an uplink for VLC system, multipath dispersion and photodetector high capacitance.

2.4.1 Light emitting diodes (LED) modulation bandwidth

The modulation bandwidth available in the transmitters (LED) is typically less than the VLC channel bandwidth, which means that the former limits the transmission rates. To achieve high data rates in VLC systems a number of different techniques can be used, for instance, optical filters, pre and post equalisation (or both), complex modulation techniques for example, modulation formats that encode multiple bits per symbol and/or modulation formats able to operate at low system bandwidth, and parallel communication (multiple input and multiple output, MIMO).

A blue optical filter at the receiver is used to filter the slow response yellowish component of the phosphor LED, and this technique is considered to be the simplest and most cost effective approach to increase data rates [64]. However, the achieved bandwidth is insignificant (8 MHz). The drop in the white LED response can be compensated for by using a simple analogue pre-equalisation at the transmitter side, and this technique can offer 40 Mb/s without the use of a blue filter [72]. However, the data rate achieved is still very low compared to the VLC spectrum. A moderate data rate (80 Mb/s) can be achieved using more complex pre-equalisation [73]. However, pre-equalisation has the drawback that the drive circuit for the LED needs to be modified, and this leads to higher costs and lower efficiency of the emitter (i.e., not all the input power is converted into light). By combining simple pre and post equalisations, 75 Mb/s can be achieved [74]. A data rate of 100-230 Mb/s was the maximum data rate achieved using phosphorescent LEDs with simple OOK modulation [75]. Higher data rates can be achieved when complex modulation approaches are used, for example, discrete multi-tone modulation (DMT) can provide data rates of about 1 Gb/s [32]. However, this type of modulation requires a complex transceiver. In terms of parallel transmission, a VLC system is the optimal choice for optical MIMO, as many LEDs (transmitters) are used for illumination and can send different data streams on every single LED to

maximise the throughput. At the same time, an array of photo detectors are necessary at the receiver side, and this setup offers improvements in security, link range and data range, while the power required is unaltered [76]. A real enhancement in the data rates can be achieved with red, green and blue (RGB) LEDs. A rate of 1.25 Gb/s was reported in [77] when using RGB LEDs in a single colour transmission mode, and 1.5 Gb/s was achieved by using a new design based on μLED arrays that use non-return-to-zero OOK (NRZ-OOK) as the modulation scheme. The 3 dB modulation bandwidth of this LED was 150 MHz [78]. The maximum data rate achieved by using commercial RGB LEDs with low complexity modulation (OOK) is up to 500 Mb/s [79]. Recently, a 3 Gb/s VLC system based on a single μLED using orthogonal frequency division multiplexing (OFDM) has been successfully demonstrated [80]. Potentially, 10 Gb/s data rates could be delivered with an RGB triplet in such devices [80]. A rate of 3.4 Gb/s has been reported in [31] using DMT, wavelength division multiplexing (WDM) and RGB LEDs. Conventional VLC systems have used organic LEDs and RGB LEDs as transmitters. However, due to their low modulation bandwidth, the highest VLC data rates achieved by LEDs was reported in [81], where the aggregate data rate was 4.5 Gb/s when using carrier-less amplitude and phase (CAP) modulation and recursive least squares (RLS) based adaptive equalisation, wavelength division multiplexing (WDM) and RGB LEDs. The design and implementation complexity are a major concern in these systems. A high modulation bandwidth transmitter in a VLC system is vital for achieving high data rates.

2.4.2 Provision of uplink for VLC system

Although VLC systems provide lighting and communications simultaneously from LEDs, the uplink channel design in such a system is a challenging task. This is due to the energy limitations of mobile devices (where such light does not need to be generated for illumination) and also due to the potential glare

from the light where VLC signals can cause discomfort to human eyes and affect the indoor illumination. Taking these reasons into considerations, VLC systems remain a strong candidate for downlink implementation within a local network. However, it is better if VLC technology is complemented with an alternative uplink technology.

Many techniques have been proposed to provide an uplink for VLC systems. In [82], retro reflecting transceivers using a corner cube modulator to provide a low data rate (few kb/s) uplink were proposed for a VLC system as shown in Figure 2.8. Recent work [83], [84] has proposed a hybrid solution where the uplink challenge is resolved by the use of a RF-VLC combination as shown in Figure 2.9. The system comprised of Wi-Fi uplink and VLC downlink to increase the overall capacity with multiple users. This solution is suitable for RF insensitive areas, such as schools and homes with relatively small data rates. Moreover, different researchers have demonstrated a bi-directional indoor communication system based on VLC RGB LEDs [85]. Each colour can be used to carry different signals. The study achieved a 300 Mb/s uplink transmission rate. A higher data rate has been enabled by higher modulation formats (quadrature amplitude modulation, QAM-OFDM), advanced digital signal processing and pre and post equalisation. However, this type of configuration requires a directional transmission beam that can lead to significant deterioration of throughput given the potential movement of users. In addition, the uplink VLC can produce light that is uncomfortable to human eyes. Therefore, there is a need to find alternative solutions with relatively high transmission speed for use in sensitive places and high-security applications.

In this thesis, an IR uplink channel is used to overcome the potential issues of uplink transmission in VLC systems. IR (invisible light) optical communications has the same advantages as VLC systems. It also has some additional advantages compared to VLC. For example, light dimming is not an issue in IR systems and uplink implementation using IR is convenient as it

avoids bright visible light next to the user equipment, next to a laptop, for example. It can also provide high transmission rates similar to VLC systems and potentially higher data rates (data rates of 5, 10 and 15 Gb/s employing OOK modulation can be achieved) [86]-[88]. This is mainly because of the wider modulation bandwidth of LD sources used in IR optical wireless instead of white LEDs. Recently, a high-speed uplink connection for VLC systems employing IR wireless links has achieved 2.5 Gb/s [89].

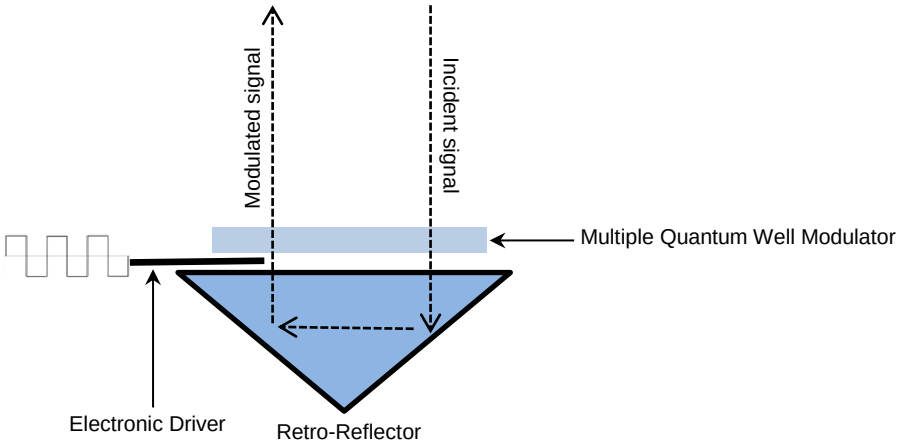

Figure 2.8: Retro reflecting technique to provide an uplink link for VLC system.

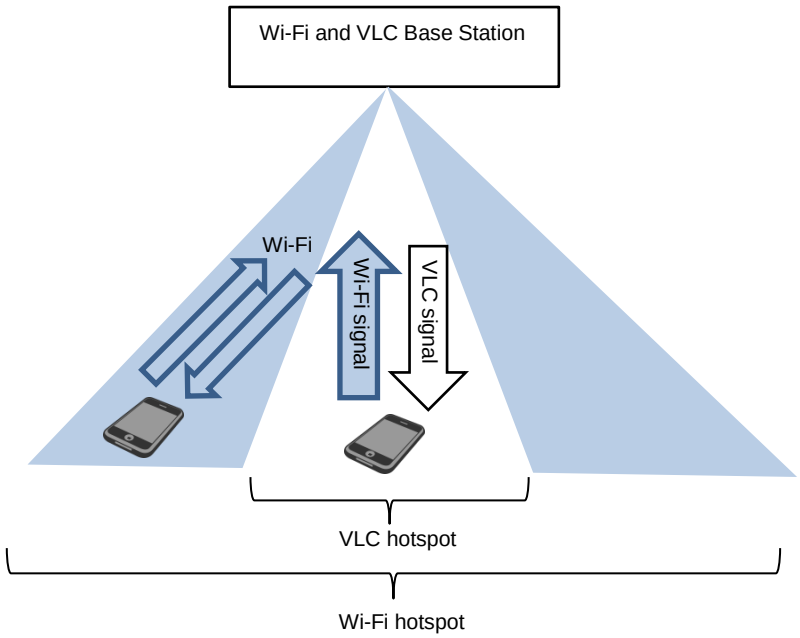

Figure 2.9: Bidirectional VLC system combination with Wi-Fi system.

2.4.3 Multipath dispersion

Multipath dispersion is an important concern in designing a VLC system for an indoor environment. This is a result of the reflective proprieties of the VLC channel. Multipath dispersion occurs when the transmitted signal reaches the receiver through different paths at different times due to reflections from the ceiling, walls and other objects. Multipath dispersion causes the received pulse to spread, hence causing ISI. The channel root mean square (rms) delay spread is an important parameter to measure the ISI induced by multipath propagation [4].

The indoor channel characteristics of VLC systems have attracted great attention to devise techniques that can help alleviate multipath dispersion. VLC systems are subjected to ISI when operated at high data rates. Therefore, various techniques have been proposed to reduce the impact of ISI in VLC systems. The authors in [90] proposed a return to zero OOK (RZ-OOK) modulation, with the space between pulses being used as a guard to reduce the effect of the delay in low data rate applications. Spread spectrum has also been considered to combat ISI, however, spread spectrum reduces the bandwidth efficiency as well [91]. The authors in [92] used zero forcing (ZF) equalisation with such a transmitter (i.e., LED) arrangements to reduce the effects of ISI. The bit error rate (BER) achieved with this technique was similar to the channel without ISI. In [28] they found that decreasing the receiver field of view leads to reduced ISI, whereas increasing the data rate lead to an increase in ISI. The authors in [93] used MIMO techniques to reduce shadowing effects. Other approaches can be used to reduce ISI in VLC systems. Adaptive equalisation with a least mean square (LMS) algorithm has been used to achieve 1 Gb/s [94]. An ADR is a simple and efficient technique that can be used to mitigate the effects of ambient light and pulse spread in OW systems [95], [96]. ADR employs multiple photo detectors with relatively small FOVs, where each photo detector is aimed in a different direction with a specific azimuth and elevation

angle to collect information signals [22]. A prism array based receiver has been investigated to provide angular diversity to mitigate the effects of ISI [97]. OFDM is a modulation technique that is extensively used in VLC systems as it successfully combats ISI caused by multipath propagation [98], [99].

In VLC systems, the impact of ISI is larger than the impact of other noise components [28]. Therefore, in this thesis, the optimisation of three and seven ADRs is proposed to mitigate the impact of multipath dispersion [100]-[102]. However, ADR presents some drawbacks, including high cost and large size due to using multiple receiving elements. An alternative approach that can be implemented to combat multipath dispersion is imaging receivers [103]-[105]. In this thesis, an imaging receiver with 50 pixels is proposed to enhance the overall system performance. A significant improvement can be achieved in SNR by using an imaging receiver at high data rates. This significant improvement in the SNR level is attributed to the ability of the imaging receiver to collect the VLC signal with minimum ISI, due to its narrow FOV pixels and large overall detection area provided by the large number of pixels.

2.4.4 Photodetector high capacitance

To collect an adequate optical signal the photodetector active area must be large, but the capacitance of the photodetector is directly proportional to its area. Therefore, a large photodetcetor area implies a large capacitance, which results in a restriction in the attainable bandwidth. The large capacitance at the input of the amplifier operates as a low pass filter (LPF), which means that the received high frequency components will be attenuated. Although, a large capacitance acts as a LPF, it does not eliminate the dominant white thermal noise that is observed after the input stage. This noise may negatively affect the SNR at higher signal frequencies. When a white noise process following a LPF is fed back into the input of the filter, its power spectral density becomes quadratic in frequency and is often called f^2 noise [106]. Due to the f^2 noise

variance being proportional to the square of the capacitance, an array of photodetectors can be used instead of a single photodetector (hence avoiding the photodetector's high capacitance) to reduce the effect of f^2 noise [107].

The authors in [108] proposed the use of an array of photo detectors instead of a single photo detector to mitigate the effects of the large capacitance and to maximise the collected power at the same time. The photo detector's effective area can be enhanced by using a hemispherical lens, as suggested in [26]. Bootstrapping was proposed by the authors in [37] to minimise the effective capacitance of a large area photo detector. In this thesis, an ADR and an imaging receiver are employed to mitigate the impact of the large photodetector area and to improve the system's performance.

2.5 Signal Modulation Techniques

OW system channels are completely different from traditional RF system channels, and this has resulted in different methods of modulation being used. Modulation schemes that fit well in RF channels do not necessarily perform well in the optical domain. There are four criteria for choosing a specific modulation technique for OW systems. The most important criterion to be applied is the average power requirement used (power efficiency), due to eye hazards and power consumption. The second criterion is the receiver's electrical bandwidth requirements. The third factor is the complexity of modulation and power consumption in portable devices. The last factor is the physical limitations in the transmitter (i.e., LD or LED). Modulation in OW systems consists of two steps: in the first step the information is coded as a waveform and then (second step) these waveforms are modulated onto the instantaneous power of the carrier [26]. This section firstly defines the intensity modulation and direct detection (IM/DD) channel, and then discusses the most common modulation schemes used over this channel: OOK and pulse position modulation (PPM).

2.5.1 IM/DD channel

IM/DD is the preferred transmission technique in OW systems [26], [109]. IM is achieved by varying the bias current of the LD or the LED. In OW systems, the transmitted signal power is always positive. Direct detection is the simplest method that can be used to detect an intensity modulated signal. The photo detector generates a current that is proportional to the incident the optical power intensity. Currently, IM/DD is considered to be the only practical approach for modulation and detection of the optical carrier in a VLC system [54]. A simple description for the IM/DD channel is given as [26]:

$$y(t) = Rx(t) \otimes h(t) + Rn(t) \tag{2.5}$$

where R is the photo detector responsivity (in amps per watt), $y(t)$ is the instantaneous photo current received, t is the absolute time, $\otimes$ denotes convolution, $h(t)$ is an impulse response, $x(t)$ is the instantaneous transmitted power and $n(t)$ is the background noise (BN), which is modelled as white Gaussian noise, and the BN is independent of the received signal.

One of the most important factors that should be considered when designing a communication system is the modulation scheme. The modulation scheme defines the power efficiency and bandwidth of the system, and these will affect the overall system performance. One of the main constraints in a mobile OW transmitter is the power consumption. Therefore, power efficient modulation is required. OOK and PPM are the most popular modulation schemes applied in OW systems [59].

The physical layer (PHY) of the IEEE 802.15.7 standard for VLC systems supports three different types of modulation schemes: OOK, PPM and colour shift keying (CSK) [70]. In this thesis all the proposed systems employ an OOK modulation scheme that adds simplicity to the VLC system. Using PPM or CSK imposes more system complexity compared to OOK.

2.5.2 On-Off Keying (OOK)

One of the simplest modulation techniques that can be implemented in a VLC system is OOK [38], [110], [111]. In OOK, a light pulse is transmitted if the bit is '1' and no light pulse is transmitted if the bit is '0'. There are two types of OOK: non return to zero OOK (NRZ-OOK) and return to zero OOK (RZ-OOK). Figure 2.10 shows NRZ-OOK and RZ-OOK signals.

Tb represents the duration of the bit. The pulse width is $Tp = Tb \times k$. If k is set to 1, the result is basically NRZ-OOK, while If k=0.5 (50% duty cycle) the scheme is known as RZ-OOK. NRZ-OOK has several advantages, including simplicity of implementation and bandwidth efficiency. However, it requires a high average optical power compared to RZ-OOK.

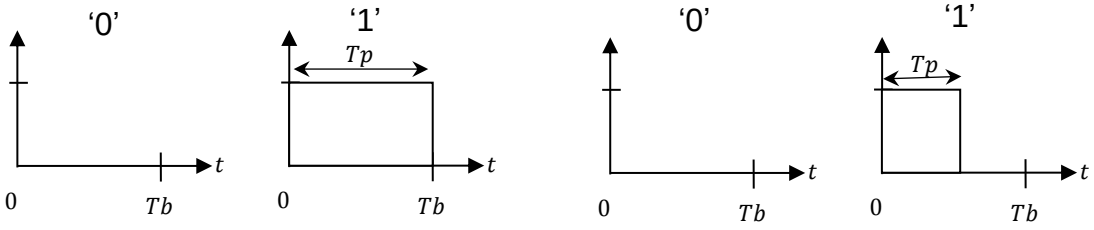

(a) NRZ-OOK (b) RZ-OOK

Figure 2.10: Basic NRZ-OOK and RZ-OOK signals.

OOK is a suitable modulation technique and easy to implement in OW systems because it is very simple for LED or LD to switch on and off quickly [21]. Many other types of modulation have been applied in OW systems, such as PPM [36]. Differential PPM (DPPM) is applied in OW systems to obtain higher data rates; it consumes less power on average than PPM. However, the distortion in the DPPM signal is greater than in the PPM signal [112]. More advanced techniques could be used in OW systems to transmit multiple carriers, such as

subcarrier modulation (SCM). This technique can provide multiple access for simultaneous users and a high data rate. However, SCM is not power efficient like single carrier schemes are [113]. For instance, each quadrature phase shift keying (QPSK) or binary PSK subcarrier requires about 1.5 dB more power than OOK. In [114] they achieved high data rates while reducing the average power requirements in SCM modulation. In [24] OFDM was applied in indoor OW systems to achieve high data rates over a noisy channel and to compact ISI. However, the system did not achieve a high SNR. The main disadvantages of OFDM are the sensitivity to frequency offset and phase noise as well as the high peak to average power ratio (PAR) [99]. In general, the use of complex modulation leads to an improvement in the performance of the OW systems, such as mitigating the ISI effect and increasing data rates. However, these modulation techniques require a complex transceiver.

In this thesis we only used NRZ-OOK with VLC and IROW systems and this is due to its simplicity and easy to implement.

2.5.3 Pulse position modulation (PPM)

PPM is a modulation scheme that offers high average power efficiency at the cost of relatively poor bandwidth efficiency [115], which makes it more sensitive than OOK to multipath dispersion. PPM is considered in optical communications due to its low average power requirements [116], [117].

PPM is a modulation scheme in which data bits are conveyed by a single pulse in one of several possible positions. The positions are represented as slots, and L-PPM has slots in a single symbol time (frame). Each frame contains a pulse occupying one slot and empty slots. The pulse is located at a slot that is proportional to the binary value of the original digital symbol. Each frame can be concluded by a guard interval to avoid inter frame interference and for timing extraction purposes. The time used for communication is divided

into equal blocks. Each block is equally divided again into *L* time slots. Figure 2.11 shows an example of 4-PPM modulation.

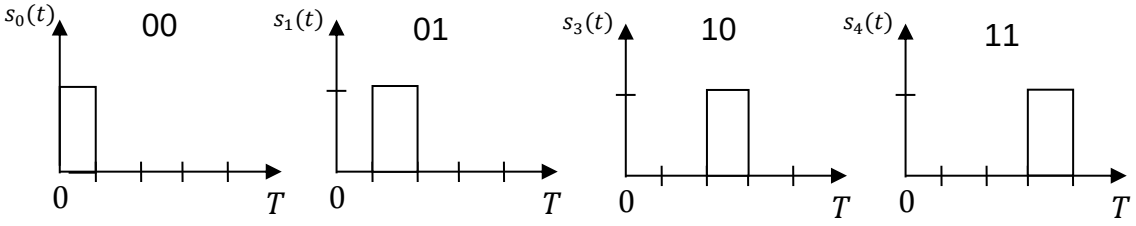

Figure 2.11: Example of 4-PPM code.

2.6 Dimming Control and Flicker Brightness of the VLC System

Brightness control for the LEDs in VLC systems is required. Light dimming is defined as controlling the perceived brightness of the light source according to the user's requirement and is a cross layer function between the PHY and MAC [70]. Many techniques have been used and implemented for dimming control in VLC systems [111], [118]-[120]. The simplest method is amplitude modulation (AM) dimming control where the luminous flux is controlled by controlling the input DC current. However, the chromaticity coordinates of the emitted light can be changed [62]. Pulse width modulation (PWM) is another method to control the width of the current pulse as shown in Figure 2.12. The main feature in the PWM dimming method is that the amplitude of the pulse remains constant. The width of the pulse varies according to the dimming level, thus the result is that the emitted light spectrum is constant. Binary code modulation or a bit angle modulation (BAM) are other dimming methods invented by artistic licence engineering (ALE), and it is a new LED drive technique that can be used in VLC systems [121]. The main advantages of using this technique are the simplicity implementation (easy to realise), potential flicker is reduced, BAM needs less processing power and simple operation to recover the data. BAM implementation of LED dimming level uses binary data patterns as shown in

Figure 2.13. In the BAM 8 bit system, the pulse width of bit 7 (most significant bit, MSB) is equal to 2^7=128, whereas the pulse width of bit 0 (least significant bit, LSB) is equal to 2^0=1 (a unit width). Usually, the brightness of the LED light depends on the average current into the LED.

Flicker in the VLC system can be defined as the fluctuations of the brightness of the LED light. The flicker occurs when the brightness changes over periods longer than the maximum flickering time period (MFTP) [70]. The flicker in VLC is classified into two groups according to its generation mechanism: intra-frame flicker and inter-frame flicker. Intra-frame flicker is defined as the perceivable brightness fluctuation within a frame. Inter-frame flicker is defined as the perceivable brightness fluctuation between adjacent frame transmissions.

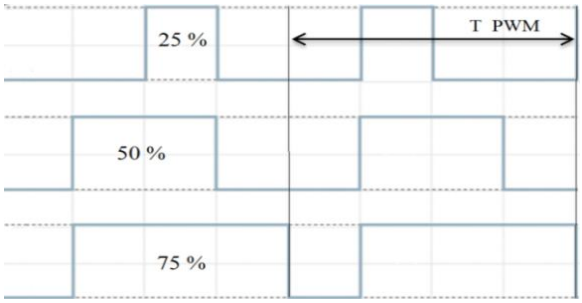

Figure 2.12: Dimming control using PWM.

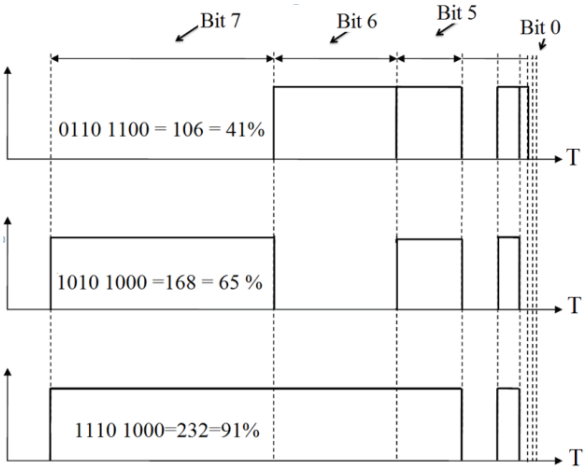

Figure 2.13: Waveform of BAM signal for dimming control.

2.7 Standards for VLC Systems

Standardisation for VLC systems started in 2003 in Japan [122]. In 2007, the Japanese electronics and information technology industries association (JEITA) proposed two standards for VLC: CP-1221 and CP-1222 [123], [124]. Significant efforts from Europe led to the start of the home gigabit access network project (OMEGA) in January 2008 to deliver high-bandwidth services for home area networks (the OMEGA project was funded by the European commission) [125]. In the same year, the national science foundation (NSF) in the US established the smart lighting engineering research centre (ERC) [126]. Recently, many organisations have been involved in integrated standards such as IEEE. In September 2011, IEEE defined standards for physical and medium access control (MAC) layers for VLC systems (802.15.7). The standard can deliver data rates appropriate for video and audio services (up to 96 Mb/s), and also considers noise and interference from light sources [70]. Similar to Wi-Fi, the light fidelity (Li-Fi) consortium was established in Norway in 2011 [127].

2.8 VLC Applications

VLC systems cover indoor to outdoor applications. Indoor applications could be data communications, indoor location estimation, indoor navigation for visually impaired people and accurate position measurements. The outdoor applications could be transportation, location information, information broadcast using the traffic light infrastructure based on the JEITA CP-1222 standard, environmental hazards, security and defence, precise control of robots and aviation [128], [129].

Like IROW systems, VLC systems can be used to transfer data within offices. User location can be estimated in an indoor environment using white LEDs, hallways are assumed to be illuminated by LEDs with a unique ID for each LED. White LEDs in conjunction with geometric sensors integrated in

smart phones could help visually impaired people move inside buildings [130]. Figure 2.14 shows a prototype of a navigation system for visually impaired people from [130]. RF signals can be undesirable inside hospital environments, especially in operating theatres and magnetic resonance imaging (MRI) scanners, therefore VLC systems can be potential solutions to such scenarios.

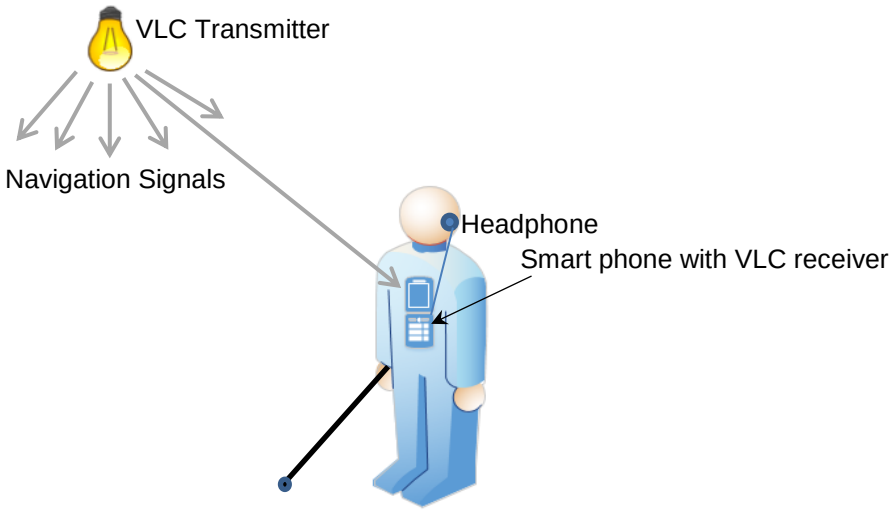

Figure 2.14: Indoor VLC navigation system for visually impaired people.

Recently, various approaches for VLC indoor positioning systems have been researched [131], [132]. VLC systems are a promising solution for indoor positioning due to many features. Firstly, there is better positioning accuracy (few millimetres) compared to radio wave systems, since VLC suffers less from interference and multipath effects. Secondly, VLC positioning systems can be used in environments where radio positioning systems are restricted, such as in hospitals [133].

White LEDs can be used to transfer digital data in the automotive field (car to car communication), head and tail LED lights can be used to communicate between cars, also there is the possibility to communicate between cars and the

traffic lights infrastructure [134]. In 2010, the geospatial information authority (GSI) of Japan started work on a standard that provides location information using visible light, the concept of this standard is to give a unique identification number to each 3×3 m^2 in Japan [128]. In risk areas, such as oil rigs and mines, safe communication and illumination can be provided by VLC systems using LEDs. Nowadays, aircraft use white LEDs for illumination, which can also be used to provide media services to passengers instead of wires. This will reduce the weight and the cost of the aircraft.

2.9 Summary

This chapter has provided an overview of VLC systems. It has introduced a comparison between VLC and RF systems. It has also explained the VLC system structure including the transmitter (LEDs) and the receiver components (concentrator, optical filter, photodetector and preamplifier), in addition to the classification of VLC links being presented. It has highlighted the significant challenges in VLC systems, such as low modulation bandwidth of transmitters (LEDs), multipath dispersion, photodetector high capacitance and the provision of an uplink, and has discussed some of the approaches that can be used to mitigate these challenges. This chapter has also addressed the most common types of modulation schemes in VLC systems. The chapter concluded with an overview of the VLC standards and current indoor and outdoor VLC applications.

3 Channel Modelling of Indoor VLC System

3.1 Introduction

To evaluate the performance of a VLC link in terms of signal integrity, modelling of the VLC channel is essential. The characteristics of the VLC system channel are fundamental to address the performance of the system and design issues. This chapter describes the tools that were used to model the VLC system communication channel in an indoor environment. The VLC signal under the effect of multipath dispersion and mobility is assessed for different link configurations (LOS and NLOS). For an indoor VLC link, multipath propagation, receiver noise, path loss and channel variation due to mobility are the major impairments. They can degrade the VLC system performance due to the introduction of heavy distortion in the received VLC signal. Light rays cannot penetrate opaque barriers such as walls, and hence are confined within the room after being reflected, which results in multipath propagation. Mathematical relations are derived to determine the received power due to multiple reflections. The simulations and calculations reported in this thesis were carried out using MATLAB.

The indoor VLC communication channel is investigated in Section 3.2. The multipath propagation model is discussed in Section 3.3. The impulse response is presented in Section 3.4. An analysis of the delay spread of the received pulse is given in Section 3.5. The SNR evaluation is provided in Section 3.6. The simulation package is explained in Section 3.7. The simulation results of the conventional VLC systems with wide FOV receiver are summarised in Section 3.8. A summary is then provided at the end of the chapter.

3.2 Indoor VLC Communication Channel

In optical wireless links, including VLC systems, IM/DD is the preferred choice [26], [109] due to its low complexity and cost. As shown in Figure 3.1, at the transmitter side IM can be simply used to modulate the desired signal into the instantaneous power of the optical carrier by varying the intensity of the optical source. At the receiver side, DD is used to generate the electrical current $I(t)$ so that it is proportional to the instantaneous received optical power. The typical detector area contains tens of thousands of very short wavelengths of the received optical signal, and hence allows spatial diversity and prevents fading [26]. An indoor OW channel that uses IM/DD can be fully characterised by the impulse response ($h(t)$) of the channel as given in [135]:

$$I(t, Az, El) = \sum_{m=1}^{M_t} Rx(t) \otimes h_m(t, Az, El) + \sum_{m=1}^{M_t} Rn_m(t, Az, El) \qquad (3.1)$$

where $I(t, Az, El)$ is the received instantaneous photocurrent in the photo-detector with photo-detector responsivity (R) using M elements to receive a transmitted signal $x(t)$ through channel h in the presence of AWGN (n_m). Az and El are the direction of arrival in the azimuth and elevation angles, respectively, t is the absolute time and $\otimes$ denotes convolution. It should be noted that $x(t)$ represents power and not amplitude. This implies that the VLC signal is non-negative.

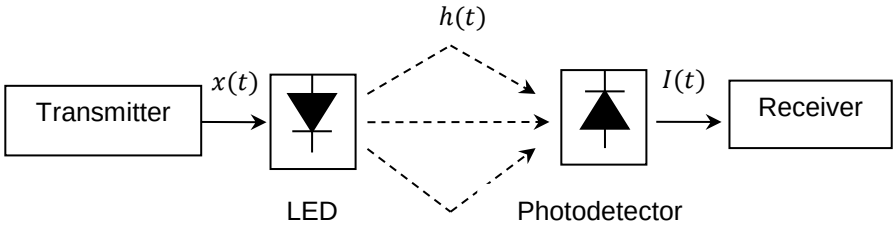

Figure 3.1: Block diagram of IM/DD VLC system.

In addition, the total average transmitted optical power in (3.1) is provided by the mean value of $x(t)$ and not an integral of $|x(t)|^2$ as is the case with RF systems.

The VLC signal emitted by the LED reaches the receiver through various paths of different lengths. These propagation paths change with the receiver movement, and/or the movement of the surrounding objects. However, the paths are fixed for a given fixed configuration. The channel impulse response can be represented approximately as the sum of scaled and delayed Dirac delta functions [26]. In this thesis a simulation package based on a ray tracing algorithm was developed to compute the impulse response on the entire communication plane. The channel impulse response can be given as:

$$h\,(t) = \sum_{k=0}^{\infty} h^{(k)}(t) \tag{3.2}$$

where $h^{(k)}$ is the impulse response due to the LOS and reflection components.

3.3 Multipath Propagation

The indoor channel propagation characteristics depend on the relative positions of the transmitter, receiver and reflectors, as well as their patterns (i.e., FOV for transmitter and receiver). These characteristics are also affected by the movement of the surrounding objects and people, but these changes are slow compared with the transmission rate. Hence, the channel can be considered as stationary for a given fixed configuration.

Multipath propagation causes the transmitted pulses to spread and may lead to ISI. Consequently, ISI restricts the attainable transmission rates. Multipath dispersion increases when the dimensions of the room increase, and this is due to the increase in the difference in paths length. Gfeller and Bapst studied the reflection coefficients for a number of materials normally used in

indoor settings [6]. They showed that the reflection coefficients ranged from 0.4 to 0.9. They also found that the power reflected by elements either on the walls or the ceiling was well approximated by an ideal Lambertian pattern. Thus, in their work and in this thesis the reflection elements on the ceiling and walls are treated as a small transmitter that transmits an attenuated version of the received signals from its centre in a Lambertian pattern. The power radiated into a solid-angle element $d\Omega$ can be modelled as [136]:

$$dP = \frac{n+1}{2\pi} \times P_s \times cos^n(\alpha) \times d\Omega \tag{3.3}$$

where the coefficient $(n + 1)/2\pi$ assures that integrating dP over the surface of a hemisphere results in the total average transmitted optical power P_s being radiated by the source (i.e., LED):

$$P_s = \int_{Hemisphere} dP \tag{3.4}$$

α is the angle of incidence with respect to the transmitter's surface normal and the parameter n represents the mode number that determines the shape of the reflected beam, which is related to the half-power semi-angle (hps) and can be defined as [26]:

$$n = \frac{-ln(2)}{ln(cos(hps))} \tag{3.5}$$

It is suitable to use n = 1 as all surfaces are presumed to be rough, and this is in agreement with experimental measurements in [6]. However, transmitters may have a high mode number, to concentrate the power at an area of interest. In this thesis, it is assumed that the reflecting elements in a plaster surface have an hps that is equal to 60^o, which corresponds to n=1.

3.3.1 Calculations of received optical power

More than one path may be present between the transmitter and the receiver as a result of multipath propagation. Temporal dispersion in the optical signal occurs as a result of multiple paths. A ray tracing algorithm can be used to compute the received optical power. The reflected optical rays from different reflectors are traced for all potential paths to the other reflectors or the receiver. Therefore, to implement ray tracing, the reflecting surfaces were divided into a number of equal-sized (square shaped) reflection elements. The optical rays reflected from these elements were in the shape of a Lambertian pattern (n = 1). The small size of these elements enhances the accuracy of the impulse response. However, the computation time increases dramatically when the surface element size is decreased.

Previous research considered only LOS and reflections up to first order [28], [77], [90]. However, this may not provide a full description of the characteristics of the system. Therefore, in this work reflections up to second order were considered, since the second order reflection can have a great impact on the system performance (especially at high data rates). In addition, our work has found that most of the received power is within the first and second reflections, but that when it goes beyond the second order the signal is highly attenuated [101].

The total received optical power (P_r) at the receiver, considering the LOS component (P_{LOS}), first order reflections (P_{FST}) and second order reflections (P_{SEC}) can be expressed as:

$$P_r = \sum_{i=1}^{S} P_{LOS} + \sum_{i=1}^{M} P_{FST} + \sum_{i=1}^{F} P_{SEC} \tag{3.6}$$

where S is the number of transmitter units, M is the number of reflecting elements in the first order reflection and F is the number of reflecting elements in the second order reflection.

Figure 3.2 shows the ray tracing setup for LOS as well as first and second order reflections. The impulse response of the VLC channel can be computed by tracing all potential light rays between the transmitter and the receiver.

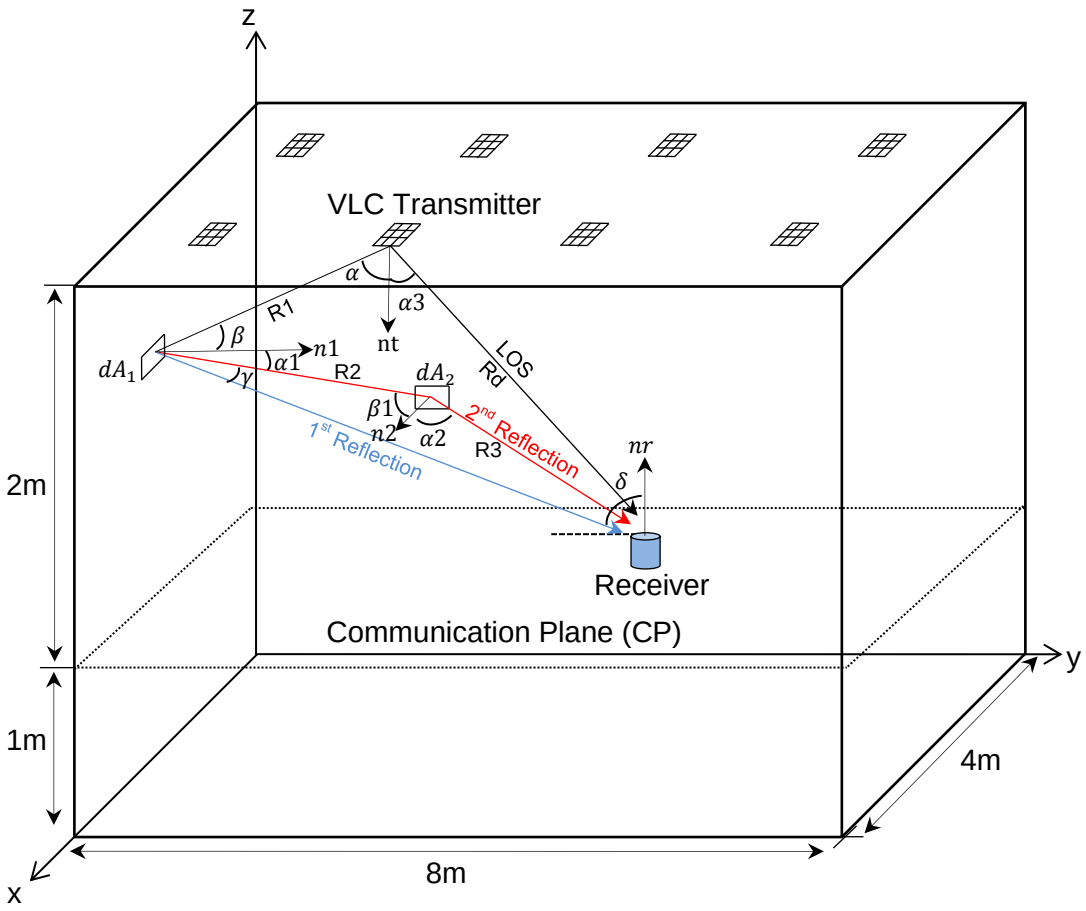

Figure 3.2: Ray tracing setup for LOS, first and second order reflections in VLC system.

3.3.1.1 Line-of-Sight (LOS) analysis

A LOS component is available when a direct path connects the transmitter and the receiver. For example, in the case of a VLC system, when the transmitter is placed on the ceiling and has an elevation angle of -90^o (facing downwards) and the receiver is on the communication plane with an elevation angle of 90^o (facing upwards), as shown in Figure 3.3, the P_{LOS} component can be written as:

$$P_{LOS} = \begin{cases} \frac{n+1}{2\pi R_d^2} \times P_s \times cos^n(\alpha) \times \cos(\delta) \times A & 0 \leq \delta \leq \psi_c \\ 0 & \delta > \psi_c \end{cases} \quad (3.7)$$

where P_s represents the total average transmitted optical power radiated by the light source (LED). A is the detector area. δ is the angle between the normal of the photodetector and the incident ray. α is the angle between the normal of the transmitter and the irradiance ray. R_d is the distance between the transmitter and the receiver. If the received angle (δ) is larger than the acceptance semi-angle (ψ_c), then the direct LOS received power approaches zero. Since, the signal must lie within the FOV of the receiver to be received, changing the receiver's FOV can be used to minimise noise (background light) or unwanted reflections.

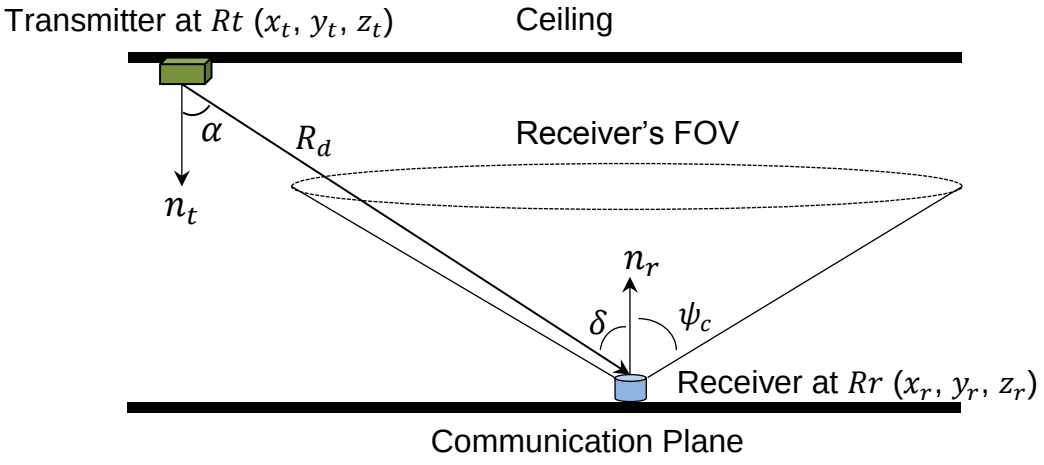

Figure 3.3: Ray tracing for LOS.

The transmitting and receiving angles (α, δ) are calculated as follows:

$$\cos(\alpha) = \frac{\hat{n}_t \cdot (Rr - Rt)}{R_d} \quad and \quad \cos(\delta) = \frac{\hat{n}_r \cdot (Rt - Rr)}{R_d} \quad (3.8)$$

where $\hat{n}_t$ is the normal of the transmitter at location Rt and $\hat{n}_r$ is the normal of the receiver at location Rr. It should be noted that both angles in (3.8) are equal if the transmitter and the receiver are placed in parallel planes, like the case in Figure 3.3. However, if the $\hat{n}_t$ is perpendicular to the $\hat{n}_r$, or vice versa, then the transmitting and receiving angles are different. Both situations were considered when computing these angles. R_d is the direct distance between the transmitter and the receiver and can be calculated as:

$$R_d = \|Rr - Rt\| = \sqrt{(x_r - x_t)^2 + (y_r - y_t)^2 + (z_r - z_t)^2} \tag{3.9}$$

where $x_t,\ y_t,\ z_t$ and $x_r,\ y_r,\ z_r$ are the transmitter and the receiver coordinates respectively.

3.3.1.2 First order reflection analysis

Figure 3.4 shows a ray incident from the transmitter on a square reflecting element and then from the reflective element to the receiver. Plaster walls can be considered as Lambertian reflectors with ne = 1 [6]. By using the Lambertian model in Equation 3.3 the received optical power of the first order reflections P_{FST} can be computed as:

$$P_{FST} = \begin{cases} \frac{(n+1)(ne+1)}{4\pi^2 R_1^2 R_2^2} \times P_s \times \rho_1 \times dA1 \times cos^n(\alpha) \times \cos(\beta) \times cos^m(\gamma) \times \cos(\delta) \times A & 0 \le \delta \le \psi_c \\ 0 & \delta > \psi_c \end{cases} \tag{3.10}$$

where R_1 is the distance between the transmitter and the reflective element, R_2 is the distance between the reflective element and the receiver and α is the angle between the normal of the transmitter and the irradiance ray.

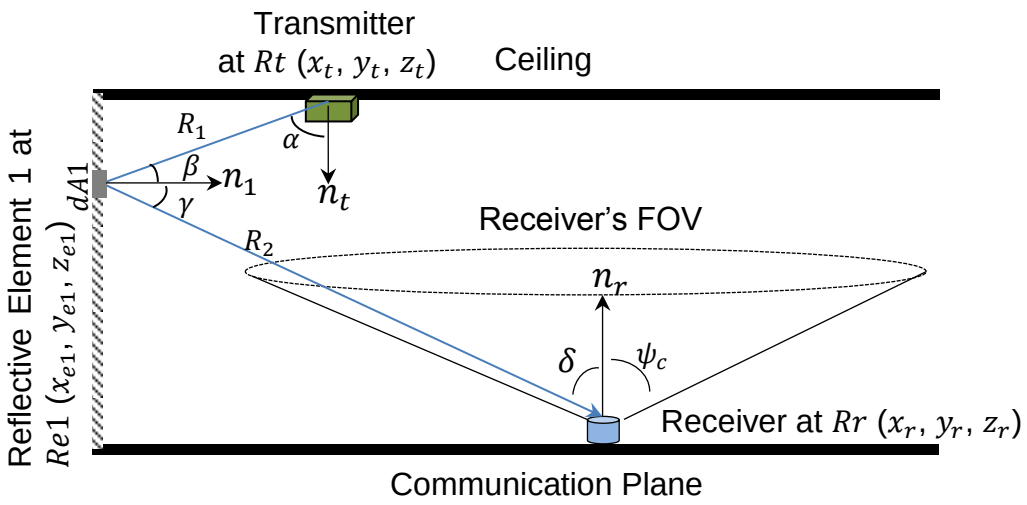

Figure 3.4: Ray tracing for first order reflections.

β is the angle between the irradiance ray from the transmitter and the reflective element's normal, γ is the angle between the reflective element's normal and the reflected ray toward the receiver and δ is the angle between the normal of the receiver and the incident ray. $dA1$ is the area of the reflective element and ρ_1 is the reflection coefficient of the reflective surface.

The reflective elements are treated as secondary small transmitters where the retransmitted power is determined by the received optical power from the transmitter and its reflection coefficient ρ_1. The four angles in Equation 3.10 can be computed as:

$$\begin{cases} \cos(\alpha) = \frac{\hat{n}_t \,.(Re1-Rt)}{R_1} & \cos(\beta) = \frac{\hat{n}_1 \,.(Rt-Re1)}{R_1} \\ \cos(\gamma) = \frac{\hat{n}_1 \,.(Rr-Re1)}{R_2} & \cos(\delta) = \frac{\hat{n}_r \,.(Re1-Rr)}{R_2} \end{cases} \tag{3.11}$$

where $\hat{n}_1$ is the normal of the reflective element 1 at location $Re1$.

3.3.1.3 Second order reflection analysis

Extending the reflection to additional surfaces and using the Lambertian model once again, the second order reflection can be calculated in three steps:

1- Compute the amount of incident optical power to the reflective element from the transmitter, which is similar to the approach used to calculate the LOS received power.
2- Compute the amount of incident optical power from the first reflective element to the second reflective element.
3- Compute the amount of received power by the receiver from the second reflective element.

It can be observed that the input power for the second reflective element is received from the first reflective element. Figure 3.5 shows the tracing of the reflected rays for the second order reflection, and P_{SEC} is given as:

$$P_{SEC} = \begin{cases} \frac{(n+1)(ne+1)^2}{8\pi^3 R_1^2 R_2^2 R_3^2} \times P_s \times \rho_1 \times \rho_2 \times dA1 \times dA2 \times cos^n(\alpha) \times \cos(\beta) \times \\ \qquad cos^m(\alpha 1) \times \cos(\beta 1) \times cos^m(\alpha 2) \times \cos(\delta) \times A \quad 0 \leq \delta \leq \psi_c \\ 0 \qquad\qquad \delta > \psi_c \end{cases} \tag{3.12}$$

where R_1 is the distance between the transmitter and the reflective element 1. R_2 is the distance between the reflective element 1 and the reflective element 2. R_3 is the distance between reflective element 2 and the receiver. $dA1$ and $dA2$ are the areas of the reflective elements 1 and 2, respectively, α is the angle between the normal of the transmitter and the irradiance ray, β is the angle between the irradiance ray from the transmitter and the normal of reflective element 1 and γ is the angle between the normal of reflective element 1 and the reflected ray toward reflective element 2. $\beta 1$ is the angle between the

incident light from the reflective element 1 and the normal of the reflective element 2. $\alpha 2$ is the angle between the normal of the reflective element 2 and the second reflected ray and δ is the angle between the second reflected ray and the normal of the receiver. ρ_1 and ρ_2 are the reflection coefficients of the first and second reflective elements, respectively.

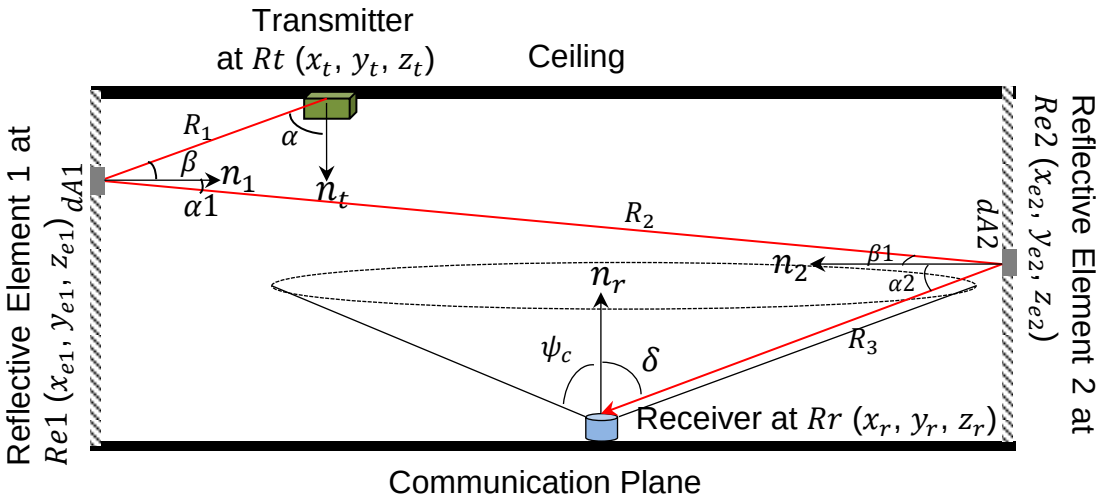

Figure 3.5: Ray tracing for second order reflections.

In the second order reflection, six angles are required and can be computed in a similar way to the direct power and first order reflection by tracing the ray from the transmitter to the receiver as:

$$\begin{cases} \cos(\alpha) = \dfrac{\hat{n}_t \,.\, (R_{e1} - R_t)}{R_1} & \cos(\beta) = \dfrac{\hat{n}_1 \,.\, (R_t - R_{e1})}{R_1} \\ \cos(\alpha 1) = \dfrac{\hat{n}_1 \,.\, (R_{e2} - R_{e1})}{R_2} & \cos(\beta 1) = \dfrac{\hat{n}_2 \,.\, (R_{e1} - R_{e2})}{R_2} \\ \cos(\alpha 2) = \dfrac{\hat{n}_2 \,.\, (R_r - R_{e2})}{R_3} & \cos(\delta) = \dfrac{\hat{n}_r \,.\, (R_{e2} - R_r)}{R_3} \end{cases} \tag{3.13}$$

where $\hat{n}_2$ is the normal of the reflecting element 2 at location $Re2$.

3.4 Impulse Response

In a practical VLC system, the impulse response is continuous, but the simulator subdivides the reflecting surfaces into discrete elements (reflecting elements on the walls, ceiling and floor). Thus, the received optical power is recorded at the receiver within time intervals (time bins). Each time bin is roughly the time light takes to travel between neighbouring elements [136]. A good choice of time bin width is provided by [41], [136]:

$$time\_bin = \sqrt{dA}/c \tag{3.14}$$

where c is the speed of light and dA is the reflection element area. Rays arriving within similar time intervals are assembled and stored for a particular receiver-transmitter location on the CP. An identical histogram of the practical impulse response is achieved as dA approaches zero. It should be noted that reducing dA leads to improved resolution of the impulse response evaluation together with an increase in the computation time exponentially. Thus, the reflective element size dA has to be selected to keep the computation requirements within a reasonable time (the computation time increases dramatically when the surface element size is decreased) [71], [137]-[139].

The indoor VLC system can be completely analysed via its impulse response $h(t)$. Several parameters can be obtained by determining the VLC impulse response, such as delay spread, 3 dB channel bandwidth and SNR.

3.5 Delay Spread

Indoor VLC systems are subject to multipath dispersion due to non-directed transmission, which can cause ISI. Delay spread is a good measure of the signal pulse spread due to the temporal dispersion of the incoming signal. The

channel spread can be quantified using the root mean square (rms) delay spread [140], [141]. The delay spread (D) of an impulse response is given by:

$$D = \sqrt{\frac{\sum(t_i-\mu)^2 P_{r_i}^2}{\sum P_{r_i}^2}} \tag{3.15}$$

where t_i is the delay time associated with the received optical power P_{ri} and μ is the mean delay given by:

$$\mu = \frac{\sum t_i P_{r_i}^2}{\sum P_{r_i}^2} \tag{3.16}$$

In this thesis, the delay spread is computed for each impulse response over the entire communication plane. In practice, for a given transmitter and receiver location the delay spread may change if the reflecting elements in the room move, for instance fans rotating and people moving. These kinds of effects are not considered in this thesis, to the best of our knowledge they have not been quantified by other researchers.

3.6 Calculations of Signal to Noise Ratio (SNR)

The VLC system's performance is best evaluated using the SNR, which gives due consideration to the noise and signal spread (eye opening). The bit error rate is expressed as:

$$BER = Q\left(\sqrt{SNR}\right) \tag{3.17}$$

where Q is the Gaussian function approximated as:

$$Q(x) = \frac{1}{2} erfc\left(x/\sqrt{2}\right) \approx \frac{1}{\sqrt{2\pi}} \frac{e^{-\left(x/\sqrt{2}\right)^2}}{x} \tag{3.18}$$

The function has the value x=6 at a BER of 10^{-9}. Hence, SNR=36 (15.6 dB) is needed for a 10^{-9} BER.

In OOK the SNR associated with the received signal can be calculated by considering P_{s1} and P_{s0} (the powers associated to logic 1 and 0, respectively). These powers (P_{s1} and P_{s0}) determine the eye opening at the sample instant, thus the ISI. The SNR is given by [142]-[145]:

$$SNR = \left(\frac{R(P_{s1}-P_{s0})}{\sigma t}\right)^2 \tag{3.19}$$

where R is the photodetector responsivity (R = 0.4 A/W) and σ_t is the standard deviation of the total noise, which is the sum of the shot noise, thermal noise and signal dependent noise. It can be calculated as:

$$\sigma t = \sqrt{\sigma_{shot}^2 + \sigma_{preamplifier}^2 + \sigma_{signal}^2} \tag{3.20}$$

where σ_{shot}^2 represents the background shot noise component, $\sigma_{preamplifier}^2$ represents the preamplifier noise component and σ_{signal}^2 represents the shot noise associated with the received signal. The detection of light by a photodiode is a discrete process since the creation of an electron-hole pair is dictated by the statistics of photon arrivals. The latter is a discrete process and obeys the Poisson distribution. The discrete nature of the photo-detection process creates a signal dependent shot noise (quantum noise). Quantum noise results from the random generation of electrons by the incident optical radiation [63].

In this thesis two schemes are considered to process the electrical signal from different branches in the ADR or different pixels in the imaging receiver: selection combining (SC) and maximum ratio combing (MRC). In the SC the receiver (ADR or imaging) simply selects the branch/pixel with the largest SNR among all the branches/pixels. The SC SNR is given by:

$$SNR_{SC} = max_i \left(\frac{R(P_{s1}-P_{s0})}{\sigma t}\right)_i^2 \quad 1 \le i \le J \tag{3.21}$$

where J represents the total number of detectors/pixels that are used in the receiver. In contrast to the SC, the MRC utilises all pixels from the imaging receiver (or branches in the ADR). The output signals of all the pixels are combined through an adder circuit. Each input to the circuit is added with a weight proportional to its SNR to maximise the SNR [146]. The weight of every pixel is obtained as [95]:

$$w_i = \frac{R(P_{s1i} - P_{s0i})}{{\sigma_t}^2{}_i} \quad 1 \le i \le J \tag{3.22}$$

The SNR at the output of the MRC is:

$$SNR_{MRC} = \frac{\left(\sum_{i=1}^{J} R(P_{s1i} - P_{s0i}) w_i\right)^2}{\sum_{k=1}^{J} (\sigma_{t_i})^2 w_i^2} \tag{3.23}$$

By substituting (W_i) in (3.23), the SNR obtained using the MRC combining method is given by:

$$SNR_{MRC} = \frac{\left(\sum_{i=1}^{j} R(P_{s1} - P_{s0})_i \left(\frac{R(P_{s1} - P_{s0})}{{\sigma_t}^2}\right)_i\right)^2}{\sum_{i=1}^{j} {\sigma_t}_i^2 \left(\frac{R(P_{s1} - P_{s0})}{{\sigma_t}^2}\right)_i^2}$$

$$= \frac{\sum_{i=1}^{j} R^2 (P_{s1} - P_{s0})_i^2 \left(\frac{R(P_{s1} - P_{s0})}{{\sigma_t}^2}\right)_i^2}{\sum_{i=1}^{j} {\sigma_t}_i^2 \left(\frac{R(P_{s1} - P_{s0})}{{\sigma_t}^2}\right)_i^2} = \sum_{i=1}^{j} \frac{(R(P_{s1} - P_{s0})_i)^2}{{\sigma_t}_i^2} = \sum_{i=1}^{j} SNR_i \tag{3.24}$$

This SNR analysis will be used throughout the thesis to evaluate new VLC systems.

3.7 Simulation Package

To evaluate the VLC system's performance under the impact of user mobility and multipath propagation, the channel impulse response has to be estimated. A simulation tool similar to one developed by Barry et al. [136], is used to produce impulse responses, the power distribution and to calculate the delay spread, 3dB channel bandwidth and SNR. The simulations and calculations reported in this thesis were carried out using MATLAB.

A simulation was conducted in an empty room (unfurnished) with dimensions of 4 m × 8 m × 3 m (width × length × height). Experimental measurements of plaster walls have shown that they are roughly a Lambertian reflector [6]. Therefore, all the walls (including ceiling) and the floor were modelled as Lambertian reflectors with high reflectivity (reflection coefficients of 0.3 for the floor and 0.8 for the walls and ceiling). These relatively high reflectivities (within the range) were selected as they result in the greatest multipath dispersion (worst case scenario), and consequently considerable pulse spread. Reflections from doors and windows are considered to be the same as reflections from walls. To model the reflections, the room was divided into a number of equally sized squares with an area of dA and reflection coefficient of ρ. Each reflection element was treated as a small transmitter that transmits an attenuated version of the received signals from its centre in the same form as a Lambertian pattern with n=1, where n is the Lambertian emission order as defined in [26].

Previous research considered only LOS and reflections up to a first order [28], [31], [80]. However, this may not provide a full description of the characteristics of the system. Therefore, in this thesis, reflections up to a second order were considered, since the second order reflection has a greater impact on system performance (especially at high data rates). It should be noted that reducing dA leads to an improved resolution in the impulse response

evaluation together with an increase in the computation time. To keep computations within practical measure, surface elements with sizes of 5 cm × 5 cm for first-order reflections and 20 cm × 20 cm for second-order reflections were used in this thesis.

The room's illumination was provided by eight LED light units. Each LED light unit was filled with 3600 (60×60) LEDs. The space between LED chips was 0.5 cm. These LED lights were installed at a height of 3 m above the floor. The height of the desk (communication plane) was 1m. The centre illumination intensity for each LED chip was 0.73 candela (cd) and the semi angle at half power of an LED chip was 70^{o} [28]. The coordinates of the LED light units were (1m, 1m, 3m), (1m, 3m, 3m), (1m, 5m, 3m), (1m, 7m, 3m), (3m, 1m, 3m), (3m, 3m, 3m), (3m, 5m, 3m) and (3m, 7m, 3m), as shown in Figure 3.6. The transmitted power from each LED chip was 20 mW. The specifications of the LED light units were adapted from [28]. A single element receiver with various FOVs (90^{o}, 60^{o} and 30^{o}) and photo sensitive area of 1 cm^{2} was used. The latter is the most basic receiver configuration widely investigated in previous research [6], [28].

We compared the results of our simulator in the case of the traditional VLC system with the theoretical results detailed in [28], [147]. In addition, the author has verified his simulator against the results of the basic IROW systems in the literature, such as a conventional diffuse system (CDS), line strip multi-beam system (LSMS) and the beam clustering method (BCM) [87], [95], [135], [136], [148]. A very good match was observed between the results of the author's simulator and other researchers' work (see appendices A and B), and this gives confidence in the capability of the author's simulator to assess new VLC systems.

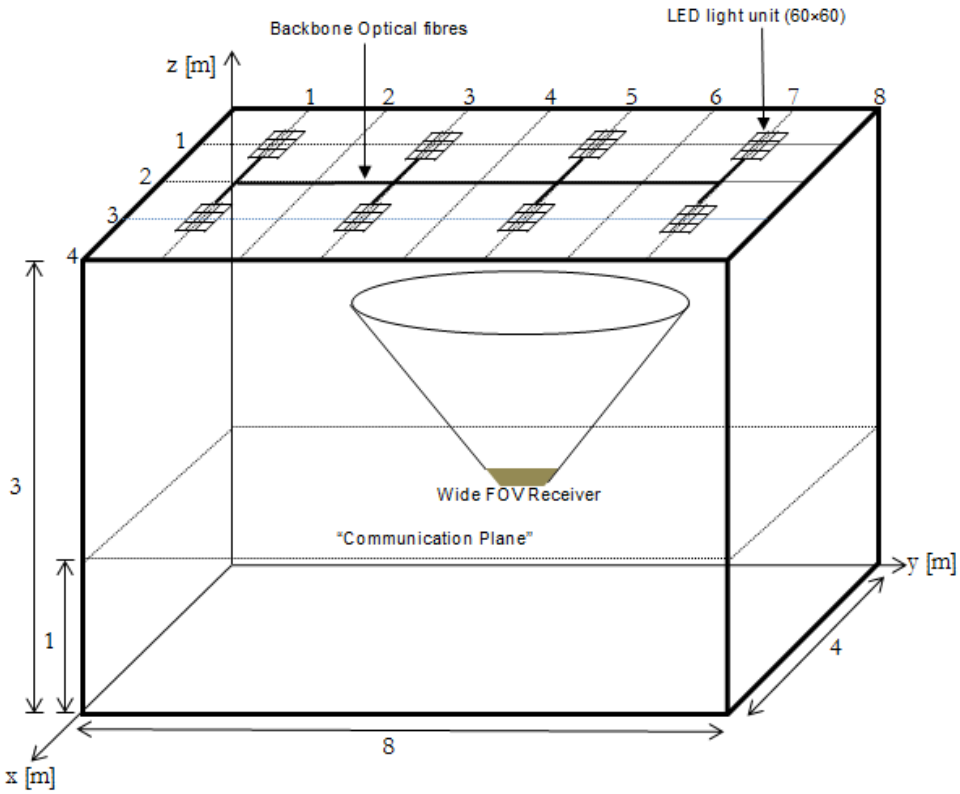

Figure 3.6: VLC system room.

3.8 Performance Analysis and Simulation Results

The simulation was used to assess the channel impulse response of the indoor VLC system. This section presents the results of the traditional VLC system with single wide FOV receiver. An optical concentrator and/or optical filter were not used in this chapter. The results of the simulation are reported in the form of impulse response, pulse response, delay spread and SNR at a low data rate of 50 Mb/s.

A traditional single optical receiver with wide FOV is the most basic receiver configuration that has been widely investigated in previous research [6], [28], [149]. A receiver with a wide FOV gathers more optical power than a narrow FOV receiver, because a wide FOV receiver collects not only the primary signal

(LOS component), but also signals that have one or more reflections, thus increasing the amount of signal power collected. On the other hand, multipath dispersion can cause increased signal spread in this case.

To evaluate the effect of FOV on the received impulse response, different receiver FOVs (90^o, 60^o and 30^o) were used. Narrower FOVs can be used to restrict the range of incident rays accepted and hence reduce the pulse spread, at the possible expense of power loss.

3.8.1 Impulse response and pulse response

The simulation of the channel impulse response was performed using a single detector with an active area of 1 cm^2 and with different reception angles (90^o, 60^o and 30^o). To compute the impulse response of the VLC channel, each ray arriving from a direct LOS component as well as the reflecting elements is added into one of the respective time bins. The delay associated with the path of each ray between transmitters (LEDs) and receiver is calculated to determine which time bin each ray should be added to. This process is repeated until all the rays falling within the FOV of the receiver have been included.

Figure 3.7 shows the impulse responses of a single photo detector (at FOV=90^o, 60^o and 30^o). Due to the symmetry of the room, the results for x=3 equal the results for x=1, therefore only x=1m and x=2m results are shown along the y-axis. The results show that the shape of the channel impulse response is a function of the position of the receiver in the room and the receiver's FOV. The impulse response of the wide FOV receiver contains many peaks corresponding to the different direct LOS components coming from different LED light units. The impulse response of the wide FOV receiver (90^o) also shows that the LOS, first and second order reflection components have a great impact on the signal, because these components make the signal spread over a larger time frame.

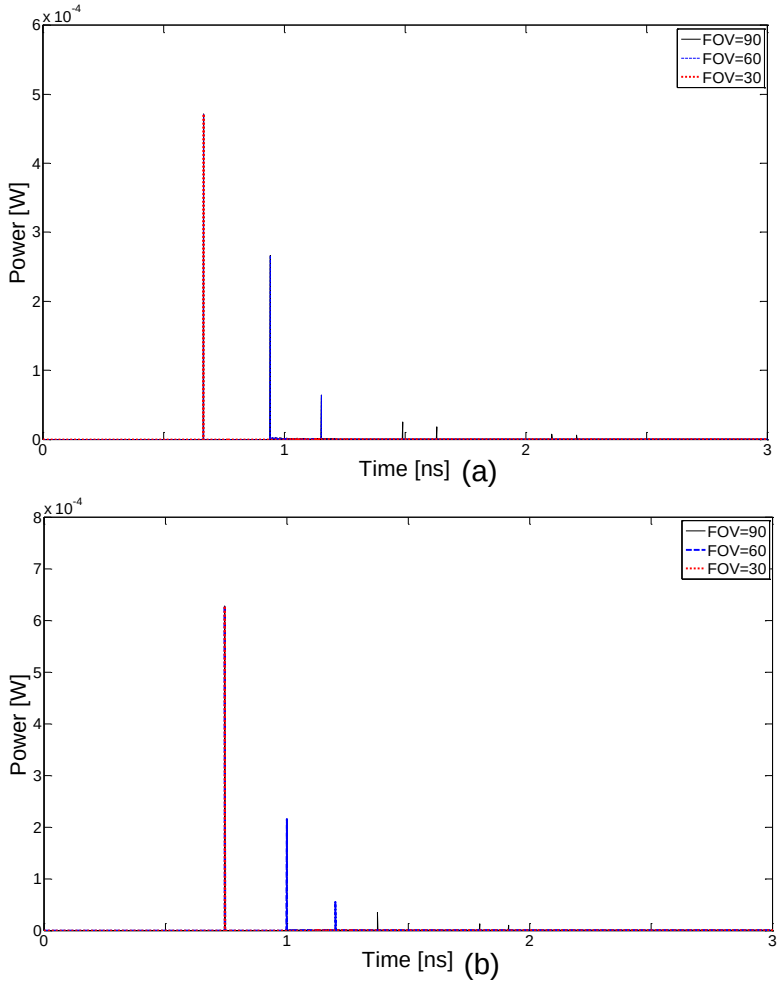

Figure 3.7: Impulse responses of traditional VLC system with single element receiver for various FOVs (90^o, 60^o and 30^o) at receiver locations of (a) (1m, 1m, 1m) and (b) (1m, 2m, 1m).

The pulse response was found through the convolution of the impulse response with a rectangular pulse with a 20 ns duration (which corresponds to 50 Mb/s). In this thesis, for the bit rate of 50 Mb/s we used the p-i-n BJT trans-impedance preamplifier in [37]. The impact of multipath propagation on the received signal was observed to result in temporal dispersion, hence potentially ISI. The effect of the pulse spread can be minimised by reducing the FOV of the receiver. However, the received optical power is reduced. For example, when the receiver was at location (1m, 1m, 1m) the received optical power is decreased

from 1.2 mW to 0.51mW (see Figure 3.8 a) when the FOV is changed from 90^o to 30^o. The pulse responses of the VLC system are depicted in Figure 3.8.

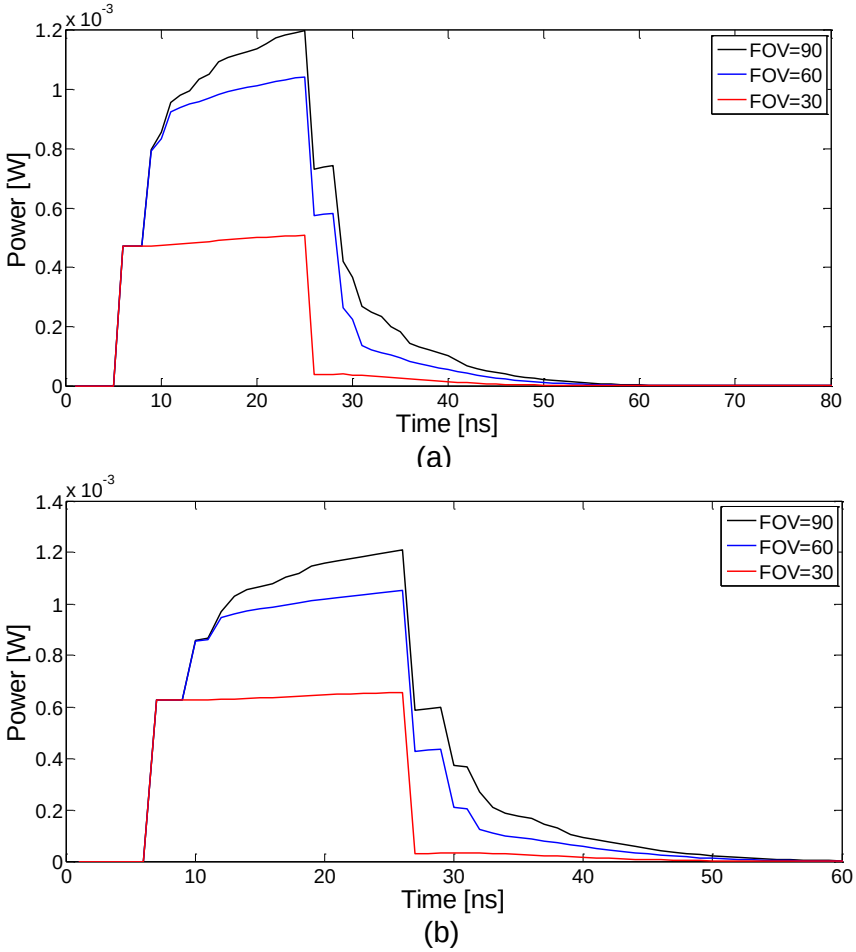

Figure 3.8: Pulse responses of traditional VLC system with single element receiver for various FOVs (90^o, 60^o and 30^o) at receiver locations of (a) (1m, 1m, 1m) and (b) (1m, 2m, 1m).

3.8.2 Delay spread

Delay spread is a measure of the multipath richness of a communications channel. Figure 3.9 presents the delay spread of the traditional VLC system when employing a single element receiver with various FOVs (90^o, 60^o and 30^o) when the receiver moves at x=1m and x=2m along the y-axis (in 1 m steps). The results show that the single element receiver with FOV=30^o has the lowest

delay spread compared with the other receivers (i.e., FOVs=90^o and 60^o). This improvement is due to the limited range of the rays accepted by the narrow FOV. However, at locations (2m, 2m, 1m), (2m, 4m, 1m) and (2m, 6m, 1m) the delay spread of the single element receiver with FOV=30^o increases dramatically, and this is due to all the LOS components from LEDs being rejected due to the narrow FOV of the receiver and only a few components of first and second order reflections can be received. Therefore, it can be concluded that the FOV should not be reduced below 60^o (in our given room geometry), where the VLC signal still preserves its good power level. It can also be noted that at FOV=60^o the delay spread is reduced due to the limited range of the rays received.

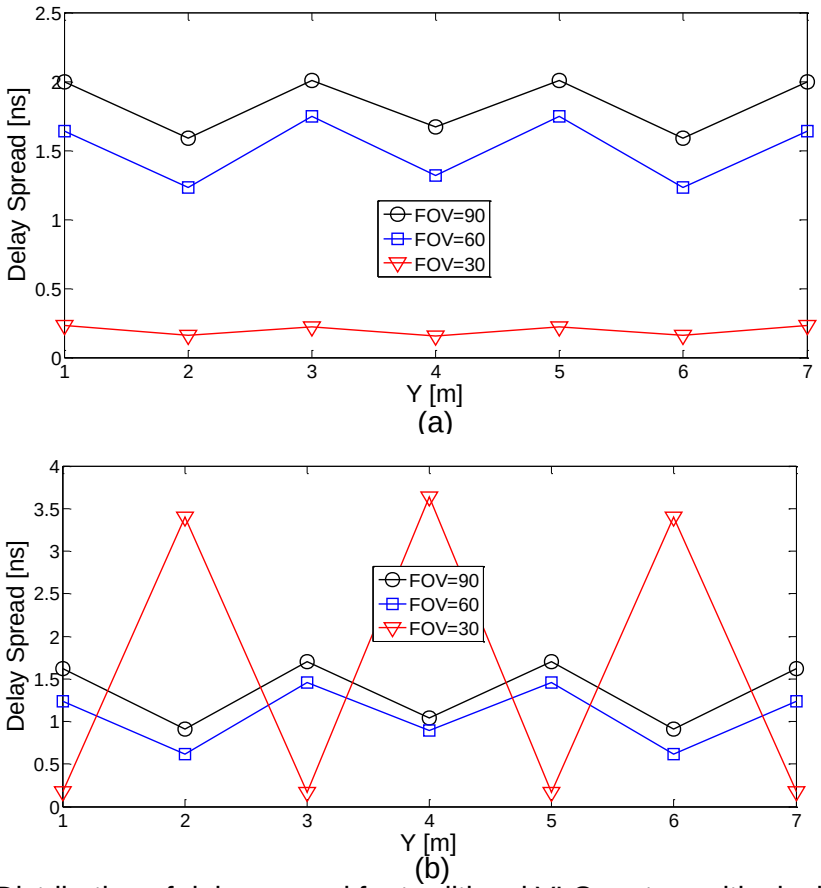

Figure 3.9: Distribution of delay spread for traditional VLC system with single element receiver for various FOVs (90^o, 60^o and 30^o) at (a) x=1m and (b) x=2m and along the y-axis.

3.8.3 SNR

Figure 3.10 shows the SNR of three mobile VLC systems operating at 50 Mb/s. Significant improvement in the SNR was achieved at 50 Mb/s when a single element receiver with FOV=30^o was used instead of 90^o and 60^o. In addition, it can be clearly seen that the VLC systems with FOVs=60^o and 30^o outperform the VLC system with a FOV of 90^o. This is attributed to reducing the contribution of the reflection component by using a narrow FOV receiver. It can be noted that the receiver at FOV=30^o achieves about 8 dB SNR gain over the wide FOV receiver (90^o) and about 4 dB gain over the receiver at FOV=60^o at the locations (1m, 1m, 1m), (1m, 3m, 1m), (1m, 5m, 1m) and (1m, 7m, 1m), which represents the worst communication paths at x=1m for the single element receiver with FOV=30^o (the SNR gain is higher in the other locations as shown in Figure 3.10).

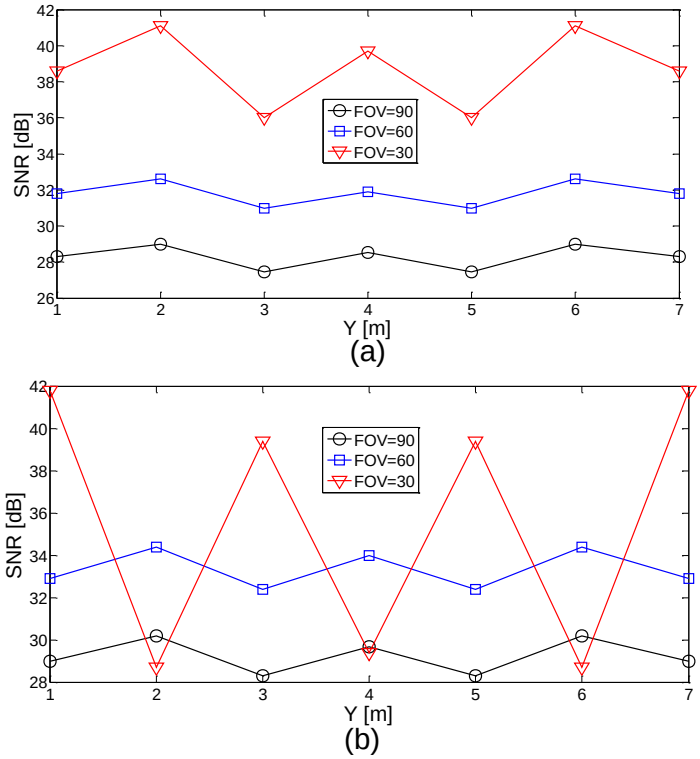

Figure 3.10: SNR of traditional VLC system with single element receiver for various FOVs (90^o, 60^o and 30^o) at (a) x=1m and (b) x=2m and along the y-axis.

3.9 Summary

The characteristics of an indoor VLC link can be evaluated by modelling the VLC channel. This chapter has provided the propagation model that is used in this thesis and an explanation was given for the different channel parameters. A ray tracing algorithm, calculations of received power and the effects of multipath propagation were explained and evaluated. The simulations and calculations reported in this thesis were carried out using the MATLAB program. Traditional IROW and VLC systems were studied and evaluated. A very good match was observed between the results of the author's simulation results and other researchers' work (see appendices A and B), and this gives confidence in the capability of the author's simulator to assess new VLC systems. The performance evaluation of a traditional VLC system with a single element receiver that has various FOVs (90^{o}, 60^{o} and 30^{o}) was studied. It was shown that reducing the FOV of such a system can lead to a significant enhancement (i.e., reducing delay spread and improving SNR). However, it should be noted that a very small FOV leads to performance degradation; therefore, an optimum FOV should be used.

4 Visible Light Communication System Employing Laser Diodes, Angle Diversity Receiver and Imaging Receiver

4.1 Introduction

Traditional RF systems suffer from insufficient transmission rate and channel capacity due to the limited radio spectrum available. There is a potential band of the electromagnetic spectrum (i.e., optical band) available that is able to provide tens of Gb/s for users in the near future [19] especially for indoor users. VLC systems are among the promising solutions to the bandwidth limitation problem faced by radio frequency systems [4]. The main challenges facing high data rate visible light communication are the low modulation bandwidth of the current transmitters (i.e., LEDs), the ISI caused by multipath propagation and CCI due to multiple transmitters. In this chapter, we propose, design and evaluate the use of laser diodes (LD) for communication as well as illumination. The main advantage of using LD is their high modulation bandwidth that enables communication at data rates of multi gigabits per second for VLC when using a suitable receiver, such as an ADR or an imaging receiver, which mitigates the ISI.

Recent research has suggested that LD can provide more-efficient lighting than LED. A prototype laser-based headlight system was demonstrated by the car maker BMW. This system uses blue lasers and phosphors to generate white light [150]. A prototype from Sandia lab showed that by using four colour

laser sources it could provide a practical white light illumination source [151]. In their experiment, four laser diodes were used (red, green, yellow and blue) to generate white light that was similar to that from other light sources, such as incandescent lights and white LEDs [151]. Lasers were not expected to be ideal light sources because of their extremely narrow line-width and extremely narrow spot size. However, the results from using four-colour laser sources have shown experimentally that the colour rendering quality of the white light is good, and this paved the way for serious consideration of the use of lasers in solid state lighting [151]. One of the main potential issues associated with using laser lighting is that lasers can be dangerous to human eyes. Therefore, it should be noted that while the original sources indeed have laser source properties (colours red, green, yellow and blue), once they have been combined (using chromatic beam-combiners) and had the beam scattered and diffused to reduce speckle then produce white light [152], [153]. In 2011, Toshiba launched LD lighting that achieves much higher luminance within a much smaller area. The lighting unit can be used for various applications that require much higher luminous flux (it produces 4500 lumens using 90 Watts) than available with conventional white LEDs [154]. Recently, different types of RGB-LD lights were investigated to generate white light, blue lasers in combination with yellow emitting YAG:Ces and RGB lasers resulted in a luminous flux of 252 lumens and luminous efficacy of 76 lm/W was reported in [155].

An ADR is considered as a simple and efficient technique that can be used to mitigate the effects of ambient light and pulse spread in OW systems [95], [96]. In this chapter, an ADR with three branches is proposed for a VLC system instead of wide FOV receiver to mitigate the impact of ISI, reduce the delay spread and increase the SNR when the VLC system operates at high data rates under the effects of mobility and multipath dispersion [100]. In addition, a custom design imaging receiver with 50 pixels is also proposed to further enhance the communication links and to provide higher SNR [103].

In this chapter, LD are introduced as the source of illumination and communication for the VLC system (LD-VLC system) in conjunction with three different receivers (wide FOV, ADR and imaging receiver). The main goal of using LD is to enable the VLC system to achieve multi-gigabit/s data rates when employing a simple modulation technique (OOK).

The reminder of this chapter is divided into sections as follows: Section 4.2 introduces the design of the laser VLC system. Section 4.3 shows laser VLC system and rooms setup. Section 4.4 presents the performance evaluation of the three branches ADR with RGB-LD. Simulation results and discussions about the use of LD in conjunction with wide FOV and imaging receivers in an empty room are presented in Section 4.5. Finally, a summary is provided in Section 4.6.

4.2 Laser Diodes Light Design

To achieve comfortable office lighting, a certain amount of illumination is required. According to European standard EN 12464-1, illumination should be at least 300 lx in an office [156]. Assuming that the LD light has a Lambertian radiation pattern, the direct LOS illumination at a point (x, y) in the floor of the room can be determined using [157], [158]:

$$E_{LOS} = I(0)\frac{cos^{n}(\theta)\,cos(\emptyset)}{D_1^2} \tag{4.1}$$

where $I(0)$ is the centre luminous intensity of the LD, θ is the irradiance angle, D_1 is the distance between the LD and any point in the floor, $\emptyset$ is the angle of incidence and n is the Lambertian emission order. Then the first reflection of illumination can be defined as shown in the following [28], [147]:

$$E_{FST} = \frac{I(0)\,cos^{n}(\theta)\,cos(\emptyset)cos(\varphi)\,cos(\delta_1)d_{A1}\rho_1}{\pi D_1^2 D_2^2} \tag{4.2}$$

where D_1 is the distance from the LD light to the first element, D_2 is the distance from the first element to the floor, d_{A1} is the area of the element in the first reflection, ρ_1 is the reflection coefficient, φ and δ_1 are the angles of irradiance and incidence for the elements respectively. The second reflection of illumination can be calculated as [28], [147]:

$$E_{SEC} = \frac{I(0)\ cos^n(\theta)\, cos(\gamma) cos(\varphi)\, cos(\delta_1) cos(\varphi_2) cos(\delta_2) d_{A1} d_{A2} \rho_1 \rho_2}{\pi^2 D_1^2 D_2^2 D_3^2} \quad (4.3)$$

where D_1 is the distance from the LD light to the first element, D_2 is the distance from first element to second element, D_3 is the distance from the second element to the floor, d_{A2} is the area of the second element in the second reflection, ρ_2 are the reflection coefficients, φ_2 and δ_2 are the angles of irradiance and incidence for the second element respectively. The total horizontal illumination at any point in the floor can be calculated as follows:

$$E_t = \sum_1^S E_{LOS} + \sum_1^M E_{FST} + \sum_1^F E_{SEC} \quad (4.4)$$

where S is the number of LD light units, M is the number of reflecting elements in the first reflection and F is the number of reflecting elements in the second reflection.

4.3 Laser VLC System and Room Setup

To evaluate the proposed VLC systems, a simulation was conducted in an empty room with dimensions 4 m× 8 m× 3 m (width × length × height) similar to the ones in Chapter 3.

A combination of red, green and blue lasers with a diffuser can be used to generate white light that has good colour rendering [159]. Therefore, the room's illumination was provided by eight RGB-LD light units which were used to ensure that ISO and European standards were satisfied [156]. Each LD light

unit has 9 (3×3) RGB-LD. The LD lights were installed at a height of 3 m above the floor. The VLC room with the coordinates of the RGB-LD light units is shown in Figure 4.1. The specifications of the RGB-LD used in this study were adopted from the practical results reported in [151], where the measured illuminace for each RGB-LD was 193 lx. Therefore, the centre illumination intensity for each RGB-LD was 162 cd. The conversion from illuminace (lx) to luminous intensity (cd) was carried out using the inverse square law which is valid if (i) the source is a point source (ii) the beam is divergent and (iii) distance of interest is greater than ten times of the source size [160]. Figure 4.2 shows the architecture of the LD light units, where the light from three lasers (i.e., RGB) is combined using beam combiners, then passes through multiple ground glass diffusers to reduce speckle before illuminating the room. This design is similar to the one studied in [151]. Beam-splitters and detectors were used to monitor and control (tune LD light engine) the different laser powers. A few percent of the beam power is needed for that purpose. Changing the power emitted by each laser can be used to obtain the exact colour desired and set the total emitted power. A number of different uniformly distributed LD light unit configurations (i.e., 4, 6 and 8 LD units) were tested to find the optimum number of units that ensure that the ISO and EU standards illumination requirements are satisfied in the room. We found that eight units were the optimum for illumination, and we used this in our study; four and six light units in the room did not achieve the minimum illumination requirement (i.e., 300 lx [156]). The height of the work desks where the transmitters and receivers associated with the user equipment are placed was 1m. This horizontal plane was referred to as the “communication plane”, (CP). Figure 4.3 shows the horizontal illumination distributions from the eight RGB-LD light units at the CP level. It is clear from this figure that there is sufficient illumination according to EU and ISO standards [156].

4.4 Performance Evaluation of LD-VLC with Three-branch Angle Diversity Receptions

The performance of the LD-VLC system is assessed in the form of impulse response, delay spread, 3 dB channel bandwidth, and SNR. Two types of receiver were used an ADR with three branches and a single wide FOV (FOV = 90^{o}) element with photo sensitive area of 1 cm^2. The proposed system is evaluated under the influence of receiver mobility, multipath dispersion and receiver noise.

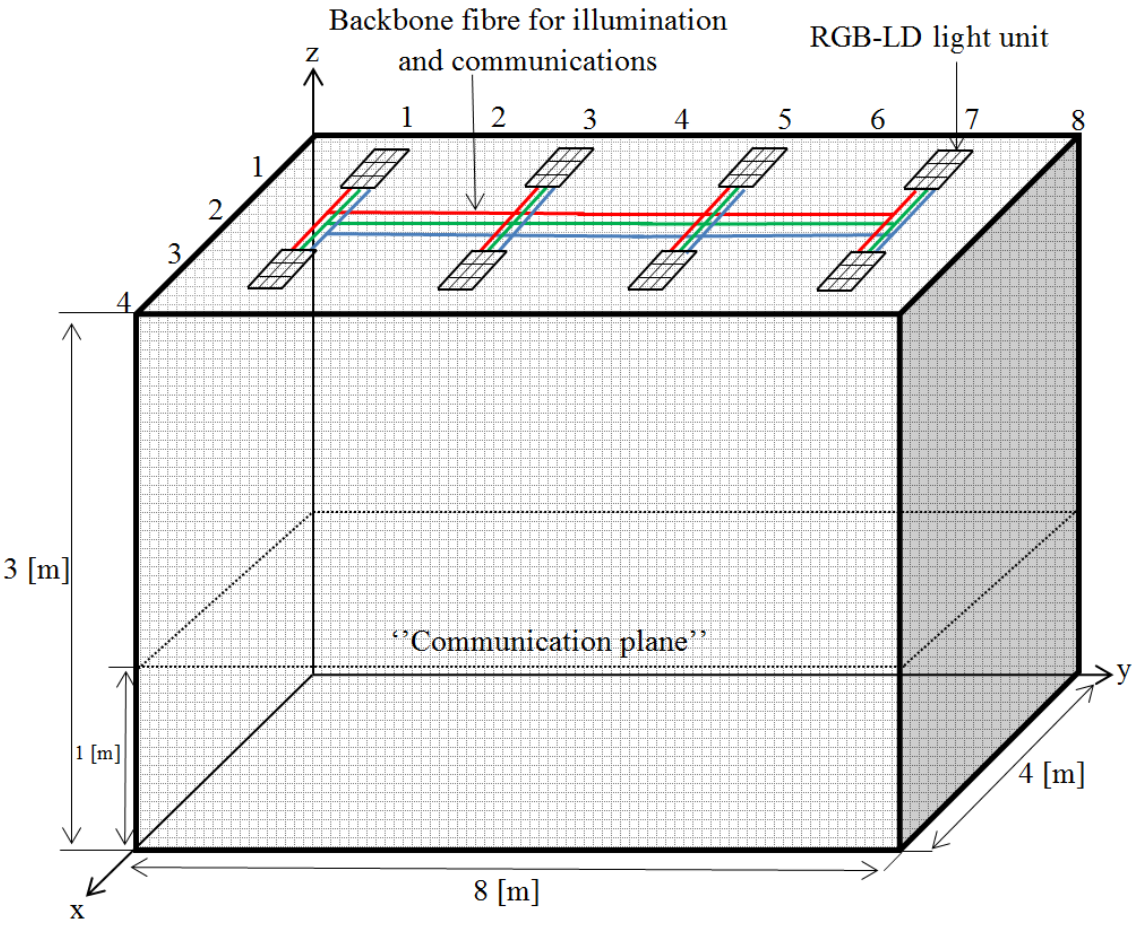

Figure 4.1: VLC system room.

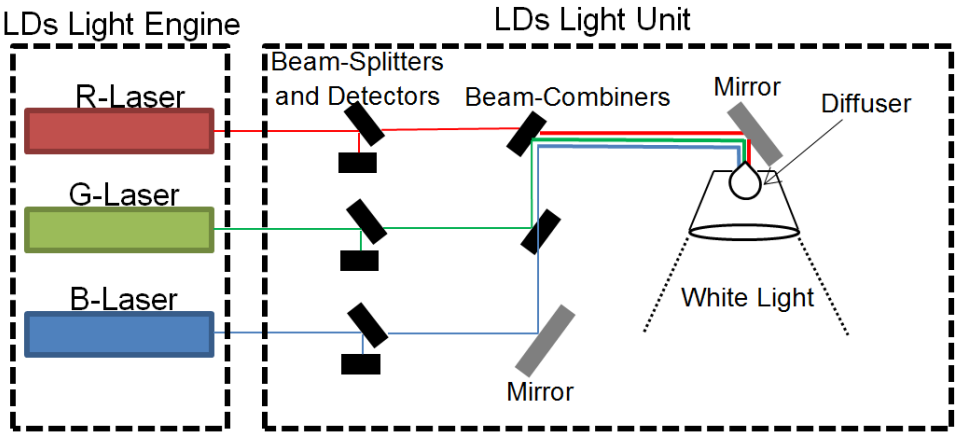

Figure 4.2: Architecture of RGB-LD white light; light from three lasers is combined using chromatic beam-combiners, then passes through multiple ground glass diffusers to reduce speckle before illuminating the room.

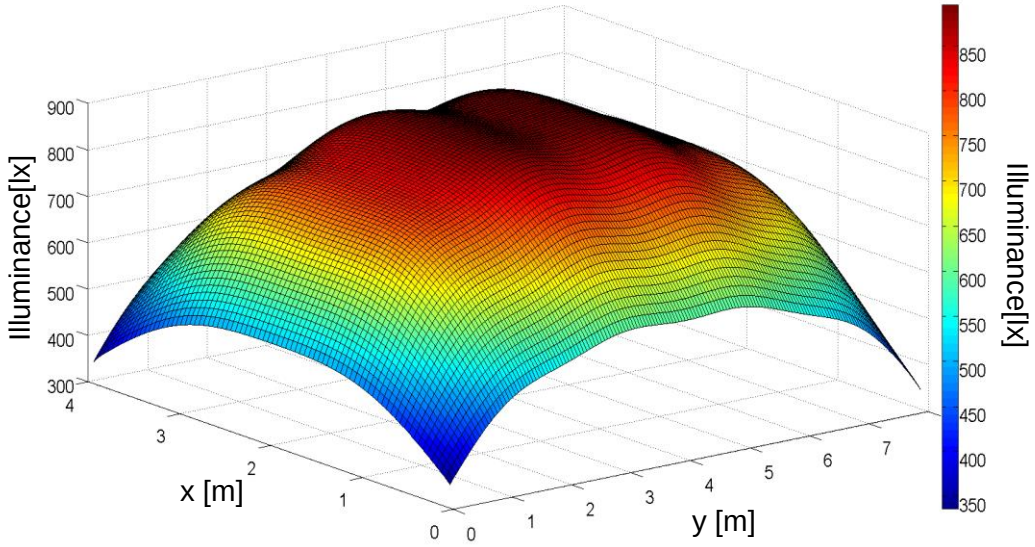

Figure 4.3: Distribution of horizontal illumination at the communication plane, Min. 336 lx and Max. 894 lx.

4.4.1 Angle diversity receiver design

An ADR is a group of narrow FOV detectors pointed in different directions. The ADR consists of three branches with photodetectors that have a responsivity of

0.4 A/W each. The ADR uses a photo detector area of 4 mm^2. The ADR was always placed on the CP, and results were obtained along the lines x=1m or x=2m. The direction of each branch in an ADR is defined by two angles: the azimuth angle (AZ) and the elevation angle (EL). The AZs of the three detectors were set at 0^o, 180^o and 0^o, and the ELs of the three branches were fixed at 90^o, 60^o and 60^o. The corresponding FOVs were fixed at 30^o, 25^o and 25^o. The AZs, ELs and FOVs were chosen through an optimisation process to achieve high SNR and low delay spread. To compute the reception angle (Φ) for any detector in the ADR, a point P has to be defined (see Figure 4.4), which is located 1 m above the detector in our case. E is an element on the wall with coordinates (x_E, y_E, z_E). Figure 4.4 shows light from a reflecting point (E) on a wall incident on one of the detectors in the ADR that is located at (x_r, y_r, z_r). Φ can be calculated as [96], [135]:

$$cos(\Phi) = \frac{\left|\overrightarrow{PR_x}^2\right| + \left|\overrightarrow{ER_x}^2\right| - \left|\overrightarrow{E_P}^2\right|}{2\left|\overrightarrow{PR_x}^2\right|\left|\overrightarrow{ER_x}^2\right|} \tag{4.5}$$

where:

$$\left|\overrightarrow{PR_x}^2\right| = 1 + \left(\frac{1}{tan\, EL}\right)^2 \tag{4.6}$$

$$\left|\overrightarrow{ER_x}^2\right| = (x_r - x_E)^2 + (y_r - y_E)^2 + (z_r - z_E)^2 \tag{4.7}$$

$$\left|\overrightarrow{E_P}^2\right| = \left[\left(\frac{cos(AZ)}{tan(EL)} + x_r\right) - x_E\right]^2 + \left[\left(\frac{sin(AZ)}{tan(EL)} + y_r\right) - y_E\right]^2 + [(z_r + 1) - z_E]^2 \tag{4.8}$$

Figure 4.5 illustrates the physical structure of the ADR and the orientation of ADR in the room. The photocurrents received in each branch can be amplified separately and can be processed using different methods, such as SC, equal gain combining (EGC) or MRC, to maximise the power efficiency of the system. MRC can achieve better performance compared to the other methods [95],

[103]. Therefore, in this section the ADR LD-VLC system employed an MRC approach.

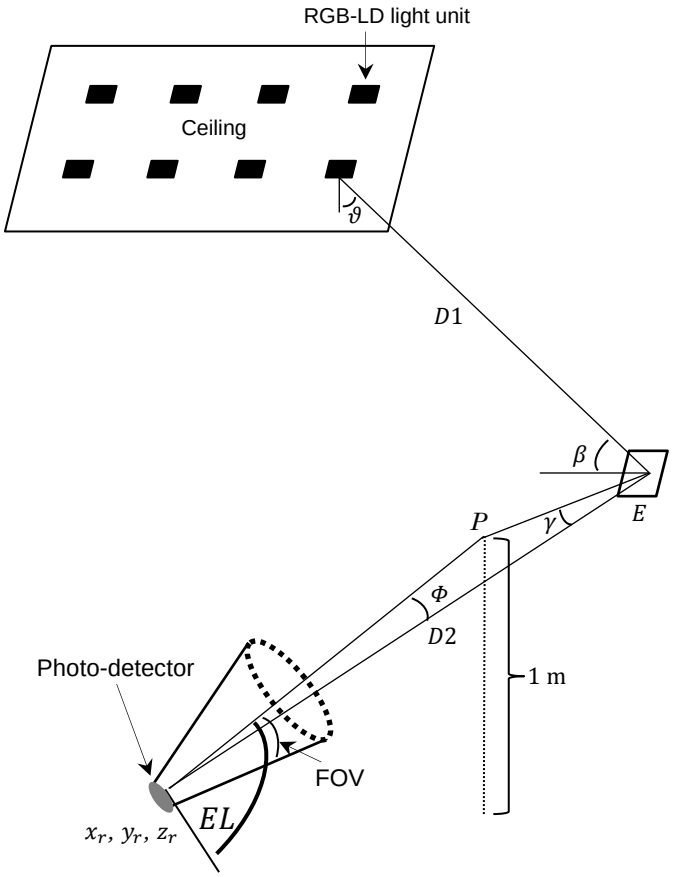

Figure 4.4: Angle diversity receiver, azimuth and elevation parameters of the diversity detection receiver.

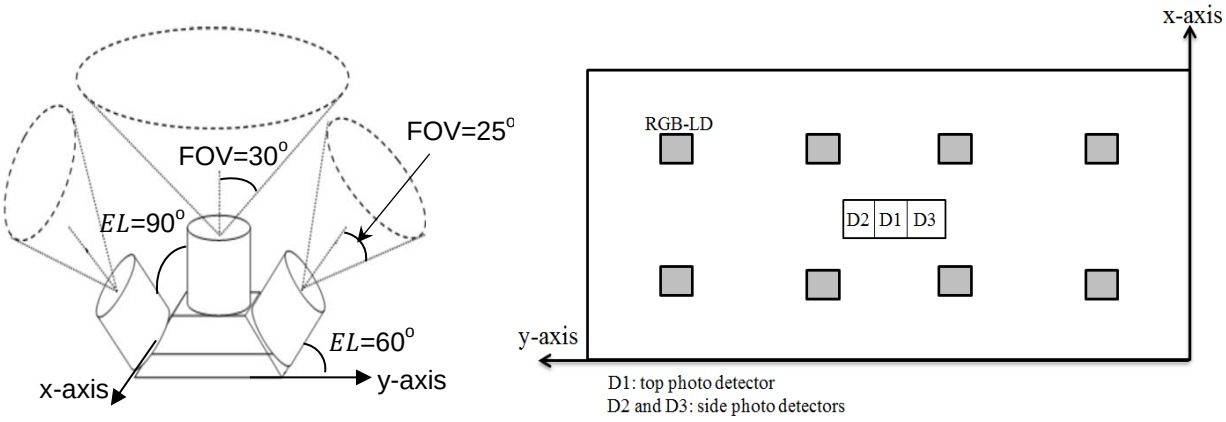

Figure 4.5: Physical structure of the ADR with top view of room that shows orientation of ADR receiver.

4.4.2 Impulse response

The impulse responses and frequency responses of the two receivers (wide FOV and ADR) at the room centre are depicted in Figure 4.6. The frequency response is found by taking Fourier transform to the impulse response. It can be seen that the ADR's impulse response (Figure 4.6b) is better than that of the wide FOV receiver in terms of signal spread. The impulse response of the wide FOV receiver (Figure 4.6a) contains many peaks that correspond to different direct LOS components coming from different RGB-LD light units. The impulse response of the wide FOV receiver also shows that the LOS as well as first and second order reflection components have a great impact on the signal, because these components cause the signal to spread over a large time-range, which is due to the wide FOV of this receiver (90^{o}). Simulation results show that the LD-VLC system in conjunction with an ADR increases the communication channel bandwidth from the 114 MHz offered by the wide FOV LD-VLC system to about 3.7 GHz at room centre(see Figure 4.6).

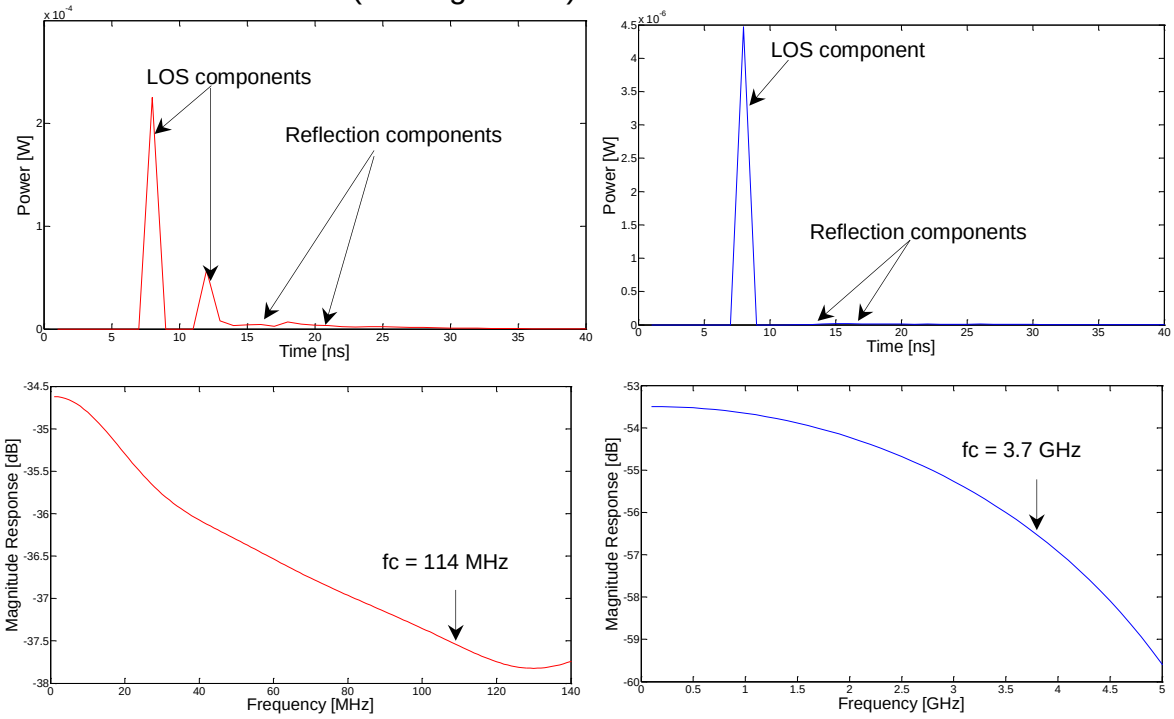

Figure 4.6: Impulse and frequency responses of (a) wide FOV and (b) ADR.

4.4.3 Delay spread and 3 dB channel bandwidth

Figure 4.7 presents the communication system delay spread associated with the wide FOV and ADR LD-VLC systems. The results show that the ADR LD-VLC system has a lower delay spread than the wide FOV LD-VLC system at all the receiver locations considered. In the ADR LD-VLC system, the results indicate that employing an ADR instead of a wide FOV receiver can reduce the delay spread by a factor of 12 in our system (when operating in a typical room) from 0.65 ns to 0.053 ns for the worst communication path (centre of the room, x=2 m and y=4m). This improvement is due to the limited range of the rays accepted by the narrow FOV associated with each branch of the ADR. In addition, it can be noticed that when the wide FOV receiver is located under one of the LD light units (i.e., at locations x=1 and y= 1, 3, 5, 7), the delay spread is higher than in other locations. This is attributed to the rays coming from the other LD light units (seven other LD light units) having to travel a longer distance to reach the receiver (distance between transmitters and receiver is maximum). In contrast, when the receiver is located midway between LD light units (i.e., at locations x= 2 and y= 2, 4, 6) the delay spread is the lowest. The ADR performance does not follow the wide FOV receiver, because it uses multiple detectors aimed towards different locations in the room, and each detector has a certain FOV.

Although, the transmitter modulation bandwidth problem in the VLC system can be solved by replacing LEDs with LD, the channel bandwidth remains an issue that needs to be solved to achieve multi-gigabit per second data rates. We dealt with channel bandwidth by using an ADR instead of a wide FOV receiver. The 3 dB channel bandwidth achieved by the two receivers is shown in Figure 4.8. The results show that the ADR provides a larger bandwidth compared to the traditional wide FOV receiver. The minimum communication channel bandwidth of the wide FOV receiver was 70 MHz at x=1m and y=1m. In contrast, the minimum channel bandwidth in the ADR LD-VLC system was 3.7 GHz at x=2m and y=4m (this value enables a data rate of up to 5.2 Gb/s [143]).

This increased channel bandwidth enables the VLC system to operate at higher data rates while using a simple modulation technique (OOK) [88]. At the least successful receiver location (x=2m and y=4m), a significant bandwidth enhancement can be achieved (a factor of 32 - from 114 MHz to 3.7 GHz) when our ADR VLC-LD is used instead of the wide FOV VLC-LD system. Note that the variation in channel bandwidth in tandem with the delay spread is due to the effects explained.

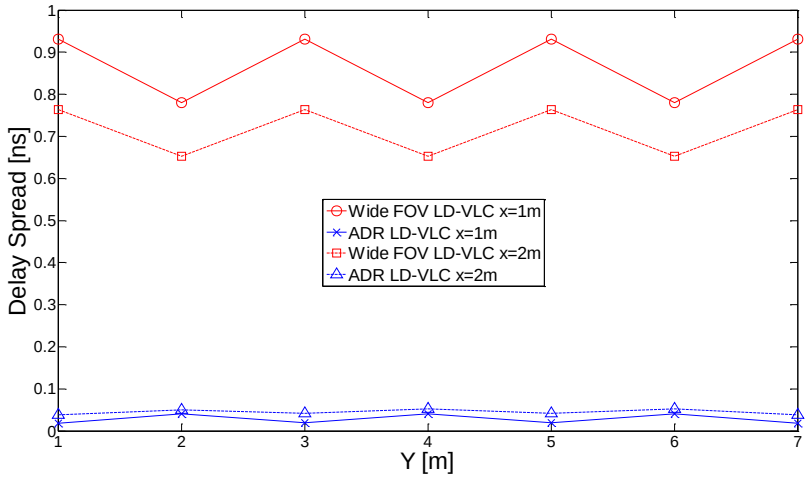

Figure 4.7: Delay spread in fourteen different locations when the receivers move along x=1m and x=2m.

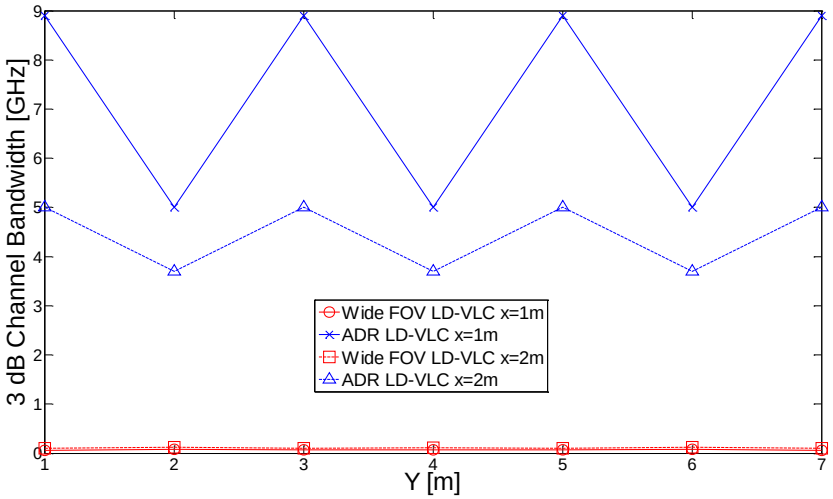

Figure 4.8: The 3 dB channel bandwidth of the two systems, when the receivers move along x=1m and x=2m.

4.4.4 SNR analysis

In this section, for the bit rate of 50 Mb/s the p-i-n BJT transimpedance preamplifier in [37] was used. A higher data rate of 5 Gb/s was also considered, and here the p-i-n FET receiver design in [161] was used. This pre-amplifier has a noise current density of 4.47 pA/$\sqrt{Hz}$ and a bandwidth of 5GHz. A significant improvement in the SNR at low data rates (50 Mb/s) was achieved when the ADR LD-VLC system was used instead of the wide FOV LD-VLC system. It can be clearly seen that the ADR achieves about 7 dB SNR gain over the wide FOV receiver at the centre of the room (x=2m and y=4m), which represents the worst communication paths for the ADR receiver (SNR gain is higher in other locations as shown in Figure 4.9). To evaluate the performance of the ADR system at higher bit rates, the SNR was calculated at 5 Gb/s. Figure 4.10 shows the SNR of the ADR when it is operated at 5 Gb/s; the lowest SNR achieved by the ADR LD-VLC system was 13.5 dB in the room corner. This means that the BER provided by our ADR LD-VLC system is better than 10^{-6} at 5 Gb/s. The 3 dB channel bandwidth achieved by the wide FOV receiver (see Figure 4.8) does not enable it to transfer data at a rate of 5 Gb/s; therefore, we only present results for the ADR at high data rates (i.e., 5 Gb/s).

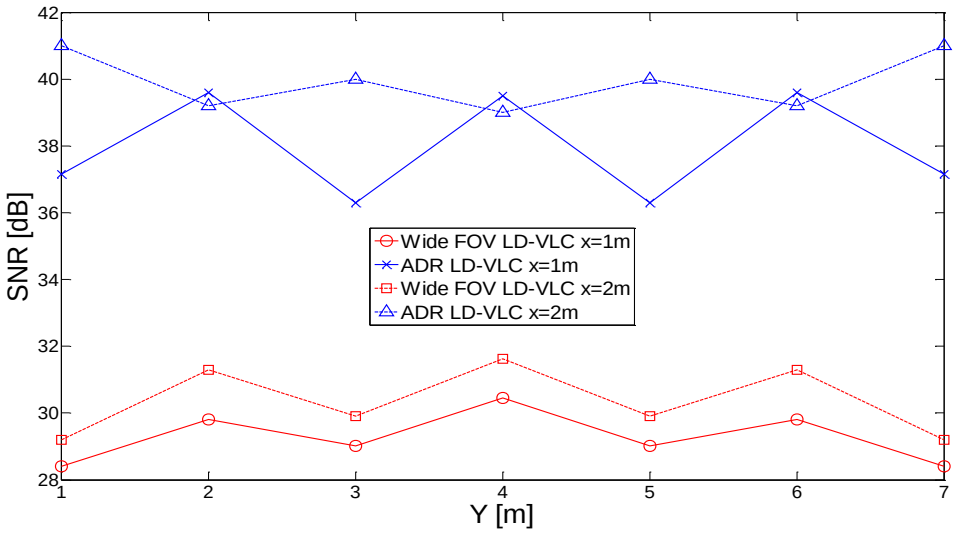

Figure 4.9: SNR of the wide FOV and the ADR LD-VLC systems at 50 Mb/s.

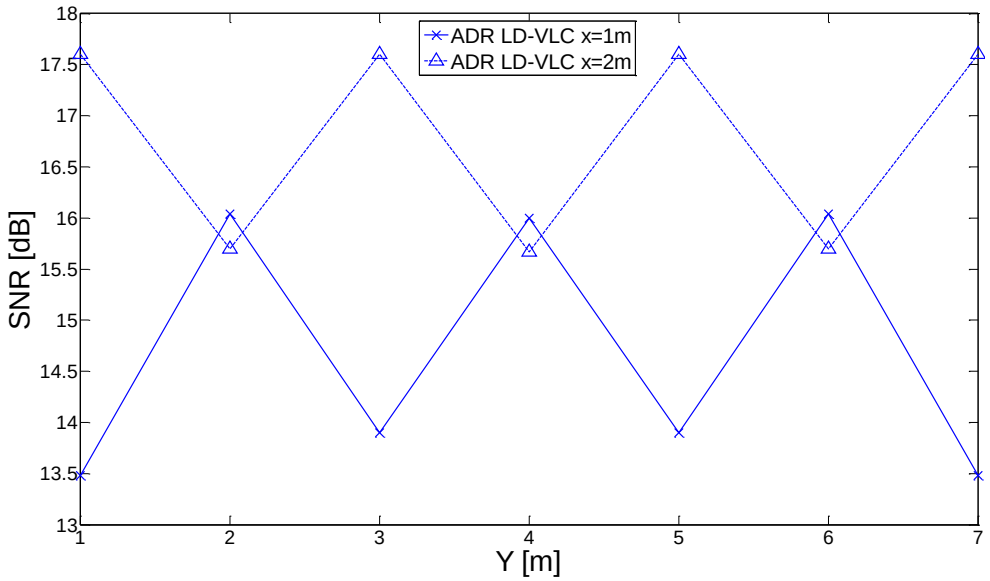

Figure 4.10: SNR of ADR LD-VLC system at 5 Gb/s when using MRC combing scheme, at x=1m and at x=2m along the y-axis.

4.5 Performance Evaluation of Mobile LD-VLC Coupled with Imaging Receiver

In this section, LD are introduced as a source of illumination and communication for a VLC system in conjunction with two different receivers (wide FOV and imaging receivers). An imaging receiver was proposed for a VLC system instead of wide FOV receiver to mitigate the impact of ISI, reduce the delay spread (increase the channel bandwidth) and increase the SNR when the VLC system operates at high data rates (5 Gb/s) under mobility and multipath dispersion. The performance of the proposed LD-VLC system using wide FOV and imaging receivers is evaluated in an empty room in the presence of multipath dispersion and mobility. The proposed systems are examined in fourteen different locations when all the receivers move along the y-axis. The results are presented in terms of impulse response, delay spread, 3 dB channel bandwidth and SNR. Due to the symmetry of the room, the results for x=3 equal

the results for x=1, therefore only x=1m and x=2m results are shown along the y-axis.

4.5.1 Imaging receiver design

The imaging receiver employs multiple pixels with narrower FOV. Narrow FOVs were chosen for the pixels to limit the range of optical rays (representing different path lengths) received hence limiting the ISI at high data rates and supporting mobility. The imaging receiver presents two potential advantages over non-imaging receivers (wide FOV and ADR): firstly, a single planner array is used for all photo-detectors, which can facilitate the use of a large number of pixels. Secondly, a common concentrator (for example, a lens) can be shared among all photo-detectors, reducing the cost and size compared to other kinds of receivers [162]. The photocurrents received in each pixel can be amplified separately and can be processed using different methods such as SC or MRC techniques to maximise the power efficiency of the system [95]. The detector array of the imaging receiver is segmented into J equal-sized rectangular shaped pixels as shown in Figure 4.11. In this case, and under most circumstances, the signal falls on no more than four pixels [163]. Therefore, the area of each pixel is the photo-detector's area, which is equal to the exit area of the imaging concentrator used, divided by the number of pixels. In this thesis the detector array was segmented into 50 pixels and the imaging receiver employed a concentrator. The transmission factor of the concentrator is given by [162], [164], [165]:

$$T_c(\delta) = -0.1982\delta^2 + 0.0425\delta + 0.8778 \tag{4.9}$$

where δ is the incidence angle measured in radians. We set the semi acceptance angle (ψ_a) of this concentrator to 65^o so that it can view the whole ceiling when the receiver is at the centre of the room. In this work, the photo detector array of the imaging receiver was segmented into 50 pixels (5 rows

and 10 columns). When the receiver is at the centre of the room it is designed to see the whole ceiling, therefore the ceiling was subdivided in this case into 50 segments (5×10) along the x and y axes respectively, and each reception area or segment is cast onto a single pixel.

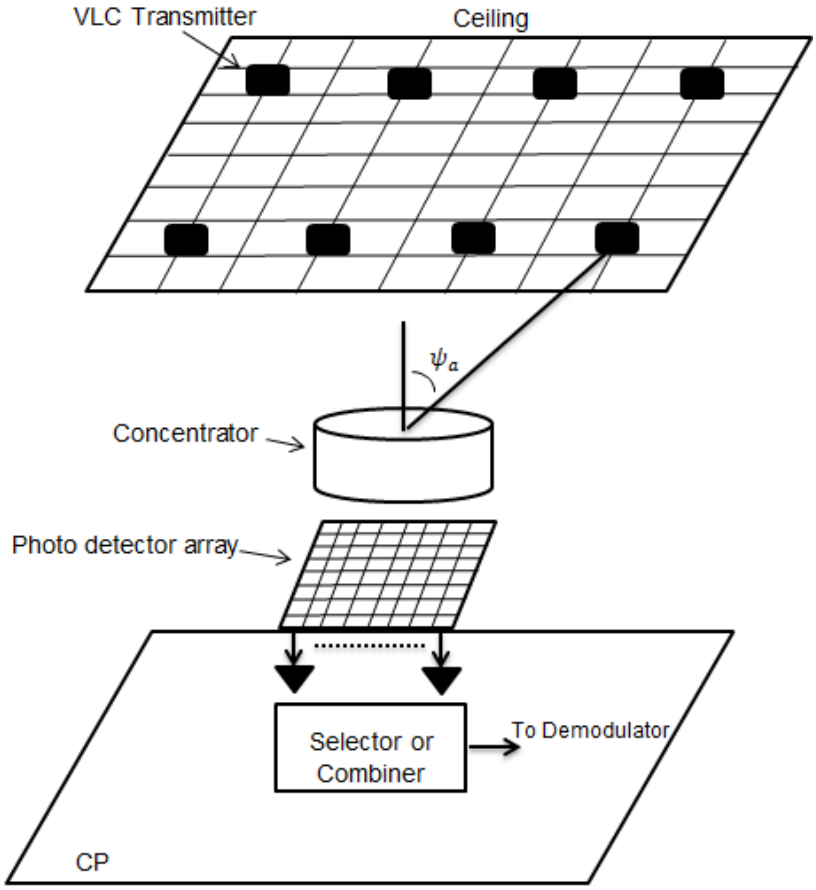

Figure 4.11: Physical structure of an imaging receiver which uses a single imaging lens with a photo-detector segmented into multiple pixels.

The detector array is assumed to fit exactly into its corresponding concentrator's exit area. Therefore, the detector array has a photosensitive area of 2 cm^2 and each pixel has an area of 4 mm^2. In our design, each reception area is cast onto a single pixel when the receiver is at the centre of the room. A pixel's reception area can be found by calculating the reception angles α_x and α_y with respect to the receiver's normal along the x and y directions as shown

in Figure 4.12. α_x and α_y can be calculated by $\alpha_x = tan^{-1}\left(\frac{d_x}{h}\right)$ and $\alpha_y = tan^{-1}\left(\frac{d_y}{h}\right)$, where d_x and d_y are the x-axis and y-axis horizontal separations and hr is the reception area height [163]. In addition, the reception area observed by each pixel varies as the imaging receiver moves (the new reception area should be calculated when the receiver moves). These reception angles (α_x and α_y) become a design property (reference points) of the imaging receiver at all locations. At certain locations on the CP, some of the reception areas on the ceiling start to appear on one of the walls, when the receiver is located at the room corner, as shown in Figure 4.13. The height of the centre of the reception area above the CP, Z_y or Z_x on the xz-wall or the yz-wall, respectively, can be calculated by:

$$Z_y = \left(\frac{Y_r}{tan\,\alpha_y}\right) \text{ and } Z_x = \left(\frac{X_r}{tan\,\alpha_x}\right) \tag{4.10}$$

where Y_r and X_r are the horizontal separation distances between the imaging receiver and the xz-wall and yz-wall respectively.

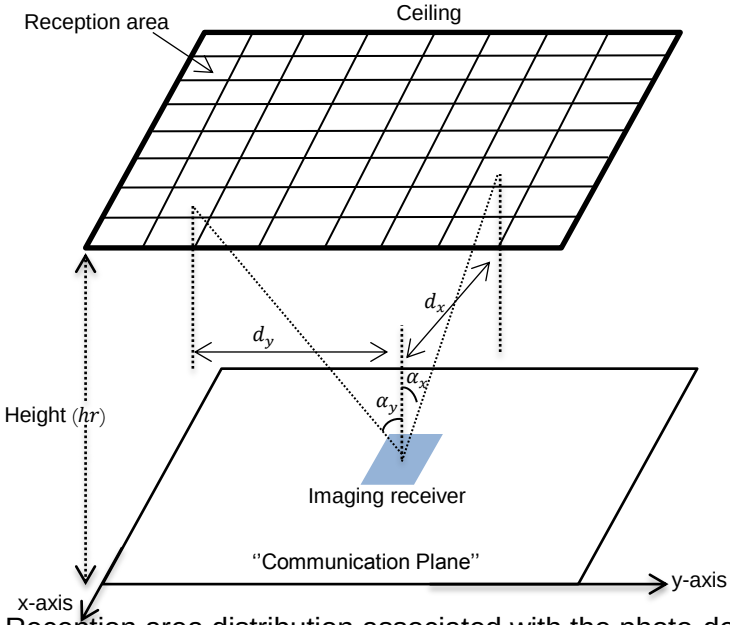

Figure 4.12: Reception area distribution associated with the photo-detector array when the receiver is placed at the centre of the room.

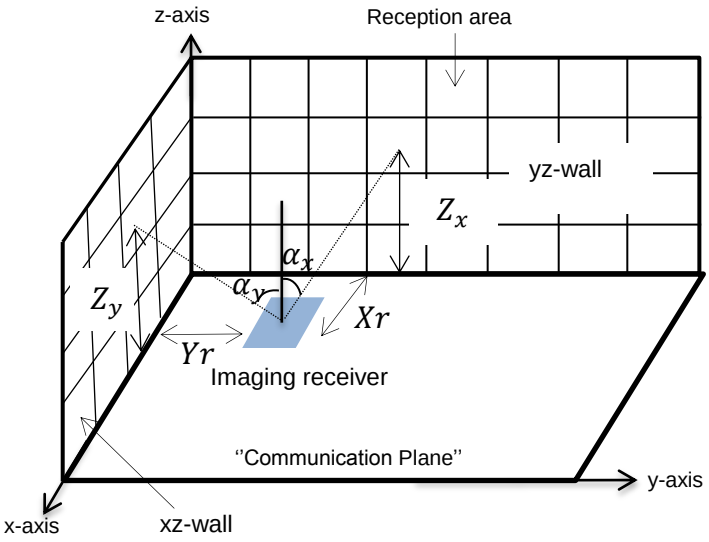

Figure 4.13: Reception area distribution associated with the photo-detector array when the receiver is placed at the corner of the room.

4.5.2 Impulse response

The impulse responses and frequency responses of the two receivers (wide FOV and imaging receivers) at the room centre are depicted in Figures 4.14 and 4.15. From Figure 4.15 it can be clearly seen that the imaging receiver's impulse response is better than that of the wide FOV receiver in terms of signal spread. The impulse response of the wide FOV receiver (Figure 4.14) contains many peaks that correspond to different direct LOS components coming from different LD light units. The impulse response of the wide FOV receiver also shows that the LOS as well as first and second order reflection components have a great impact on the signal, because these components cause the signal to spread over a large time-range (see Figure 4.14), which is due to the wide FOV's of this receiver. From Figure 4.15 we can see that the first and the second order reflections were significantly reduced when using the imaging receiver at this location, which means the ISI was almost eliminated. In addition, the power received by the imaging receiver was low (6.7 μW for single pixel and 34.8 for all pixels) compared to the wide FOV receiver (345 μW) as shown in Figure 4.15. This difference in received power between the imaging receiver

and wide FOV receiver is due to three reasons: 1) the concentrator acceptance angle in the imaging receiver is 65^o which reduces the number of rays accepted (to reduce ISI) 2) the narrow FOV of each pixel (about 21^o) also restricts the number of rays and hence the overall received power 3) the photo detector area for each pixel is 4 mm^2 while the wide FOV receiver has 1 cm^2 area with 90^o FOV. However, when SNR is calculated (see equation 3.19) most of the received power in the wide FOV receiver contributes to P_{s0} (powers associated with logic 0) due to dispersion in the signal received by the wide FOV receiver, which leads to ISI.

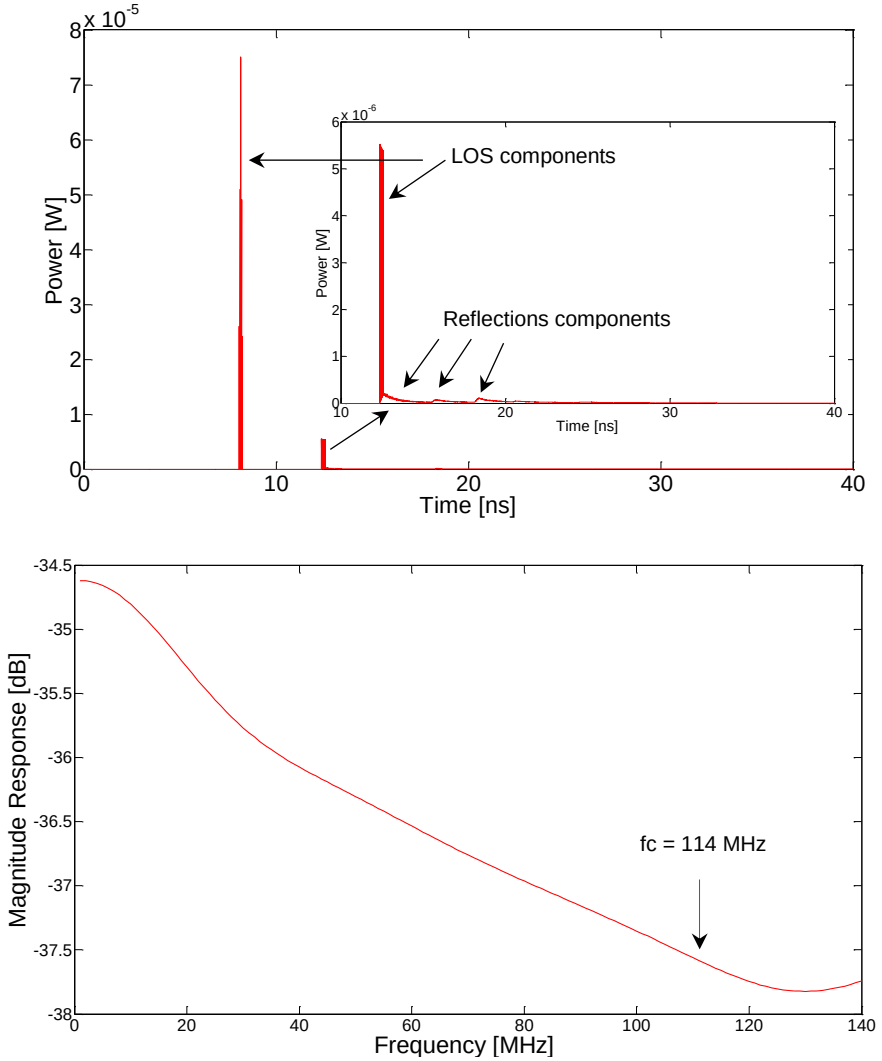

Figure 4.14: Impulse and frequency responses of wide FOV receiver at room centre (x=2m, y=4m, z=1m).

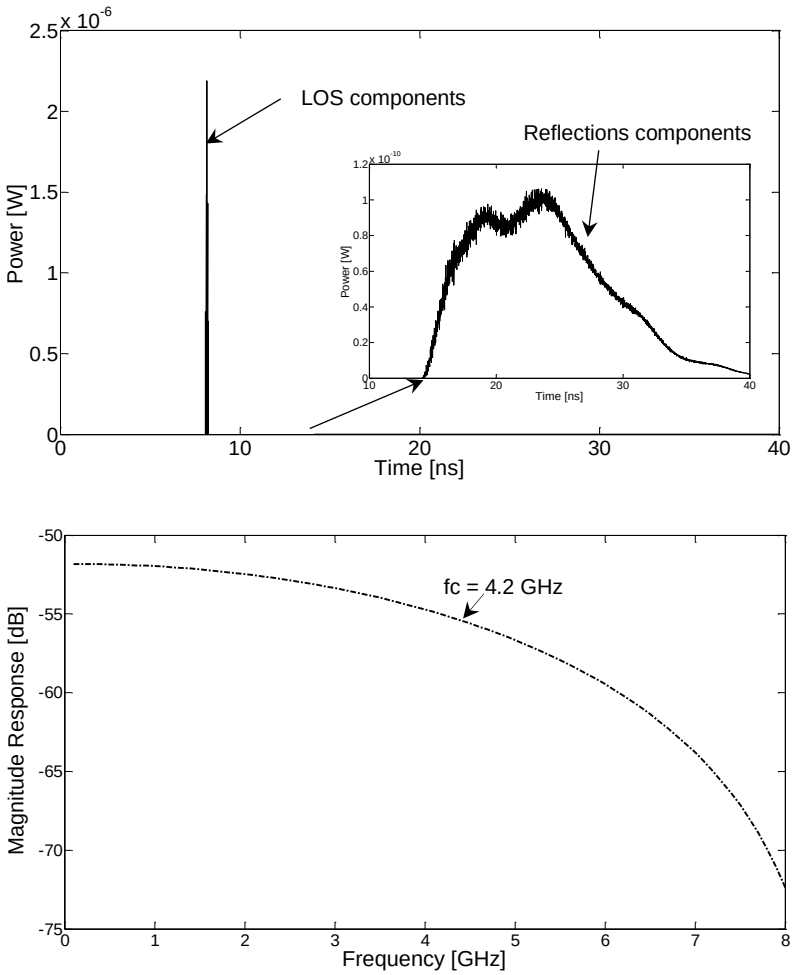

Figure 4.15: Impulse and frequency responses of imaging receiver at room centre (x=2m, y=4m, z=1m).

4.5.3 Delay spread and 3dB channel bandwidth

Figure 4.16 presents the communication system delay spread associated with the wide FOV LD-VLC and imaging LD-VLC systems. The results show that the imaging LD-VLC system has lower delay spread compared to the wide FOV LD-VLC system at all the receiver locations considered. In the imaging LD-VLC system, the results indicate that employing an imaging receiver instead of a wide FOV receiver can reduce the delay spread by a factor of 17 in our system (operated in a typical room) from 0.7 ns to 0.04 ns at the worst communication

path (centre of the room, (x=2m, y=4m)). This improvement is due to the limited range of the rays accepted by the small pixels with narrow FOV. The variation in delay spread along the x=1m and x=2m is due to the dominance of the direct line of sight component under a VLC light source and its weakness at locations between VLC light sources.

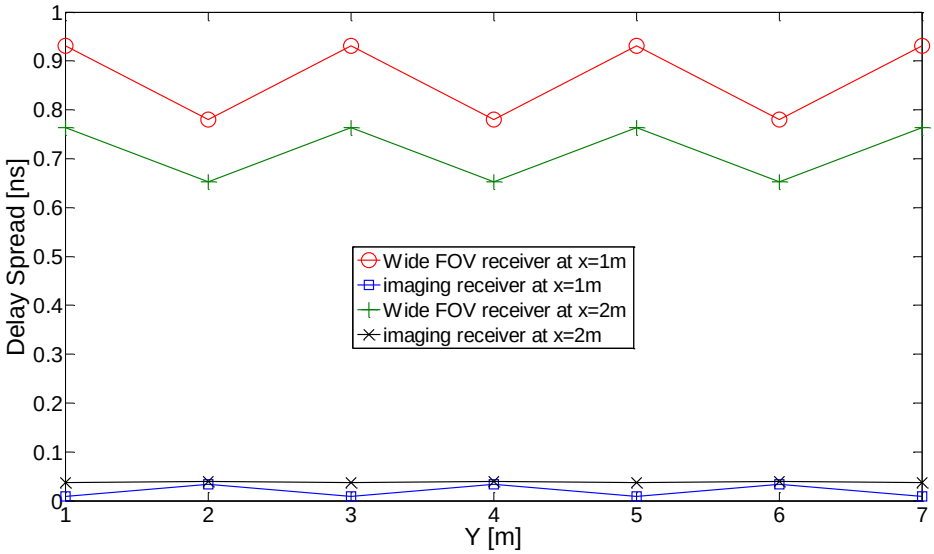

Figure 4.16: Delay spread of the wide FOV and the imaging LD-VLC systems in fourteen different locations when the receivers move along the y-axis.

The 3 dB channel bandwidth achieved by the two receivers is shown in Figure 4.17, note the variation in channel bandwidth in tandem with the delay spread due to the effects explained. The results show that the imaging receiver provides a larger bandwidth compared to the traditional wide FOV receiver. The minimum communication channel bandwidth of the wide-FOV receiver was 70 MHz at x=1m and y=1m (worst communication path for the wide FOV receiver due to high multipath propagation). In contrast, the minimum channel bandwidth in the imaging LD-VLC system was 4.2 GHz at x=2m and y=4m (this value enables a data rate of up to 6 Gb/s [143]). This increased channel bandwidth enables the VLC system to operate at higher data rates [87]. The imaging LD-VLC system produced significant improvements in the channel bandwidth at all receiver locations compared to the wide FOV system. This is attributed to

reducing the contribution of the reflection components by using a narrow FOV pixel and by appropriately weighing (MRC fashion) the pixels' contributions resulting in an emphasis on the direct power component (i.e., LOS). For instance, at location x=2m and y=4m, a significant bandwidth enhancement can be achieved, a factor of 36 (from 116 MHz to 4.2 GHz), when our imaging LD-VLC is used instead of the wide FOV LD-VLC system. To the best of our knowledge, this is the highest channel bandwidth and data rates reported for an indoor mobile VLC system with simple modulation format and system design. Also, it should be noted that the results in Figure 4.17 are in agreement with the general observation made in Figure 4.16. For instance, in the imaging system at the point x=1m and y=1m the delay spread is lowest resulting in the highest channel bandwidth (Figure 4.17). Similar agreement is observed when comparing other locations. In an optical direct detection system, the optimum receiver bandwidth is 0.7 times the bit rate. Therefore, the maximum data rate that can be achieved by a wide FOV receiver is 100 Mb/s due to the channel bandwidth being 70 MHz. The 0.7 figure is based on Personick's optical receiver design [143].

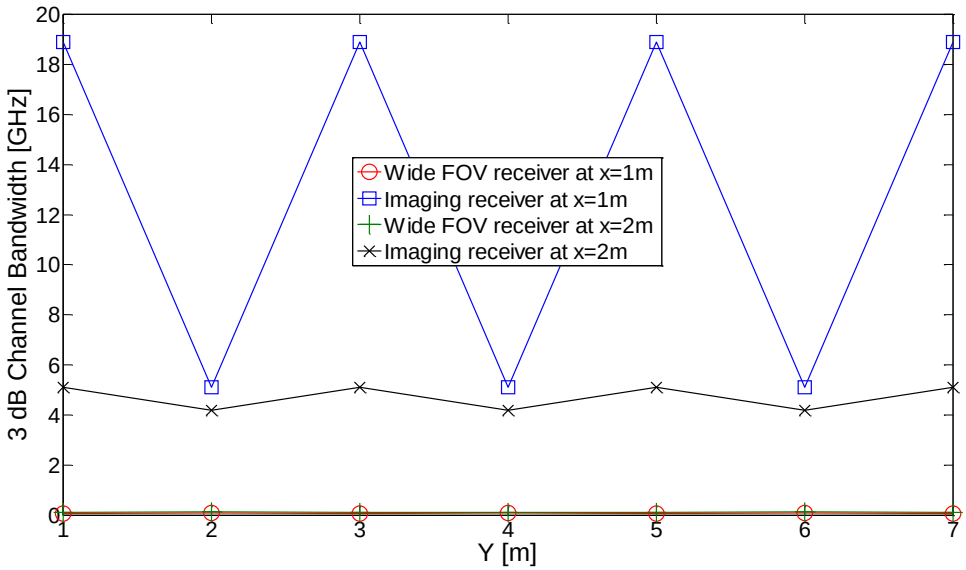

Figure 4.17: The 3 dB channel bandwidth of the wide FOV and the imaging LD-VLC systems in fourteen different locations when all the receivers move along the y-axis.

4.5.4 SNR results

In this section, for the bit rate of 30 Mb/s we used the p-i-n FET [162] receiver. Note that this lower data rate of 30 Mb/s was used to compare the performance of the imaging receiver with results in the literature [163], [165] to verify our equations and simulator. Higher data rates of 5 Gb/s is also considered, and here we used the p-i-n FET receiver designed in [161]. Significant improvement in the SNR was achieved at 30 Mb/s when the imaging LD-VLC system was used instead of the wide FOV LD-VLC system. It can be clearly seen that the imaging receiver achieves about 3 dB SNR gain over the wide FOV receiver when the SC technique was applied and about 8 dB when the MRC technique was applied at the centre of the room (x=2m and y=4m), which represents the worst communication paths for the imaging receiver (SNR gain is higher in other locations as shown in Figure 4.18). In the VLC systems, the impact of ISI is larger than other noise components, typically up to 20 Gb/s [28]. Therefore, significant improvements can be achieved by using an imaging receiver at high data rates. This significant improvement in the SNR level is attributed to the ability of the imaging receiver to collect the VLC signal with minimum ISI, due to its narrow FOV pixels and large overall detection area provided by the large number of pixels.

To evaluate the performance of the imaging system at higher bit rates, the SNR was calculated at 5 Gb/s. Figure 4.19 illustrates the SNR of the imaging system when it operated at 5 Gb/s; the imaging LD-VLC system achieved about 16.1 dB SNR when using the SC approach and approximately 19.1 dB SNR at the room centre when using MRC. This means that the BER provided by our imaging system is better than 10^{-9} at 5 Gb/s. It should be noted that an MRC imaging system outperforms an SC imaging system. SC is a simple form of diversity, where the receiver simply selects the pixel with the largest SNR among all the pixels. In contrast, MRC utilises all the pixels in the imaging receiver and combines the output signals from the pixels with weights dictated

by the SNR observed by each pixel. A pixel that observes a better SNR is given a higher weight. Therefore, SC is a subset of MRC and the MRC receiver is as such comparable to or better than SC as our results show. In Figure 4.17 the 3 dB channel bandwidth achieved by the wide FOV receivers does not enable them to transfer data at a rate of 5 Gb/s, therefore, we only present results for the imaging receiver at high data rates (i.e., 5 Gb/s).

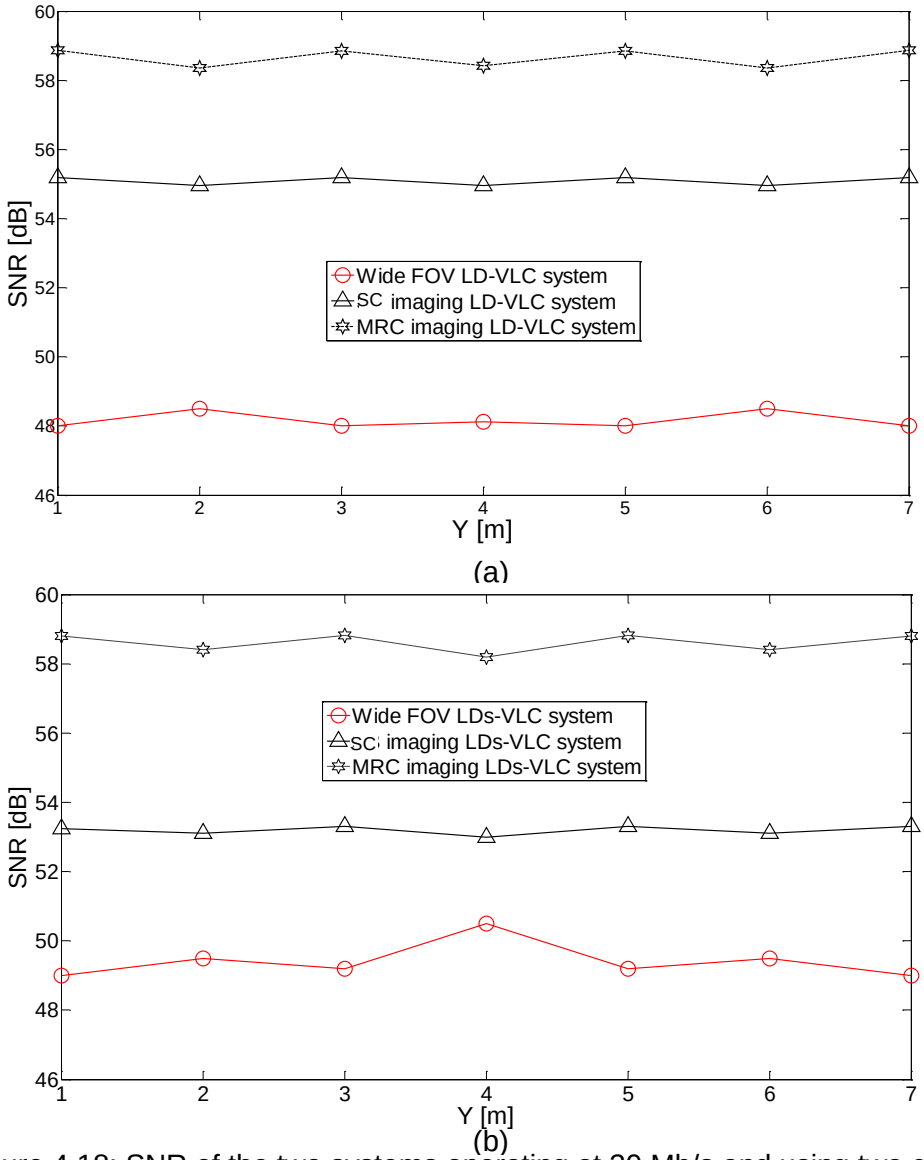

Figure 4.18: SNR of the two systems operating at 30 Mb/s and using two combing schemes (SC and MRC for imaging receiver), (a) at x=1m and (b) at x=2m along the y-axis.

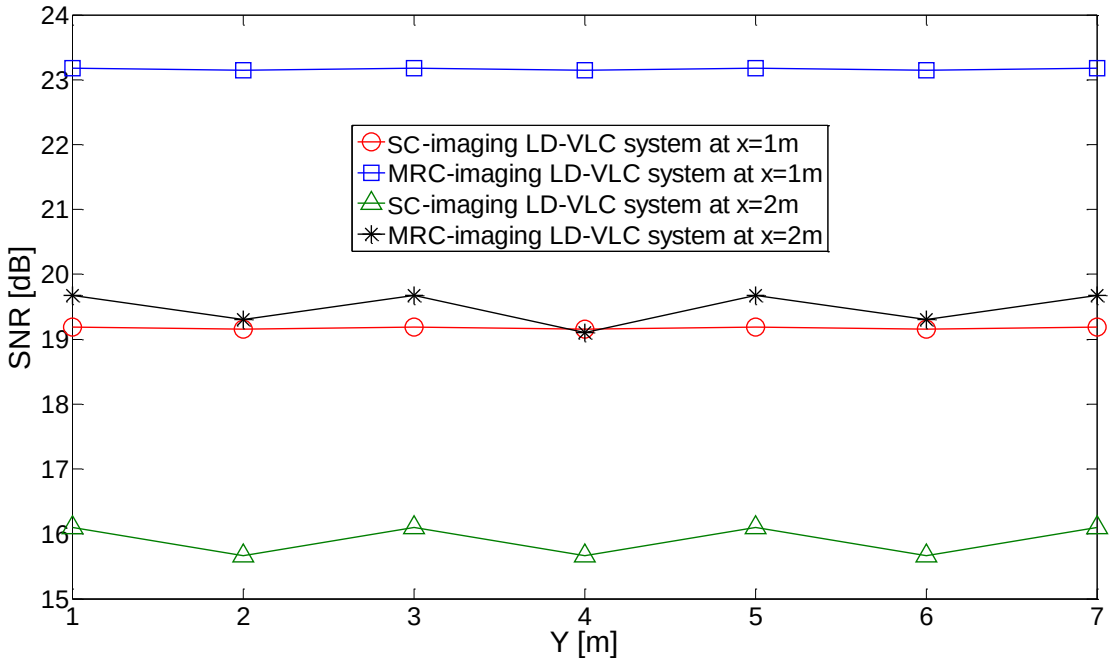

Figure 4.19: SNR of imaging LD-VLC system operating at 5 Gb/s and using two combing schemes (SC and MRC), at x=1m and at x=2m along the y-axis.

4.6 Summary

In this chapter, we proposed, designed and investigated a novel LD-VLC system that uses LD instead of LEDs as the transmitters in conjunction with three different receivers (wide-FOV receiver, an ADR and an imaging receiver) to deal with the main constraints of the traditional VLC system, namely the low modulation bandwidth of the LEDs and ISI caused by multipath dispersion.

The ADR with three branches is introduced for VLC system. The AZs, ELs and FOVs were chosen through an optimisation process to achieve high SNR and low delay spread. The ADR LD-VLC system has the ability to decrease the delay spread of the wide FOV LD-VLC system by 91% from 0.65 ns to 0.053 ns at the room centre (x = 2 m and y = 4 m), which leads to an increase in the channel bandwidth by a factor of 32 from 114 MHz to 3.7 GHz. Our ADR LD-VLC system provides full mobility within the test area in the presence of

multipath propagation and achieves a BER better than 10^{-6} at 5 Gb/s when using a simple modulation format (OOK).

In this chapter, a custom design imaging receiver is introduced for VLC systems. The imaging LD-VLC system has the ability to decrease the delay spread associated with the wide FOV LD-VLC system by 94% from 0.7 ns to 0.04 ns at the room centre (x=2m and y=4m), which leads to an increase in the channel bandwidth by a factor of 36 from 116 MHz to 4.2 GHz. Furthermore, at a low data rate (30 Mb/s) our proposed system (imaging LD-VLC) offers SNR improvement of 8 dB, and the lowest SNR achieved was 19.2 dB at a high data rate (5 Gb/s) at the room centre. Moreover, our imaging LD-VLC system employs an OOK modulation scheme that adds simplicity to the VLC system. Our system provides full mobility within the test area in the presence of multipath propagation and achieves a BER better than 10^{-9} at 5 Gb/s.

Chapter 5 will address methods to enhance the SNR of the imaging LD-VLC system to achieve data rates higher than 5 Gb/s.

5 Mobile Multi-gigabit Indoor Visible Light Communication Systems Employing Angle Diversity Receiver, Imaging Receiver and Delay Adaptation Technique in Realistic Environment

5.1 Introduction

In a mobile indoor VLC system the distance between the LD light units and the receiver is a key factor; thus, sending the information signals from all LD units at the same time increases the delay spread which decreases the 3 dB channel bandwidth. To further enhance the communication links and to provide higher data rates (beyond 5 Gb/s) with the ADR and the imaging LD-VLC systems, a novel delay adaptation technique (DAT) is introduced in this chapter coupled with a seven branch ADR (DAT ADR) and imaging LD-VLC system (DAT imaging LD-VLC system) to mitigate the ISI, the CCI due to multiple transmitters and reduce the impact of multipath dispersion due to mobility at the receiver. Instead of transmitting the signals at the same time from different LD light units, the proposed algorithm sends the signal that has the longest journey first, and then it sends the other signals with different differential delays (Δt) so

that all the signals reach the receiver at the same time. To ensure that all the transmissions reach the receiver at the same time, the beam delay adaptation technique introduces a differential delay (Δt) between the transmissions. We also model two different room scenarios: an empty room and a realistic environment room that has a door, windows, bookshelves, mini cubicles and other objects. The difficulty related with all two room arrangements is the ability to establish LOS communication link between transmitter (i.e., LD light unit) and receiver at all possible locations. The results showed an enhancement in channel bandwidth from 4.2 GHz to 23 GHz when the imaging LD-VLC system was combined with our algorithm in a worst case scenario (i.e., real environment). In addition, the DAT imaging LD-VLC system has the ability to maintain a strong LOS component in a harsh realistic environment in all receiver locations which leads to receiving high optical power in addition to reducing multipath dispersion. Our results indicate that the DAT imaging LD-VLC system achieves significant 3 dB channel bandwidth enhancements over DAT ADR, imaging LD-VLC and wide FOV systems when a realistic environment is considered.

The reminder of this chapter is divided into sections as follows: Section 5.2 describes the delay adaptation technique. Section 5.3 describes the rooms' setup. Section 5.4 presents the DAT ADR system configuration and simulation results. Simulation results and discussions of the DAT imaging LD-VLC system in an empty room are presented in Section 5.5. The robustness of the proposed DAT imaging system against mobility, shadowing and signal blockage is investigated in Section 5.6. At the end of the chapter a summary is provided.

5.2 Delay Adaptation Technique (DAT)

All the LD units typically emit signals simultaneously, which means the signal from the closest LD light unit reaches the receiver first before signals from distant LD units, and this causes significant induced performance degradation.

To reduce the impact of this impairment we proposed a delay adaptation technique coupled with an ADR and an imaging receiver (ADR and imaging receiver eliminate the effect of ISI) to enhance the SNR and system bandwidth. To ensure that all the transmissions reach the receiver at the same time, our beam delay adaptation technique introduces a differential delay (Δt) between the transmissions. It should be noted that DAT cannot be employed in a straight forward fashion with VLC systems when employing MIMO transmission. This technique can be easily applied when all VLC transmitters send the same information signal at the same time. The delay adaptation adjusts the transmission times of the signals as follows:

1- Send a pilot signal from the first RGB-LD unit to calculate the mean delay (μ) at the receiver for this RGB-LD unit.
2- Repeat step 1 for all branches in the ADR or pixels in the imaging receiver (the aim of this step is to find the best pixel that has the lowest mean delay (μ) among all pixels).
3- Repeat steps 1 and 2 for all RGB-LD units.
4- The receiver calculates the differential delays (Δt) between the received pulses from each of the RGB-LD units.
5- The receiver uses an infrared beam at a low data rate to send a control feedback signal to inform all the transmitters of the delays associated with each transmitter (eight delay values relayed to each transmitter in the case of an empty room or a realistic room both have eight RGB-LD light units).
6- The transmitters send signals from the RGB-LD units in an ascending order according to the delay values such that a RGB-LD unit that has the largest delay, i.e. longest path to the receiver transmits first.

A pedestrian speed of 1 m/s is typical for indoor users [166], we therefore propose that the receiver re-estimates its delay values for all LD light units at the start of a 1 second frame and if these have changed compared to the

previous frame values then the receiver uses the feedback channel to update the transmitters. If the time taken to determine the value of each delay associated with each LD unit (relative to the start of the frame) is equal to 1 ms (based on typical processor speeds), we have used a Microchips 32 bits microcontroller (PIC32MX110F016B) with clock rate of 50 KHz (1/50 KHz × 50 pixels =1ms) therefore the value of each delay associated with each LD unit is equal to 1 ms. The delay adaptation method set up or training time is 72 ms (9 RGB-LD in each unit × 8 light units × 1 ms). This training rate (once every 1 second frame) is sufficient given that the delay adaptation has to be carried out at the rate at which the environment changes (pedestrian movement). Therefore, the adaptive system can achieve 100% of the specified data rate when it is stationary, and 92.8% in the case of typical user movement. The MAC protocol used to share the VLC medium between users should include a repetitive training period to perform the beam delay adaptation. The design of the MAC protocol is not considered in this work. Our delay adaptation algorithm has been considered at one given receiver location in a single user scenario. In the case of a multiuser scenario, scheduling [167] can be used where the delay adaptation algorithm is chosen to maximise the 3 dB channel bandwidth and the SNR in a given region for a given time period. The delay adaptation can be implemented through delayed switching of the VLC sources. It should be noted that the RGB-LD light units (i.e. eight transmitters) should always be ‘ON’ to provide illumination for the room. Therefore, to prevent flickering dimming technique may be used [70].

5.3 Rooms Setup

To study the benefits of the DAT technique for an indoor VLC system, a simulation based on a ray tracing algorithm was performed in two room configurations. The simulation model was developed using room dimensions of 4m × 8m (width × length) with a ceiling height of 3 m, and the room

configurations were denoted as room (A) and room (B). Figures 5.1 a and b show room A, which is an empty room, and room B, which is a realistic environment as normally experienced in office arrangements where a door, windows, furniture and mini cubicles block the optical signal. Both rooms experience multipath propagation. Given typical indoor walls and floor colours and textures, typical reflection coefficients of 0.3 for the floor and 0.8 for the walls and ceiling were used for room A [6], [88]. These relatively high reflectivities (within the typical range) were selected as they result in the greatest multipath dispersion (worst case scenario), and consequently considerable pulse spread. Figure 5.1b shows room B which has three large windows, a door, bookshelves, furniture, chairs and cubicles that have surfaces parallel to the walls of the room. These objects can create shadowing. In room B, the door and three glass windows were assumed to not reflect any signal; therefore, their diffuse reflectivities were set to zero. Moreover, the walls and the ceiling have a diffuse reflectivity of 0.8 and the floor has a 0.3 diffuse reflectivity. Two of the walls: x=4m (excluding the door) and y=8m were covered by filling cabinets and bookshelves with diffuse reflectivity of 0.4. It was assumed that signals encountering a physical barrier were either blocked or absorbed. Additionally, desks, tables and chairs inside room B have similar reflectivities to the floor (i.e., 0.3). The complexity is distinct in room B where low reflectivity objects and physical partitions can create significant shadowing and signal blocking.

Experimental measurements of plaster walls have shown that they are roughly a Lambertian reflector [6]. Therefore, all the walls, the ceiling and the floor in rooms A and B were modelled as Lambertian reflectors with high reflectivity. To model the reflections, the room was divided into a number of equally sized squares with an area of dA and reflection coefficient of ρ. Each reflection element was treated as a small transmitter that transmits an attenuated version of the received signals from its centre in a Lambertian pattern with n =1.

To ensure computations can be performed within a reasonable time, surface elements of size 5 cm × 5 cm for first-order reflections and 20 cm × 20 cm for second-order reflections were used. In our evaluation channel characteristics, optical power received, delay spread, 3 dB channel bandwidth, and path-loss calculations were determined in similar way to that used in [26], [88]. The simulations and calculations reported in this chapter were carried out using the MATLAB program. Simulation tool is similar to one developed by Barry et al. [136], and is used to produce impulse responses, the power distribution and to calculate the delay spread, 3 dB channel bandwidth and SNR. The LD lights were installed at a height of 3 m above the floor. The height of the work desks where the transmitters and receivers associated with the user equipment are placed was 1m. This horizontal plane was referred to as the CP.

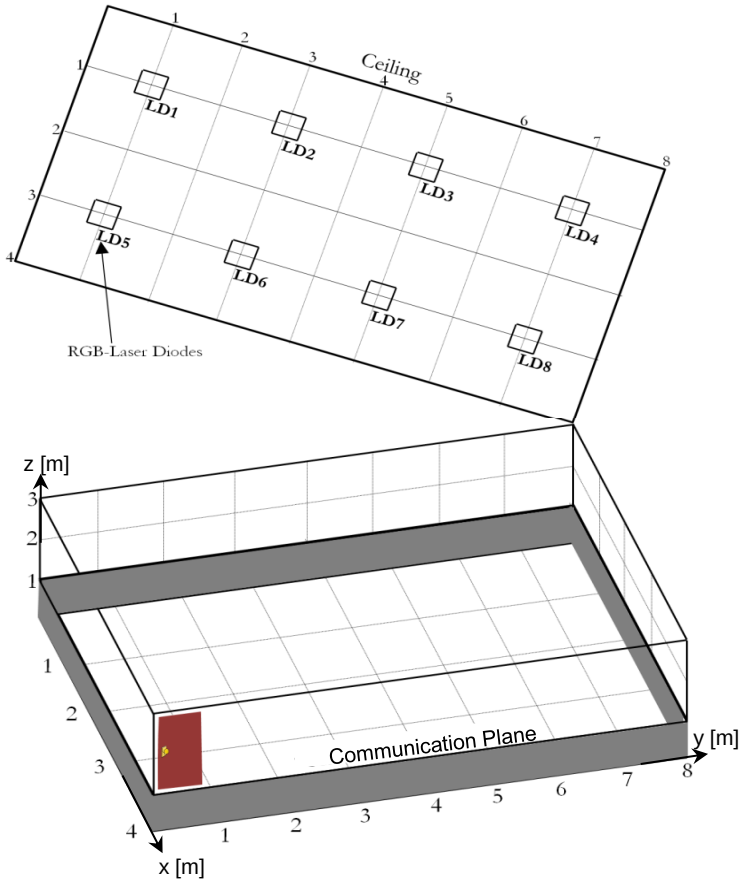

(a)

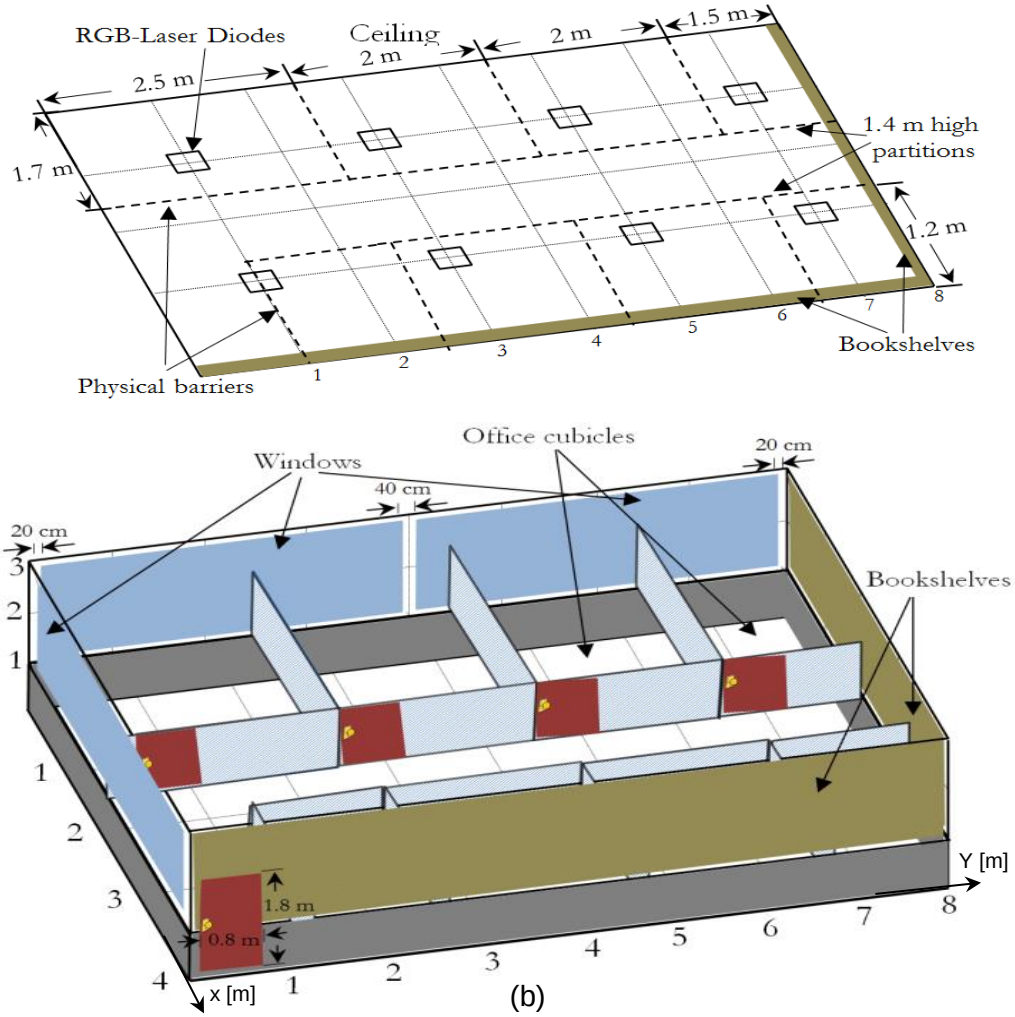

Figure 5.1: VLC system rooms (a) an empty room (Room A) and (b) a realistic room which has a door, three large glass windows a number of rectangular-shaped cubicles with surfaces parallel to the room walls (Room B).

5.4 DAT Angle Diversity Receiver (DAT ADR)

This section presents a performance evaluation of a mobile multi-gigabit VLC system in the two different environments. The VLC channel characteristics and links were evaluated under the diverse situations of an empty room and a room with very strong shadowing effects resulting from mini cubicle offices. RGB-LD were used to mitigate the low modulation bandwidth of conventional transmitters (LEDs) in the VLC system. In addition, an ADR was introduced to mitigate ISI. The proposed ADR has seven sub-detectors. We optimised the

azimuth angle, elevation angle and FOV for each detector to obtain high system performance (i.e. low delay spread and high SNR) under the impact of mobility and multipath propagation. Furthermore, a DAT was used to further reduce the effect of ISI and multipath dispersion. The combination of delay adaptation and ADR (DAT ADR system) added a degree of freedom to the link design, which resulted in a VLC system that has the ability to provide high data rates (i.e., 5 Gb/s) in the considered harsh indoor environment. The proposed system used a OOK modulation format and it was able to provide data rates of 5 Gb/s and a BER of 10^{-3} in the worst case scenario in the considered realistic indoor environment.

In this section, the performance of the proposed system (i.e., DAT ADR) was evaluated in two different environments: in an empty room in the presence of multipath dispersion and mobility as well as in a realistic room environment with mobility. In the realistic environment, signal blockage (as a result of cubicles), a door, windows, furniture, multipath propagation and mobility are all present. To evaluate the effect of signal blockage, mobility and shadowing on the VLC communication link, we considered the room shown in Figure 5.1b. The results of the DAT ADR was compared in rooms A (an empty room) and B (realistic room) in terms of impulse response, path loss, delay spread and SNR. The proposed system is examined in fourteen different locations when the ADR moves along the y-axis.

In this chapter, for the bit rate of 30 Mb/s we used the p-i-n FET preamplifier receiver [162]. Higher data rates of 5 Gb/s and 10 Gb/s are also considered, and here we used the p-i-n FET receivers designed in [161], [168], respectively.

5.4.1 Angle diversity receiver design

The ADR is a group of narrow FOV detectors. A responsivity of 0.4 A/W and a photo detector area of 4 mm^2 were used for each branch. The ADR was always

placed on the CP along the lines x=1m or x=2m. The direction of each branch in the ADR was defined by two angles: the azimuth angle (AZ) and the elevation angle (EL). The AZs of the seven detectors were set at 0^o, 45^o, 90^o, 135^o, 225^o, 270^o and 315^o, and the ELs for the seven branches were fixed at 90^o, 45^o, 60^o, 45^o, 45^o, 60^o and 45^o. The corresponding FOVs were fixed to 20^o, 15^o, 25^o, 15^o, 15^o, 25^o and 15^o. The AZs, ELs and FOVs were chosen through an optimisation process to achieve the best SNR and minimum delay spread. The reception angle calculations for any detector in the ADR are given in detail in Chapter 4, Section 4.4.1. Figure 5.2 illustrates the physical structure of the ADR. The photocurrents received in each branch can be amplified separately and can be processed using different methods, such as SC, EGC or MRC, to maximise the power efficiency of the system. In this section, SC and MRC were used. SC is a simple form of diversity, where the receiver simply selects the branch with the largest SNR among all the branches. In contrast, MRC utilises all branches in the ADR.

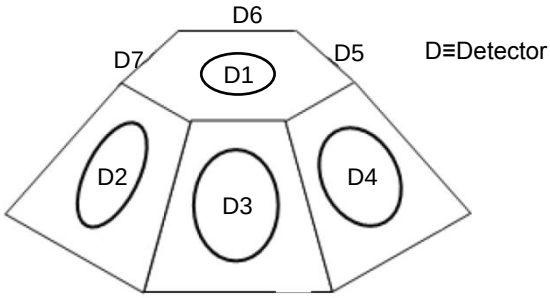

Figure 5.2: Physical structure of the angle diversity receiver with seven branches.

5.4.2 Impulse response

Channel impulse responses at the room centre (i.e., x=2m and y=4m) for the DAT ADR system are shown in Figure 5.3 for rooms A and B. It should be noted that both impulse responses of the proposed system are dominated by short initial impulses due to the LOS path between the transmitter and receiver. It can be clearly seen that the effect of shadowing is clear when the receiver is

located at the room centre in room B (see Figure 5.3). The LOS received power in room A is 4.5 μW, whereas it is 2.25 μW in room B (about 3 dB reduction in received power), and this is due to one of the LOS components being blocked by the wall of a cubicle. It should also be noted that the amount of received optical power from the reflections in room B was less than that received in room A, as shown in Figure 5.3, and this is due to the existence of the door, windows, cubicles, partitions and bookshelves in room B that lead to reduced multipath propagation. These impulse responses suggest that the DAT ADR system performs better in room A (without shadowing) than in room B.

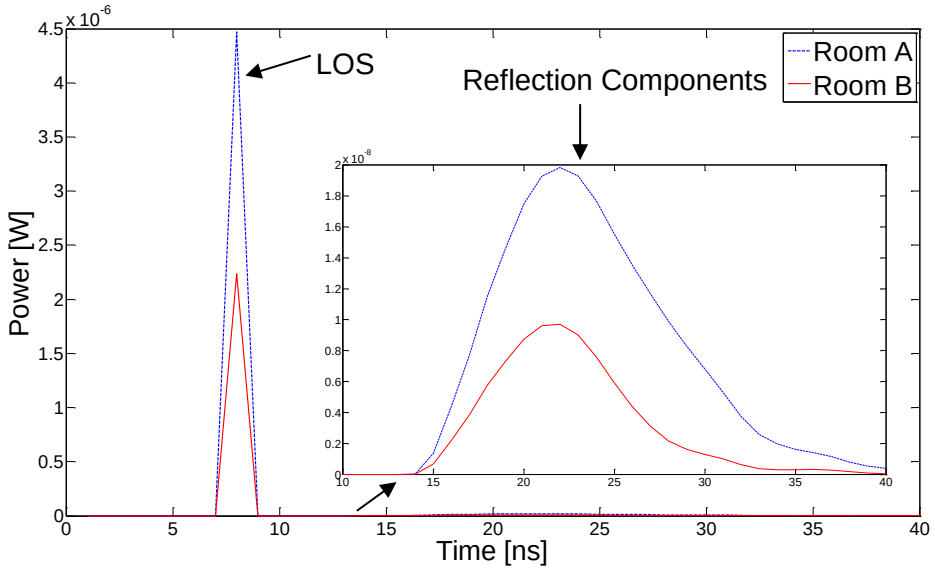

Figure 5.3: Impulse responses of DAT ADR system at room centre (2m, 4m, 1m) in two different environments (rooms A and B).

5.4.3 Optical path loss

One of the main targets of any communication system is to achieve high SNR at the receiver. The SNR in OW systems is based on the square of the received optical signal power and receiver and ambient noises [26]. Therefore, the average received optical power and path loss explain part of the main VLC system performance in the two different environments. Optical path loss can be defined as [169]:

$$PL(dB) = -10log_{10}(\int h(t)dt) \quad (5.1)$$

where $h(t)$ is the system impulse response. Figure 5.4 shows the optical path loss of the DAT ADR system in rooms A and B. It should be observed that the performance of the proposed system is degraded in room B at x=2m (the path loss increased by 3 dB in room B at x=2m), and this can be attributed to signal blockage as a result of cubicles, which lead to reduced received optical power. It can be noticed that the path loss is comparable in rooms A and B when the receiver moves along x=1m. This is due to the LOS links available at this line (i.e., x=1m), which protect against shadowing and mobility in this system.

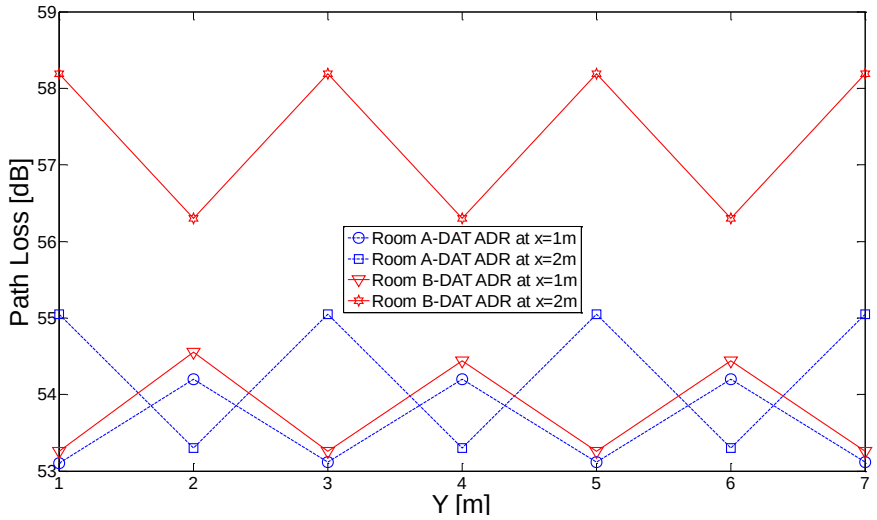

Figure 5.4: Optical path loss distribution of DAT ADR system in two different environments (rooms A and B) at x=1m and x=2m along y-axis.

5.4.4 Delay spread

Figure 5.5 illustrates the delay spread of the DAT ADR system in two different environments (i.e., rooms A and B). It can be noted that the proposed system has lower delay spreads in room B than in room A, and this is attributed to two reasons: firstly, the proposed system has the ability to establish a LOS link at all receiver positions. Secondly, reflections from the door and windows were set to zero, while the other two walls in room B were covered by filling cabinets and

bookshelves with a smaller diffuse reflectivity of 0.4. This means that the power contribution from the reflections was minimal and this reduced the delay spread. The non-symmetry in the delay spread curve in room B is due to the presence of windows at one end of the room and the presence of bookshelves at the other end. In room B, when the receiver position is close to the windows, for example, at points (x=1m and y=1m) and (x=2m and y=1m) the delay spread becomes very low because the received power from the reflections is very low. However, when the receiver moves towards the other side of the room (i.e. receiver positions close to bookshelves), for instance, at points (x=1m and y=7m) and (x=2m and y=7m), the delay spread increased due to the power received from the signals reflected by the bookshelves.

The minimum communication channel bandwidth of the DAT ADR system in rooms A and B was 8.3 GHz (where the delay spread is 0.02 ns at points x=2m, y=1m, 3m, 5m, 7m). The significant increase in the channel bandwidth enables our proposed system to operate at higher data rates using a simple modulation technique, OOK [87].

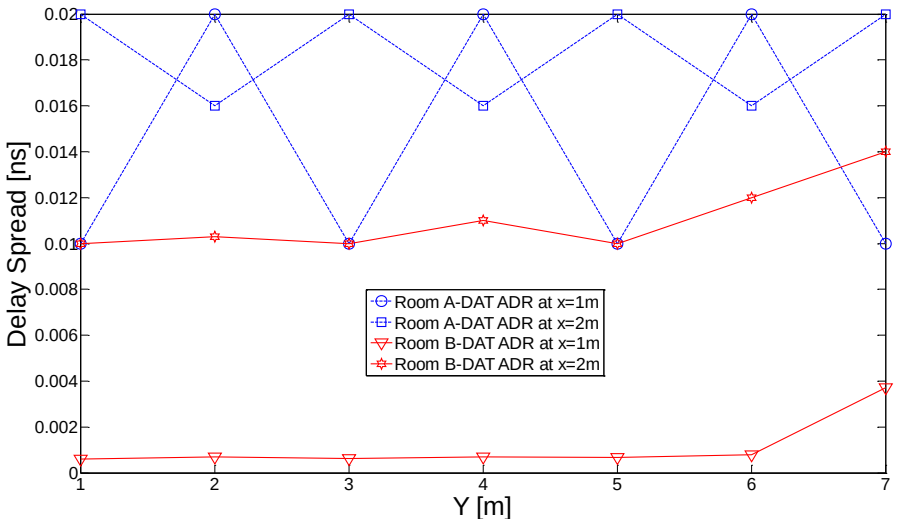

Figure 5.5: Delay spread of DAT ADR system in two different environments (rooms A and B) at x=1m and at x=2m and along y-axis.

5.4.5 SNR analysis

In this section, for the bit rate of 5 Gb/s we used the p-i-n FET receiver designed in [161]. Figure 5.6 shows the SNR_{SC} results against receiver location for the DAT ADR system in the two room scenarios. The DAT ADR system has a slightly lower SNR in room B at x=1m and this is due to the reduction in received power. In addition, at x=2m the SNR decreased by 3 dB in room B in all receiver locations, this is because when the receiver moves along the middle of the room some transmitters cannot be detected by the receiver due to the cubicles. It should be noted that the results in Figure 5.6 are in agreement with the general observation made in Figure 5.4. For instance, the DAT ADR system in room B at x=2m had a path loss higher than that in room A, which led to a decrease in SNR. Note the variation in SNR in tandem with the path loss (see Figure 5.4) due to the effects explained.

Figure 5.7 illustrates the SNR_{MRC} of the DAT ADR system in the two environments. At x=1m, the simulation results of the SC and MRC techniques in rooms A and B show comparable SNR results (about 1 to 2.5 dB difference, see Figures 5.6 and 5.7). This is due to the fact that the power received by one of the detectors is dominant, compared to other detectors, and also due to the limited number of detectors that can collect direct LOS optical signals. It is observed that at x=2m the MRC technique outperformed SC (see Figures 5.6 and 5.7), the SNR gain was over 3 dB in all receiver locations in both environments. This is due to the two branches of ADR having received the same amount of optical signals.

The highest BER provided by our proposed system in room A was about 10^{-5}, whereas it was approximately 10^{-3} in room B when the proposed system operated at 5 Gb/s (when using MRC method). Forward error correction codes (FEC) can be used to further reduce the BER in this proposed DAT ADR system.

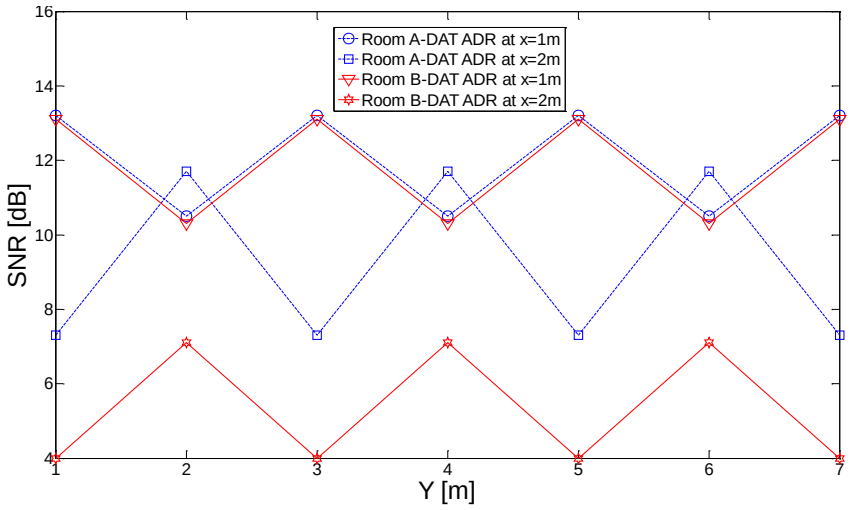

Figure 5.6: SNR_{SC} of DAT ADR system in two different environments (rooms A and B) when operated at 5 Gb/s at x=1m and at x=2m and along y-axis.

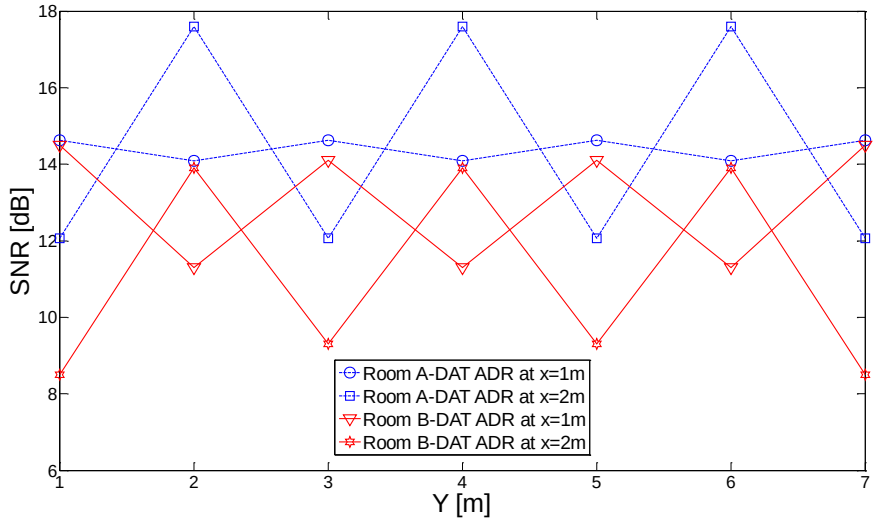

Figure 5.7: SNR_{MRC} of DAT ADR system in two different environments (rooms A and B) when operated at 5 Gb/s at x=1m and at x=2m and along y-axis.

5.5 DAT Imaging LD-VLC system in Empty Room

To further improve the communication links and to provide higher data rates (beyond 5 Gb/s) with the imaging LD-VLC system (this system was presented in Chapter 4, Section 4.5), a novel delay adaptation technique coupled with

imaging LD-VLC system (DAT imaging LD-VLC system) to mitigate the ISI, CCI due to multiple transmitters and reduce the impact of multipath dispersion due to mobility at the receiver. We evaluated the performance of the DAT in the presence of multipath propagation, ISI and mobility for the two VLC systems in an empty room. The results of the imaging LD-VLC system are compared with those of the DAT imaging LD-VLC system. The results are presented in terms of impulse response, delay spread, 3 dB channel bandwidth and SNR.

5.5.1 Impulse responses

The impulse responses of the imaging LD-VLC and DAT imaging LD-VLC at the room centre (worst case scenario) are depicted in Figure 5.8. At the room centre the distance between the transmitter and receiver becomes maximum which leads to increase in delay spread, path loss and decrease in SNR. Therefore, the location ((2m, 4m, 1m), room centre) is the worst case scenario. The LOS components have a great impact on the system performance. Therefore, we magnified the impulse response for these systems to show the LOS clearly. It can be seen that the DAT imaging system impulse response is better than the imaging system in terms of signal spread. By reducing the signal spread, this leads to an increase in the 3 dB channel bandwidth which decreases the multipath induced ISI and enables higher throughput for the VLC system.

5.5.2 Delay spread and 3 dB channel bandwidth

Figure 5.9 presents the delay spread performance of the imaging and DAT imaging systems in a worst case scenario (when the receiver moves along the line x=2m). The results show that the DAT imaging LD-VLC system outperforms the imaging LD-VLC system by decreasing the delay spread by a factor of 6, from 0.04 ns to 0.007 ns at the room centre. The 3 dB channel bandwidth of the

two systems (i.e. imaging LD-VLC and DAT imaging LD-VLC) when the receiver moves along the x=2m line is given in Table 5.1.

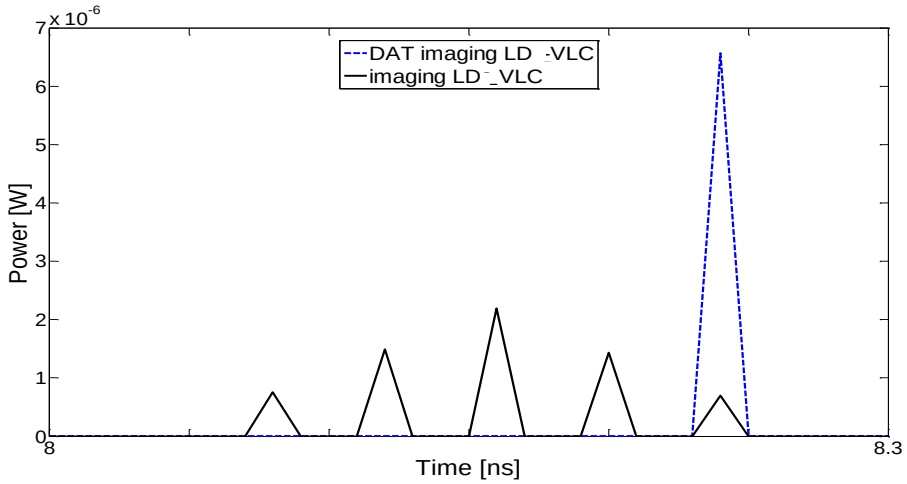

Figure 5.8: Impulse responses of two systems at room centre (2m, 4m, 1m).

The results show that the DAT imaging LD-VLC system offers 3 dB channel bandwidth of more than 16 GHz in the worst case in the rooms examined (which are of typical size), which is the highest channel bandwidth reported for a VLC system to the best of our knowledge. The significant increase in channel bandwidth enables our proposed systems to operate at higher data rates. For example, a 10 Gb/s data rate requires a 7 GHz channel bandwidth with simple OOK modulation, the new DAT imaging LD-VLC system can achieve higher data rates [143].

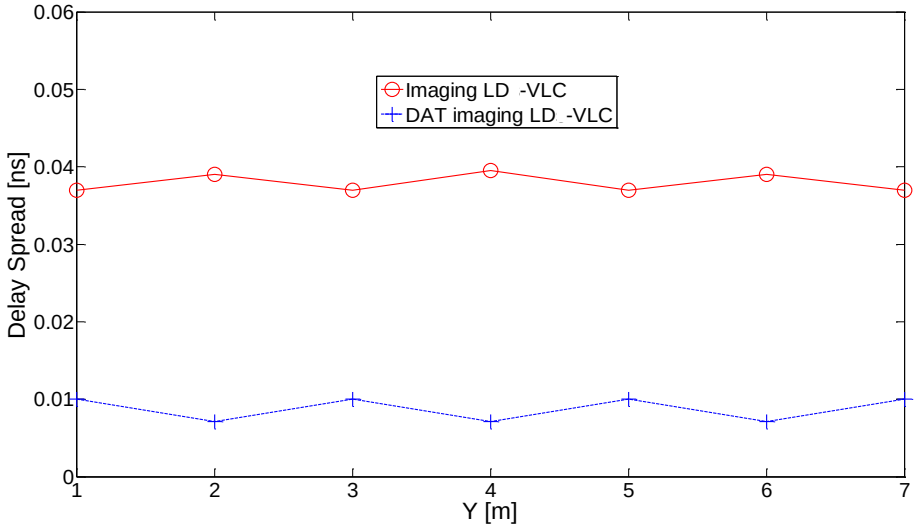

Figure 5.9: Delay spread of two systems at x=2m and along y-axis.

Table 5.1: Channel bandwidth of proposed systems.

System	3 dB channel Bandwidth [GHz]						
	Receiver Locations along the y-axis, Y [m]						
	1	2	3	4	5	6	7
Imaging LD-VLC	5.2	4.2	5.2	4.2	5.2	4.2	5.2
DAT Imaging LD-VLC	16.6	23.4	16.6	23.4	16.6	23.4	16.6

5.5.3 SNR performance

Figure 5.10 illustrates the SNR (SC and MRC) of the imaging and DAT imaging systems when operating at 30 Mb/s. It is observed that the DAT system does not give any advantage over the imaging system at low data rates due to the high channel bandwidth achieved by the imaging system (i.e., 4.2 GHz), which guarantees low ISI at the low operating bit rate considered (30 Mb/s). Figure 5.11 shows the SNR of the imaging and DAT imaging systems at a high data rate (10 Gb/s). These results show that the SNR fluctuations in the imaging system at high data rates are reduced and the SNR is improved by 6 dB when using MRC combing (BER about 10^{-5}) in the DAT imaging system. The DAT imaging system has the ability to achieve more than 23 Gb/s (16 GHz channel bandwidth is achieved). FEC can be used to further reduce the BER form 10^{-5} to 10^{-9} in this proposed DAT imaging LD-VLC system.

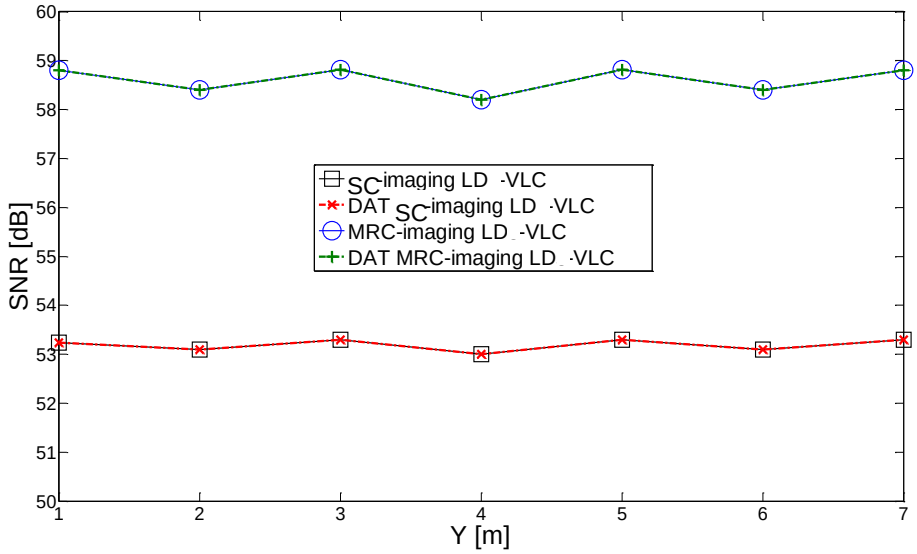

Figure 5.10: SNR of imaging system and DAT imaging system when both operate at 30 Mb/s, when the receivers move at x=2m and along y-axis.

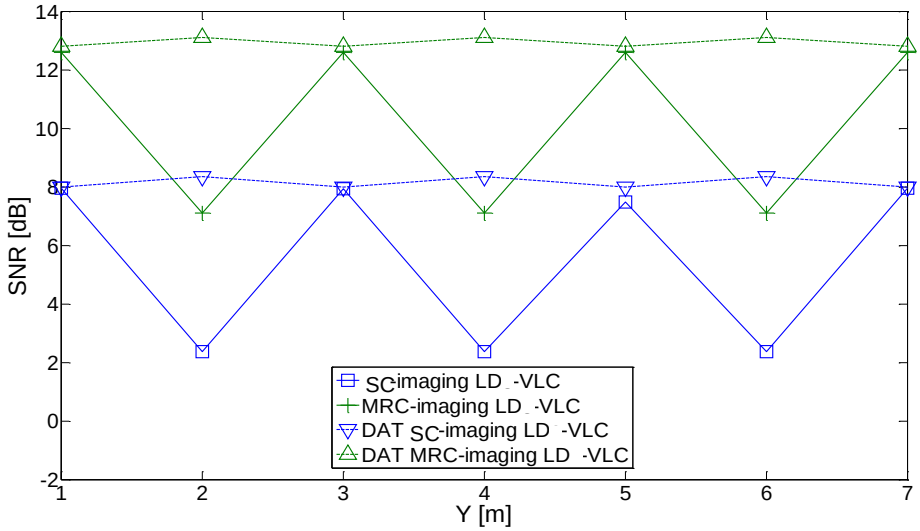

Figure 5.11: SNR of imaging system and DAT imaging system when both operate at 10 Gb/s, when the receivers move at x=2m and along y-axis.

5.6 DAT Imaging LD-VLC System in Realistic Room

We extended the analysis and evaluation of the performance of the proposed system (i.e., DAT imaging LD-VLC system) to a realistic room environment with mobility. In this realistic environment, signal blockage (as a result of cubicles), a

door, windows, furniture, multipath propagation and mobility all present. To evaluate the effect of signal blockage, mobility and shadowing on the VLC communication link, we considered the room shown in Figure 5.1b. The results of the DAT system was compared in rooms A (an empty room) and B (realistic room) in terms of impulse response, path loss, delay spread and SNR. We have considered a mobile user with a speed of 1 m/s moving along the y-axis in the lines x=1m or x=2m, the results in this section are presented in two places in the room 1) when the user is inside a mini cubicles (x=1m and along y-axis) and 2) when the mobile user is in the middle of the room (x=2m and along y-axis). In this section a simulation package based on a ray tracing algorithm was developed using MATLAB to compute the impulse response of the DAT imaging LD-VLC system in a realistic environment. Additional features were introduced for a realistic room. In the realistic environment for each receiver location the first step is to check the availability of LOS component (certain conditions were introduced to the simulator to check the existence of LOS, 1^{st} and 2^{nd} order reflection components in each location) then the received power due to 1^{st} and 2^{nd} order reflections is also calculated.

5.6.1 Impulse response

Channel impulse responses at the room centre for the DAT imaging system are shown in Figure 5.12 for rooms A and B. It should be noted that both impulse responses of the proposed system are dominated by short initial impulses due to the LOS path between transmitter and receiver. In addition, it can be clearly seen that the proposed system has good robustness against shadowing and mobility, and it has the ability to maintain LOS even in this harsh environment (i.e., room B), which is attributed to the number of transmitters that are distributed on the ceiling (i.e., eight RGB LD light units). However, the amount of received optical power from the reflections in room B is less than that received in room A, as shown in Figure 5.12, and this is because of the existence of the door, windows, cubicles, partitions and bookshelves in room B

that lead to reduced multipath propagation. Although the received power from reflections was severely affected in room B, the LOS component remained the same in both room configurations in both systems, and the LOS component has the largest impact on the system performance. For example, the received optical power associated with the DAT imaging LD-VLC system in room A was 6.69 μW, whereas it was 6.63 μW in room B, which indicates that the reduction in power is negligible (the reduction in power was 0.063 μW).

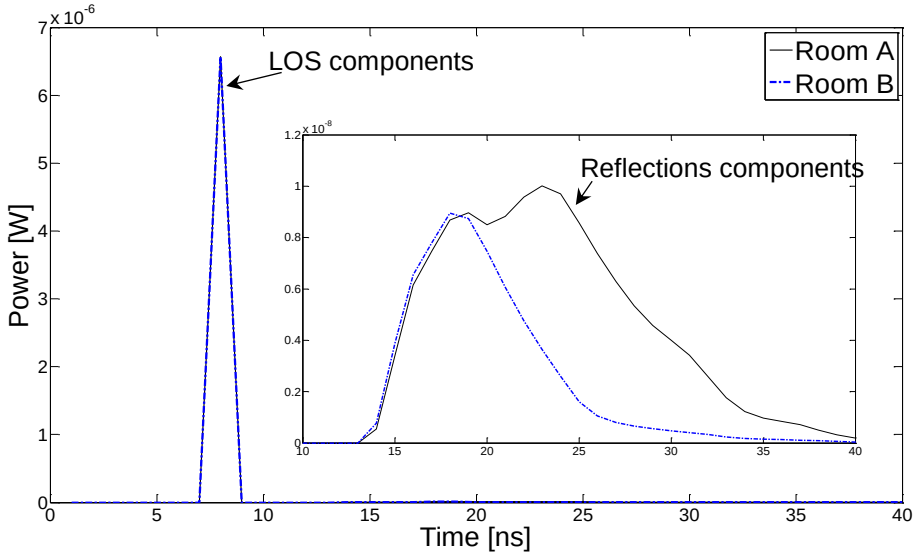

Figure 5.12: Impulse responses of DAT imaging system at room centre (2m, 4m, 1m) in two different environments (rooms A and B).

5.6.2 Path loss

Figure 5.13 illustrates the optical path loss of the DAT imaging system in rooms A and B. It is observed that the performance of the proposed system is comparable in rooms A and B, and this can be attributed to the LOS links available on the entire CP, which protects against shadowing and mobility in this system. It can be noticed that the path loss can be higher when the receiver moves along x=2m. This is due to the larger distance between the receiver and transmitter. Overall, the proposed systems were evaluated and it was shown

that they are able to achieve similar performance levels in an empty room and in a realistic indoor environment.

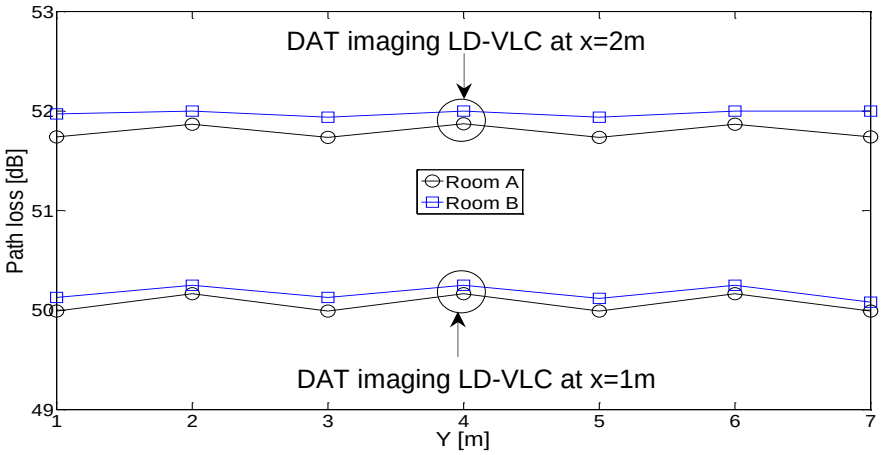

Figure 5.13: Optical path loss distribution of DAT imaging system in two different environments (rooms A and B) at x=1m and x=2m along y-axis.

5.6.3 Delay spread and 3 dB channel bandwidth

Figure 5.14 shows the delay spread of the DAT system in two different environments (i.e., rooms A and B). It can be clearly seen that the DAT imaging system has lower delay spreads in room B than in room A, and this is attributed to two reasons: firstly, the proposed system has the ability to establish a LOS link at all receiver positions. Secondly, reflections from the door and windows are set to zero, while the other two walls in room B are covered by filling cabinets and bookshelves with a small diffuse reflectivity of 0.4. This means that the power contribution from the reflections is minimal and this reduced the delay spread. The non-symmetry in the delay spread curve in room B is due to the presence of windows at one end of the room and the presence of bookshelves at the other end. In room B, when the receiver position was close to the windows, for example, at points (x=1m and y=1m) and (x=2m and y=1m) the delay spread becomes very low because the received power from the reflections is very low. However, when the receiver moves towards the other side of the room (i.e. receiver positions close to bookshelves), for instance, at

points (x=1m and y=7m) and (x=2m and y=7m), the delay spread increases due to the power received from the signals reflected by the bookshelves. The 3 dB channel bandwidth of the DAT imaging LD-VLC in two different environments (rooms A and B) when the receiver moves along the x=2m line is given in Table 5.2. The results show that the DAT imaging LD-VLC system offers 3 dB channel bandwidth of more than 24 GHz in room B. Therefore, room B outperforms room A in terms of 3 dB channel bandwidth as the delay spread decreased in room B (see Figure 5.14).

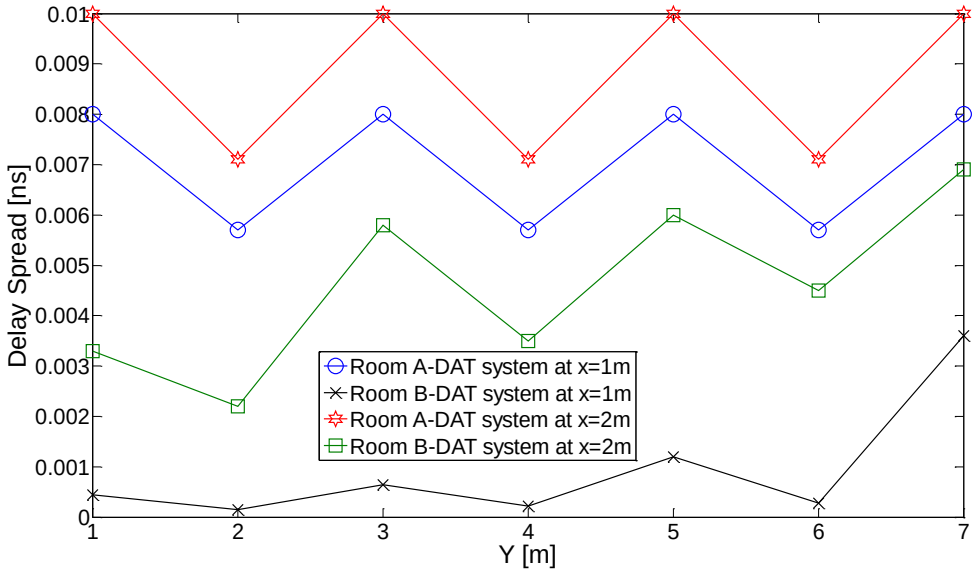

Figure 5.14: Delay spread of DAT imaging system in two different environments (rooms A and B) at x=1m and at x=2m and along y-axis.

Table 5.2: Channel bandwidth of the DAT imaging LD-VLC in two different environments.

DAT Imaging LD-VLC	3 dB channel Bandwidth [GHz]						
	Receiver locations along the y-axis, Y [m]						
	1	2	3	4	5	6	7
Room A	16.6	23.4	16.6	23.4	16.6	23.4	16.6
Room B	37.1	38.9	28.7	36.7	27.7	31.6	24.1

5.6.4 SNR

Figure 5.15 shows the SNR_{SC} results against receiver location for the DAT system in two room scenarios. The DAT imaging system has a slightly lower SNR in Room B and this due to the reduction in received power. It should be noted that the results in Figure 5.15 are in agreement with the general observation made in Figure 5.13. For instance, the DAT system in room B has a path loss higher than that in room A which leads to a decrease in SNR.

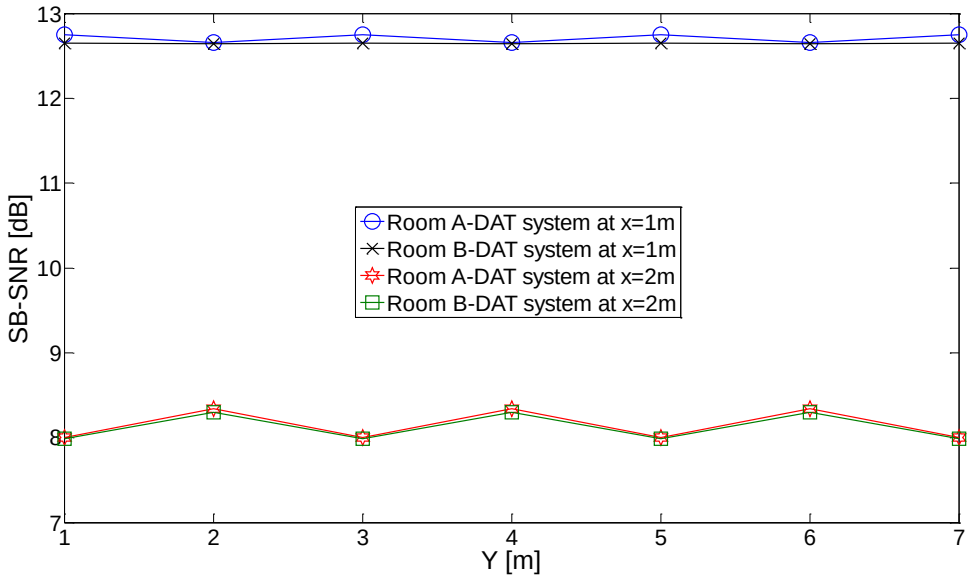

Figure 5.15: SNR_{SC} of DAT system in two different environments (rooms A and B) when system operated at 10 Gb/s at x=1m and at x=2m and along y-axis.

5.7 Summary

A novel delay adaptation technique was introduced for a VLC system and an ADR and an imaging receivers were used to improve the SNR and channel bandwidth as well as to reduce the effect of multipath dispersion. In addition, our proposed systems were evaluated in a harsh environment with mobility, and the results showed that our systems are robust in the presence of shadowing and mobility.

In this chapter, we proposed, designed and evaluated a novel LD-VLC system with ADR and delay adaptation in two different environments (an empty room and a realistic room). The DAT ADR system achieved 5 Gb/s and a BER of 10^{-5} at the least successful point in the empty room with simple modulation format (OOK). However, there was degradation in the performance (BER increase) when the DAT ADR system operated in the realistic environment considered. The DAT ADR system in a realistic room (room B) had a lower delay spread (high 3 dB channel bandwidth) but also a lower received power and overall lower SNR. From the results of DAT ADR we can conclude that the room design can play an important role in changing the SNR distribution, delay spread and impulse response uniformity.

The DAT imaging LD-VLC system has the ability to decrease the delay spread of the imaging LD-VLC system by 83% from 0.04 ns to 0.007 ns at the room centre, which leads to an increase in the channel bandwidth by a factor of 5.4 from 4.2 GHz to 23 GHz, and this channel bandwidth has the ability to provide data rates of up to 33 Gb/s. Moreover, at low data rates (30 Mb/s), the proposed algorithm does not offer SNR improvements, which is due to the low ISI at these data rates. The BER provided by our DAT imaging LD-VLC system is better than 10^{-5} at 10 Gb/s, in the worst case scenarios. The DAT imaging system in a realistic room has lower delay spread (higher 3 dB channel bandwidth) but also lower received power and overall has slightly lower SNR.

6 10 Gb/s Mobile Visible Light Communication System Employing Angle Diversity, Imaging Receivers and Relay Nodes

6.1 Introduction

In the near future, indoor wireless systems will be required to offer multi-gigabit per second connectivity. VLC systems are potential candidates to provide high data rates services for indoor users. However, the traditional VLC system suffers from limitations in the modulation bandwidth of the transmitters (i.e. LEDs) [4]. Therefore, alternative transmitters are needed for VLC systems to achieve high data rates. An ADR and an imaging receiver are solutions that can tackle the signal spread caused by multipath in a VLC system [4], [170]. A three branch ADR with RGB-LD has been proposed in [100], and 5 Gb/s was achieved in an empty room (see Chapter 4). Our previous work in this area has shown that significant enhancements can be achieved when using an imaging receiver (see Chapter 4) [103]. The data rate achieved by this previously developed VLC system was 5 Gb/s by introducing a LD and an imaging receiver [103].The main limitations in the traditional VLC system (i.e., the low modulation bandwidth of the LEDs and ISI) have been addressed previously by using LD instead of LEDs and the wide FOV receiver has been replaced by the imaging receiver which has narrow FOV pixels [103]. The data rate achieved by this previously developed VLC system was 5 Gb/s in the worst case scenario

[103]. However, its link performance was negatively affected by mobility and this leads to performance degradation in the SNR and channel bandwidth. Therefore, in this chapter we introduce the concept of relay assisted VLC systems to improve the overall system performance.

Relays have been previously considered for use in different networks to reduce the transmission distances and increase system capacity [171], [172]. Relays were introduced by Meulen in 1971 [173] and spread widely in radio communication after the emergence of the cooperative communication idea [172]. In the literature, relay assisted FSO wireless systems have been proposed [174], [175]. Relays were used in FSO system to provide multi-hop diversity to the destination. In [176] an LED light bulb in a desk lamp is used as a relay when it receives a radio signal from a mobile device and broadcasts it back to the desk with larger coverage and higher light intensity. In an infrared OW system the concept of relays is studied in [177]. The use of intermediate nodes in OW systems can lead to significant improvements in SNR and considerable extra bandwidth in the channel. Relays can either be idle users present in the communication plane who can cooperate in the transmission, or they can be transceivers deployed solely for this purpose [177].

In this chapter three new VLC systems, an ADR relay assisted LD-VLC (ADRR-LD), an imaging relay assisted LD-VLC (IMGR-LD) and select-the-best imaging relay assisted LD-VLC (SBIMGR-LD) are modelled and their performance is compared at 10 Gb/s in two VLC room sizes (5×5×3 m^3 and 4×8×3 m^3). We also model two different room scenarios: an empty room and a real environment room that has a door, windows, bookshelves, mini cubicles and other objects. The challenge in both rooms is the ability to establish LOS communication link between transmitter and receiver at all relevant locations. We have used the previously introduced LD and imaging receiver in Chapter 4 and delay adaptation technique in Chapter 5 and we have achieved 10 Gb/s in a realistic environment, which is a 2x increase in data rate compared with [100]

and [103], and in the current work we introduce the concept of relays in VLC systems for the first time to the best of our knowledge. The main difference between the proposed VLC systems in this study and traditional VLC systems is the use of RGB LD as the transmitters instead of LED. The main advantage of using visible LD is their wide modulation bandwidths ranging from hundreds of MHz to more than 10 GHz.

The remainder of this chapter is organised into the following sections: Section 6.2 explains the simulation environment and VLC channel model; Section 6.3 describes the proposed VLC systems' configurations. Section 6.4 provides the simulation results and discussion of the ADRR-LD system, IMGR-LD system and SBIMGR-LD system in an empty room. Section 6.5 presents the simulation results and discussion of the proposed systems in a small office environment. The robustness of the proposed systems against mobility, shadowing and signal blockage is investigated in Section 6.6. Finally, a summary is provided in Section 6.7.

6.2 Simulation Environment

To study the benefits of our techniques for an indoor VLC system, a simulation based on a ray tracing algorithm was performed in an empty room.

Three new VLC systems are considered in this work: ADRR-LD, IMGR-LD and SBIMGR-LD systems. All the proposed systems use an upright transmitter at the CP and the transmitter is placed at three different locations on the CP: (1 m, 1 m, 1 m), (2 m, 1 m, 1 m) and (2 m, 4 m,1 m). These transmitter locations represent three main cases: transmitter underneath relay (best case), transmitter between two relays and transmitter at the centre of the room, which is considered the worst case scenario due to the large distance between transmitter and relay. Figure 6.1 shows the VLC room with eight RGB-LD light units (eight relays) with upright transmitter and receiver both located on CP.

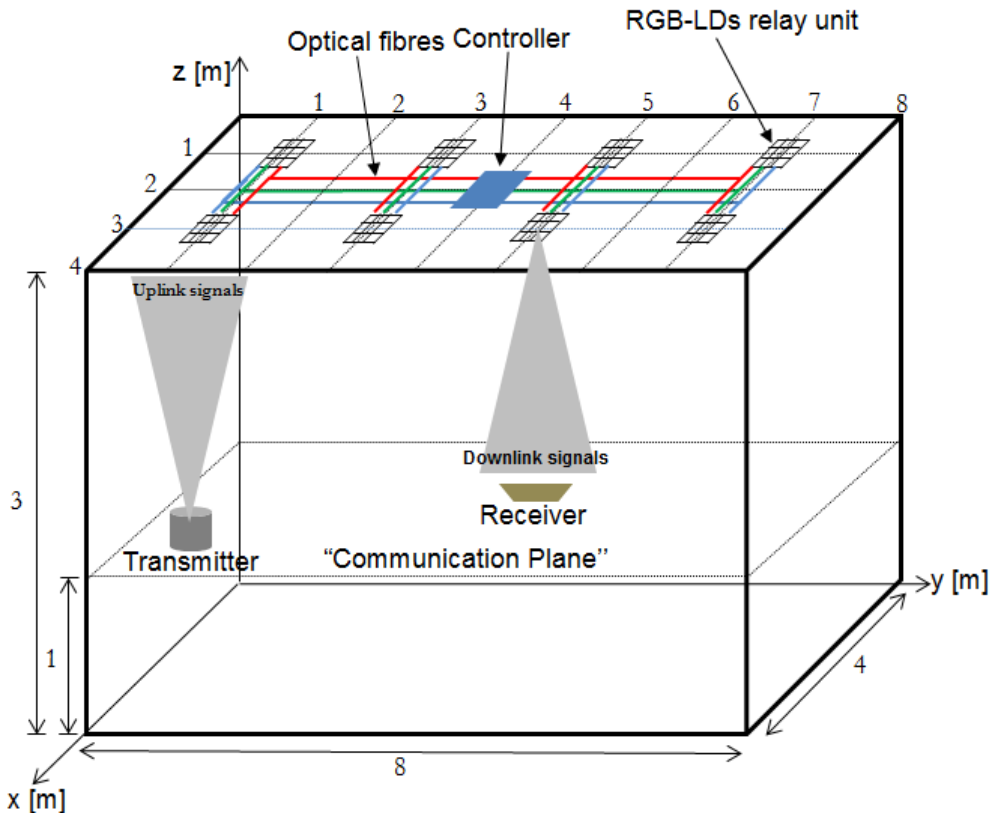

Figure 6.1: VLC system room.

6.3 Systems' Configurations

In this section, three new VLC systems are presented, analysed and compared in order to identify the most appropriate system for use in multi-gigabit VLC systems.

6.3.1 ADRR-LD

The ADRR-LD system employs one upright transmitter on the CP, eight relays (lighting fixtures) on the ceiling connected by fibre interconnects and controlled by a central controller and a seven branch ADR (similar to that in Chapter 5) located on the CP as shown in Figure 6.2. A communication set up (CS)

algorithm is proposed to select the optimum link between the transmitter and the relays (under mobility, this algorithm can be called periodically). For a single transmitter at a given set of positions, the CS algorithm identifies the optimum link according to the following steps:

1- The controller activates a listening mode in all the relays (eight relays).
2- The transmitter on the CP sends a pilot signal.
3- SNR is computed at each relay.
4- The relay that yields the best SNR is chosen by the controller (which is mostly the closest relay to the transmitter).
5- The controller deactivates the remaining seven relays and keeps the closest relay 'ON'.
6- The closest relay sends a feedback signal to the transmitter to start operating mode (i.e., start sending information signals).

Once the information signals are sent by the transmitter, the closest relay to the transmitter receives it and the controller broadcasts the information to the rest of the relays to start transmission to the destination (ADR). Switching 'ON' the relays and emitting signals simultaneously from the relays (light fixtures) may result in receiving the signals at different times due to multipath propagation. Therefore, a DAT is coupled with the ADRR-LD system to enhance the SNR and channel bandwidth. The delay adaptation technique was previously proposed in Chapter 5 [103].

If the time taken to determine the value of each SNR and delay associated with each relay (relative to the start of the frame) is equal to 1 ms, then our CS algorithm and delay adaptation method training time is 80 ms (8 relays × 1 ms + 9 RGB-LD in each relay unit × 8 relay units × 1 ms). This rate (80 ms, once every 1-second frame) is sufficient given that the CS and delay adaptation have to be carried out at the rate at which the environment changes (pedestrian movement). Therefore, the adaptive system can achieve 100% of the specified data rate when it is stationary, and 92% in the case of transmitter or user

movement, i.e. 10 Gb/s when it is stationary and 9.2 Gb/s when there are environmental changes (user or object movement in the room). Our delay adaptation algorithm has been considered at one given receiver location in a single user scenario. In the case of a multiuser scenario, opportunistic scheduling can be employed [167].

The photocurrents received in each branch can be processed using different approaches (SC, EGC or MRC). The MRC technique can achieve better performance compared to other methods [95]. Therefore, the ADRR-LD system employs an MRC approach.

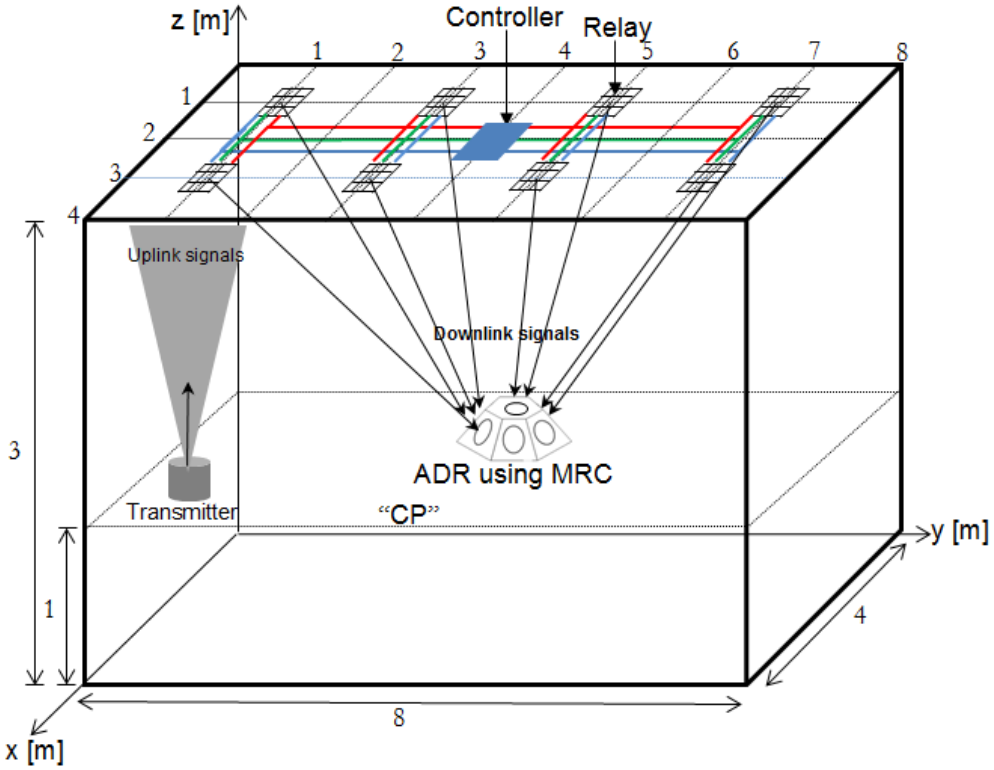

Figure 6.2: ADRR-LD system.

6.3.2 IMGR-LD

The IMGR-LD system has a similar room configuration and uses the same algorithms as the previous system (i.e., CS and delay adaptation). However, the main difference between the two systems is the type of receiver (see Figure 6.3). An imaging receiver with 50 pixels is employed here. The IMGR-LD system combines the signals coming from eight relays by using the MRC method. It should be noted that the uplink signal from the transmitter is only received by one relay (the closest relay to the transmitter) then the controller broadcasts the information to the rest of the relays to start transmission to the destination (imaging receiver).

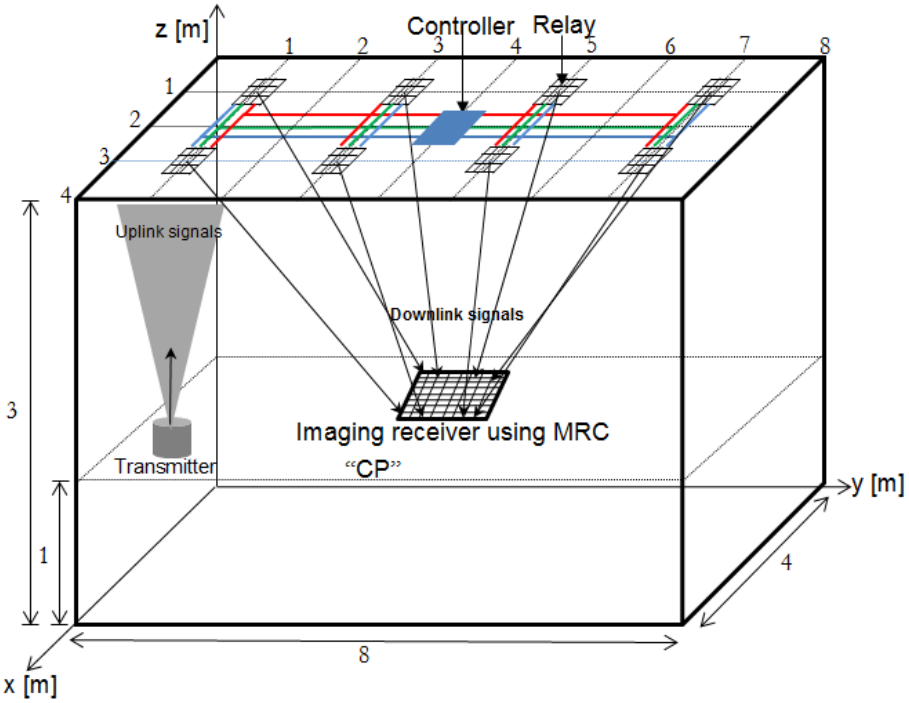

Figure 6.3: IMGR-LD system.

6.3.3 SBIMGR-LD

In contrast to IMGR-LD, in the SBIMGR-LD system only one relay sends the information to the receiver (i.e., the relay closest to the receiver) as shown in Figure 6.4. The CS algorithm is used to find the optimum path between

transmitter and relay. Then, a select-the-best (SB) algorithm is applied between relays and receiver to find the closest relay to the receiver. The SB algorithm identifies the closest relay to the receiver according to the following steps:

1- A pilot signal is sent from one of the relays.
2- SNR is estimated at the receiver by pixel 1 of the imaging receiver.
3- Repeat step 2 for other pixels in the imaging receiver.
4- Repeat steps 2 and 3 for other relay units.
5- The receiver sends a low data rate control feedback signal to inform the controller of the SNRs associated with each relay.
6- The relay that yields the best SNR is chosen by the controller (typically the closest relay to the receiver in our simulations).
7- The controller activates a silent mode for the remaining six relays and keeps the closest relay to the transmitter 'ON' to receive information signals from the transmitter, and it also keeps the closest relay to the receiver 'ON' for transmission (see Figure 6.4). When the transmitter and receiver are at the same position (special case) only one relay will be 'ON' to receive and transmit information signals.

Like IMGR-LD, SBIMGR-LD employs a delay adaptation technique to improve SNR. The time taken by our algorithms (i.e., CS, SB and delay adaptation) is equal to 25 ms (8 relays × 1 ms (for CS) + 8 relays × 1 ms (for SB) + 9 RGB-LD in each relay unit × 1 relay unit × 1 ms (for delay adaptation)). Therefore, 100% of the specified data rate can be achieved by the adaptive system when it is stationary and 97.5% in the case of transmitter or receiver movement. The proposed algorithms (SB, CS and DAT) require a repetitive training and feedback channel from the receiver to the controller at a low data rate. An IR diffuse channel is suggested to achieve this.

Figure 6.5 shows a block diagram of the transmitter, relay and receiver with uplink and downlink channels (note that if a VLC transmitter near the user (laptop for example) is deemed too bright for user comfort, an IR uplink can be

implemented). After CS the VLC transmitter sends the information signals, the relay unit receives the data and then the controller (a Microchips 32 bits microcontroller was used as the controller (PIC32MX110F016B) [178]) broadcasts the information to all relays. The backbone of our room network is for example based on plastic optical fibre (POF) cables (multimode fibres or even single mode fibres can be used to support higher data rates in future) and there are used for illumination (LD light engine is used to generate RGB lasers) and to carry the data. RGB LD emit the same information signal simultaneously.

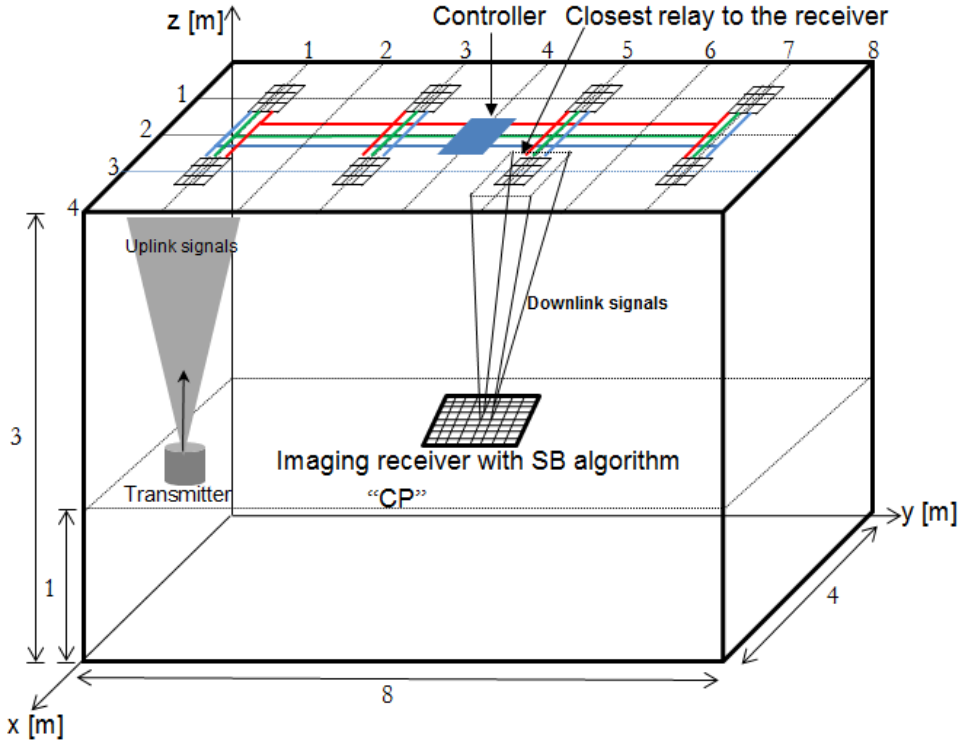

Figure 6.4: SBIMGR-LD system.

The use of a RGB triplet in such devices could potentially deliver data rates in the order of 30 Gb/s by using WDM. It should be noted that the source of the information (transmitter) is fixed and located on the CP, its main function is to send the information signals to relays. Each mobile user has a compact transceiver that has the ability to send and receive data. The size of the photo detector and concentrator are acceptable in mobile terminals and they can be

securely fixed to the mobile unit.

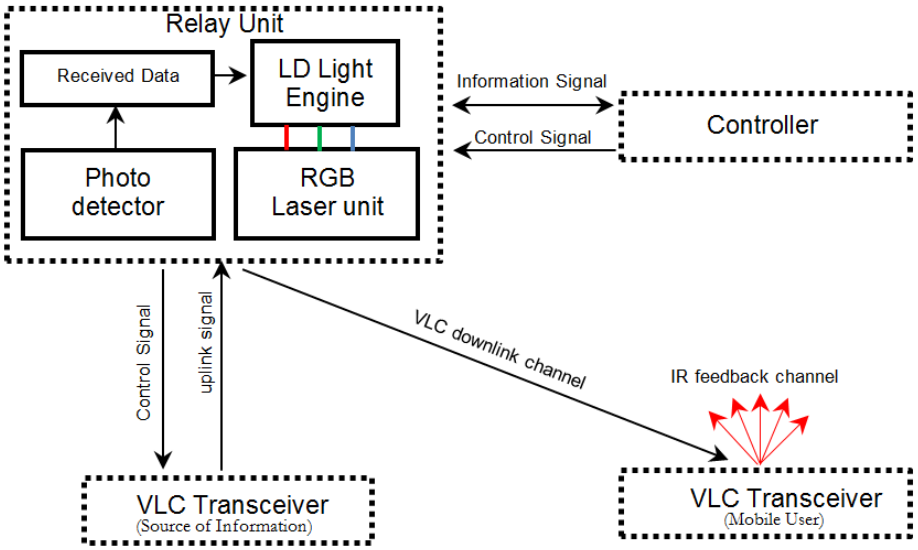

Figure 6.5: Block diagram of relay assisted VLC system.

6.4 Simulation Results in an Empty Room

We evaluated the performance of the proposed systems (ADRR-LD, IMGR-LD and SBIMGR-LD) using ADR and imaging receivers in an empty room in the presence of multipath dispersion and mobility. The proposed systems are examined in fourteen different locations when the receivers move along the y-axis and the transmitter is at the room centre (worst case scenario). The results are presented in terms of impulse response, delay spread, 3 dB channel bandwidth and SNR.

6.4.1 Impulse responses

The impulse responses of the ADRR-LD, IMGR-LD and SBIMGR-LD at the room centre are depicted in Figures 6.6 a, b and c, respectively. It can be seen that the SBIMGR-LD impulse response is better than that of ADRR-LD and IMGR-LD systems. The impulse responses of the three systems consist of first

and second reflection components as well as LOS. It can be noted that received power from reflection components in the SBIMGR-LD system has lower power than in ADRR-LD or IMGR-LD. This is because only the closest relay to the receiver transmits the information signals, whereas in the case of the ADRR-LD and IMGR-LD systems, eight relays emit optical signals together.

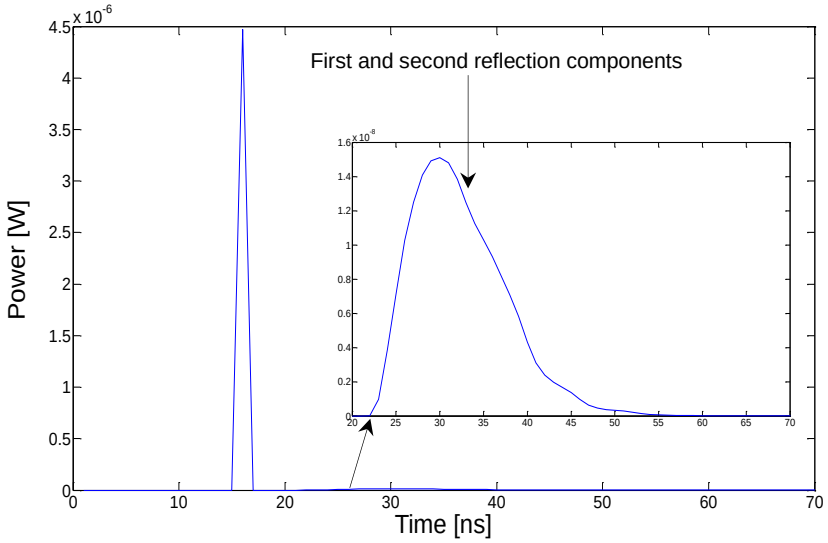

(a)

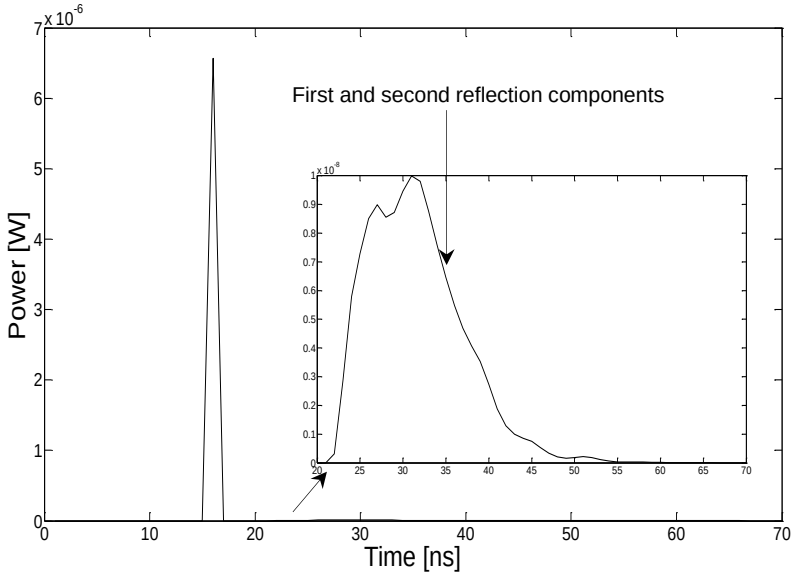

(b)

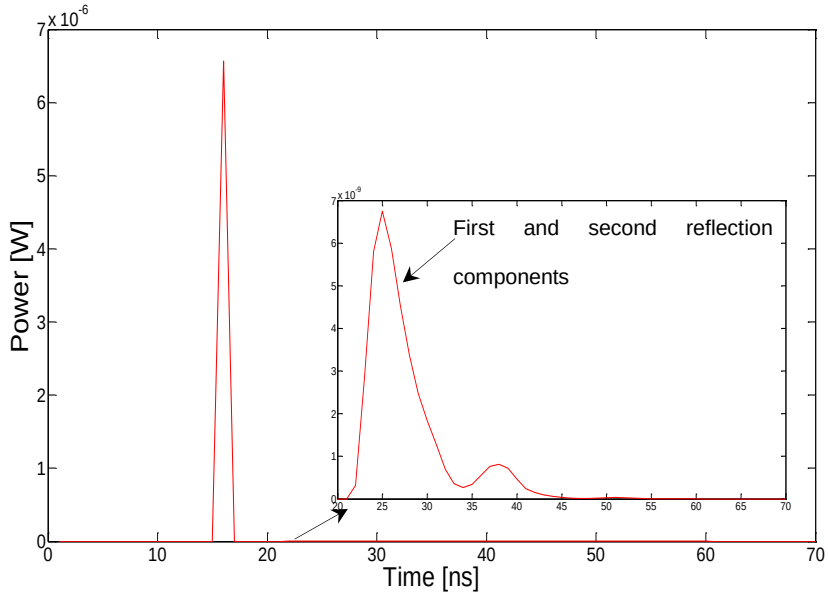

(c)

Figure 6.6: Impulse responses at room centre (x=2m, y=4m, z=1m) (a) ADRR-LD, (b) IMGR-LD and (c) SBIMGR-LD.

6.4.2 Delay spread distribution

Figure 6.7 presents the delay spread of the proposed systems when receivers move at x=1m and x=2m along the y-axis (in 1 m step). A 0.2 m user step has been considered and combined with the results of the 1 m step as shown in Figures 6.7, 6.8 and 6.9. Reducing the step size from 1 m to 0.2 m led to smoothing the results curves for the delay spread, 3 dB channel bandwidth and SNR. The results show that the SBIMGR-LD has the lowest delay spread compared with ADRR-LD and IMGR-LD. This is attributed to two reasons: first, in SBIMGR-LD only one relay sends information signals towards the receiver. Second, LOS is dominant over other components. The results indicate that employing the SBIMGR-LD system instead of the ADRR-LD system can reduce the delay spread by a factor of 1.6, from 0.01 ns to 0.006 ns in the worst communication path. It was observed that, at x=1m in the ADRR-LD and the IMGRR-LD systems, the delay spread can be lower than at x=2m. This is due to

link distances which increase at x=2m leading to increase in delay spread. However, the SBIMGR-LD system delay spread is about the same in both lines x=1m and x=2m.

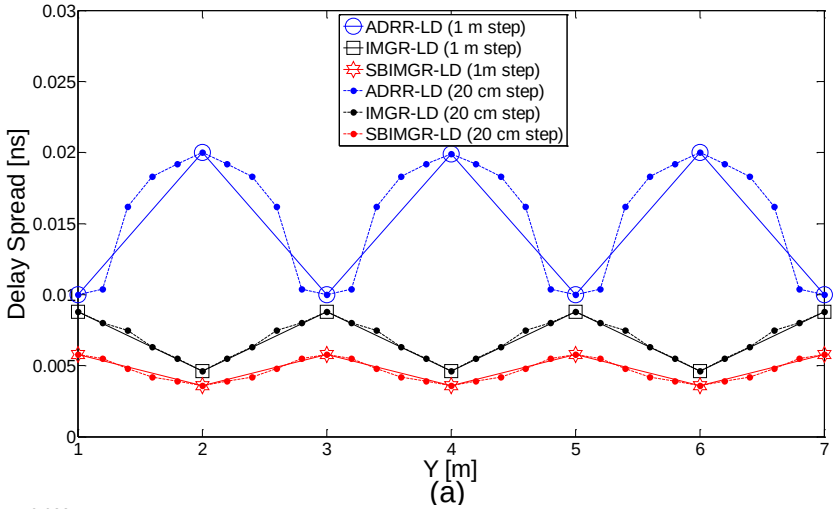

(a)

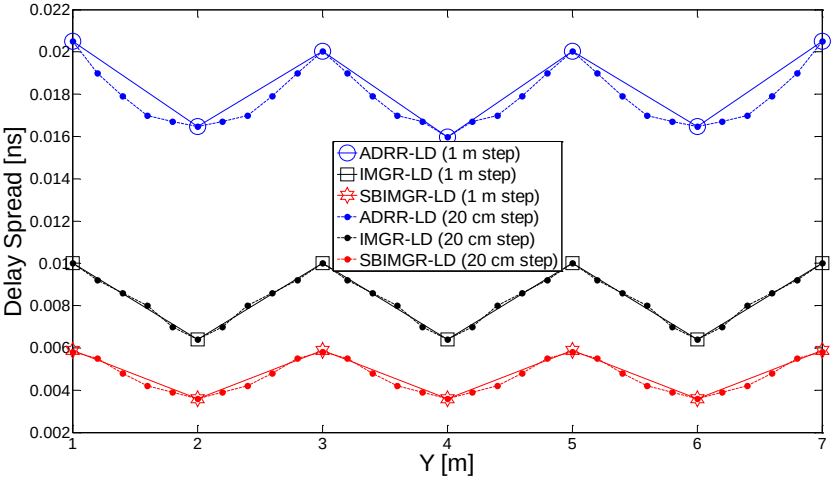

(b)

Figure 6.7: Delay spread of the three systems, (a) at x=1m and (b) at x=2m.

6.4.3 The 3 dB channel bandwidth

Although the transmitter modulation bandwidth problem in the traditional VLC system can be tackled by replacing LEDs with LD, channel bandwidth remains an issue that needs to be solved to achieve multi-gigabit data rates. Previous work has shown that adopting LD with an imaging receiver can provide a 3 dB channel bandwidth of more than 4 GHz [103]. The 3 dB channel bandwidth

achieved by three systems at x=1m and x=2m is depicted in Figure 6.8. The results show that the SBIMGR-LD system offers 3 dB channel bandwidth of more than 26 GHz in the worst case. The minimum communication channel bandwidth of the ADRR-LD system was 8.3 GHz at x=2m. The significant increase in the channel bandwidth enables our proposed systems to operate at higher data rates using a simple modulation technique, OOK [87]. Also, it should be noted that the results in Figure 6.8 are in agreement with the general observation made in Figure 6.7. For instance, in the SBIMGR-LD system at the point x=1m and y=2m, the delay spread is the lowest resulting in the highest channel bandwidth (see Figure 6.8 a). Similar agreement is observed when comparing other locations.

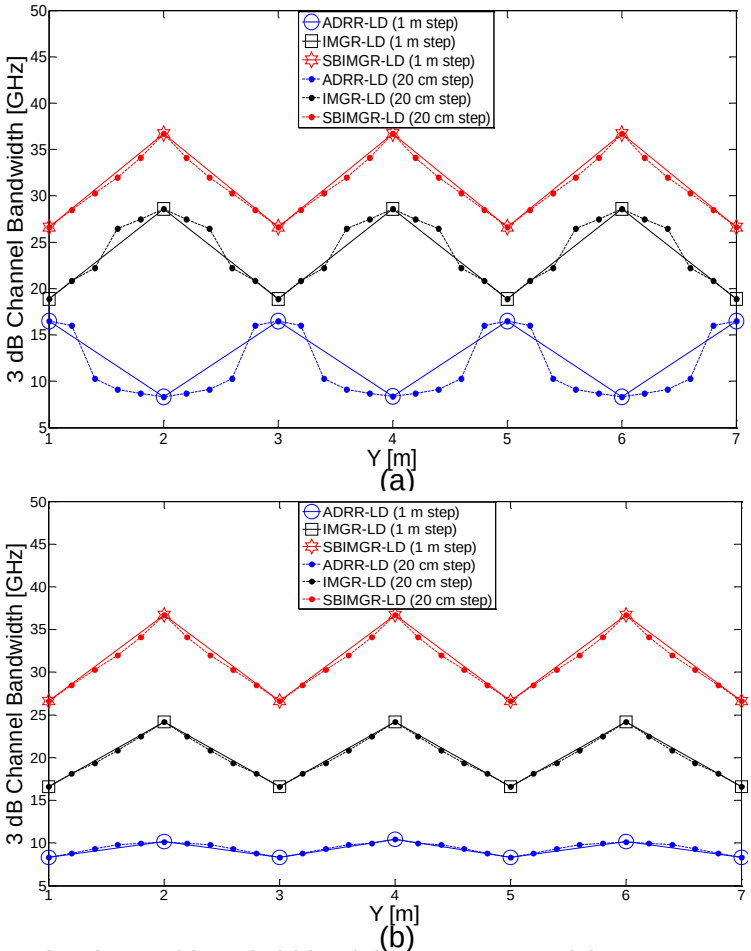

Figure 6.8: The 3 dB channel bandwidth of three systems, (a) at x=1m and (b) x=2m and along y-axis.

Third order reflections were also considered when the receiver was located at the worst case scenario position (2m, 4m, 1m). Table 6.1 shows the delay spread and 3 dB channel bandwidth of the proposed systems with and without third order reflections. The increase in the delay spread and reduction in receiver bandwidth were extremely small when the third order reflections were included. This can be attributed to strong LOS components and the limited range of the rays accepted by the small FOV branches of the ADR and pixels in the imaging receiver with narrow FOV. This is an important distinction between VLC systems and IROW systems, where, in the latter, third order reflections may play a significant role at high data rates [34]. Received power from the third order reflections for the three systems was extremely low compared to LOS, first order and second order reflections. For example, in the IMGR-LD system, the LOS, first order, second order and third order received powers were 6.36 μW, 0.2 μW, 0.131 μW and 0.01 μW respectively, which means that the third order reflections have a power contribution of about 0.14% of the total power received. Therefore, for convenience, computer analysis up to second order reflections has been considered in this thesis.

Table 6.1: Delay spread and 3 dB channel bandwidth with and without 3rd order reflections.

Receiver at (2m, 4m, 1m)	ADRR	IMGR	SBIMGR
Delay spread [ns] up to 2nd order reflections	0.0159	0.0064	0.0036
Delay spread [ns] up to 3rd order reflections	0.0162	0.0066	0.0037
3 dB channel bandwidth [GHz] up to 2nd order reflections	10.42	24.2	36.7
3 dB channel bandwidth [GHz] up to 3rd order reflections	10.28	23.5	36.2

6.4.4 SNR results

To evaluate the performance of ADRR-LD, IMGR-LD and SBIMGR-LD at high bit rates, the SNR was calculated at 10 Gb/s. Figure 6.9 shows the SNR_{MRC} of three mobile VLC systems operating at 10 Gb/s. The IMGR-LD and the SBIMGR-LD systems outperform the ADRR-LD system. The imaging receiver produced significant improvements in SNR compared to the ADR. This is attributed to reducing the contribution of the reflection component by using narrow FOV pixels and by appropriately weighing (MRC-fashion) the pixels' contributions resulting in an emphasis on the direct power component (i.e. LOS). SBIMGR-LD has lower SNRs values at x=1m and x=2m compared with the IMGR-LD system. This is due to only one source of information transmitting data (one relay transmits information), whereas in IMGR-LD eight relays emit information signals simultaneously and, at the receiver side, MRC is used which leads to significant improvement in SNR. Simulation results at x=1m showed that the IMGR-LD system achieved about 15.7 dB SNR when using the MRC approach. This means that the BER provided by our IMGR-LD system is better than 10^{-9} at 10 Gb/s. However, the SNR is observed to decay slightly when the receiver moved along the x=2m (BER better than 10^{-7}). This decay occurs due to the increased distance between relay and receiver. FEC can be used to reduce further the BER from 10^{-7} to 10^{-9} in this proposed IMGR-LD system.

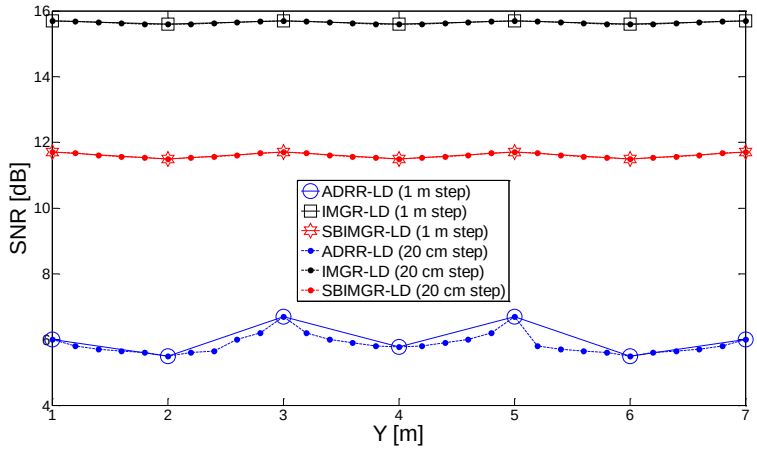

(a)

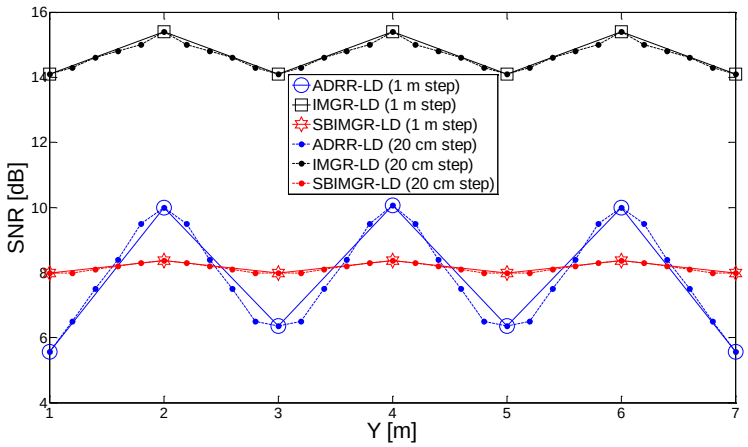

(b)

Figure 6.9: SNR of ADRR-LD, IMGR-LD and SBIMGR-LD systems when operated at 10 Gb/s (a) at x=1m and (b) at x=2m and along y-axis.

Higher data rates of 10 Gb/s is considered, and here we used the p-i-n FET receiver designed in [168].

Tables 6.2, 6.3 and 6.4 present the BER at 10 Gb/s of the ADRR-LD, IMGR-LD and SBIMGR-LD, respectively. Due to room symmetry, we calculated BER for 1 m to 4 m along the y-axis. If we compare the values in Tables 6.3, 6.4 and 6.5 for x=1m and x=2m, we can clearly see that the IMGR-LD system has the best performance compared to the other systems. At x=2m, the BER of the IMGR-LD system has increased slightly. However, this increase does not severely affect the performance of the system; for example, the smallest value of BER in Table 6.3 at x=2m is equal to 2.9×10^{-7}, and this value can provide a strong communication link.

Table 6.2: BER performance of ADRR-LD system.

x=1m				
Receiver Location y-axis	1m	2m	3m	4m
BER	2.8×10^{-2}	3.6×10^{-2}	1.4×10^{-2}	3×10^{-2}
x=2m				
Receiver Location y-axis	1m	2m	3m	4m
BER	2.9×10^{-2}	7.2×10^{-4}	2.3×10^{-2}	7.2×10^{-4}

Table 6.3: BER performance of IMGR-LD system.

x=1m				
Receiver Location y-axis	1m	2m	3m	4m
BER	5.6×10^{-10}	8.6×10^{-10}	5.6×10^{-10}	8.6×10^{-10}
x=2m				
Receiver Location y-axis	1m	2m	3m	4m
BER	2.9×10^{-7}	3.3×10^{-9}	2.9×10^{-7}	3.3×10^{-9}

Table 6.4: BER performance of SBIMGR-LD system.

x=1m				
Receiver Location y-axis	1m	2m	3m	4m
BER	7.2×10^{-5}	9.2×10^{-5}	7.2×10^{-5}	9.2×10^{-5}
x=2m				
Receiver Location y-axis	1m	2m	3m	4m
BER	6.2×10^{-3}	4.6×10^{-3}	6.2×10^{-3}	4.6×10^{-3}

In Figure 6.10, the SNR penalty was calculated based on the old CS and old DAT settings while in motion. The results show the SNR penalty incurred as a result of mobility. The proposed systems' design should allow a link margin. For instance, with a link power margin of 3 dB for ADRR-LD, Figure 6.10 shows that adaptation has to be done every time the receiver moves by 0.6 m approximately. If the SNR penalty is lower than 1 dB, as desired in ADRR-LD, then Figure 6.10 shows how often the system has to adapt its settings. For example, for the SNR penalty to be below 1 dB, the system has to adapt the CS and delay adaptation every 0.2 m approximately, which corresponds to a 0.2 second adaptation frequency. It should be noted that this adaptation has been done at the rate at which the environment changes and not at the system's bit rate. In addition, we can clearly see that the IMGR-LD and SBIMGR-LD systems outperform the ADRR-LD and this is due to using the imaging receiver instead of the ADR.

6.5 Small Office Environment

A simulation tool was developed to model a new VLC room with dimensions of 5×5×3 m^3 to enable comparison with previous work [28], [147] (room dimensions, source distribution, surrounding surface reflectance and receiver positions are similar to [28]), and to evaluate the performance of the proposed systems in two different room sizes. The results are presented in terms of delay spread and SNR, and compared to the results presented in the previous Section. Figure 6.11 shows the new VLC room (small office).

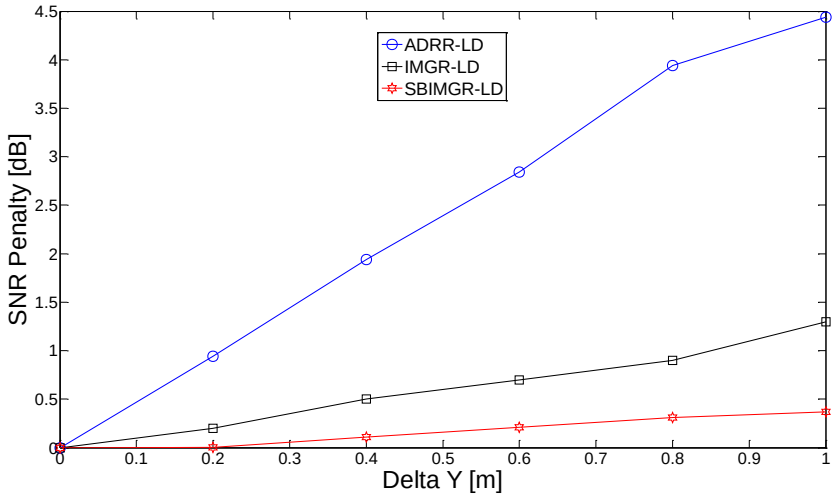

Figure 6.10: The SNR penalty of proposed systems when the receiver moves from the optimum location at (2m, 1m, 1m) along y-axis.

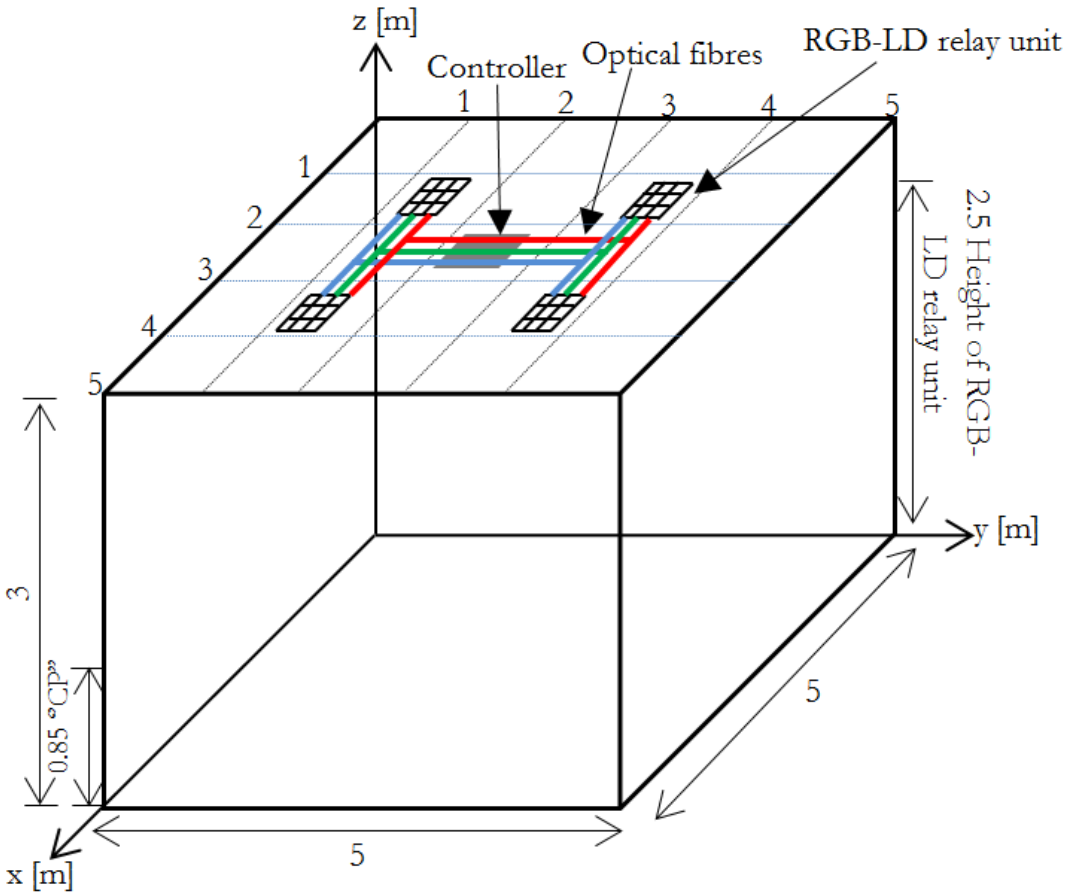

Figure 6.11: VLC system room with dimensions of 5×5×3 m^3.

6.5.1 Delay spread

Figure 6.12 presents the delay spread of the proposed systems when receivers were moved at x=1.25m (line underneath relay units) and x=2.5m (middle of the room) along the y-axis. It should be noted that the delay spread of the proposed systems in the small office (5×5×3 m^3) is much lower than that in the large office (4×8×3 m^3), and this could be due to two reasons: 1) the distance between the relay unit and receiver is less than that in the large office and 2) decreasing the room size leads to a decrease in the number of reflectance elements which decreases the power received from the reflections. The delay spread results are comparable to the results in [147]. However, in the current work the delay spread becomes very low because we used an imaging receiver and ADR with narrow FOV, which lead to a reduction in the effect of the reflection components. Due to the symmetry of the room, the results for x=1.25m, y=1 are equal to the results for x=1.25m, y=4 (or y=2 and y=3); a similar behaviour was observed when the receiver moved along the x=2.5m line.

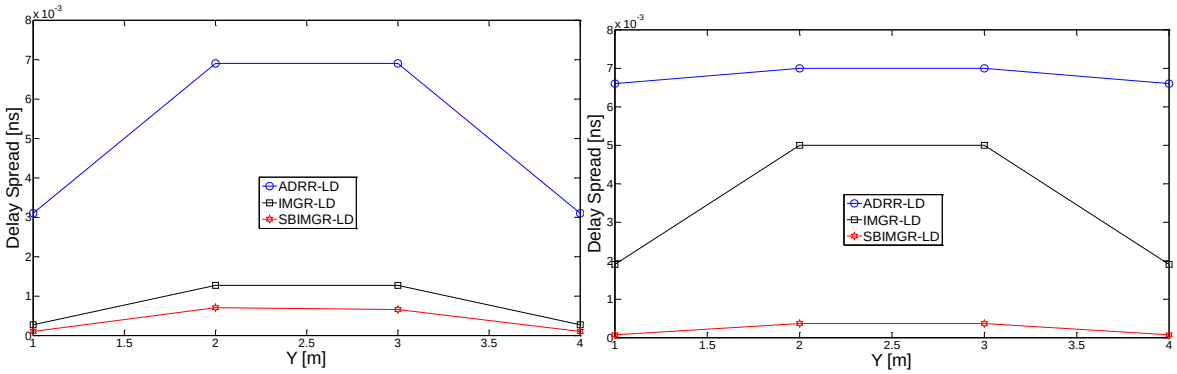

Figure 6.12: Delay spread of three systems, (a) at x=1.25m and (b) at x=2.5m and along y-axis.

6.5.2 SNR

Figure 6.13 illustrates the SNR of the proposed systems at high data rates (10 Gb/s) in the small office. It was observed that the SNR of the three systems in

the small room was higher than that in the large room due to the small distance between the transmitter and receiver, which lead to a reduced path loss and increased SNR. It should be noted that the IMGR-LD system outperformed the other systems (ADRR-LD and SBIMGR-LD) in the small office (5×5×3 m^3), as it did in the large office (4×8×3 m^3).

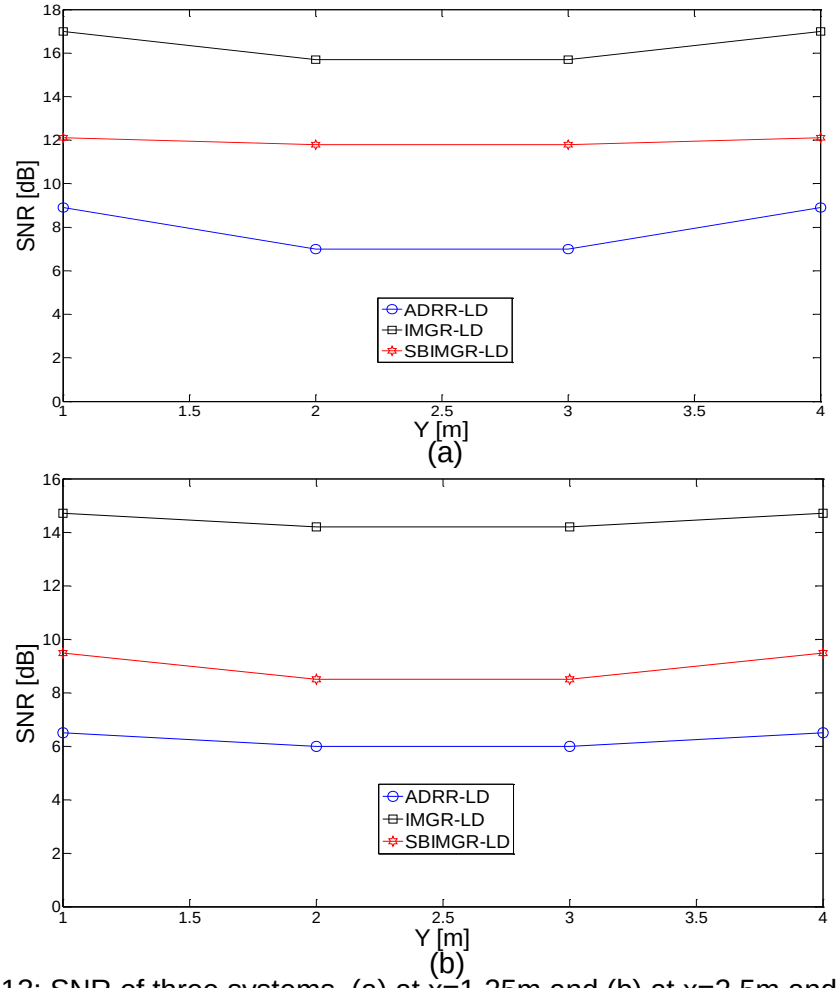

Figure 6.13: SNR of three systems, (a) at x=1.25m and (b) at x=2.5m and along y-axis.

6.6 Effect of Realistic Indoor Environment

Shadowing, signal blockage and mobility are among the main impairments that impact the performance of VLC systems in indoor environments. Therefore, we extended the analysis and evaluation of the performance of the proposed systems to a harsh indoor environment with mobility. The simulation was

conducted in a room that was comparable in dimensions to that explained in Section 6.2 (see Figure 6.1). The realistic room environment is similar to that in Chapter 5, Section 5.3 (Figure 5.1b). In Section 6.3 a simulation package based on a ray tracing algorithm was developed using MATLAB to compute the impulse response of the different VLC systems in an empty room. In the realistic environment for each receiver location, the first step is to check the availability of the LOS component (certain conditions were introduced to the simulator to check the existence of LOS, first and second order reflection components in each location) and then the received power due to first and second order reflections is calculated. In some locations over the CP some of the LOS components were blocked by mini cubicles, and this affected the SNR severely. Figure 6.14 shows a block diagram of the simulator with ADR and imaging receiver.

6.6.1 Impulse response

Channel impulse responses at the room centre (i.e. x=2m and y=4m, chosen as they represent the worst communication link over the entire CP (motion between cubicles)) for the ADRR-LD, IMGR-LD and SBIMGR-LD systems are shown in Figure 6.15 for rooms A and B (room A is an empty room and room B is a realistic room). It should be noted that the impulse responses of the proposed systems were dominated by short initial impulses due to the LOS paths between the transmitters and receiver. In addition, it can be clearly seen that the IMGR-LD and SBIMGR-LD systems have good robustness against shadowing and mobility.

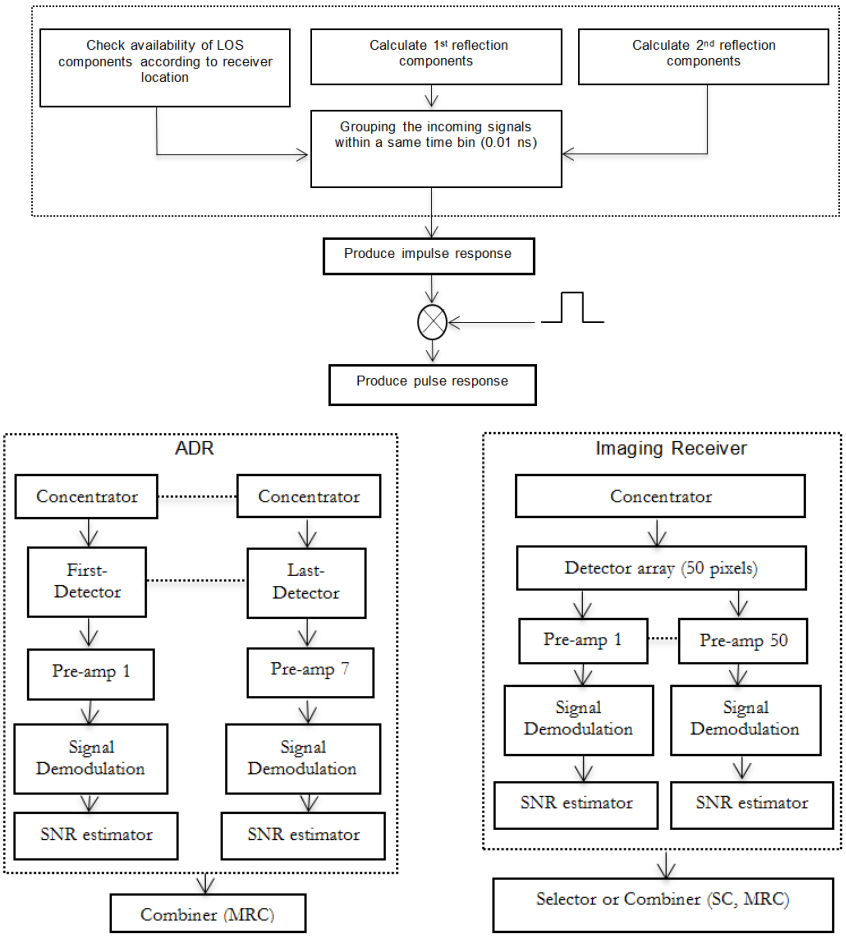

Figure 6.14: Block diagram of simulator.

However, the amount of received optical power from the reflections in room B was less than that received in room A, as shown in Figure 6.15, and this was due to the existence of the door, windows, cubicles, partitions and bookshelves in room B that lead to reduced multipath propagation. Although the received power from the reflections was severely affected in room B, the LOS component remained the same in both room configurations in both systems, and the LOS component had the largest impact on the system performance. For example, the received optical power associated with the IMGR-LD system in room A was 6.69 μW, whereas it was 6.63 μW in room B, which indicates that the reduction in power was negligible (the reduction in power was 0.063

μW). Moreover, it can be noted that the effect of shadowing on the ADRR-LD system was clear when the receiver was located at the room centre in room B. The LOS received power in room A was 4.5 μW, whereas it was 2.25 μW in room B (about 3 dB reduction in received power), and this was due to one of the LOS components being blocked by the wall of a cubicle. These impulse responses suggest that the ADRR-LD system performs better in room A (without shadowing) than in room B, and the IMGR-LD and SBIMGR-LD systems were affected by the shadowing geometry considered (office cubicles).

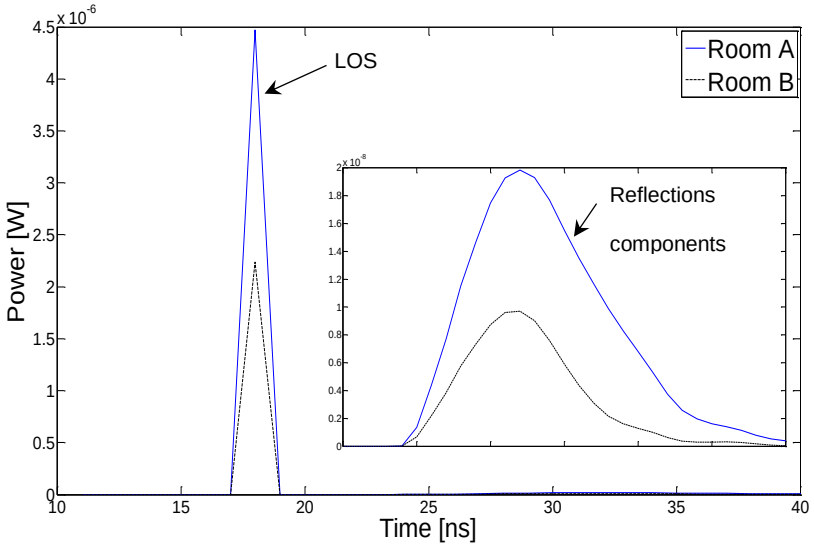

(a)

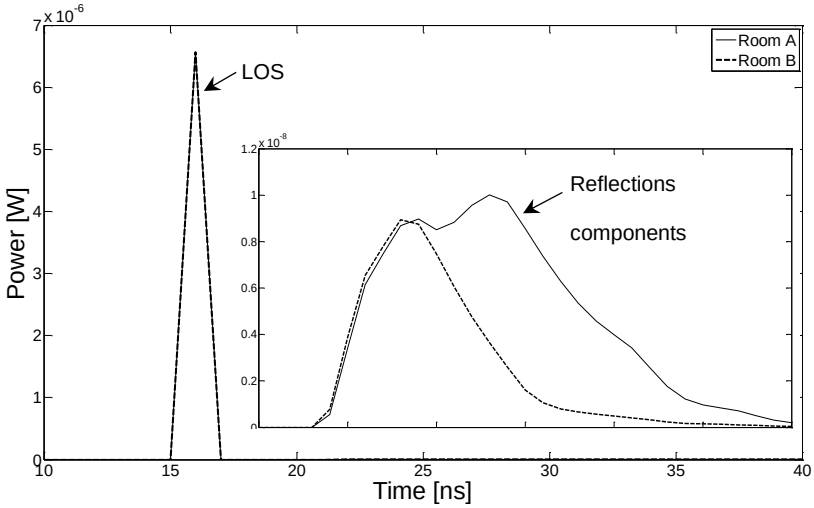

(b)

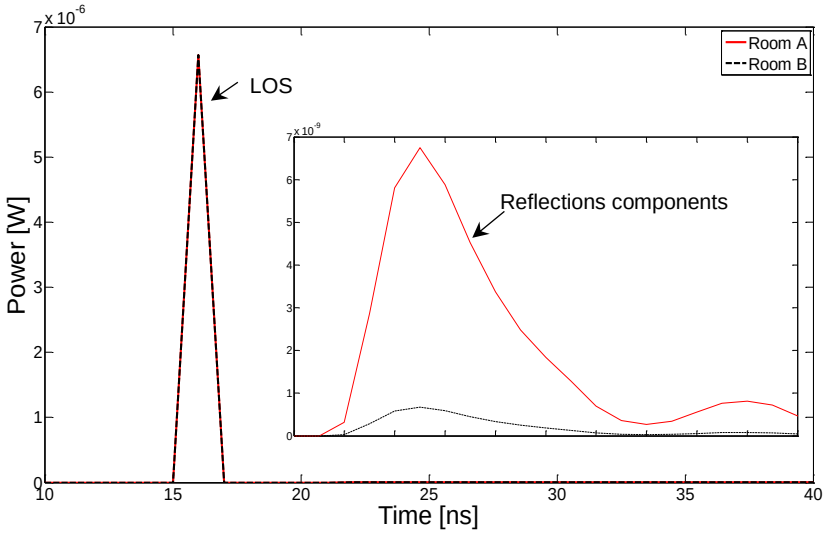

(c)

Figure 6.15: Impulse responses at room centre (x=2m, y=4m, z=1m) in two different environments (rooms A and B) (a) ADRR-LD, (b) IMGR-LD and (c) SBIMGR-LD.

6.6.2 SNR

Figure 6.16 shows the SNR results against receiver location for the proposed systems in the two room scenarios. It is observed that the performance of the IMGR-LD and SBIMGR-LD systems are comparable in rooms A and B, and this can be attributed to the LOS links available in the entire CP, which protects against shadowing and mobility in these systems. It can be noticed that the ADRR-LD system has lower SNR in room B than in room A (3 dB SNR reduction approximately). This is because, when the ADR moves along lines x=1m and x=2m, some transmitters (RGB-LD relay unit) cannot be detected by receivers due to cubicles. The proposed systems are able to achieve a very high channel bandwidth (8.3 GHz and beyond, see Figure 6.8), which is more than enough to operate at 10 Gb/s. In addition, the backbone of the room network is fibre cable that is able to carry 10 Gb/s, and the modulation bandwidth of the LD (the sources used in our work) can be in the GHz range (off-the-shelf LD). Furthermore, the photo detector (PD) area that was used in our work (imaging receiver and ADR) was very small (4 mm^2) to ensure that the

internal capacitance of the PD would not affect the performance of our receivers. The fabrication and testing of a high speed VLC receiver array are very challenging tasks. To the best of our knowledge, there is no commercial high speed VLC receiver to date that has specially been designed for indoor VLC use. At a data rate of 10 Gb/s, most of the components will probably be adopted from the IROW and optical fibre domain [179], which is not ideal for VLC.

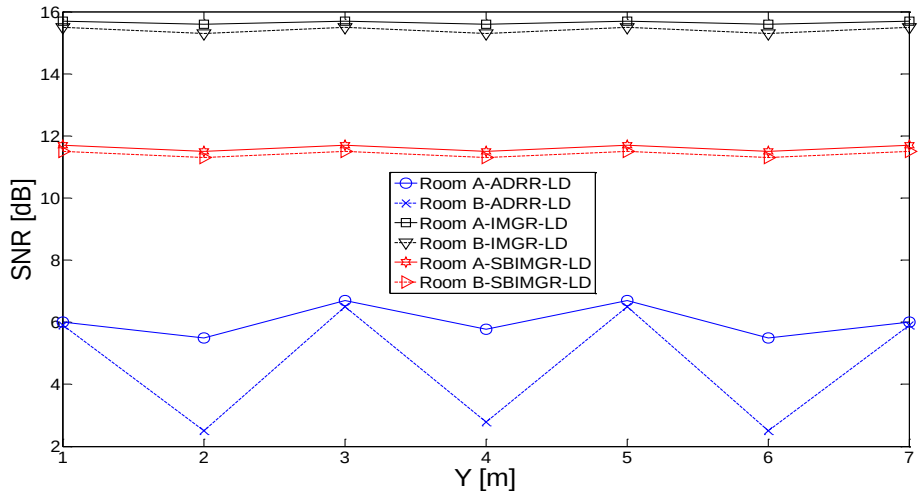

(a)

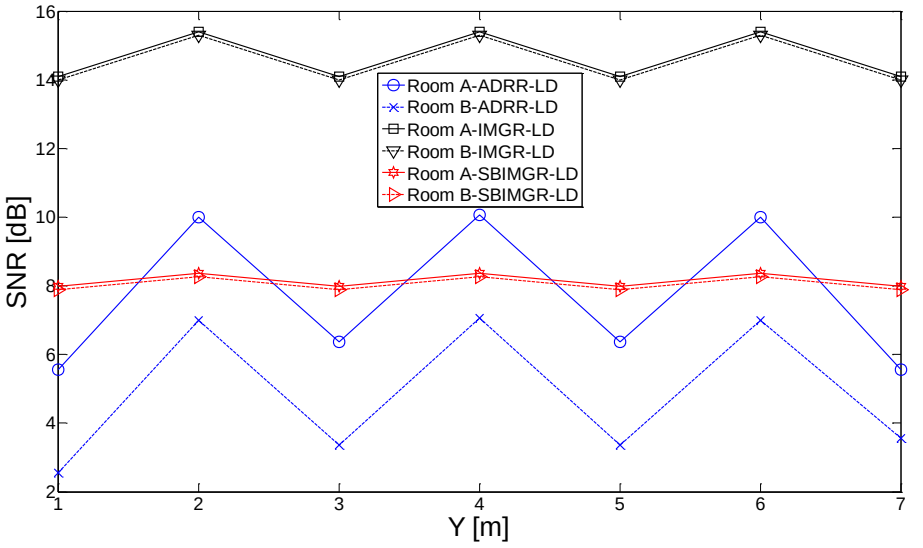

(b)

Figure 6.16: SNR of ADRR-LD, IMGR-LD and SBIMGR-LD systems in two different environments (rooms A and B) when the systems operated at 10 Gb/s at (a) x=1m and (b) x=2m and along the y-axis.

6.7 Summary

In this chapter, we proposed, designed and investigated the concept of relays in a VLC system. We introduced two novel algorithms (CS and SB) to create optimum transmitter-relay and relay-receiver communication links. Three novel VLC systems (ADRR-LD, IMGR-LD and SBIMGR-LD) are introduced. These VLC systems use LD instead of LEDs as transmitters, and they use two different types of receiver: an ADR with 7 branches and an imaging receiver with 50 pixels. We optimised the FOVs, AZs and ELs of the ADR and the FOVs of the imaging receiver. In the worst case scenario, SBIMGR-LD achieves significant improvements in VLC channel bandwidth and delay spread over the ADRR-LD and IMGR-LD systems. It has the ability to achieve 26 GHz channel bandwidth (about 0.0058 ns delay spread). On the other hand, the IMGR-LD outperforms the ADRR-LD and the SBIMGR-LD systems in SNR (14.1 dB in the worst case scenario). The BER provided by our IMGR-LD system is better than 10^{-7} at 10 Gb/s in the worst case scenario.

Different room sizes were also considered to examine the performance of the proposed systems. The performance of the proposed systems was better in the small office than the large office and this is due to the distance between the transmitter and receiver, which was smaller and led to reduced path loss, delay spread and increased SNR.

The proposed systems were evaluated under diverse situations including an empty room and a realistic room. The IMGR-LD and SBIMGR-LD systems have good robustness against shadowing and mobility. However, the ADRR-LD system performance was severely affected when it is operated in the realistic environment characterised by shadowing.

7 Mobile Indoor Visible Light Communication System Employing Beam Steering and Computer Generated Holograms

7.1 Introduction

VLC systems have typically operated at data rates below 10 Gb/s and operation at this data rate was shown to be feasible by using LD, imaging receivers, relay nodes and delay adaptation techniques (DAT imaging LD-VLC system in Chapter 5 and IMGR-LD system in Chapter 6). However, higher data rates, beyond 10 Gb/s, are challenging due to the low SNR and ISI. In this chapter, for the first time, to the best of our knowledge, we propose, design and evaluate a VLC system that employs beam steering (of part of the VLC beam) using adaptive finite vocabulary of holograms in conjunction with an imaging receiver and a delay adaptation technique to enhance SNR and to mitigate the impact of ISI at high data rates (20 Gb/s). An algorithm was used to estimate the receiver location, so that part of the white light can be directed towards a desired target (receiver) using beam steering to improve SNR. Simulation results of our location estimation algorithm (LEA) indicated that the required time to estimate the position of the VLC receiver is typically within 224 ms in our system and environment. A finite vocabulary of stored holograms is introduced to identify the best location to steer the beam to the receiver location. The beam steering approach improved the SNR of the fully adaptive VLC system by 15 dB at high data rates (20 Gb/s) over the DAT imaging LD-VLC system in the worst case scenario.

Previous chapters have shown that significant enhancements in the VLC system data rates can be achieved by replacing LEDs with LD coupled with the use of an imaging receiver instead of the conventional wide FOV receiver [100], [103]. In addition, performance evaluations were carried out for a mobile multi-gigabit VLC system in two different environments in the previous chapters. A rate of 10 Gb/s in a realistic environment has been shown to be possible with a VLC system when a delay adaptation technique in conjunction with laser diodes and imaging receiver were used with a simple modulation format (OOK) [103]. Significant improvements were shown to be possible when a VLC relay assisted system is combined with an imaging receiver and a delay adaptation technique [101]. However given typical parameters, the latter system cannot provide a throughput beyond 10 Gb/s due to its low SNR.

Beam steering has been widely investigated in communication systems to maximise the SNR at the receiver [86], [163], [180]. Therefore, beam steering can also be an attractive option to consider in VLC systems to enhance the system performance. Recently, transmission beam steering for MIMO IROW systems with intensity modulation and direct detection has been developed [181]. In addition, recent work has demonstrated optical wireless energy transmission using optical beam steering and beam forming with a spatial light modulator (SLM). They focused light on the desired target using optical beam steering and beam forming to transfer optical wireless energy [182]. A VLC beam steering array can be constructed using electronically controlled mirrors in front of the receiver. An inexpensive approach that can be used to provide good link quality during mobility is to use mirrors with piezoelectric actuators in front of the receiver [4], [129]. Another approach is the tilting of the transmitter and receiver together using piezoelectric actuators that are controlled electronically. As with the mirror method, the tilting method also needs to be controlled by an electronic circuit. However, these methods lead to a bulky receiver and cannot be used for mobile devices [4].

Recently, various approaches for VLC indoor positioning systems have been researched [131], [132]. VLC systems are a promising solution for indoor positioning due to many features. Firstly, there is better positioning accuracy (few millimetres) compared to radio wave systems, since VLC suffers less from interference and multipath effects. Secondly, VLC positioning systems can be used in environments where radio positioning systems are restricted, such as in hospitals [133].

The work presented in this chapter aims to address the impairments of VLC systems and provide practical solutions, hence achieving data rates beyond those reported in the previous chapters. In this chapter, we propose a novel LEA and beam steering (BSR) technique to improve the SNR of a VLC system at high data rates (20 Gb/s and beyond). In addition, we introduce a new adaptive finite vocabulary hologram approach for beam steering making use of simulated annealing optimisation. To best of our knowledge this represents the first time these techniques are used in VLC systems. The holograms are pre-calculated and stored in the proposed system (each is suited for a given (range of) transmitter and receiver locations) and eliminate the need to calculate holograms real time at each transmitter and receiver location. The concept of finite adaptive computer-generated holograms has been recently proposed in [183], [184] and it is adapted here for the first time to VLC systems.

The first step is to estimate the receiver location using the LEA algorithm then the BSR technique steers part of RGB-LD white light to the VLC receiver, which leads to enhanced received SNR. The enhancement in the signal strength by the BSR approach can improve the transmission distance. Imaging receivers were shown to be attractive and efficient in mitigating the effects of ambient light and pulse spread in infrared optical wireless systems [87], [88], [162], [170]. In our previous work we proposed the use of an imaging receiver for a VLC system to provide a robust link and mitigate multipath dispersion, as well as to improve the overall system performance. In this chapter we used an

imaging receiver and two types of diversity schemes SC and MRC to choose or add the received power collected by different pixels. A DAT for a VLC system was proposed in and it is used here as it was shown to offer channel bandwidths of more than 36 GHz, which enables the VLC system to operate at data rates of more than 20 Gb/s. The adaptation techniques (LEA, BSR and DAT) require a repetitive training and feedback channel from the receiver to transmitter at a low data rate. An IR diffuse channel is suggested to achieve this channel. The ultimate goal of this work is to enhance the SNR at high data rates, reduce the effect of receiver mobility and minimise delay spread (maximise channel bandwidth) within a realistic environment.

The rest of the chapter is organised as follows: The VLC system model is described in the next Section. Section 7.3 describes the VLC systems' configurations. The impact of beam steering on illumination is investigated in Section 7.4. Adaptive finite vocabulary of holograms for VLC is considered in Section 7.5. The simulation results in an empty room are outlined in Section 7.6. Robustness against shadowing is evaluated in Section 7.7. A high speed adaptive mobile VLC system is introduced in Section 7.8. Finally, a summary is presented in Section 7.9.

7.2 Simulation Setup

To evaluate our proposed techniques (LEA, BSR and DAT), a simulation was conducted in an empty room with dimensions of 4m×8m×3m (width × length × height). The simulation tool used is similar to the ones used in previous chapters (3, 4, 5, and 6). The simulations and calculations reported in this chapter were carried out using MATLAB. In our evaluation, the channel characteristics, optical power received, delay spread, 3 dB channel bandwidth and SNR calculations were determined in similar ways to those used in Chapters 3, 4, 5 and 6. Imaging receiver with 50 pixels is used to reduce the impact of multipath dispersion. The imaging receiver design provided in

Chapters 4 and it is used here with BSR technique. To enable BSR technique three different holograms should be used at each light unit and this is due to using RGB-LD (i.e., a different hologram for each colour). The VLC room with the coordinates of the RGB-LD light units and the imaging receiver is shown in Figure 7.1.

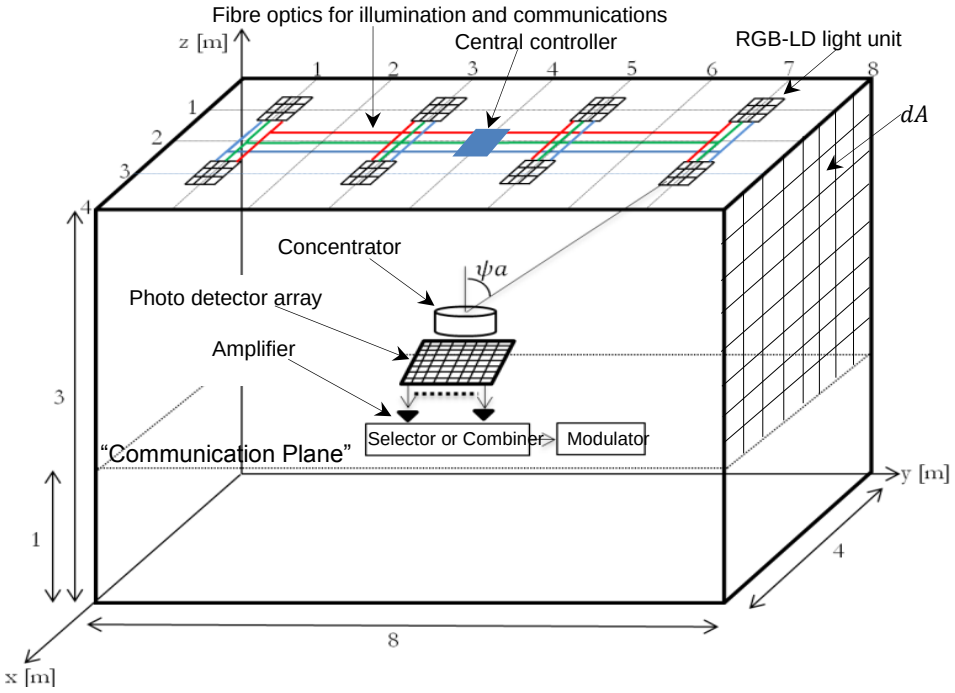

Figure 7.1: VLC system room and the physical structure of imaging receiver.

The imaging receiver is always placed on the communication plane along the x=1m and x=2m lines (see Figure 7.2). Each pixel in the imaging receiver has its own amplifier to amplify the received photocurrent (see Figure 7.1). In our previous work, a simulation package based on a ray tracing algorithm was developed to compute the impulse response for different VLC systems. In this chapter, additional features were introduced to enable LEA, BSR and delay adaptation.

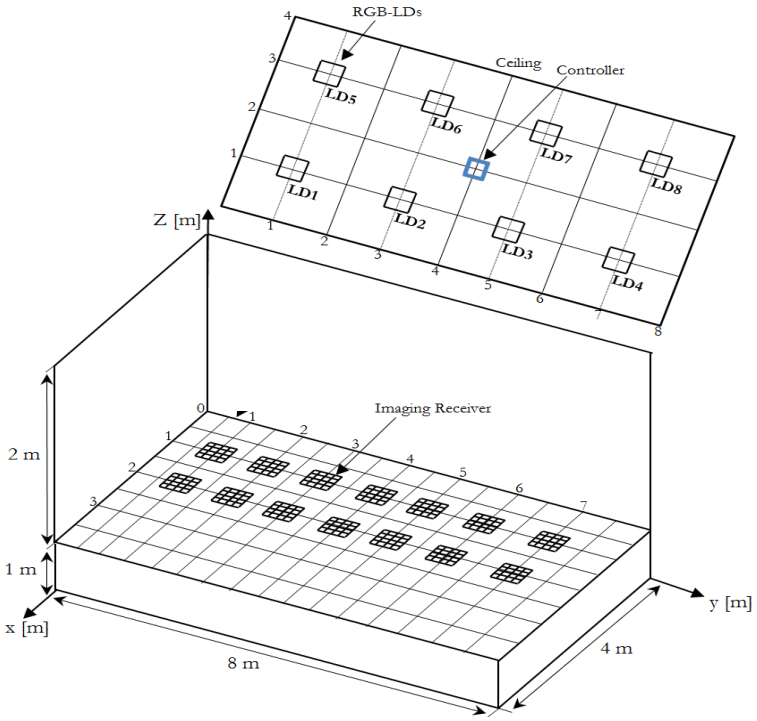

Figure 7.2: Imaging receiver test area locations on communication plane.

7.3 VLC Systems' Configurations

In this section, four VLC systems are presented, analysed and compared to identify the most appropriate system for use in high-speed VLC systems (20 Gb/s and beyond).

7.3.1 Imaging LD-VLC system

The imaging LD-VLC system employed eight RGB-LD transmitters (lighting fixtures) on the ceiling connected by fibre interconnect and controlled by a central controller and an imaging receiver with 50 pixels. The imaging LD-VLC system was proposed in Chapter 4 [103] and it is considered here to compare it with our new proposed VLC systems.

7.3.2 DAT imaging LD-VLC system

The DAT imaging LD-VLC system has a similar configuration as the previous system. However, the delay adaptation technique is combined with imaging LD-VLC (DAT imaging LD-VLC) to enhance the overall system performance. The DAT imaging LD-VLC system was previously proposed in Chapter 5 [103].

7.3.3 Beam steering LD-VLC system

The newly proposed beam steering LD-VLC system has a similar room configuration and uses the same transmitters and receiver as in the previous systems. However, three new algorithms were introduced to enable the system to achieve data rates higher than 10 Gb/s. Select-the-best (STB), LEA and BSR algorithms were used to enhance the SNR of the new VLC system.

7.3.4 Fully adaptive VLC system

In contrast to the beam steering LD-VLC system, the fully adaptive VLC system employed the delay adaptation technique to further improve the communication link performance. In contrast to our previous work in [100]-[103] where the RGB-LD light unit had a fixed form pattern, we propose here a fully adaptive VLC system where the transmitter (RGB-LD light unit) has the ability to direct part of the white light towards the receiver location to enhance the SNR when operating at high data rates. LEA and BSR were implemented in a certain RGB-LD light unit for a single receiver at a given set of positions; when the receiver starts moving, they are applied in another RGB-LD light unit according to the new receiver location (coordinates). The SNR improvement at high data rates (i.e., 20 Gb/s) could be achieved according to the following algorithms:-

- STB algorithm is proposed to locate the closest transmitter (RGB-LD) to the receiver to implement LEA and BSR. The STB algorithm identifies the closest transmitter to the receiver according to the following steps:

  1- A pilot signal is sent from one of the VLC transmitters.
  2- The SNR is estimated at the receiver by pixel 1 of the imaging receiver.
  3- Repeat step 2 for the other pixels in the imaging receiver.
  4- Repeat steps 2 and 3 for the other VLC transmitter units.
  5- The receiver sends (using an infrared beam) a low data rate control feedback signal to inform the controller of the SNRs associated with each transmitter.
  6- The transmitter that yields the best SNR is chosen by the controller (typically the closest transmitter to the receiver in our simulations).

It should be noted that the RGB-LD light units should always be ‘ON’ to provide illumination for the room. The information signals are coded (each RGB-LD unit has its own code) and sent from each RGB-LD light unit by the central controller. Once the receiver receives the coded signal from the RGB-LD light unit, the SNR is computed and a feedback signal is sent. If the time taken to calculate the value of each SNR with each RGB-LD unit is equal to 1 ms then the STB algorithm training time is 8 ms (8 RGB-LD units × 1 ms).

- A new LEA is introduced to the VLC system to identify the optimum location to carry out optical BSR. The RGB-LD light unit that has been chosen in the STB algorithm initially produces a single beam using a computer generated hologram (CGH) and scans it along a number of possible locations in the room to identify the location of the receiver. At each beam setting the receiver computes the SNR and the optimum beam location is selected at the controller. The location estimation algorithm is an effective approach

that can help identify the optimum direction for BSR in a way that gives the best SNR at the receiver.

The RGB-LD light unit is followed by the CGH that generates beams whose locations can be varied where the transmission angles θ_x and θ_y in the xy-axes are varied between -70^o and 70^o (half power beam angle of RGB-LD light unit was 70^o) with respect to the transmitter's normal in both the x and the y (α_{-x} to α_x and α_{-y} to α_y) directions respectively. The LEA produces a single beam and scans it with step angle (β) along a range of rows and columns in the room to identify the location that yields the best receiver SNR. The coordinates of this location are used as the centre of the BSR direction. β is chosen to be large in the first iteration (26.5^o, which allows the spot to move 100 cm) to reduce the number of locations that have to be scanned. The angle is then reduced by a factor of two in each following iteration. The position that results in the best SNR is identified as a sub-optimum location, and the area that includes this sub-optimum location is selected as a new scanning area for the next iteration. A number of iterations are carried out until the final optimum location is identified (eight scan iterations are considered to achieve β=0.28^o or step size of 1 cm). The LEA scans 224 possible locations in eight iterations until reaching the target step size (1 cm). The LEA determines the two transmission angles θ_x and θ_y that identify the coordinates (x, y, z) of the best SNR location according to the following steps:

1- Configure the RGB-LD light unit to implement scan locations according to the associated parameters: the x-axis scan range (θ_x^{Start} to θ_x^{End}), the y-axis scan range ($\theta_y^{Start}$to θ_y^{End}) and the step angle (β). A single beam is moved by changing the beam angles between -70^o and 70^o in steps of β to determine the sub-optimum location. Some of the scan points will be on the walls due to the RGB-LD light unit's position, as shown in Figure 7.3.

2- The SNR is computed at each step and the receiver sends a control feedback signal at a low rate to inform the controller of the SNR associated with each scan. This feedback channel can be implemented using an infrared beam.
3- Compare the SNR computed and recorded with the associated transmission angles θ_x and θ_y that give the maximum SNR.
4- Determine the sub-optimum coordinates (xs, ys, zs) of the beam that produces the sub-optimum SNR based on its transmission angles θ_x and θ_y.
5- To configure the next iteration, the controller identifies the area that includes the sub-optimum location from θ_x and θ_y and assigns it as the boundary angles of the new scanning area (α_{-x} to α_x and α_{-y} to α_y).
6- β is reduced by a factor of two.
7- Repeat steps 1 to 4 to identify the best location that gives the highest SNR. The iterations stop when $\beta \leq 0.28^o$ (beam step is 1 cm).
8- The controller assigns the optimum location with the coordinates (x, y, z) to the transmitter.

❖ The new BSR technique focuses a part of the light of one of the RGB-LD towards the coordinates that were found by the LEA algorithm. According to the illumination results, which will be discussed in the next section, up to 20% of the RGB-LD light unit can be beam steered towards the receiver's location while the remaining white light (i.e., 80%) is used for illumination.

The adaptation techniques (LEA, BSR and DAT) require a repetitive training and feedback channel from the receiver to transmitter at a low data rate. A diffuse IR channel (λ=850 nm) is suggested to achieve this channel. An IR detector is attached to the RGB-LD light unit.

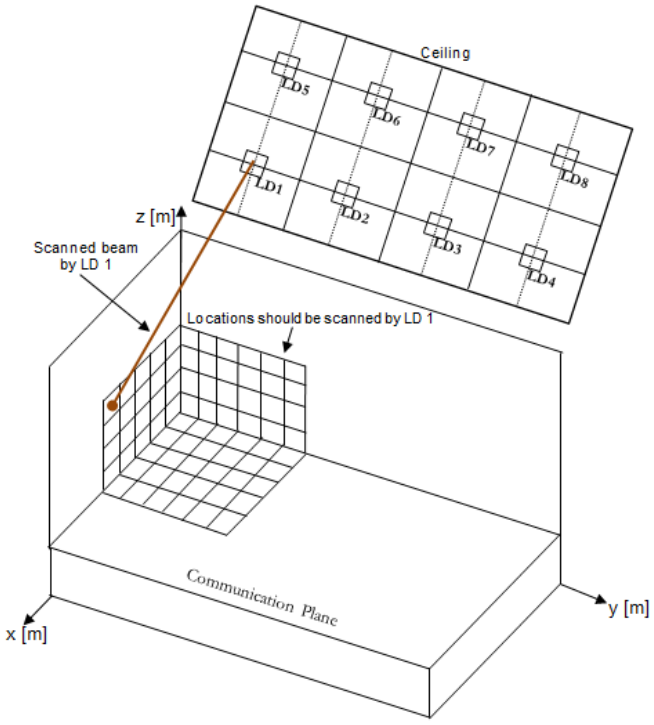

Figure 7.3: LEA implemented at one of corner RGB-LD light units.

Heat sources such as RGB-LD light unit may negatively affect the performance of the feedback channel (IR diffuse) as they may be considered as interference sources [185]. However, it should be noted that in this work we have used the RGB-LD light units which have lower heat emission than conventional lamps such as halogen or incandescent. In addition, the main function of this channel is to send a feedback signal and the data rates used in this channel are very low (i.e., tens of kb/s). Figure 7.4 shows a block diagram of the transmitter and receiver with uplink and downlink channels. The CGH in the transmitter is used for beam steering, and it is a transparent or reflective device that is used to spatially modulate the phase or amplitude of each pixel [186]. The CGH devices have μs to ms response times that are sufficient to carry out the BSR technique at the rate of mobile receiver movements [187]. The CGH and control circuit can generate beams to scan the communication plane and estimate the receiver location (see Figure 7.5). Changing the holographic function through the control circuit can generate variable optical beam locations on the

communication plane with different switching times. Once, the beam steering technique is applied, delay adaptation can be utilised to reduce the effect of multipath and reduce the delay spread (increase channel bandwidth). An imaging receiver employing narrow FOV pixels can be used to mitigate the effect of multipath propagation due to the limited range of rays received. However, it has been seen in a VLC system that the delay spread is influenced by the RGB-LD spots' relative positions and the number of RGB-LD spots seen by the FOV of each pixel [103]. Thus, emitting signals from all RGB-LD units at the same time may cause a time delay differential between the signals received at the pixel, which results in spreading the received pulse and hence limiting the bandwidth. The delay adaptation algorithm for a VLC system was proposed in Chapter 5 [103], and it is used here to offer improvements in terms of bandwidth efficiency. The delay adaptation can be implemented through array elements delayed switching.

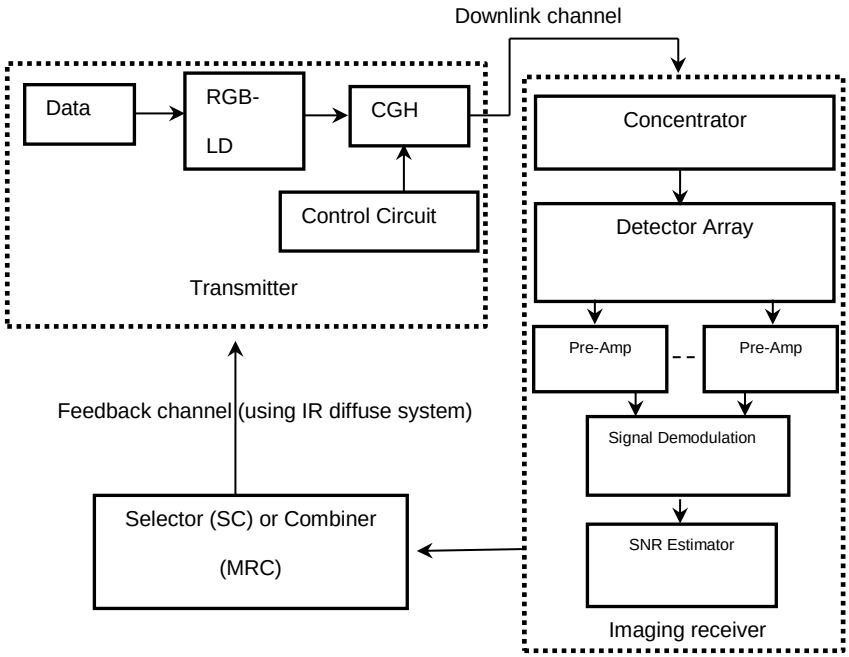

Figure 7.4: Block diagram of fully adaptive VLC system.

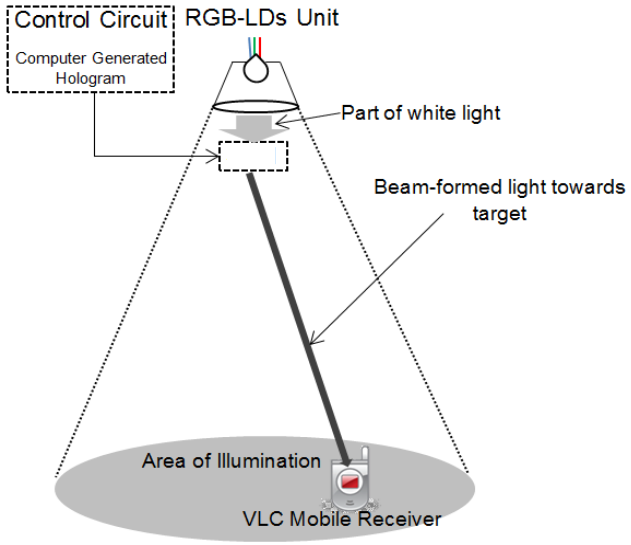

Figure 7.5: Beam steering technique applied at one of RGB-LD light unit.

A pedestrian user moves indoor at a speed of about 1 m/s [166]. We therefore propose that the receiver re-estimates its SNR and delay values for all RGB-LD light units at the start of a one second frame, and if these have changed compared to the previous frame's values then the receiver uses the feedback channel to update the controller. The LEA and the delay adaptation method training time will be 296 ms (224 possible locations should be scanned in all iterations × 1 ms + 9 RGB-LD in each transmitter unit × 8 transmitter units × 1 ms). This time (296 ms, once every one second frame) is sufficient given that LEA and delay adaptation have to be carried out at the rate at which the environment changes (pedestrian movement). Therefore, the beam steering LD-VLC system can achieve 100% of the specified data rate when it is stationary, and 70.4% in the case of user movement, (user or object movement in the room). The 30 % overhead (data loss in the case of user movement) is considered too high. Therefore, fast and efficient algorithms should be implemented to reduce the loss in data rate during mobility. LEA, BSR and delay adaptation algorithms are carried out at one given receiver location for the single user scenario to enhance the SNR and bandwidth at the receiver, and

this can be achieved through the algorithms given in Figure 7.6. In the case of a multiple user scenario, opportunistic scheduling [167] can be used where LEA, BSR and delay adaptation algorithms are implemented opportunistically (or randomly between users/regions) to maximise the 3 dB channel bandwidth and the SNR in a given region for a given time period. The MAC protocol should include a repetitive training period to perform the algorithms in Figure 7.6.

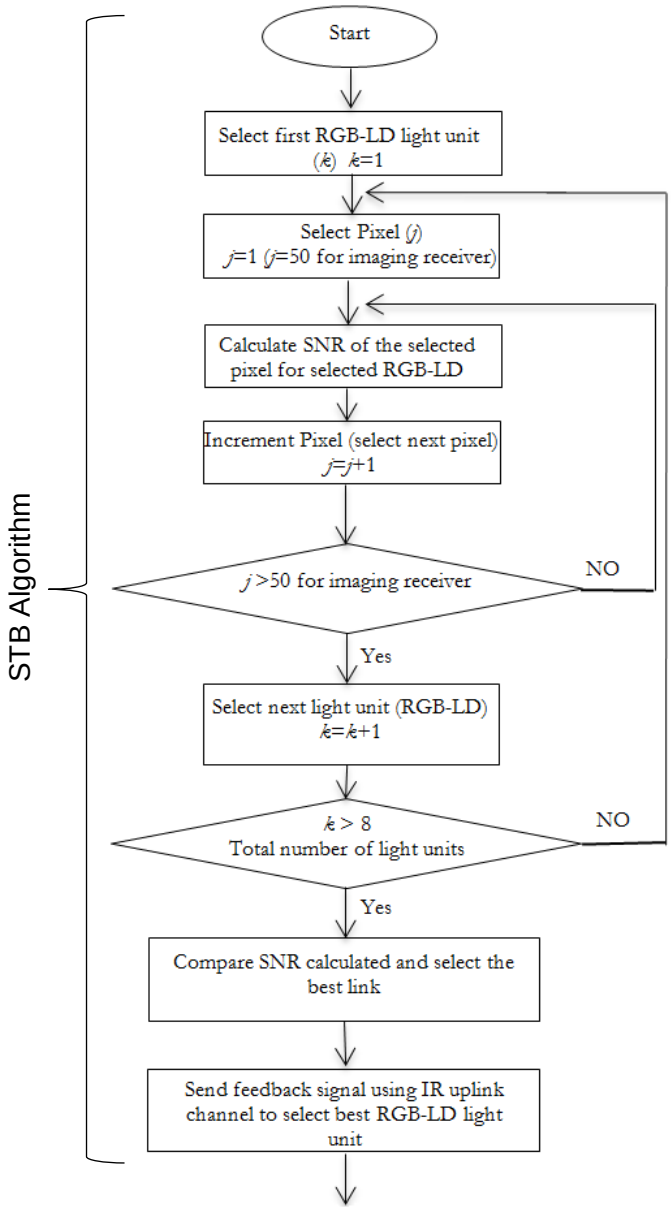

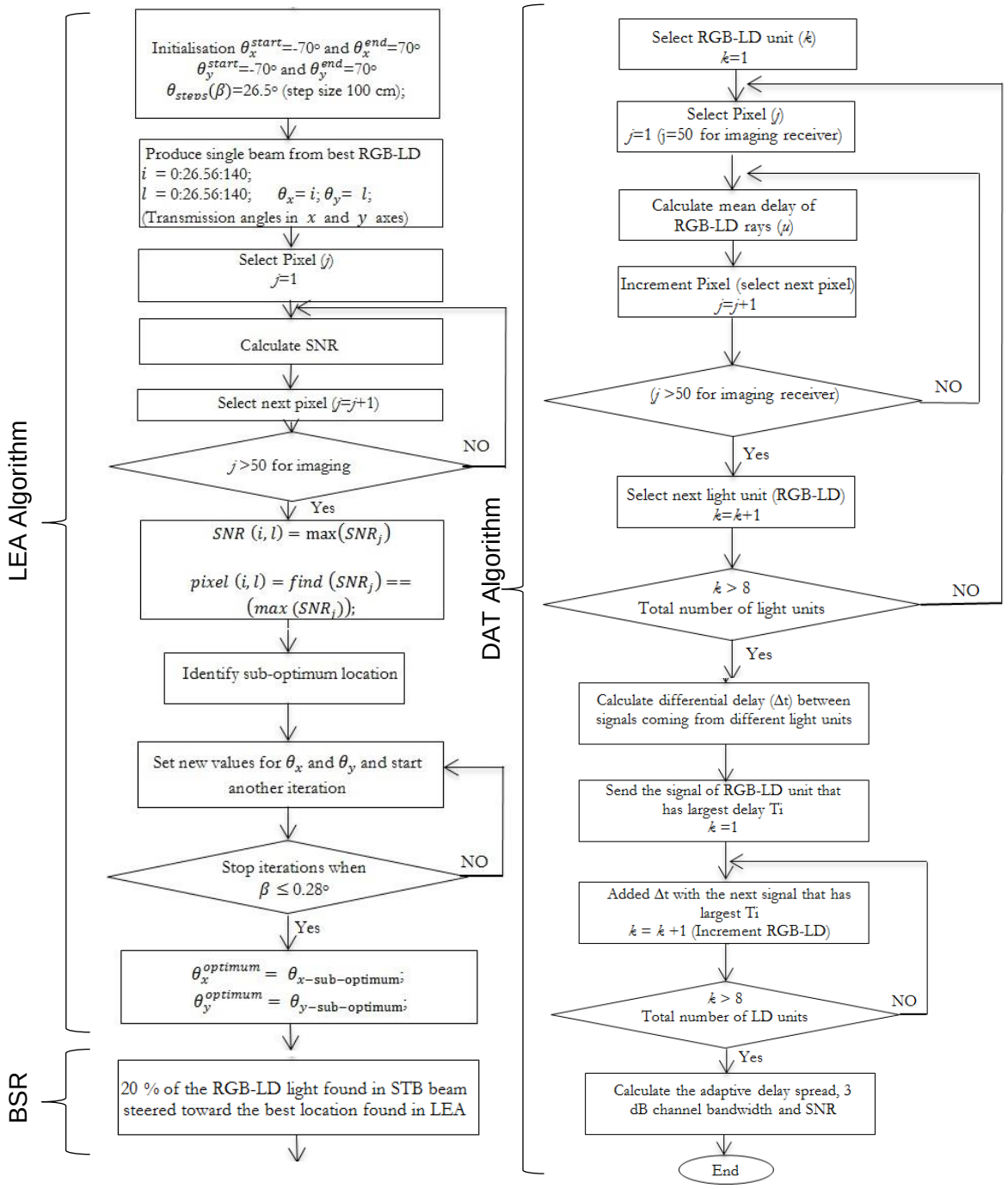

Figure 7.6: Flow chart of STB, LEA, BSR and DAT algorithms.

7.4 The Impact of the Beam Steering Technique on Illumination

The main function of the RGB-LD light units is to provide sufficient illumination according to ISO and European standards [156]. Therefore, to ensure the illumination is at an acceptable level we controlled the white light directed towards the receiver so that only a small amount of the RGB-LD light is beam steered towards the receiver (20% of light of RGB-LD unit), and the remaining light is used for illumination. We examined different values of light beam steering (10%, 20% and 30%) and we found that 20% achieves good performance in terms of the improvement in the achievable channel bandwidth and data rate while obeying the illumination standards with an acceptable change in illumination (i.e., the reduction in illumination is within the threshold level of European standards, which is 300 lx).

Figure 7.7 shows the horizontal illumination distribution for the eight RGB-LD units, the comparison is carried out for the illumination with and without beam steering when 10%, 20% and 30% of the beam power is steered, applied at LD1 (see Figure 7.2 for RGB-LD numbers and locations). The LD1, LD4, LD5 and LD8 light units were located at the room corners, and when beam steering of more than 20% is carried out at one of these light units, this led to reduced illumination in the room corners that is less than the threshold level (i.e. less than 300 lx, see Figure 7.7c). The minimum illumination in the corner without beam steering was 336 lx, as shown in Figure 7.7 a, b and c. However, when beam steering was applied at one of the corner RGB-LD units (worst case scenario) the illumination decreased, due to a part of the RGB-LD' light being steered towards the receiver location (e.g. at 1m, 1m, 1m). The minimum illumination values of 10%, 20% and 30% beam steering were 323 lx, 300 lx and 275 lx respectively. Therefore, we chose 20% beam steering as an acceptable value that kept the illumination at an acceptable level (300 lx) and improved the

SNR. We emphasise that the beam steering technique is carried out at one RGB-LD light unit that is nearest to the receiver location (the RGB-LD that has been chosen by the STB), while the remaining RGB-LD light units (seven RGB-LD light units) operate normally. Note that steering light to a receiver, not only increases the received power, it more importantly reduces the delay spread by increasing the power received through the direct ray well beyond the power received through reflections.

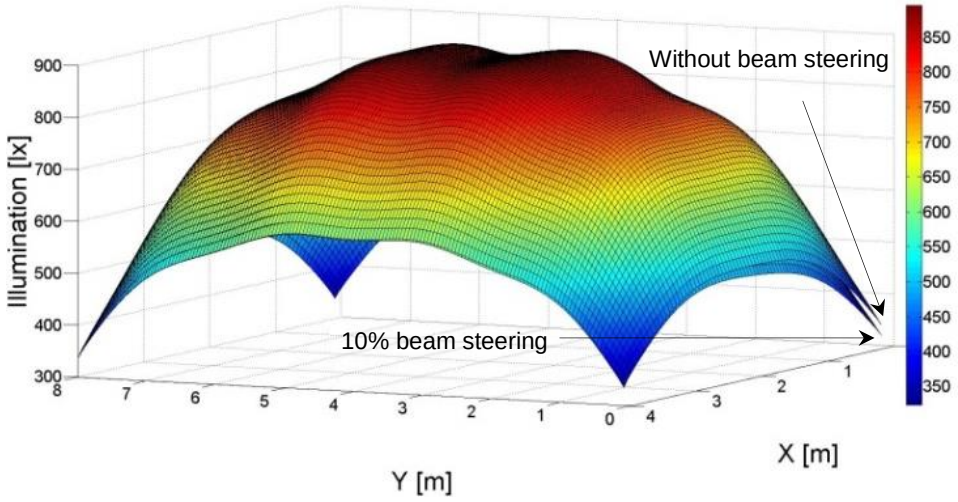

(a)

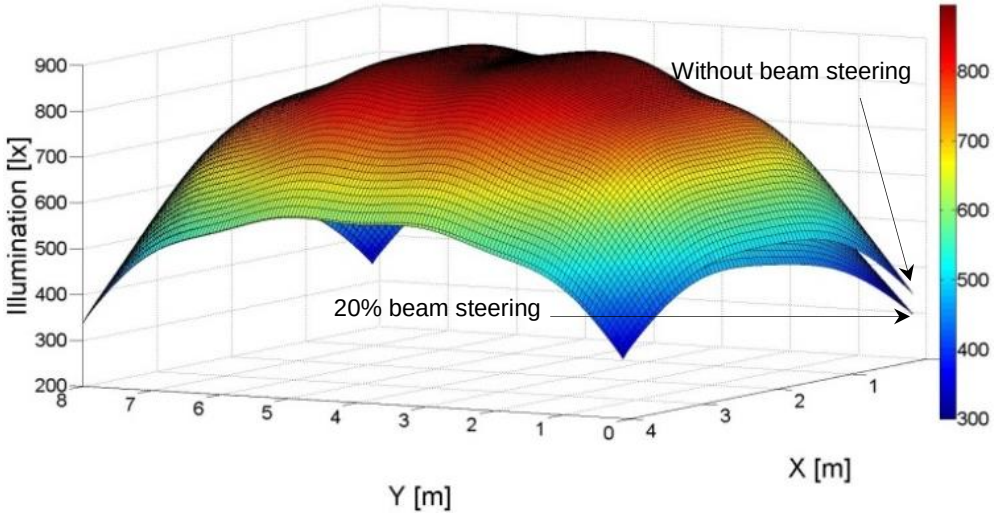

(b)

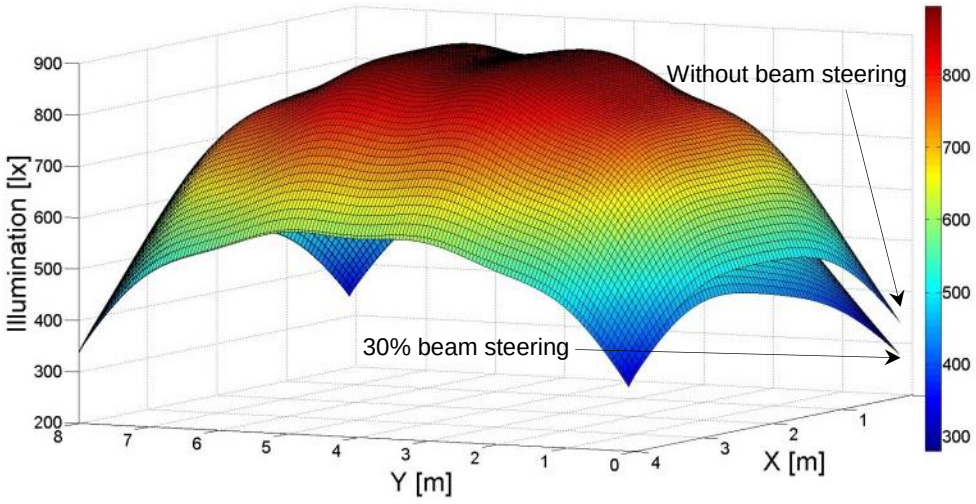

(c)

Figure 7.7: The distribution of horizontal illumination on the communication plane without beam steering minimum illumination 336lx and maximum illumination 894lx: (a) 10% beam steering minimum illumination 323 lx and maximum illumination 892 lx (b) 20% beam steering minimum illumination 300 lx and maximum illumination 889 lx (c) 30% beam steering minimum illumination 275 lx and maximum illumination 887 lx.

7.5 Adaptive Finite Vocabulary of Holograms for VLC

An angle and power adaptive IROW system has recently been introduced [86], [163]. Beam angle adaptation for VLC systems can be an effective technique that helps to provide the strongest path between the transmitter and the receiver at every receiver location. The adaptive transmitter first produces a single spot to scan the communication plane at approximately 224 possible locations in order to identify the best location. Once the optimum angles are found, the transmitter generates the hologram. These processes require intensive calculations and time from a digital signal processor (DSP). Figure (7.8) shows an example of VLC communication architecture when the transmitter is placed at (1m,1m,3m) and the receiver is at (1m,1m,1m).

Computer generated holograms can produce spots with any prescribed amplitude and phase distribution. The CGH's have many useful properties. Spot distributions can be computed on the basis of diffraction theory and encoded into a hologram. Calculating a CGH means the calculation of its complex transmittance. The transmittance is expressed as:

$$H(u,v) = A(v,u).exp[j\phi(u,v)] \tag{7.1}$$

where $A(u,v)$ is the hologram's amplitude distribution, $\phi(u,v)$ is its phase distribution, and (u,v) are coordinates in the frequency space. The relative phases of the generated spots are the objects of interest. The hologram is able to modulate only the phase of an incoming wave front, the transmittance amplitude being equal to unity.

The analysis used in [183], [184], [188] was used for the design of the CGHs. The hologram $H(u,v)$ is considered to be in the frequency domain. The pixels' locations in the hologram are defined by the frequency coordinates u and v (two dimensions). The observed diffraction pattern $h(x,y)$ is in the spatial domain (far field). They are related by the continuous Fourier transform:

$$h(x,y) = \iint H(u,v)exp[-i2\pi(ux+vy)]dudv \tag{7.2}$$

The hologram structure is an $M \times N$ array of rectangular cells, with dimension $R \times S$. Each cell represents a complex transmittance value H_{kl}: - $M/2 < k < M/2$ and $-N/2 < l < N/2$. If the hologram is placed in the frequency plane, the diffraction pattern is given by [184], [189]:

$$h(x,y) = RSsinc(Rx,Sy)\sum_{k=-\frac{M}{2}}^{\frac{M}{2}-1}\sum_{l=-\frac{N}{2}}^{\frac{N}{2}-1} H_{kl}\, exp[i2\pi(Rkx+Syl)] \tag{7.3}$$

where $sinc(a,b)= sin(\pi a)\, sin(\pi b)/\pi^2 ab$. The hologram is designed such that the complex amplitude of the spots is proportional to some value of interest.

However, because of the finite resolution of the output device and the complex transmittance of the resulting hologram, the reconstruction will be in error. This error can be used as a cost function. Simulated annealing was employed to minimise the cost function. The amplitudes and phases of every spot are determined by the hologram pixels' pattern and are given by its Fourier transform.

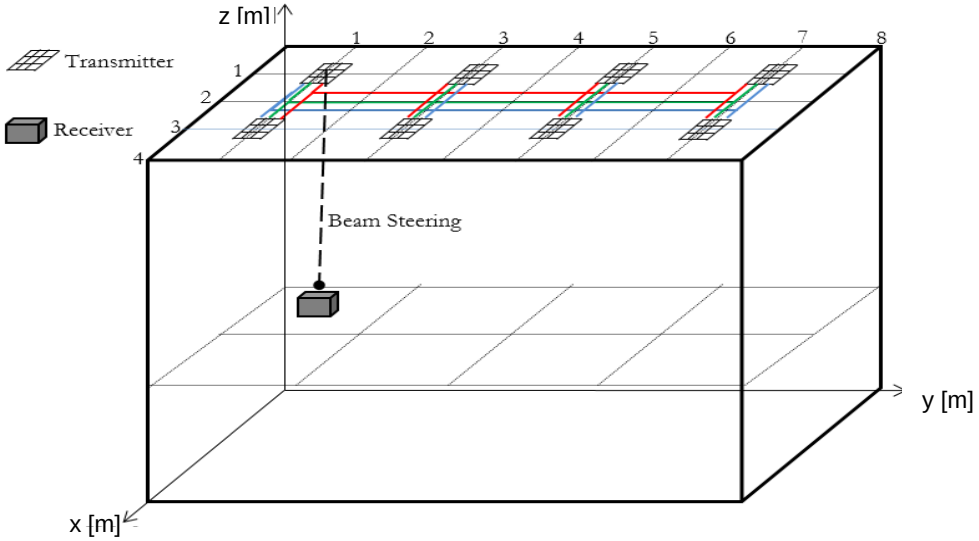

Figure 7.8: VLC communication architecture of our proposed system when the transmitter is placed at (1m,1m,3m) and the receiver is at (1m,1m,1m).

The desired distribution of spots in the far field is $f(x,y) = |f(x,y)|exp(i\varphi(x,y))$. The main goal of the design is to determine the CGH distribution $g(v,u)$ that generates a reconstruction $g(x,y)$ as close as possible to the desired distribution $f(x,y)$. The cost function (CF) is defined as a mean squared error which can be interpreted as the difference between the normalized desired object energy $f"(x,y)$ and the scaled reconstruction energy $g"(x,y)$:

$$CF_k = \sqrt{\sum_{i=1}^{M}\sum_{j=1}^{N}(|f"(i,j)|^2 - |g"_k(i,j)|^2)^2} \quad (7.4)$$

where $f"(x$, y) represents the normalised desired object energy and $g"_k(i,j)$ represents the scaled reconstruction energy of the k^{th} iteration. Simulated annealing was used to optimise the phase of the holograms offline by minimising the cost function.

A large number of holograms are required in order to accurately identify the receiver location within the region [184]. Each hologram produces the optimum pattern which was pre-calculated based on the LEA. An example of one hologram, when the transmitter is placed in the corner of room at: (1m, 1m, 3m) and the receiver is present at (1m, 1m, 1m), as shown in Figure 7.8. Simulated annealing was used to optimise the phase of the CGHs. Figure 7.9 shows three snapshots of hologram phase distributions, $g(x,y)$, in the far filed at different iterations. When the number of iterations increases, the hologram phase distributions improve. The cost function versus the number of iterations completed is shown in Figure 7.10.

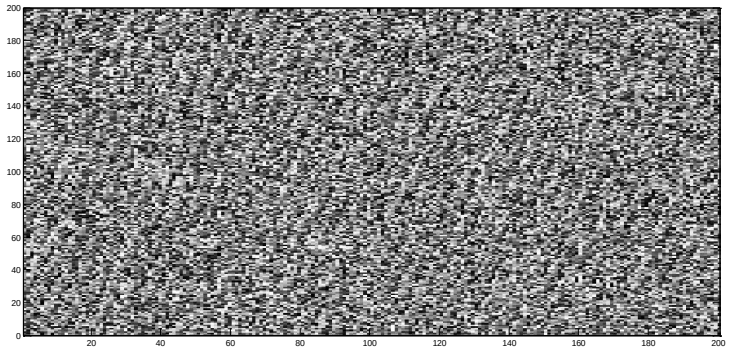

Hologram phase distributions (iteration 5)

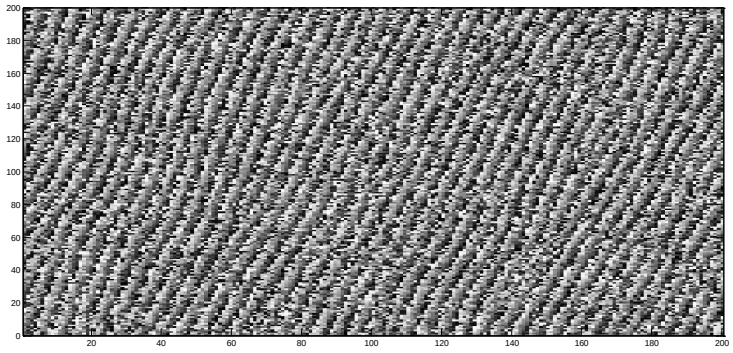

Hologram phase distributions (iteration 15)

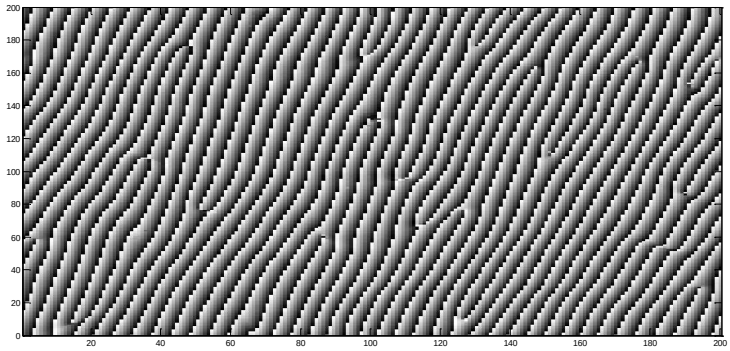

Figure 7.9: The hologram phase pattern at iterations 5, 15 and 100 using simulated annealing optimisation.

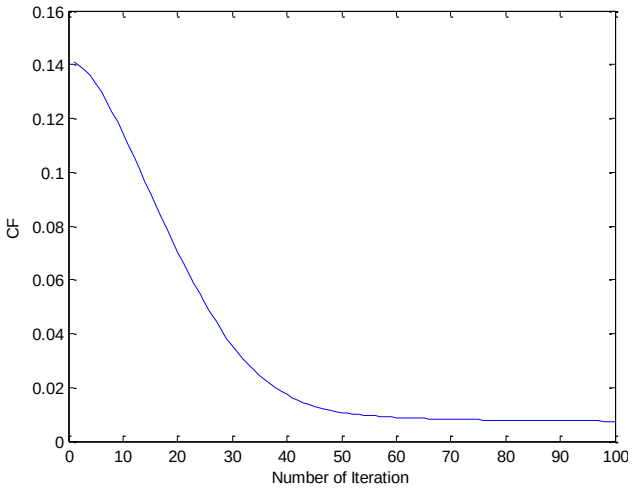

Figure 7.10: Cost function versus number of iterations.

7.6 Simulation Results and Performance Analysis

In this section, we evaluate the performance of LEA, BSR and delay adaptation techniques in the presence of multipath propagation, ISI and mobility of the VLC system in an empty room. Two new VLC systems, beam steering LD-VLC and fully adaptive LD-VLC, were compared with imaging LD-VLC and DAT imaging

LD-VLC. The results are presented in terms of impulse response, delay spread, 3 dB channel bandwidth and SNR.

7.6.1 Impulse response

The impulse responses of the four VLC systems: imaging LD-VLC, DAT imaging LD-VLC, beam steering LD-VLC and fully adaptive LD-VLC, at the room centre are depicted in Figure 7.11. The LOS components have a great impact on the system performance; therefore, we magnified the impulse responses for these systems to show the LOS contributions clearly. First and second order reflection components exist in the original impulse response, but they do not appear in this figure due to magnification of the LOS components. It can be clearly seen that the systems that employ the delay adaptation technique (DAT imaging LD-VLC and fully adaptive) are significantly better than the other systems (imaging LD-VLC and beam steering LD-VLC) in terms of signal spread (recall that there are multiple VLC light sources in the room). The imaging LD-VLC system (black line) produces 6.68 μW received power with a much greater signal spread due to sending the signals at the same time from different LD light units. A considerable reduction in the signal spread is observed when the delay adaptation technique is adopted in the imaging the LD-VLC system as shown in blue line Figure 7.11. However, there is no increase in the amount of received optical power (the sum of received power is the same in both systems in imaging LD-VLC and DAT imaging LD-VLC). On the other hand, a significant increase in the received optical power can be achieved when the beam steering LD-VLC system replaces the DAT imaging LD-VLC system, by a factor of 7, from 6.68 μW to 47.46 μW, as shown in red line Figure 7.11. This significant improvement in the received power is due to steering a beam of white light towards the receiver location. However, signal spread still exists in this system, and this lead to degradation in the system performance at high data rates. It can be clearly seen that the fully adaptive LD-VLC system's impulse response is better than the other systems in terms of

signal spread and received optical power, as shown in Figure 7.11 compared to other systems. Reducing the signal spread of the beam steering LD-VLC system leads to an increase in the 3 dB channel bandwidth that enables higher data rates in the VLC system and decreases the ISI caused by multipath.

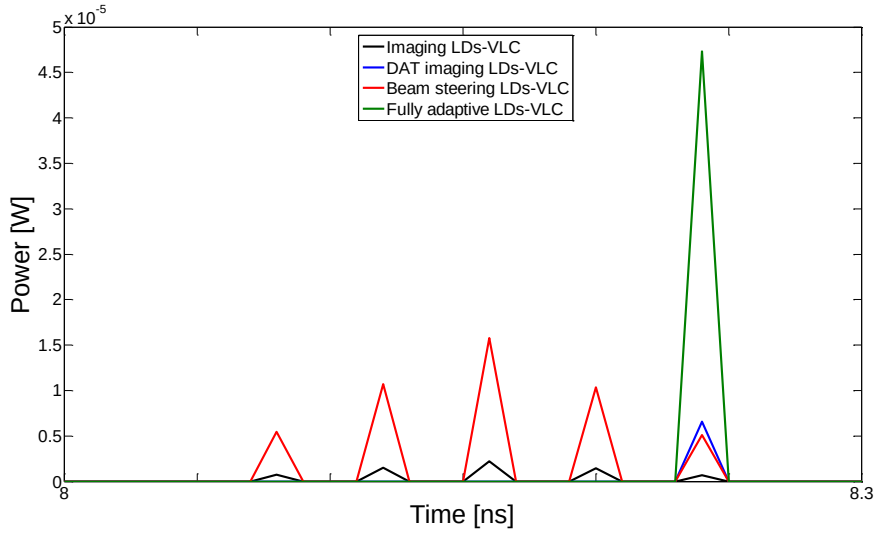

Figure 7.11: Impulse responses of different VLC systems at room centre: laser diodes transmitters with an imaging receiver (imaging LD-VLC), delay adaptation technique with laser diodes transmitters and imaging receiver (DAT imaging LD-VLC), location estimation and beam steering techniques with laser diodes transmitters and imaging receiver (beam steering LD-VLC) and location estimation, beam steering, delay adaptation, CGHs with laser diodes transmitters and imaging receiver (fully adaptive LD-VLC).

7.6.2 Delay spread and 3 dB channel bandwidth

Figure 7.12 evaluates the delay spread of the four systems under the worst case scenario (when the receiver moves along x=2m). The middle of the room (x=2m) is considered to be the worst communication link in the communication plane area due to its associated high ISI and multipath propagation level; therefore, we only consider the x=2m line. The delay spread for the imaging LD-VLC system is relatively low (0.04 ns in the worst case) and this is due to the narrow FOVs associated with each pixel in the imaging receiver, and this

limitation in the FOV minimises the number of rays accepted. However, to operate at high data rates (10 Gb/s and beyond) the delay spread should be further reduced (i.e., less than 0.04 ns). To improve the quality of the link we combined the delay adaptation technique with imaging LD-VLC system. The DAT imaging LD-VLC system outperforms the imaging LD-VLC system, as it dramatically decreases the delay spread from 0.04 ns to 0.007 ns (by a factor of 5) at the room centre. The beam steering LD-VLC system has a slightly lower delay spread (0.036 ns at the room centre) compared to the imaging LD-VLC system and this is due to the advantage of beam steering, which increases the amplitude of the LOS components (see Figure 7.11) and this makes this LOS component dominant compared to the first and second order reflections. Moreover, the DAT imaging LD-VLC system performs better than the beam steering system in terms of delay spread. This is due to the signal spread in the beam steering system, as shown in Figure 7.11. Thus, to further enhance the performance of the beam steering system we combined the delay adaptation technique with beam steering to produce a fully adaptive VLC system that has the lowest delay spread reported to date to the best of our knowledge (0.0035 ns in the worst case scenario) compared with other systems. The results show that the fully adaptive system reduces the delay spread by a factor of 13 compared with the imaging LD-VLC system (from 0.04 ns to 0.0035 ns) at the room centre. The receiver's locations of y=2m, 4m and 6m in the non-adaptive systems (imaging LD-VLC and beam steering LD-VLC) in Figure 7.12 are considered to be the worst receiver locations (due to high multipath propagation). However, by employing the delay adaptation approach, these locations become better than other locations (y=1m, 3m, 5m and 7m) due to the ability of this delay adaptation method to reduce the effect of multipath propagation to the lowest level.

Previous work [103] has shown that delay adaptation with an imaging receiver can provide a 3 dB channel bandwidth of more than 16 GHz under the worst

case scenario. However, the main problem with such a system is the low SNR at high data rates (10 Gb/s and beyond).

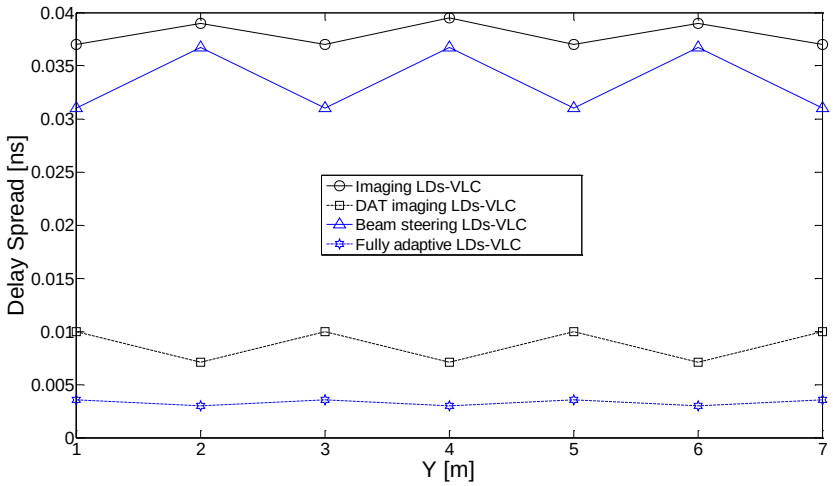

Figure 7.12: Delay spread of four systems at x=2m and along the y-axis.

Therefore, to enable it to operate at 20 Gb/s we proposed the beam steering technique to enhance the SNR at high data rates and to utilise the significant increase in the channel bandwidth that will enable our proposed system (fully adaptive VLC system) to operate at 20 Gb/s. The 3 dB channel bandwidth at x=2m in our four systems is given in Table 7.1. The results show that the fully adaptive VLC system has the ability to offer a communication channel with 3 dB channel bandwidth greater than 36 GHz.

It should be noted that the channel bandwidth is negatively affected by the number of light spots seen within the pixel's FOV, because when the number of spots increases this can result in the introduction of a time delay between the signals received from the spots within the receiver's FOV, and hence this limits the bandwidth. For instance, the impulse response of non-adaptive systems (systems that do not employ the delay adaption approach) has many peaks (see Figure 7.11), which increases the delay spread for these systems (see Figure 7.12). However, when the delay adaptation technique is combined with

those systems the channel bandwidth increases dramatically, as shown in Table 7.1.

Table 7.1: The 3 dB channel bandwidth of proposed systems.

System	3 dB Channel Bandwidth [GHz]						
	Receiver Locations along the y-axis, y[m]						
	1	2	3	4	5	6	7
Imaging LD-VLC	5.1	4.19	5.1	4.19	5.1	4.19	5.1
DAT Imaging LD-VLC	16.6	23.4	16.6	23.4	16.6	23.4	16.6
Beam steering LD-VLC	5.37	4.54	5.37	4.54	5.37	4.54	5.37
Fully Adaptive LD-VLC	36.7	38.5	36.7	38.5	36.7	38.5	36.7

7.6.3 SNR

In this section, we consider a low data rate (30 Mb/s) to enable a comparison with previous work in Chapter 5. A higher data rate of 20 Gb/s is also considered. For a bit rate of 30 Mb/s we employed the p-i-n FET trans-impedance preamplifier used in [162]. For the higher data rate we used the p-i-n HEMT receiver designed in [190]. Figure 7.13 illustrates the SNR_{SC} and SNR_{MRC} of the imaging LD-VLC, DAT imaging LD-VLC, beam steering LD-VLC and fully adaptive LD-VLC systems at low data rates (30Mb/s). It is observed that the adaptive systems (systems that applied the delay adaptation technique) did not give any advantage over non-adaptive systems at low data rates due to the high channel bandwidth achieved by all systems, which guarantees low ISI at the low operating bit rate considered (30 Mb/s). The beam steering LD-VLC and fully adaptive LD-VLC systems achieved about a 10 dB SNR gain over the imaging LD-VLC and DAT imaging LD-VLC systems when the beam steering technique is applied with the low data rate systems. In addition, it can be seen that the difference between SC and MRC is about 4 dB on average in all

systems. This is because the MRC receiver effectively produces an SNR which is equal to the sum of the SNRs experienced by all the pixels versus SC which simply chooses the pixel with the best SNR. Moreover, the number of RGB-LD visible within the pixel's FOV is a key to achieving a high SNR. As a result of this fact, the beam steering technique has the ability to enhance the SNR by directing a part of the white light towards the receiver location and thus increases the number of LOS components within the pixel's FOV.

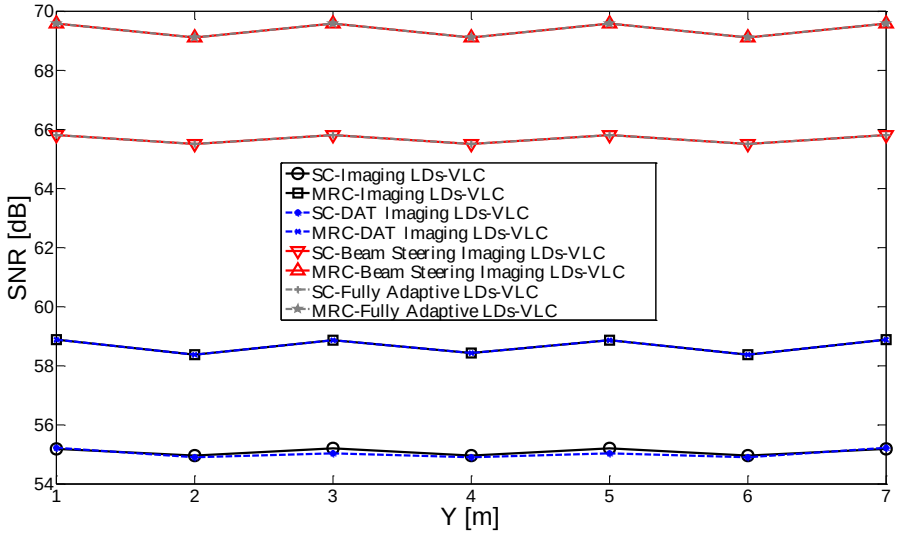

(a)

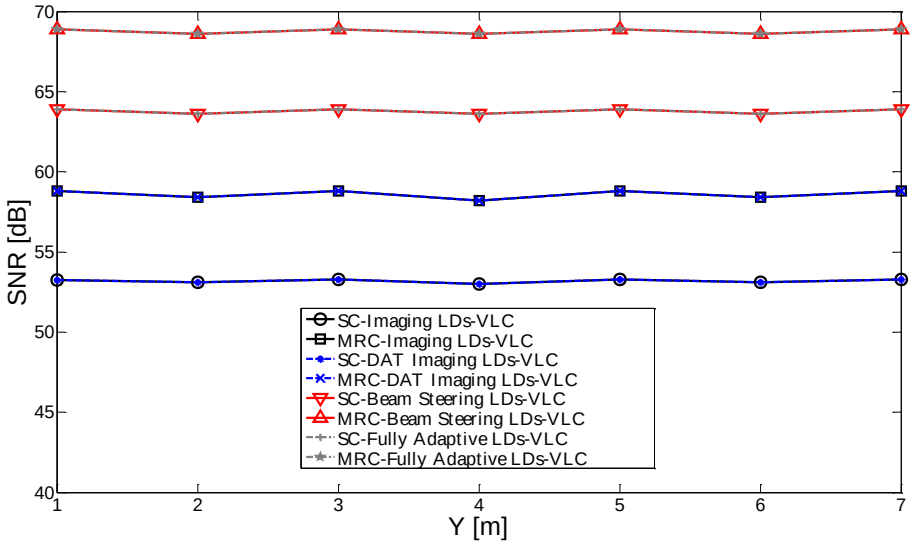

(b)

Figure 7.13: SNR of four systems (imaging LD-VLC, DAT imaging LD-VLC, beam steering LD-VLC and fully adaptive LD-VLC) when operated at 30 Mb/s and using two combing schemes (SC and MRC), (a) at x=1m and (b) at x=2m along the y-axis.

To evaluate the performance of our four systems at higher bit rates, the SNR is calculated at 20 Gb/s. Figure 7.14 shows the SNR_{SC} and SNR_{MRC} of the four VLC systems at 20 Gb/s. To achieve a BER of 10^{-9} for OOK, a SNR of 15.6 dB is required [87], [191]. It can be noted that the fully adaptive system has the ability to provide SNR values higher than this required value in all the receiver locations. The fully adaptive VLC system outperforms other systems in terms of SNR, it achieves about a 15 dB SNR gain over the DAT imaging LD-VLC system in the middle of the room. This significant improvement in the SNR level is attributed to the ability of the beam steering technique to steer a part of the light towards the receiver location and thus increase the power received by the pixels. Although, the beam steering technique increases the power level at the receiver with the beam steering LD-VLC system as shown in Figure 7.11 and increases the SNR at low data rates as shown in Figure 7.13, at high data rates (20 Gb/s) the performance decreases dramatically. This is due to the high multipath dispersion and ISI at the high data rates. Therefore, when the delay adaptation technique is combined with the beam steering system (fully adaptive system) we can achieve considerable enhancements in terms of SNR and 3 dB channel bandwidth, as shown in Table 7.1 and Figure 7.14. In addition, the delay adaptation technique adds a degree of freedom to the link design for the adaptive systems (DAT imaging and fully adaptive VLC), resulting in VLC systems that can provide higher SNR compared to the non-adaptive systems (imaging LD-VLC and beam steering LD-VLC). At x=1m, the SNR fluctuations in the non-adaptive systems due to ISI and multipath propagation can be mitigated by employing the delay adaptation approach. Moreover, when the VLC receiver moves along x=1m in all four systems, we noticed that it has a high SNR compared to when the receiver moves along x=2m, and this is due to the high multipath, ISI and path loss in the middle of the room (x=2m).

Table 7.2 presents the BER values corresponding to the achieved SNRs at 20 Gb/s for the imaging LD-VLC, DAT imaging LD-VLC, beam steering LD-VLC and fully adaptive LD-VLC systems respectively at line x=2m when using SC (due to room symmetry, we calculated BER for 1 m to 4 m along the y-axis). It can clearly be seen that the fully adaptive LD-VLC system has the best performance compared to the other systems. The highest value of BER in the fully adaptive LD-VLC system is equal to 4.1×10^{-16}, and this value can provide a strong communication link.

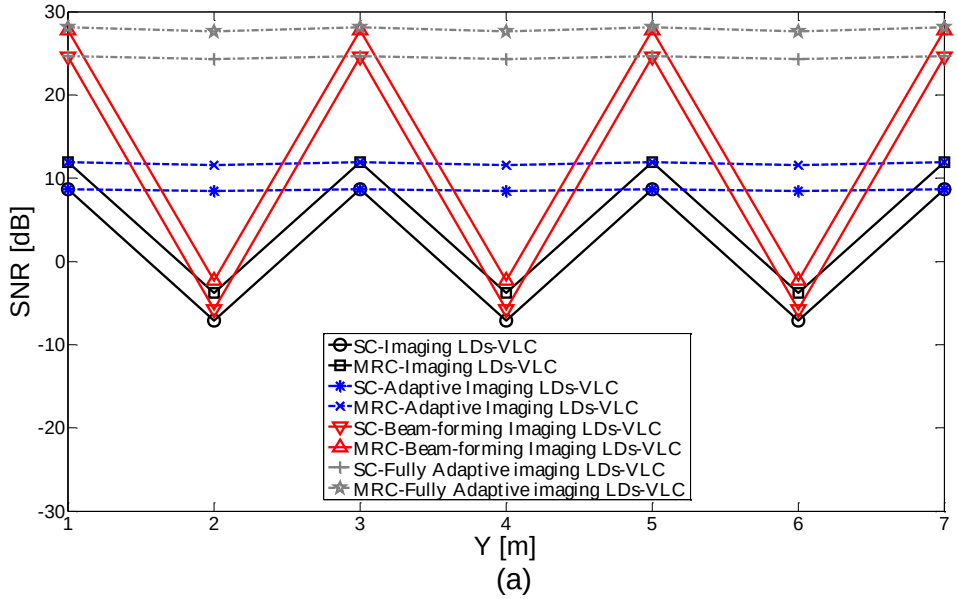

(a)

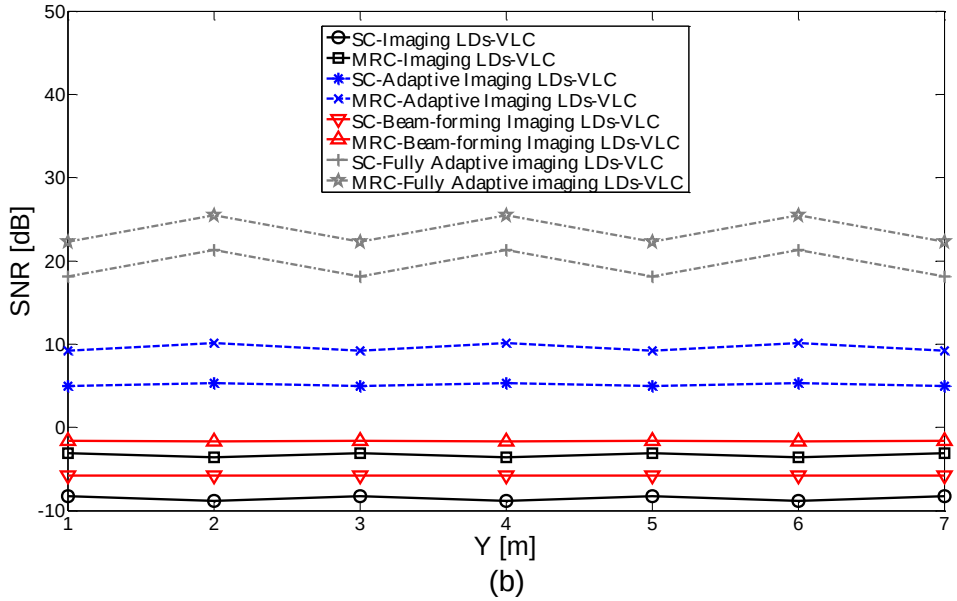

(b)

Figure 7.14: SNR of four systems (imaging LD-VLC, DAT imaging LD-VLC, beam steering LD-VLC and fully adaptive LD-VLC) when operated at 20 Gb/s and using two combing schemes (SC and MRC), (a) at x=1m and (b) at x=2m along the y-axis.

System	BER			
	Receiver Locations along the y-axis, y[m]			
	1	2	3	4
Imaging LD-VLC	7.9×10^{-1}	9.9×10^{-1}	7.9×10^{-1}	9.9×10^{-1}
DAT Imaging LD-VLC	4.7×10^{-2}	3.9×10^{-2}	4.7×10^{-2}	3.9×10^{-2}
Beam steering LD-VLC	6.8×10^{-1}	6.8×10^{-1}	6.8×10^{-1}	6.8×10^{-1}
Fully Adaptive LD-VLC	4.1×10^{-16}	Error free	4.1×10^{-16}	Error free

Table 7.2: BER performance of the proposed systems at x=2m.

7.7 Robustness to Shadowing, Signal Blockage and Mobility

In this section we extended the analysis to evaluate performance of proposed systems in realistic indoor environment. For realistic indoor environment we have used the same parameters and characteristics of the room in Chapter 5 (see Figure 5.1b).

Comparisons were performed between the fully adaptive and DAT imaging LD-VLC systems in two different environments (i.e., room A that is an empty room, see Figure 7.1 and room B that is a realistic room, see Figure 5.1b) when operating at 20 Gb/s with full mobility. The complex environment in this room results in shadowing created by low reflectivity objects and physical partitions. In this section, the results of the adaptive systems are compared in rooms A and B in terms of impulse response, path loss and SNR. We have considered a

mobile user with a speed of 1 m/s moving along the y-axis in the lines x=1m, x=2m and x=3m, the results in this section are presented in two places in room 1) when the user is inside a mini cubicle (x=1m and x=3m along the y-axis) and 2) when the mobile user is in the middle of the room (x=2m and along the y-axis). In this section a simulation package based on a ray tracing algorithm was developed using MATLAB to compute the impulse response of the proposed systems.

7.7.1 Impulse response

It is observed that in all room locations both systems have the ability to establish LOS links between the transmitters and receiver, which is due to a good distribution of RGB-LD on the ceiling. For example, Figure 7.15 shows the impulse responses at the room centre (2 m, 4 m, 1 m) for the fully adaptive system and for the DAT imaging LD-VLC system in rooms A and B (room A is an empty room and room B is a realistic environment). In both room scenarios for the two systems the LOS components are the same. However, the power collected from the signals coming to the receiver from the ceiling, strip walls that surround the windows and bookshelves is decreased due to many reasons. Firstly, the physical partitions prevent rays from reaching the receiver. In addition, the reflectivity of the two windows is zero, which means no signals will be received from the two walls at x=0 and y=0. Moreover, the bookshelves have a reflectivity of 0.4, and this reduces the power of the signals received from them. However, we should note that the LOS link has the largest amount of received power and the reduction in received power from reflections is negligible. For instance, the associated power at the room centre position for the fully adaptive system in room A is 47.46 μW whereas it was 47.41 μW in room B.

7.7.2 Path loss analysis

Figure 7.16 illustrates the path loss distributions for rooms A and B at x=1m, and x=2m along the y-axis. It can be seen that the path loss for the two systems is comparable in both room scenarios.

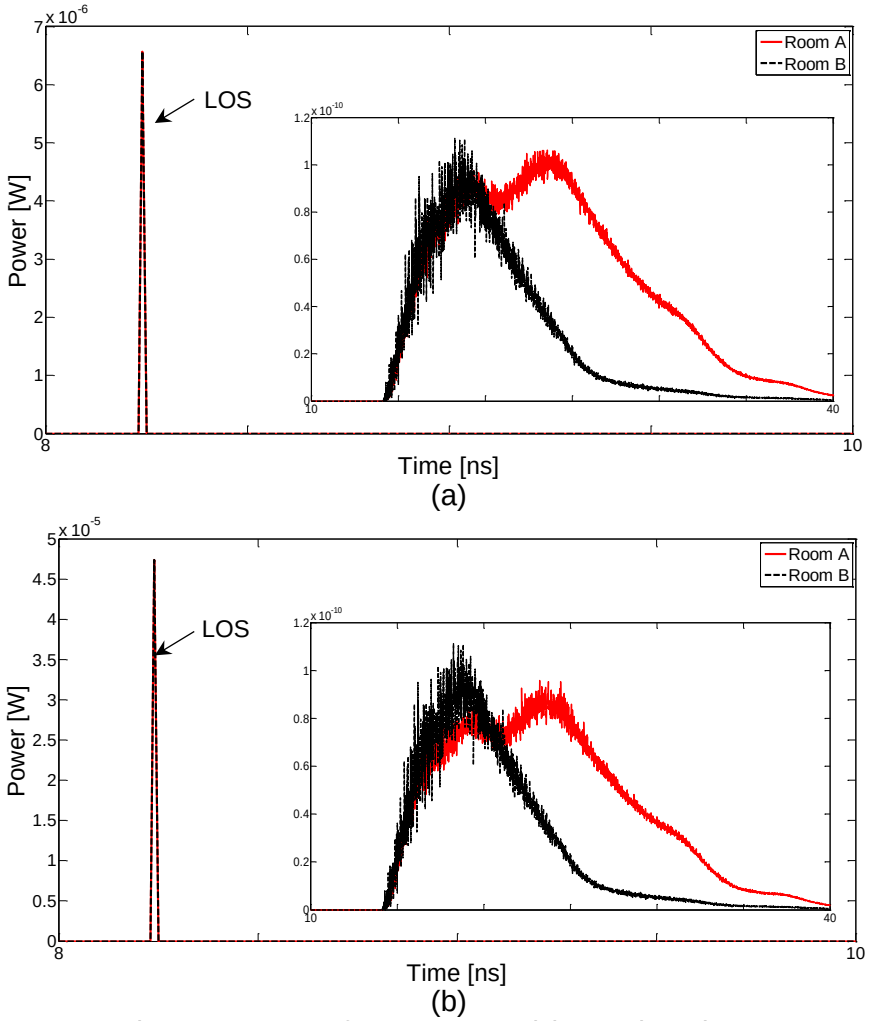

Figure 7.15: Impulse responses of two systems (a) DAT imaging LD-VLC and (b) fully adaptive LD-VLC in two different environments at room centre.

The path loss increased less than 0.5 dB when both systems were evaluated in room B. This insignificant increase in the path loss is attributed to the fact that our systems have the ability to establish LOS links in both rooms (i.e. A and B),

which leads to similar performances when operated in different environments. Therefore both systems possess robustness against shadowing and mobility and they are able to achieve similar performance levels in an empty room and a realistic environment. In DAT imaging LD-VLC system when the receiver position was close to the windows (along x=1m), for example, at point (x=1m and y=1m) the path loss becomes higher because the received power from the reflections is very low (glass windows are considered to not reflect any signal). However, when the receiver moves towards the other side of the room (i.e., receiver positions close to bookshelves). In addition, it can be seen that the path loss in the two systems is higher when the receiver moves along x=2m. This is due to the larger distance between the receiver and transmitter.

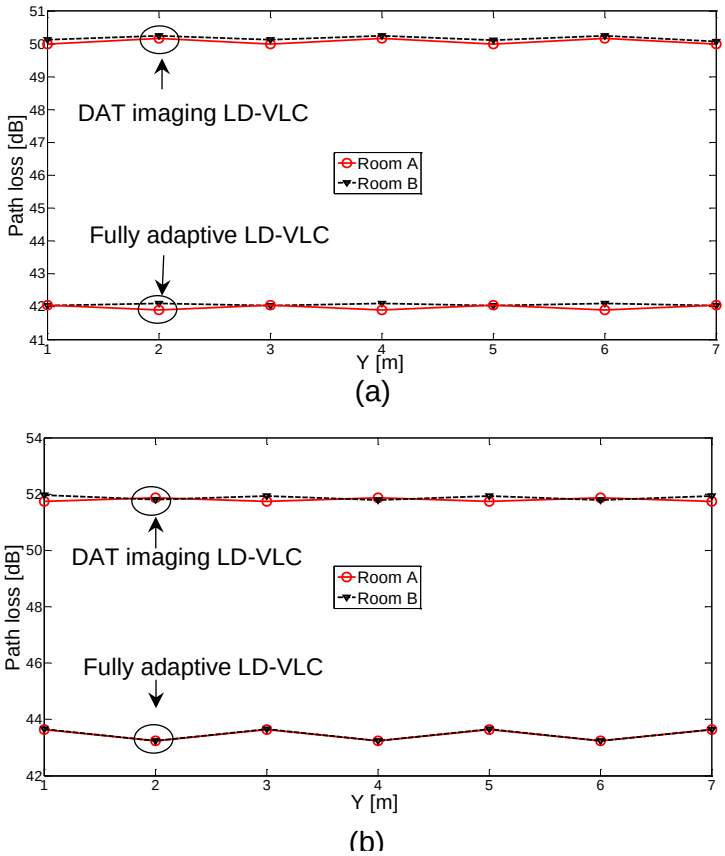

Figure 7.16: Path loss of DAT imaging LD-VLC and fully adaptive LD-VLC systems in two different environments (a) at x=1m and (b) at x=2m.

7.7.3 SNR and BER

Figure 7.17 shows the SNR of four systems (imaging LD-VLC, DAT imaging LD-VLC, beam steering LD-VLC and fully adaptive system) at x=1m and x=2m along the y-axis over the communication plane for different environments (i.e., rooms A and B). In rooms A and B both adaptive systems have comparable results, there was very low degradation in the SNR when both systems operated in room B. This is attributed to the ability of our adaptive systems to adapt to such an environment. Also, it should be noted that the results in Figure 7.17 are in agreement with the general observation made in Figure 7.16. For example, for the DAT imaging LD-VLC system at the point x=1m and y=4m, the path loss is highest resulting in the lowest SNR. Similar behaviour was observed when comparing Figure 7.16 and Figure 7.17 for the fully adaptive system.

In a realistic environment when the user is inside a mini cubicle (x=1m along the y-axis) the SNRs of the proposed systems are comparable. In addition, it should be noted that the systems that employ the delay adaptation technique (DAT imaging and fully adaptive VLC) can provide higher SNR compared to the non-adaptive systems (imaging LD-VLC and beam steering LD-VLC). It can be noted that the fully adaptive system has smooth SNR at all relevant locations in the room (see Figures 7.14 and 7.17).

Table 7.3 shows the BER at 20 Gb/s of the proposed systems (imaging LD-VLC, DAT imaging LD-VLC, beam steering LD-VLC and fully adaptive LD-VLC) at line x=2m when using SC. It can be noted that the fully adaptive LD-VLC system has the best performance compared to the other systems. In the realistic environment, the BER of the fully adaptive VLC system has increased slightly compared to an empty room. However, this increase does not severely affect the performance of the system; for example, the maximum value of BER provided by the fully adaptive LD-VLC system is equal to 6.9×10^{-16}.

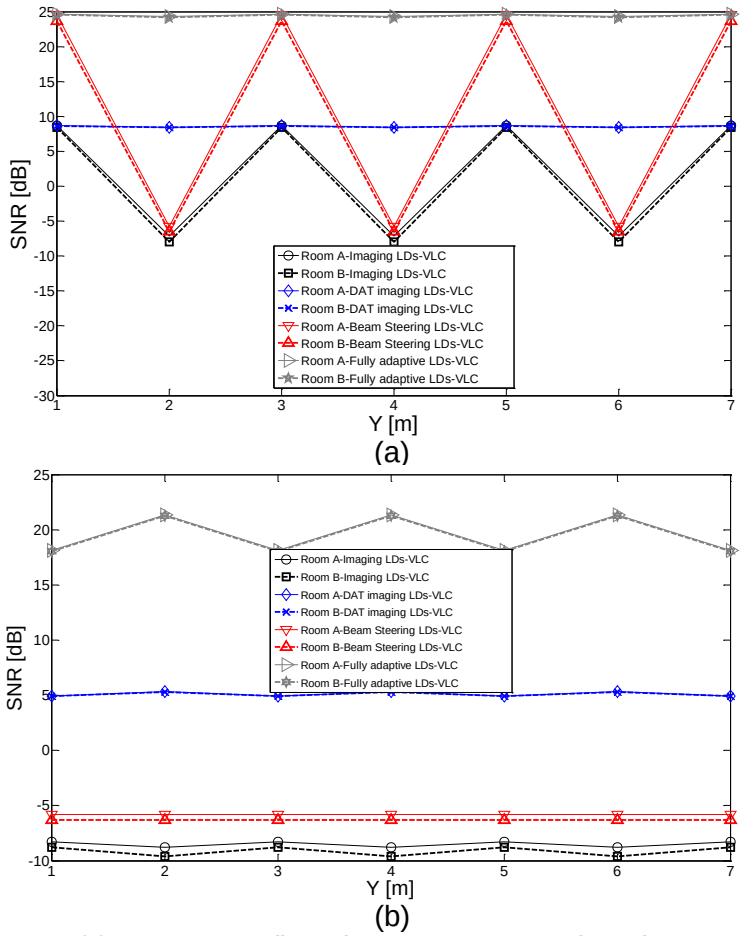

Figure 7.17: SNR_{SC} of four systems (imaging LD-VLC, DAT imaging LD-VLC, beam steering LD-VLC and fully adaptive LD-VLC) when operated at 20 Gb/s in two different room scenarios at (a) x=1m and (b) at x=2m, along y-axis.

Table 7.3: BER performance of the proposed systems at x=2m.

System	BER			
	Receiver Locations along the y-axis, y [m]			
	1	2	3	4
Imaging LD-VLC	9.8×10^{-1}	9.9×10^{-1}	9.8×10^{-1}	9.9×10^{-1}
DAT Imaging LD-VLC	4.8×10^{-2}	4×10^{-2}	4.8×10^{-2}	4×10^{-2}
Beam steering LD-VLC	7×10^{-1}	7×10^{-1}	7×10^{-1}	7×10^{-1}
Fully Adaptive LD-VLC	6.9×10^{-16}	Error free	6.9×10^{-16}	Error free

7.8 High Speed Adaptive Mobile VLC System

The high channel bandwidth achieved through the delay adaptation technique coupled with the additional SNR accomplished by the beam steering technique, can be used to provide high data rates (20 Gb/s and beyond) with the new VLC system. The p-i-n HEMT optical receiver proposed by Gimlett [190] was used for the fully adaptive VLC system to operate at 20 Gb/s. The noise current spectral density for this preamplifier is 12 $\mathrm{pA}/\sqrt{\mathrm{Hz}}$ and the preamplifier has a bandwidth of 16 GHz. Through the use of a suitable filter the preamplifier bandwidth can be limited to 14 GHz.

Transmitters for data rates of up to 40 Gb/s are established in fibre systems [192], therefore the rise and fall times of the LD based transmitter is not considered in this thesis. A laser driver with high power is required to enable our light unit to emit 2 W from each RGB-LD at bandwidth of 14 GHz. This may incurred more cost and complexity to our system. The OOK modulation format is used with intensity modulation and direct detection. The OOK modulation is an appropriate modulation scheme for high data rates in OW systems [193] due to its simplicity, however higher order modulation formats can be investigated. Adaptive equalisation can be used to further reduce the ISI [94]. The SNR calculations in equation (3.19) take into account eye closure $(P_{s1} - P_{s0})$, and therefore the SNR values reported consider ISI and receiver preamplifier noise. The imaging LD-VLC, DAT imaging LD-VLC and beam steering LD-VLC systems performed identically at a bit rate of 30 Mb/s, and this is evident due to the excess channel bandwidth available. ISI increased noticeably at 20 Gb/s which results in significant SNR degradations. The fully adaptive LD-VLC system can offers high SNR (18 dB at the least successful point) and bandwidth of more than 36 GHz (see Table 7.1), which enables it to support data rates of 20 Gb/s. Figure 7.14 shows that an SNR gain of 27 dB can be achieved when the fully adaptive system is used instead of the beam steering system in the

middle of the room (worst case scenario). This improvement is due to the use of the delay adaptation technique with beam steering (fully adaptive system), and it significantly reduces the effect of ISI and multipath dispersion. The SNR results of the fully adaptive system in the real environment (see Figure 7.17) show that our proposed system achieves an SNR_{SC} of 18 dB under the worst case scenario (at point x=2, y=1, 3, 5 and 7 in Figure 7.17b), which is greater than the 15.6 dB needed to achieve 10^{-9} BER. This SNR is obtained when multipath propagation, shadowing, signal blockage and mobility are all present.

The feedback link is vital for the proposed systems as it affects directly the performance of the systems. The feedback channel is used to send information (such as SNR measured for STB algorithm and mean delay for DAT algorithm) at very low data rate. If any error occurs in this channel, this will degrade the performance of the fully adaptive system. The feedback channel operates at a very low data rate, which means that SNRs in excess of 33 dB can be achieved at data rates up to 30 Mb/s [22], [32], [44]. This in turn means that the BER achieved in the feedback channel is extremely small which would be considered an almost ideal communication link. However, FEC coding can be used to ensure that any errors in the feedback channel are minimised.

Simulation results have shown that LEA and beam steering coupled with imaging receiver detection, can significantly improve performance in the proposed system (beam steering LD-VLC system). However this is at the cost of complexity in the design of beam steering LD-VLC. The complexity is associated with the computation time required to identify the optimum location to perform beam steering. For example, in a typical room with dimensions of 4m × 8m × 3m (width × length × height), LEA generates a single spot which scans the communication plane changing the beam angle associated with the spot between -70^{o} and 70^{o}, a total of 224 possible locations, which requires 224 ms adaptation time in order to identify the optimum location.

7.9 Summary

In this chapter, for the first time to best of our knowledge, we introduced beam steering and location estimation algorithms for a mobile multi-gigabit/s VLC system. We also combined these algorithms with the concept of delay adaptation to produce a fully adaptive VLC system that has the ability to achieve 20 Gb/s with full receiver mobility in a realistic indoor environment. The LEA estimates the best locations to steer the beam to by scanning a single beam over the communication plane and computing the resultant SNR for every single beam.

We investigated the effect of beam steering on the illumination and found that up to 20% of the light from the RGB-LD can be beam steered towards the receiver position to improve SNR without affecting the illumination. The beam steering technique steers 20% of the white light from a certain RGB-LD light unit (close to receiver) towards the optimum location that was found by LEA to maximise the SNR. In addition, at a low data rate (30 Mb/s) our fully adaptive system offers an SNR improvement of 10 dB over the imaging LD-VLC system when using the MRC approach. At a high data rate (20 Gb/s) a 29 dB SNR gain is achieved when the fully adaptive system replaces the imaging LD-VLC system under the worst case scenario, and these improvements in the SNR enable our fully adaptive system to provide a BER of better than 10^{-9} at all receiver locations when operated at 20 Gb/s in a harsh room environment.

Furthermore, the delay adaptation technique was combined with the beam steering technique and location estimation algorithm to mitigate the effect of ISI and multipath dispersion. The delay adaptation adjusts the switching times of the signals in a fashion that allows the signals to reach the receiver at the same time. The significant improvements in channel bandwidth and SNR enhance the performance of our VLC system and enable it to operate at higher data rates (20 Gb/s and beyond). Moreover, the fully adaptive VLC system can achieve

100% of the data rate (20 Gb/s) when it is stationary and 70.4% (14 Gb/s) in the case of user movement, and this is due to the time needed (296 ms) for the adaptation process.

Next Chapter will address methods to accelerate the location estimation algorithm and reduce the time required to find the receiver location below 224 ms.

8 Fast and Efficient Adaptation Techniques for Visible Light Communication Systems

8.1 Introduction

Beam steering fully adaptive VLC system has been shown to offer performance enhancements over traditional VLC systems in the previous chapter (Chapter 7). However, an increase in the computational cost is incurred. In this chapter, we introduce fast computer generated holograms (FCGHs) to speed up the adaptation process. The new, fast and efficient fully adaptive VLC system can improve the receiver SNR and reduce the required time to estimate the position of the VLC receiver. It can also adapt to environmental changes, providing a robust link against signal blockage and shadowing. In addition, an ADR and a delay adaptation technique are used to reduce the effect of ISI and multipath dispersion. Significant enhancements in the SNR, with VLC channel bandwidths of more than 26 GHz are obtained, resulting in a compact impulse response and a VLC system that is able to achieve higher data rates (25 Gb/s) with full mobility in the considered realistic indoor environment. VLC systems are among the promising solutions to the bandwidth limitation problem faced by microwave systems. They are also among the potential candidates for 5G indoor systems [194].

Recently, beam steering has been proposed in VLC systems to maximise the SNR at the receiver [104]. Simulation results have shown that a significant improvement in the data rate (20 Gb/s for a stationary user and 14 Gb/s for a mobile user) can be achieved in a mobile VLC system that employs beam

steering. The improvements achieved are however at the cost of complex adaptation requirements. The complexity is associated with the computation time required to identify the optimum location to steer the beam to. In this chapter, for the first time to the best of our knowledge, we report the use of holograms and beam steering in VLC systems with efficient adaptation. The concept of finite computer generated holograms has been recently proposed in VLC system [104]. The work in Chapter 7 investigated a very limited case of finite pre-stored holograms and studied it in a realistic indoor environment to examine the impact of shadowing. Here we extend the work in [104] by (i) introducing FCGHs, (ii) studying the VLC system complexity and SNR penalty, (iii) employing angle diversity receiver with narrow FOVs, (iv) evaluating a high data rate system (25 Gb/s), and (v) considering a real environment that experiences shadowing to assess the utility of FCGHs.

In Chapter 4, we proposed the use of an ADR for a VLC system to provide a robust link and mitigate multipath dispersion, as well as to improve the overall system performance. In this chapter we used an ADR with selective combining to choose the best branch. A DAT for a VLC system was proposed in Chapter 5 and it is used here as it is shown to offer channel bandwidths of more than 26 GHz (in a worst case scenario), which enables the VLC system to operate at data rates of more than 25 Gb/s. The adaptation techniques (FCGHs and DAT) require repetitive training and a feedback channel from the receiver to transmitter at a low data rate. An infrared diffuse channel is suggested to realise this link. The ultimate goal of this study is to enhance the 3 dB channel bandwidth, minimise the impact of ISI, and increase the SNR when the VLC system operates at a high bit rate of 25 Gb/s under the effect of multipath dispersion, shadowing, mobility and receiver noise.

The rest of the chapter is organised as follows: Section 8.2 describes the VLC system configurations and fast computer generated holograms for VLC system. The VLC system complexity is considered in Section 8.3. The

simulation results in an empty room are outlined in Section 8.4. Robustness against shadowing is evaluated in Section 8.5. The simulation results of fully adaptive employing imaging receiver are outlined in Section 8.6. Finally, a summary is provided at the end of the chapter.

8.2 VLC Systems' Configurations

In this section, two VLC systems are presented, analysed and compared to find the most suitable system for use in high-speed VLC systems (25 Gb/s and beyond).

8.2.1 DAT ADR LD-VLC system

The DAT ADR LD-VLC system employed eight RGB-LD transmitters (lighting fixtures) on the ceiling connected by fibre interconnect and controlled by a central controller and an ADR with three branches (similar to one that used in Chapter 4). The DAT is combined with ADR LD-VLC (DAT ADR LD-VLC) to enhance the overall system performance. The DAT ADR LD-VLC system was previously proposed in Chapter 5 and it is considered here to compare it with our new proposed VLC system.

8.2.2 Fully adaptive ADR VLC system

The recently proposed fully adaptive VLC system has achieved 20 Gb/s for stationary user and 14 Gb/s for mobile user (the time required for adaptation algorithms during mobility was 296 ms). However, high complexity is associated with the computation required to identify the optimum beam steering location. In order to solve this problem, we introduce a new FCGHs using simulated annealing to speed up the beam steering process. In this chapter the RGB-LD light unit has the ability to direct part of the white light towards the receiver location to enhance the SNR when operating at high data rates.

The adaptation algorithms are implemented in a certain RGB-LD light unit for a single receiver at a given set of positions. When the receiver starts moving, they are applied in another RGB-LD light unit according to the new receiver location (coordinates). The reduction in complexity and SNR improvement at high data rates (i.e., 25 Gb/s) can be achieved according to the following algorithms:-

- Select-the-best (STB)

STB algorithm is introduced in Chapter 7 and it is used here to locate the closest transmitter (RGB-LD) to the receiver to implement the fully adaptive ADR VLC system.

- Fast computer generated holograms (FCGHs)

For a large room of 4m × 8m, the communication plane is divided into eight regions (2m × 2m per region). The floor (2m × 2m) under the visible light sources is subdivided into small areas, for example we divided it to 256 subdivisions (see Figure 8.1). In the case of classic beam steering [104] the transmitter first sequentially tries all *m* holograms (256 holograms in this case) and the receiver computes the SNR associated with each hologram at the receiver and relays this information to the transmitter for the transmitter to identify the best hologram to use (update the holograms). This is an exhaustive search mechanism among the stored holograms. If each SNR computation is carried out in 1 ms (based on typical processor) then the total adaptation time when the receiver moves is 256 ms. A further improvement in SNR can be achieved by increasing the number of regions on the floor which leads to smaller regions and improved SNR, but a larger number of holograms to choose from leading to an increase in the time required to identify the best holograms. For instance, increasing the number of regions from 256 to 512 will lead to an increase in the total number of holograms to 512. Hence the

computation time required to identify the optimum holograms is increased to 512 ms. In order to overcome this problem, a FCGHs algorithm is introduced to effectively improve the SNR (through the use of more holograms) while reducing the computation time required to identify the optimum hologram.

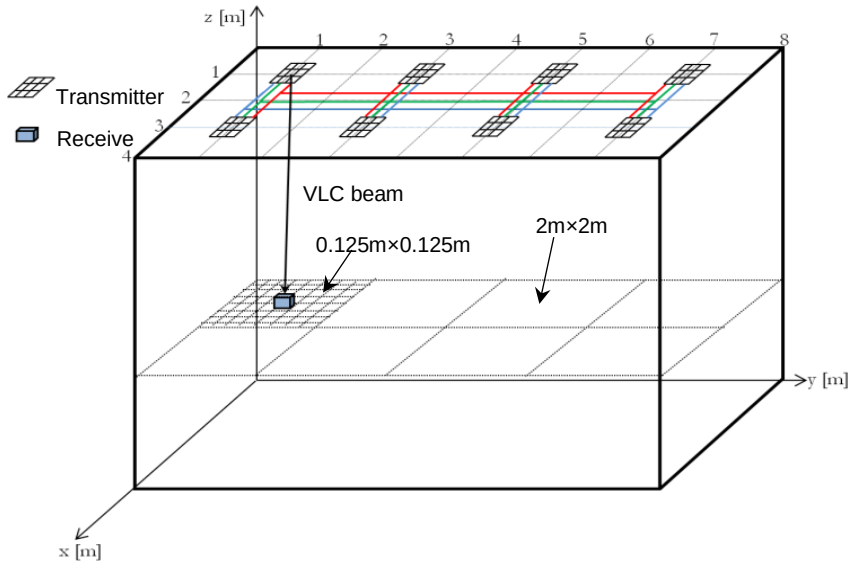

Figure 8.1: Architecture of our proposed VLC communication system when the transmitter is placed at (1m,1m,3m) and the receiver is on communication plane.

The FCGHs algorithm determines the optimum hologram that yields the best receiver SNR based on a divide and conquer (D&C) algorithm. The transmitter divides the stored holograms into four quadrants with a boundary based on the hologram transmission angles ($-\delta_{min}$ to 0) and (0 to δ_{max}) in both x, y axes. The transmitter first tries the middle hologram at each quadrant (four holograms will be first tried) to identify the sub-optimal quadrant; hence reducing the number of holograms that need to be tried by a factor of 4 in the first step. The receiver sends a feedback signal at a low rate, which informs the transmitter about the SNR associated with each hologram. The hologram that results in the best receiver SNR is identified as a sub-optimum hologram, and the quadrant that includes this sub-optimum hologram will be divided in the next step into four sub-quadrants. The transmitter again scans the middle hologram at four new sub-quadrants and identifies the second sub-optimal hologram; hence

identifying the second sub-optimal quadrant. The transmitter again divides the new second sub-optimal quadrant into four quadrants in a similar manner to the first and second sub-optimal quadrants to identify the third sub-optimal quadrant. The quadrant that is represented by the third sub-optimal hologram will be scanned. This technique helps to reduce the computation time required to identify the optimum hologram when a very large number of holograms is used. The proposed FCGHs algorithm can be described for a single transmitter and receiver as follows:

1- The RGB-LD light unit that has been chosen in the STB algorithm first divides the stored holograms into four main groups associated with quadrants based on the hologram transmission angles. The boundary angles associated with the first quadrant are δ_{max-x} to 0 in the x-axis and δ_{max-y} to 0 in y-axis.
2- The RGB-LD transmits a pilot signal using the middle hologram in each quadrant in order to determine the first sub-optimum hologram.
3- The SNR is computed at each step (each hologram) and the receiver sends a control feedback signal at a low rate to inform the controller of the SNR associated with each scan. This feedback channel can be implemented using an infrared beam.
4- The hologram that yield the best SNR is chosen by the controller (identifies sub-optimal quadrant for next iteration).
5- The new scanning area is divided into four quadrants and repeats steps 2 to 4 to identify the second sub-optimal quadrant.
6- Repeat steps 2 to 5 to identify the best location that gives the highest SNR (the divide and conquer process continues and the transmitter determines the optimal hologram transmission angles that maximise the receiver's SNR).

The proposed FCGHs reduce the computation time from 224 ms taken by the classic beam steering LD-VLC system to 32 ms (32 possible locations should be scanned in all iterations × 1 ms).

❖ Delay adaptation technique (DAT)

DAT is proposed in Chapter 5 and it is used here to reduce time delay differential between the signals received at the detector and to improve channel bandwidth. The MAC protocol should include a repetitive training period to perform the algorithms in Tables 8.1 and 8.2. It should be noted that the FCGHs described apply to a single transmitter and a single receiver position. If there is more than a single receiver (multi user) in the room, then a MAC protocol should be used. This will regulate which transmitter-receiver pair can use which resources (for example time slots, code, wavelength) and when.

Table 8.1: STB algorithm.

Inputs:	N =8; (Number of RGB-LD light units) j =3; (Number of branches in ADR) $p(.)$ is a rectangular pulse over $[0, Tb]$, $Tb = 1/B$ (B is the bit rate).
1.	for S =1: j;
2.	for R = 1: N;
3.	Calculate and sum the received powers within a time bin (0.01 ns duration)
4.	Produce the impulse response $h_j(t)$
5.	Calculate the pulse response $h_j(t) \otimes P(t - Tb)$ and then calculate $(PS_1 - PS_0)$
6.	Compute $SNR_j = \left(\frac{R(P_{S1} - P_{S0})}{\sigma_t}\right)^2$
7.	end for
8.	$SNR_N = max\ (SNR_j)$
9.	end for
10.	$SNR_{max} = max\ (SNR_N)$
11.	Select RGB-LD unit that yields SNR_{max}

Table 8.2: DAT algorithm.

1.	for S =1: j;
2.	for R =1: N;
3.	Compute the impulse response observed by the desired branch.
4.	$\mu_{NLD_S} = \frac{\sum_i t_i P_{ri}^2}{\sum_i P_{ri}^2}$; (compute mean delay associated with each signal from each RGB-LD unit).
5.	end for
6.	end for
7.	$\mu_{max} = max(\mu_{NLD_S})$;
8.	for R = 1: N;
9.	Δt_N_{LD}=μ_{max}- μ_{NLD_S}; (Calculate the time delay).
10.	Compute the impulse response $h_{NLD}(t)$ observed by the desired branch.
11.	Introduce time delay as $h_{NLD}(t - \Delta t\_N_{LD})$; (shift the impulse response)
12.	end for
13.	Produce the optimised impulse response $h_{optimised}(t)$
14.	Calculate the pulse response $h_{optimised}(t) \otimes P(t - Tb)$ and then calculate $(PS_1 - PS_0)$
15.	Compute the delay spread, 3dB channel and SNR optimised.

8.3 VLC System Complexity

Significant SNR and 3dB channel enhancements can be achieved by introducing beam steering and computer generated holograms in VLC systems, however the implementation complexity increases. This complexity is associated with the resources and computational time (computing the SNR and

time delay) required to identify the optimum location to steer the optical beam to. In this section we evaluate the efficiency of the proposed FCGHs by considering time complexity.

The nature of a function $T(m)$ [195] can be used to measure the computational complexity of algorithms, for example a linear algorithm of input size m can induce a linear time complexity of $T(m)=O(m)$. A single pass implementation algorithm with complexity order of $O(m)$ has an acceptable performance with a small value of m. However, a large value of m makes it too complex. The classical beam steering algorithm with computer generated holograms [104] can identify the optimum hologram by scanning all the areas underneath the best transmitter (see Figure 8.1), which has similar properties as the "one-pass" style algorithms. Therefore, the time complexity of the classical computer generated holograms is linear and can be given $T(m) = O(m)$. Here m represents the total number of regions that should be covered for each transmitter. Significant SNR improvements can be achieved by increasing the value of m. However, the time complexity increases dramatically and this is due to the total number of holograms required, which is m. In contrast, the FCGHs is a recursive algorithm based on a D&C method, where the process used to find the optimum hologram is recursively broken down into a number of iterations S. For example, in the case of four iterations (S=4), then the complexity can be given as [195]:

$$T(m) = j\ log_2\left(\frac{m}{j}\right) \tag{8.1}$$

where j is the number of sub-problems (quadrants in our FCGHs). In each iteration the transmitter divides the stored holograms into four quadrants (i.e., j = 4). For instance, in the case of m=256 (number of regions underneath the transmitter), hence the number of holograms required for classical computer generated hologram is 256. Then the computation time required to identify the optimum holograms is 256 ms (If each SNR computation is carried out in 1 ms,

based on typical processor). On the other hand, the computation time required to identify the optimum holograms in the FCGHs is 24 ms (based on equation 8.1).

8.4 Simulation Results in Empty Room

In order to study the performance of our proposed system, under mobility and multipath dispersion, consideration was given to an unoccupied rectangular room that had no furnishings, with dimensions of 8m × 4m × 3m (length × width × height). The simulation model was created with room measurements comparable to the one used in Chapters 3, 4, 5, 6 and 7.

In this section, we evaluate the performance of the proposed fully adaptive ADR VLC system in an empty room in the presence of multipath dispersion and mobility. The proposed system is examined in fourteen different locations when the receiver moves along the y-axis. The results are presented in terms of impulse response, delay spread, 3 dB channel bandwidth, SNR and BER.

An ADR with three branches is used for both systems (DAT ADR LD-VLC and fully adaptive ADR VLC). The ADR consists of three branches with photodetectors that have a responsivity of 0.4 A/W each. The ADR uses photodetectors with an area of 4 mm^2 each. The ADR was always placed on the communication plane, and results were obtained along the lines x=1 m or x=2 m. The direction of each branch in an ADR is defined by two angles: the azimuth angle (AZ) and the elevation angle (EL). The AZs of the three detectors were set at 0^o, 180^o and 0^o, and the ELs for the three branches were fixed at 90^o, 60^o and 60^o. The corresponding FOVs were fixed to 30^o, 25^o and 25^o. The AZs, ELs and FOVs were chosen through an optimisation process to achieve high SNR and low delay spread. For simplicity, SC is considered here in order to process the resulting electrical signals. SC represents a simple form of diversity, where the receiver simply selects the branch with the best SNR.

8.4.1 Impulse response

The impulse responses of the two systems (DAT ADR LD-VLC and fully adaptive ADR) at the room centre are depicted in Figure 8.2. It can be seen that the fully adaptive ADR VLC's impulse response is better than that of the DAT ADR LD-VLC in terms of received optical power. A significant increase in the received optical power can be achieved when the fully adaptive ADR replaces the DAT ADR LD-VLC system. A factor of 4 improvement is achieved, from 4.6 μW to 18.64 μW. This significant improvement in the received power is due to steering a beam of white light towards the receiver location.

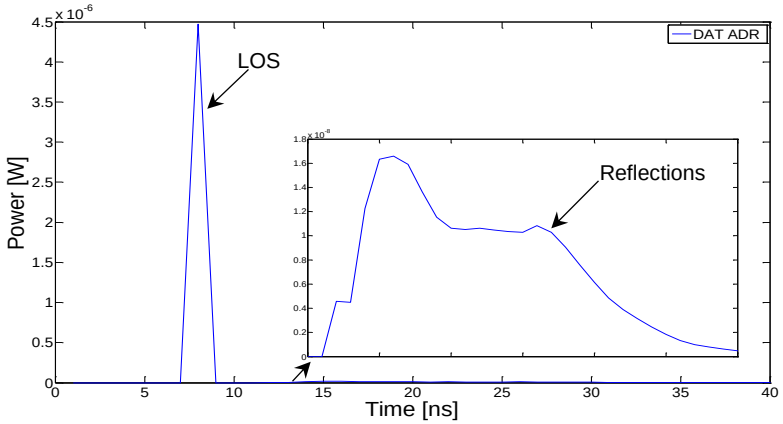

(a)

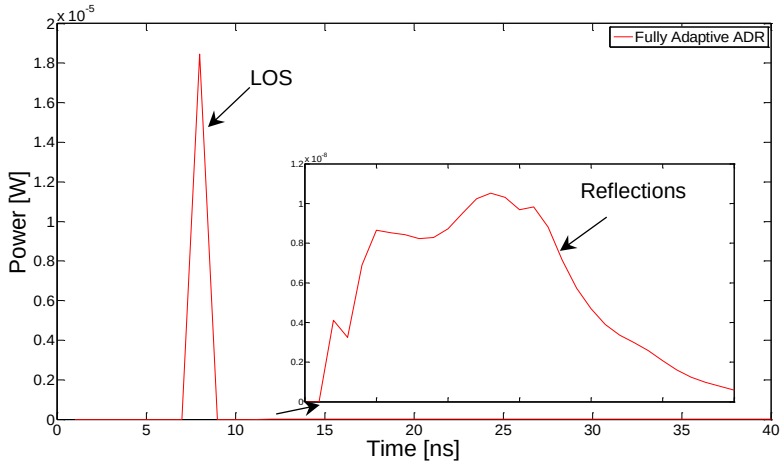

(b)

Figure 8.2: Impulse responses of different VLC systems at room centre: (a) DAT ADR LD-VLC and (b) fully adaptive ADR VLC.

8.4.2 Delay spread and 3 dB channel bandwidth

Figure 8.3 presents the communication system delay spread associated with the DAT ADR LD-VLC and fully adaptive ADR VLC systems. The results show that the fully adaptive system has a lower delay spread than the DAT ADR LD-VLC system at all the receiver locations considered. The delay spread for the DAT ADR system is relatively low (0.02 ns in the worst case) and this is attributed to two reasons: firstly, due to the narrow FOVs associated with each branch in the ADR, and this limitation in the FOV minimises the number of rays accepted. Secondly, DAT is used. However, to operate at high data rates (25 Gb/s and beyond) the delay spread should be further reduced (i.e. less than 0.02 ns). The fully adaptive ADR system outperforms the DAT ADR system, as it dramatically decreases the delay spread from 0.02 ns to 0.0058 ns (by a factor of 3.4) at the room centre. The minimum communication channel bandwidth of the fully adaptive ADR was 26 GHz (where the delay spread is 0.0058 ns at points x=2m, y=2m, 4m, 6m). It should be observed that the performance of both systems is degraded at x=2m (high delay spread), and this can be attributed to the high ISI due to multipath propagation in the middle of the room (i.e. x=2m). It should be noted that steering light to a receiver, not only increases the received power, it more importantly reduces the delay spread by increasing the power received through the direct ray well beyond the power received through reflections. Chapter 5 has shown that DAT with an ADR can provide a 3 dB channel bandwidth of more than 8.3 GHz under the worst case scenario. However, the main problem with such a system is the low SNR. Therefore, to enable it to operate at 25 Gb/s we proposed FCGHs to enhance the SNR and to utilise the significant increase in the channel bandwidth that will enable our proposed system (fully adaptive ADR VLC system) to operate at 25 Gb/s. The 3 dB channel bandwidth at x=2m in our systems is shown in Table 8.3. The results show that the proposed system has the ability to offer a communication channel with 3 dB bandwidth greater than 26 GHz.

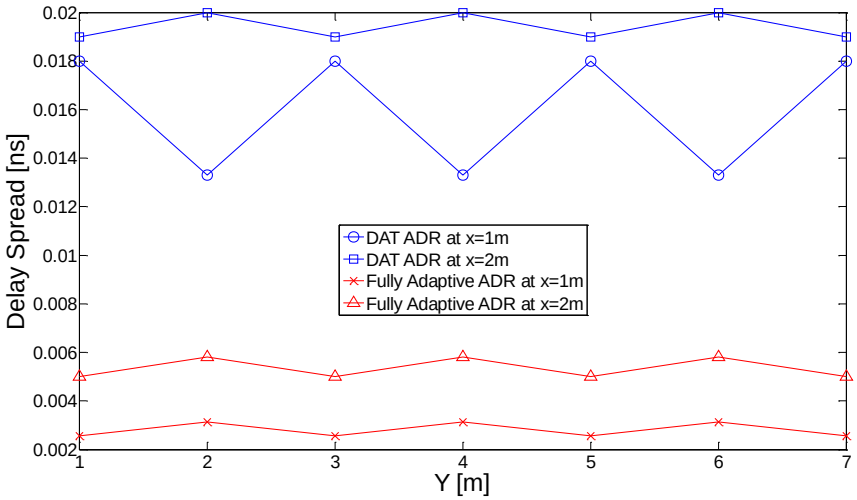

Figure 8.3: Delay spread of two systems at x=1m, x=2m and along y-axis.

Table 8.3: Channel bandwidth of proposed systems.

System	3 dB channel Bandwidth [GHz]						
	Receiver Locations along the y-axis, Y [m]						
	1	2	3	4	5	6	7
DAT ADR	8.7	8.3	8.7	8.3	8.7	8.3	8.7
Fully Adaptive ADR	29.5	26	29.5	26	29.5	26	29.5

8.4.3 SNR and BER

The p-i-n HEMT optical receiver proposed by Klepser [196] was used for the fully adaptive 25 Gb/s ADR VLC system. The noise current spectral density for this preamplifier is 12 $\mathrm{pA}/\sqrt{\mathrm{Hz}}$. In this study we considered SC method of processing the electrical signal from different branches in an ADR.

It should be noted that the fully adaptive ADR system has the ability to provide SNR values higher than those associated with the DAT ADR system. The results in Figure 8.4 are in agreement with the general observation made in

Figure 8.3. For instance, the DAT ADR system at x=2m and y=4m had a delay spread higher than other locations, which led to a decrease in SNR. Note the variation in SNR in tandem with the delay spread (see Figure 8.3) due to the effects explained. The DAT ADR system does not have the ability to operate at 25 Gb/s due to the impact of ISI and multipath propagation. However, these effects can be mitigated by employing fully adaptive ADR VLC. It can be noticed that for both systems the SNR can be lower when the receiver moves along x=2m. This is due to the larger distance between the receiver and transmitter.

Table 8.4 presents the BER values corresponding to the achieved SNRs at 25 Gb/s for the DAT ADR and fully adaptive ADR systems at the line x=2m (due to room symmetry, we calculated BER at 1 m to 4 m along the y-axis). It can clearly be seen that the fully adaptive ADR system has the best performance compared to the other systems. The highest value of BER in the fully adaptive ADR system is equal to 2.9×10^{-6}, and this value can provide a good communication link. FEC can be used to further reduce the BER from 10^{-6} to 10^{-9} in the proposed system.

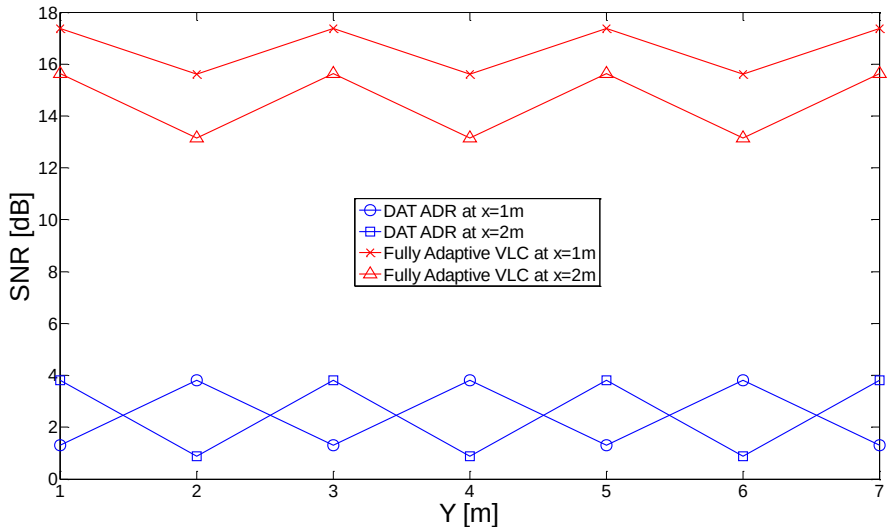

Figure 8.4: SNR of two systems (DAT ADR and fully adaptive ADR) when operated at 25 Gb/s at x=1m, x=2m and along the y-axis.

The system may choose to update its holograms less frequently even in the presence of mobility. This simplification is at the cost of an SNR penalty. In Figure 8.5, the SNR penalty was calculated based on the old holograms settings while in motion. The results show the SNR penalty incurred as a result of mobility. The proposed system (fully adaptive ADR) design should allow a link margin. For instance, with a link power margin of 3 dB, Figure 8.5 shows that adaptation has to be done every time the receiver moves by ~1.4 m. If the SNR penalty is lower than 1 dB as desired in the proposed system, then Figure 8.5 shows how often the system has to adapt its settings. For example, for the SNR penalty to be below 1 dB, the system has to adapt every 0.4 m, which corresponds to a 0.4 s adaptation rate. It should be noted that this adaptation has been done at the rate at which the environment changes and not at the system's bit rate.

Table 8.4: BER performance of proposed systems at x=2m.

System	BER			
	Receiver Locations along the y-axis, Y[m]			
	1	2	3	4
DAT ADR	7.7×10^{-2}	10×10^{-1}	7.7×10^{-2}	10×10^{-1}
Fully Adaptive ADR	1.6×10^{-9}	2.9×10^{-6}	1.6×10^{-9}	2.9×10^{-6}

8.5 Simulation Results in Realistic Room

In this section, we expand the analysis and the evaluation of the fully adaptive ADR system in realistic office arrangements where VLC signal blockage (as a result of mini-cubicles), doors and windows, furniture and multipath propagation all exist. The simulation model was created with room measurements comparable to the one used in Chapter 5 (see Figure 5.1b).

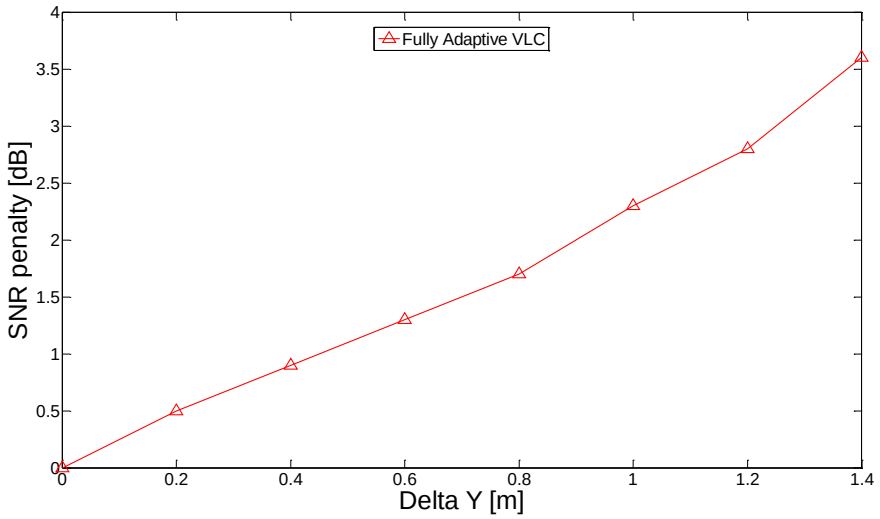

Figure 8.5: SNR penalty of proposed system when receiver moves from optimum location at (2m,1m,1m) along the y-axis.

Comparisons are performed of the proposed system in two different environments (i.e., an empty room A and a realistic room B) when operating at 25 Gb/s with full mobility. The results of the fully adaptive ADR VLC system were compared in rooms A (an empty room) and B (realistic room) in terms of impulse response, path loss and SNR. The proposed system is examined in fourteen different locations when the receiver moves along the y-axis.

8.5.1 Impulse response

Channel impulse responses at the room centre (i.e., x=2m and y=4m) for the fully adaptive ADR VLC system are shown in Figure 8.6 for rooms A and B. It should be noted that both impulse responses of the proposed system are dominated by short initial impulses due to the LOS path between the transmitter and receiver. It can be clearly seen that the amount of received optical power from the reflections in room B is less than that received in room A, as shown in Figure 8.6, and this is due to the existence of the door, windows, cubicles, partitions and bookshelves in room B that lead to reduced multipath propagation. These impulse responses suggest that the proposed system has good robustness against shadowing and mobility, which is attributed to the

FCGHs that maintain acceptable SNR in different environments. Although the received power from reflections was severely affected in room B, the LOS component remained the same in both room configurations in both systems, and the LOS component has the largest impact on the system performance. For instance, the power received by the proposed VLC system in room A was 18.64 μW, whereas it was 18.61 μW in room B, which indicates that the reduction in received power is negligible.

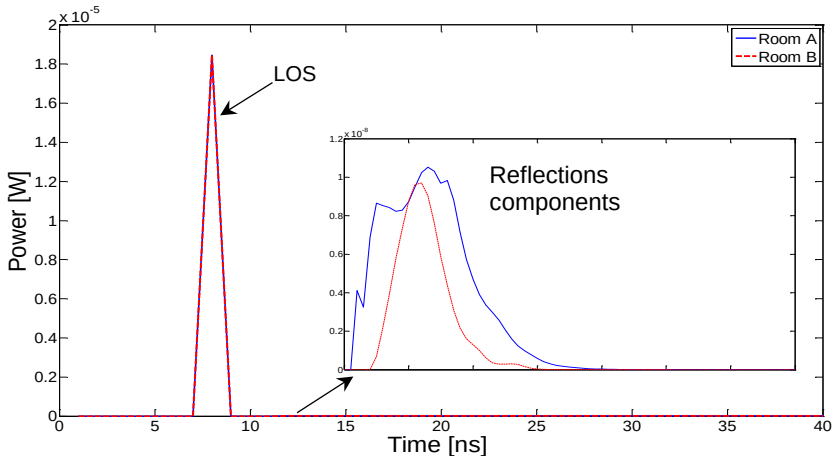

Figure 8.6: Impulse responses of fully adaptive ADR VLC system at room centre (2m, 4m, 1m) in two different environments (rooms A and B).

8.5.2 Path loss

Figure 8.7 shows the optical path loss of the proposed system in rooms A and B. It should be observed that the performance of the proposed system is comparable in rooms A and B, and this can be attributed to the LOS links available on the entire communication plane, which protects against shadowing and mobility in this system. It can be noticed that the path loss can be higher when the receiver moves along x=2m. This is due to the larger distance between the receiver and transmitter. Overall, the proposed system was evaluated and it was shown that it is able to achieve similar performance levels in an empty room and in a realistic indoor environment.

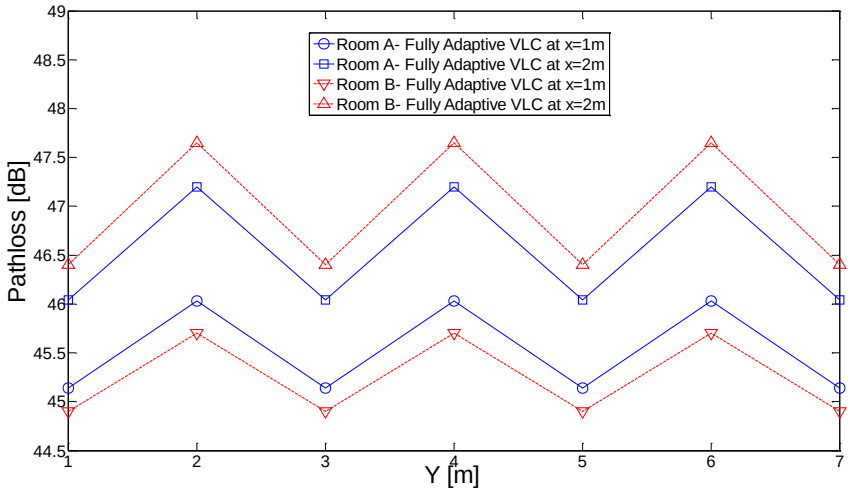

Figure 8.7: Optical path loss distribution of fully adaptive ADR VLC system in two different environments (rooms A and B) at x=1m and x=2m along y-axis.

8.5.3 SNR and BER

Figure 8.8 shows the SNR of the fully adaptive ADR VLC system at x=1m and x=2m along the y-axis over the communication plane for different environments (i.e. rooms A and B). In rooms A and B the proposed system has comparable results. There is very low degradation in the SNR when the proposed system operated in room B. This is attributed to the ability of our fully adaptive VLC system to adapt to such an environment. Also, it should be noted that the results in Figure 8.8 are in agreement with the general observation made in Figure 8.7. For instance, at the point x=2m and y=4m, the path loss is highest resulting in the lowest SNR.

Table 8.5 shows the BER at 25 Gb/s of the proposed system at line x=2m. It can be noted that in the realistic environment, the BER of the fully adaptive VLC system has increased slightly compared to an empty room. However, this increase does not severely affect the performance of the system; for example, the maximum value of BER provided by the proposed system is equal to 4.1×10^{-6}.

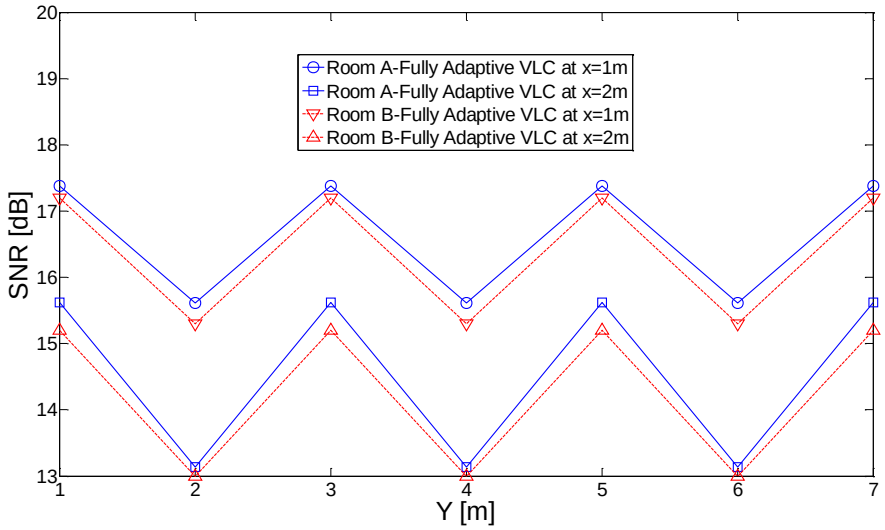

Figure 8.8: SNR of fully adaptive VLC when operated at 25 Gb/s in two different room scenarios at x=1m and at x=2m along the y-axis.

Table 8.5: BER performance of proposed system at x=2m in different environments.

System	BER			
	Receiver Locations along the y-axis, Y[m]			
	1	2	3	4
Room A-Fully Adaptive ADR VLC	1.6×10^{-9}	2.9×10^{-6}	1.6×10^{-9}	2.9×10^{-6}
Room B-Fully Adaptive ADR VLC	4.4×10^{-9}	4.1×10^{-6}	4.4×10^{-9}	4.1×10^{-6}

8.6 Fully Adaptive System Employing Imaging Receiver

The fully adaptive imaging (FAI) system has a similar room configuration and uses the same algorithms as the previous system (i.e., fully adaptive ADR). However, the main difference between the two systems is the type of receiver. An imaging receiver with 50 pixels is employed here (similar to the ones used in Chapter 4). In this section we used an imaging receiver with SC to choose the best pixel. We evaluate the performance of the proposed fully adaptive imaging VLC system in an empty room in the presence of multipath dispersion and

mobility. In this section, two VLC systems (FAI and imaging LD-VLC) are compared to identify the most appropriate system for use in high-speed VLC systems (25 Gb/s and beyond). The imaging LD-VLC system was previously introduced in Chapter 4 and it is considered here to compare it with FAI system. The results are presented in terms of delay spread, 3 dB channel bandwidth and SNR.

8.6.1 Delay spread and 3 dB channel bandwidth

Figure 8.9 evaluates delay spread and 3 dB channel bandwidth of the two systems under the worst case scenario (when the receiver moves along x=2m). The delay spread for the imaging LD-VLC system is relatively low (0.04 ns in the worst case). But, to operate at high data rates (25 Gb/s and beyond) the delay spread should be further reduced (i.e. less than 0.04 ns). The results show that the FAI system reduces the delay spread by a factor of 11.4 compared with the imaging LD-VLC system (from 0.04 ns to 0.0035 ns) at the room centre. The results show that the fully adaptive imaging VLC system has the ability to offer a communication channel with 3 dB bandwidth greater than 36 GHz.

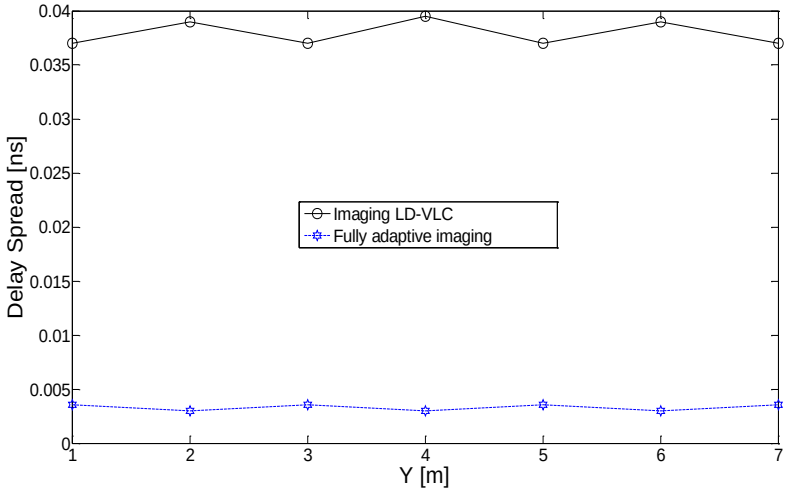

(a)

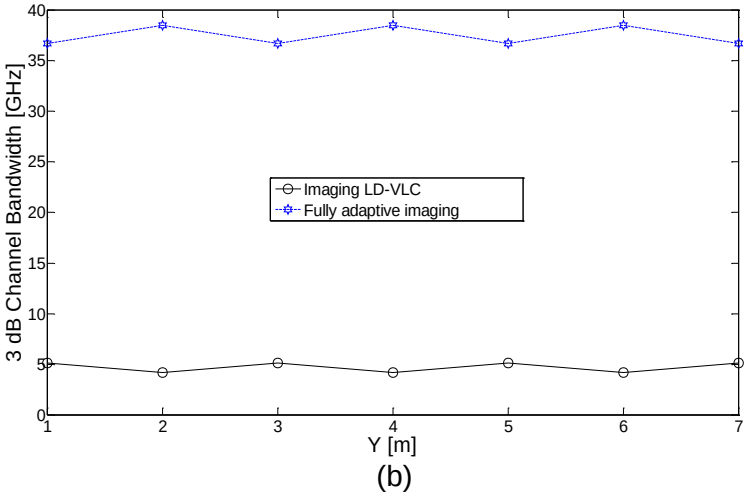

(b)

Figure 8.9: Delay spread and 3 dB channel bandwidth of two systems, (a) delay spread (b) 3 dB channel bandwidth.

8.6.2 SNR

It can be noted that FAI system has the ability to provide SNR values higher than this required value in all the receiver locations. The fully adaptive imaging system outperforms imaging LD-VLC system in terms of SNR (see Figure 8.10). It achieves about a 25 dB SNR gain over the imaging LD-VLC system at the worst case scenario. The imaging LD-VLC system does not have the ability to operate at 25 Gb/s due to the impact of ISI and multipath propagation. However, these effects can be mitigated by employing fully adaptive imaging system. The highest value of BER in the fully adaptive imaging system is equal to 4×10^{-12}, and this value can provide very good communication link.

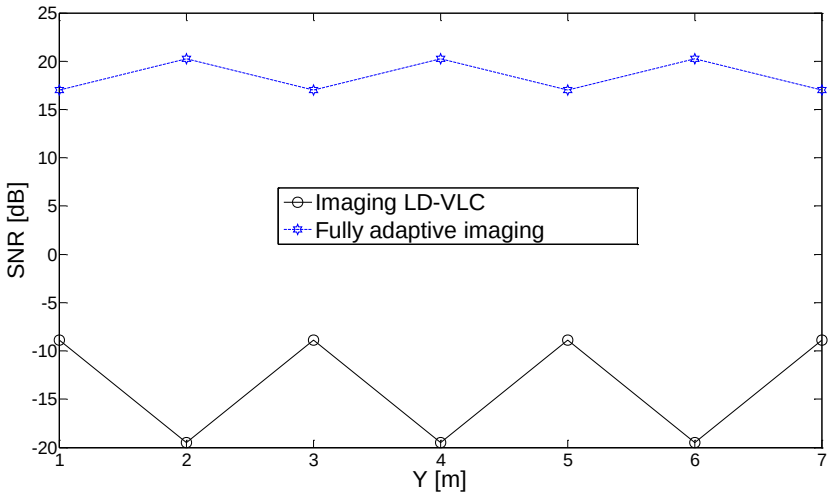

Figure 8.10: SNR of two systems when operating at 25 Gb/s at x=2m and along the y-axis.

8.7 Summary

In this chapter, we introduced a FCGHs VLC system and introduced a new fully adaptive VLC system that has ability to achieve 25 Gb/s. In addition, DAT was introduced to FCGHs to reduce the effect of multipath dispersion, delay spread and increase the 3dB channel bandwidth and SNR when the system operates at high data rates.

Increasing the number of holograms/regions helps the transmitter accurately identify the receiver's location, hence improving the system performance. A search algorithm based on D&C was used in order to reduce the time needed to select the best pre-calculated hologram which leads to high SNR. The proposed system is coupled with an ADR to improve the received VLC signal in the presence of multipath dispersion, mobility, and shadowing.

The proposed FCGHs can effectively steer the VLC beam nearer to the receiver location at each given receiver location. The time required to find the optimum location to steer the beam to, was reduced from 224 ms to 32 ms.

The simulation results show that the fully adaptive ADR VLC system can significantly improve the impulse response, SNR, as well as the delay spread compared to DAT ADR VLC system. In addition, the proposed system can also adapt to environmental changes, offering a link that is robust against signal blockage and shadowing. The BER provided by our proposed system in realistic indoor environment is about 10^{-6} at 25 Gb/s in the worst case scenario.

To the best of our knowledge, the data rates achieved by our proposed system (i.e. 25 Gb/s for a stationary user and 22.2 Gb/s for a mobile user) are the highest data rates to date for an indoor VLC system.

Finally, further improvement can be achieved when our fully adaptive system is used in conjunction with the imaging receiver. The highest value of BER in the fully adaptive imaging system is equal to 4×10^{-12}.

9 High Data Rate Backup Systems for Visible Light Communication

9.1 Introduction

Dimming is an important feature of an indoor lighting system where the illumination level can be controlled by the user. Therefore, integrating a VLC system with an illumination system poses some challenges. One of the main issues is that the light unit should be ‘‘ON’’ all the time to ensure continuous communication. Using light units (i.e., LED or LD) for communications raises a key question relating to establishing communication channels when the lights are off. The power at the VLC receiver is reduced when the user dims the lights to low levels, and this may lead to a degradation in the SNR and affect the achievable data rate. In the case of light dimming and ultimately turning off the light, the SNR degrades and the communication link is disconnected. Recently, hybrid schemes were proposed to support VLC systems, RF based systems are used to supplement the VLC system [197], [198], [199]. However, achieving a high transmission rate (multi gigabits per second) and security are the most challenging parts. The main goal of the work presented here is to provide practical solutions when the light is switched off and achieving data rates higher than those reported in [197], [198], [199]. In this chapter, we report the use of IR systems that utilise a LD source to support the VLC system when the light is totally switched off. IR optical communication has the same advantages as VLC systems. It can also provide high transmission data rates similar to VLC systems and potentially higher data rates (data rates up to 15 Gb/s employing OOK modulation can be achieved) [87], [88]. This is mainly because of the wider modulation bandwidth of the LD sources used in IROW systems instead of white LEDs. Despite these advantages, wireless IR systems encounter two

major impairments. The first is concerned with sensitivity to additive shot noise owing to sunlight or artificial background lighting. The second is the multipath dispersion associated with reflections from walls, the ceiling and room surfaces as well as the NLOS transmission of OW signals. Various techniques have recently been proposed to combat the impairments of IR systems, and higher bit rates have been achieved [86], [200]. Our goal in this chapter is to achieve high data rates when the VLC system is turned off by employing a hybrid diffuse IR system (HDIR) coupled with (i) a wide FOV receiver, (ii) a custom design imaging receiver, (iii) a beam steering IR (BSIR) system or (iv) a cluster distributed IR (CDIR) system. The data rates achieved (i.e., 1.25 Gb/s and 2.5 Gb/s) by our proposed backup systems are high compared with the ones provided by RF systems with the additional advantage that an infrared source can easily be integrated in current solid state lighting systems. In Chapter 4, we proposed the use of an imaging receiver for a VLC system to provide a robust link and mitigate multipath dispersion, as well as to improve the overall system performance. In this study we used two types of receivers: wide FOV and an imaging receiver (similar to the one that used in Chapter 4) with selective combining to choose the best pixel. The ultimate goal of this study is to provide alternative high data rate systems when the VLC system is disabled. The simulation results show that the proposed systems have the ability to achieve high data rates (1.25 Gb/s and 2.5 Gb/s) with a BER of 10^{-9} in the presence of multipath dispersion, receiver noise and mobility.

The rest of the chapter is organised as follows: Section 9.2 describes the simulation setup. Section 9.3 describes the backup system's configurations for VLC. The simulation results in an empty room are outlined in Section 9.4. The impact of the power transmitted and photo detector area are evaluated in Section 9.5. Finally, a summary is provided at the end of the chapter.

9.2 Simulation Setup

To study the performance of our proposed system, under mobility and multipath dispersion, simulations were run in a typical rectangular room that was unfurnished similar to the ones used in previous chapters. Previous research on IROW has found that the majority of the transmitted power is inside the first and second reflections, and that the power within the third and higher order reflections is very small [6], [136]. Therefore, reflections up to the second order were taken into account in our simulator. In this study, we do not consider the background noise from other artificial lights, since the light is off when the IR communication link is used. Higher bit rates of 1.25 Gb/s and 2.5 Gb/s are evaluated in our backup systems. We used the preamplifier design proposed in [161].

9.3 Backup Systems' Configurations

In this section, four IROW systems are presented, analysed and compared to identify the most proper system for use as a backup for VLC systems.

9.3.1 Hybrid diffuse IR (HDIR) system employing wide FOV receiver

The hybrid diffuse system employed one IR transmitter located at the centre of the ceiling, which can provide a direct LOS link at the receiver on the CP. Figure 9.1 shows the hybrid diffuse IR (HDIR) communication architecture. In this case, the majority of the power is collected from the direct link and lower power is collected through reflections. Our proposed transmitter (HDIR) uses a single wide beam source, typically with a Lambertian pattern where the transmitted optical signal fully diffuses over the environment. The IR transmitter is connected to all the visible light sources via fibre links (to link to main network in the building) and simple control circuits (located at the centre of the room). When the light is dimmed or the received optical power falls below a certain

threshold, the receiver sends a feedback signal at a low rate to the controller to switch the link into the backup system (i.e., HDIR). In this system we used a conventional single element wide FOV (90^{o}) photodetector with photo sensitive area of 4 mm^2. The HDIR transmitter is positioned at the centre of the room at (2m, 4m, 3m), is pointed downwards and emits 1 W with an ideal diffuse pattern. Exposure to optical radiation at such power levels can be hazardous to the skin and eyes. Nevertheless, different techniques can be used to reduce the impact of the high laser power, such as extending the source size, destroying its spatial coherence using holograms mounted on the transmitter or the use of arrays of transmitters. Pohl et al. have shown that such a source may use an integrating sphere as a diffuser to emit optical power in the range of 100 mW to 1 W [201]. Therefore, a transmitter power of 1 W will be assumed in this system.

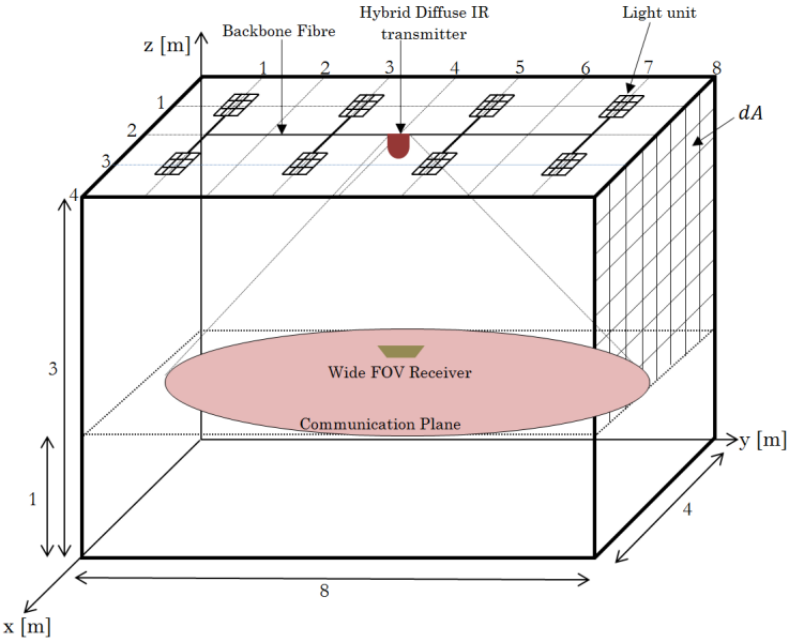

Figure 9.1: Architecture of HDIR with wide FOV receiver on communication plane.

9.3.2 Hybrid diffuse IR (HDIR) system employing imaging receiver

The HDIR system with imaging receiver has a similar room configuration and uses the same IR transmitter as the previous system. However, the main difference between the two systems is the type of receiver (see Figure 9.2). An

imaging receiver with 50 pixels is employed here. The imaging receiver offers two main advantages over the traditional non imaging receivers. Firstly, all detectors share a common concentrator (e.g., a lens). Hence, it can be fabricated with a smaller size and lower cost. Secondly, all photodetectors can be placed on a single plane. Therefore, the designer can opt to use a larger number of detectors with small detector areas and narrow FOV. This will reduce the impact of multipath dispersion and reduce the high capacitance associated with large area detectors, and consequently improve the receiver bandwidth.

In this chapter, we employed the imaging receiver design proposed in [103]. It is comprised of a single imaging lens and detector array that is subdivided into 50 pixels. The receiver detector array has a photosensitive area of 2 cm^2 and each pixel has an individual area of 4 mm^2. The reception zone of each pixel (on the ceiling) varies as the receiver terminal moves around the room over the CP. The calculation of the new reception zone associated with each pixel is discussed in detail in Chapter 4 [103]. The calculation of the received optical power is discussed in [103]. The simulation results were obtained at various receiver positions within the indoor environment.

9.3.3 Beam Steering IR (BSIR) system employing imaging receiver

In contrast to the HDIR, in the BSIR system the IR transmitter uses beam steering to steer the IR beam towards the receiver location. The IR transmitter faces downward at the centre of the ceiling as shown in Figure 9.3. Angle adaptation techniques, based on liquid crystal devices, have been investigated in IROW systems to maximise the SNR at the receiver [86], [87]. It has been shown to be an effective technique that can help optimise the distribution of the diffusing spots to maximise the receiver's SNR, regardless of the transmitter's position, the receiver's orientation and the receiver's FOV. However, this technique requires intensive calculations and time on a DSP to generate a hologram at each step.

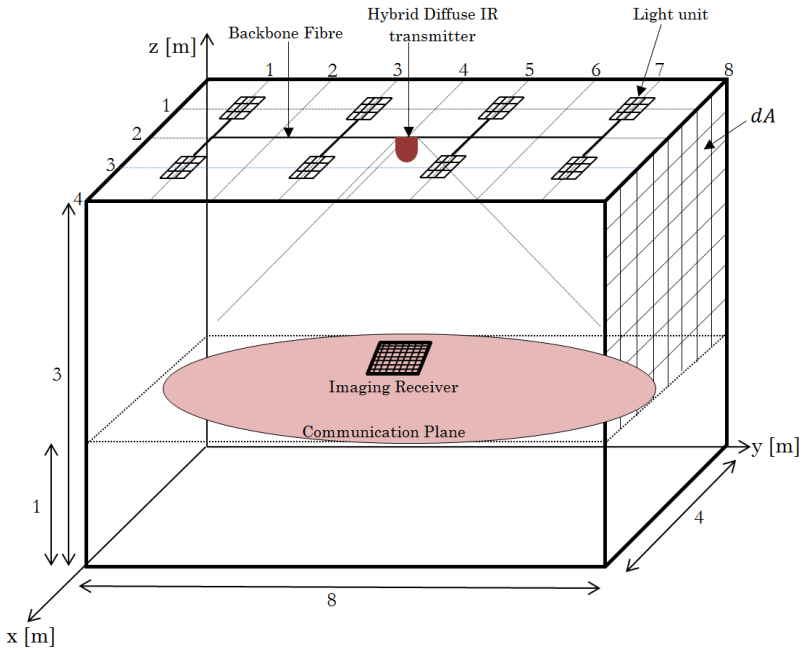

Figure 9.2: Architecture of HDIR with imaging receiver on communication plane.

In our new BSIR system, we propose an adaptive finite vocabulary (stored) hologram approach for beam steering in our backup system. For a large room of 4 m × 8m, the floor (i.e., CP) is divided into number of regions. The total number of holograms to be stored in our design is N, where N represents the number of regions into which the CP is divided. This large number of regions has been chosen to accurately identify the receiver location during its motion (user mobility). Since the transmitter is fixed at the centre of the room (close to the controller), the transmitter uses a hologram that steers the beam (narrow direct LOS link) to the optimum location if the receiver is present in any one of the regions. The concept of finite computer generated holograms has been recently proposed in IR diffusing spot systems and VLC systems [104], [184], and it is developed here for the first time in the BSIR system to improve the performance of the HDIR system.

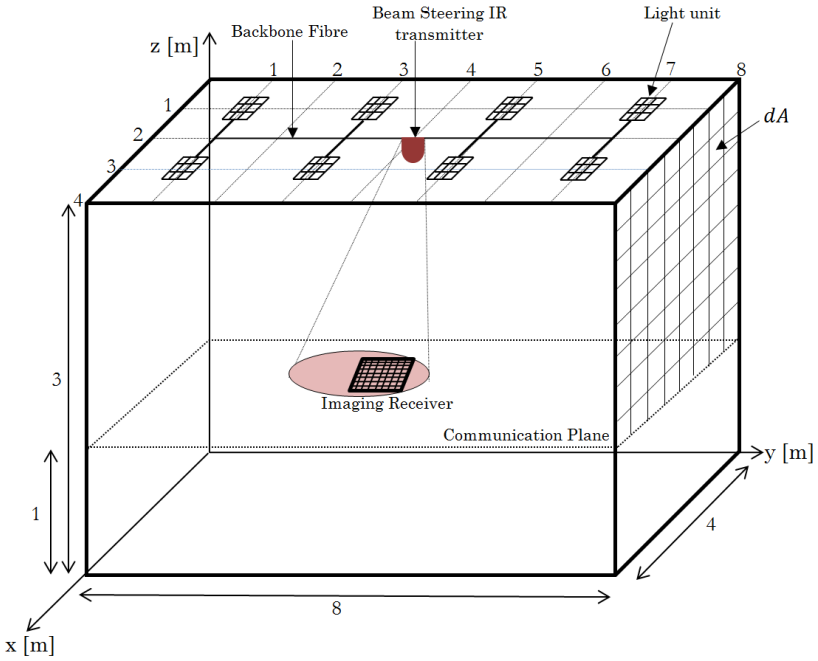

Figure 9.3: Architecture of BSIR with imaging receiver on communication plane.

9.3.4 Cluster distributed IR (CDIR) system employing imaging receiver

In the CDIR system, IR transmitters are used that utilise LD sources to support the VLC systems when the light is switched off. The CDIR system employs more than one IR source and distributes them on the ceiling, i.e., each IR source is attached to a VLC transmitter (i.e., light unit). All IR sources are connected via fibre and a control unit to perform cluster mechanisms. The new concept of using IR clusters is employed to design a new geometry that can achieve a good performance in mobile IR communications. A custom design for the imaging receiver (similar to the one in the previous systems) is used to reduce the impact of multipath dispersion and ISI. Figure 9.4 shows the architecture of our CDIR system. The proposed system consists of eight IR sources, and each is attached to a visible light source located on the ceiling, which can provide a direct LOS link to the receiver on the CP. The IR transmitters are connected to all visible light sources via fibre links (to link to the

main network in the building) and simple control circuits. As shown in Fig. 4, each IR source forms part of a cluster that can cover over 2m × 2m. When the light is dimmed or the received optical power falls below a certain threshold, the receiver sends a feedback signal at a low rate to the VLC transmitter to switch the link into the supporting CDIR system. A STB algorithm is used (similar to the ones used in Chapter 7) to select the optimum link between the IR transmitter and receiver (under mobility, this algorithm can be called periodically). The first step is to switch ON each IR source individually. Each source uses a single wide beam, typically with a Lambertian pattern with n=1, where n is the Lambertian emission order (the transmitted optical signal fully diffuses over the environment). The receiver then computes the received power and the SNR associated with each source. The receiver sends a signal, at a low rate, back to the control unit conveying the information about the SNR weight associated with each source to identify the receiver location (the receiver is located near to the source that has the highest SNR). The transmitter switches ON only the optimal IR source (source that is nearest to the receiver location) and other sources remain off to reduce the impact of multipath dispersion.

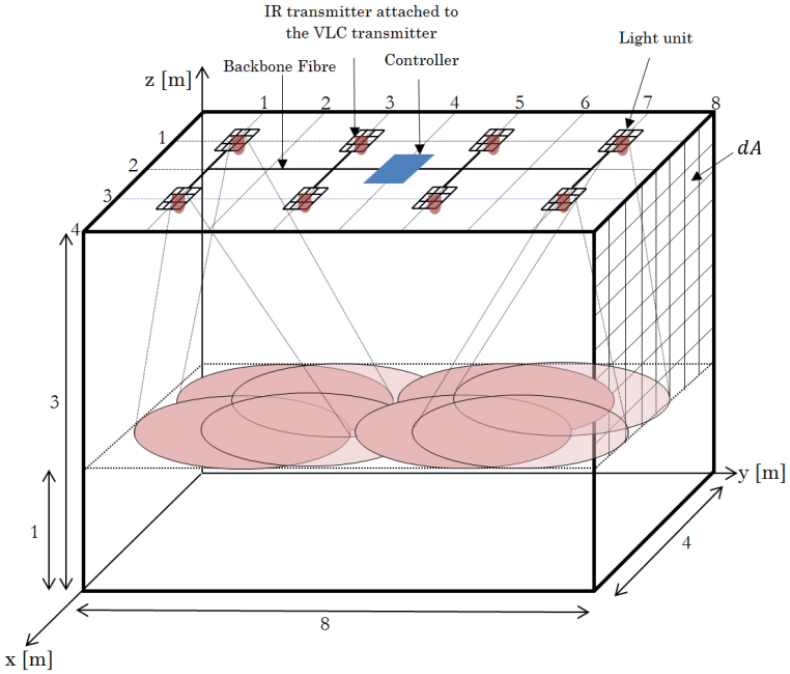

Figure 9.4: Architecture of CDIR when all IR transmitters are ‘‘ON’’.

The selected IR transmitter in the STB algorithm will then start to send information signals to the receiver. Figure 9.5 shows CDIR after employing STB. For the first step in the CDIR system (when applying the STB algorithm), each IR transmitter emits 100 mW (800 mW from eight transmitters). A 100 mW signal will be fully diffuse within the indoor environment (see Figure 9.4), while for next step (when the controller selects only one IR transmitter) only a 100 mW signal will be transmitted from the best IR transmitter as shown in Figure 9.5.

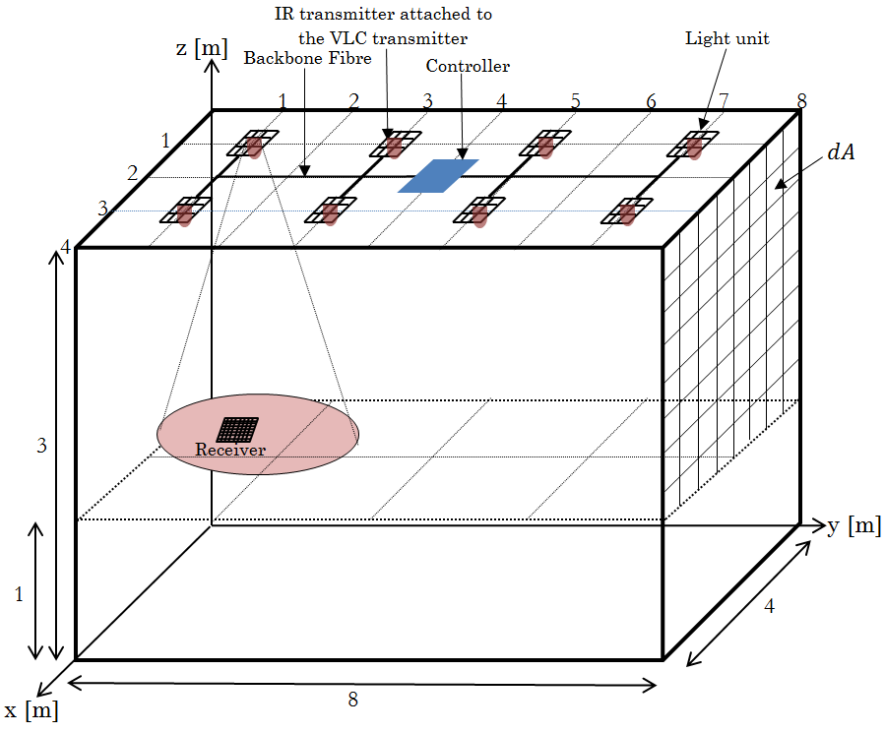

Figure 9.5: Architecture of CDIR when only one IR transmitter is ‘‘ON’’.

9.4 Simulation Results in Empty Room

In this section, we evaluate the performance of the proposed backup systems in an empty room in the presence of multipath dispersion, receiver noise and mobility. The results are presented in terms of delay spread, 3 dB channel bandwidth, SNR and BER.

9.4.1 Delay spread and 3 dB channel bandwidth

A comparison of the channel delay spreads of our proposed systems is given in Figure 9.6. The receiver moves along the x=1 m line in the HDIR (with wide FOV and imaging receiver) and BSIR systems, where this line is considered to be the worst communication link in the CP area due to its associated high ISI, path loss and multipath propagation level. In the CDIR system, the receiver moves along x=2m, which is considered the worst communication path. The HDIR system with wide FOV receiver shows much more signal delay spread due to the wide receiver FOV (FOV = 90^{o}), which accepts a wide range of rays with different path lengths from the transmitter to the receiver. In the HDIR system with an imaging receiver the delay spread results are quoted when the system employs selection combining of the imaging receiver pixels where the pixel with the best SNR (note the SNR expression accounts for delay spread) is selected. The delay spread of our HDIR is reduced from almost 1.55 ns to 0.1 ns when an imaging receiver replaces the wide FOV receiver. This is attributed to the narrow FOV associated with each pixel, which limits the rays received by using 50 small FOV (about 21°) pixels and selecting the best imaging receiver pixel. The proposed BSIR system coupled with an imaging receiver reduces the delay spread from 1.55 ns to 0.07 ns. This is attributed to two reasons: firstly, due to the narrow FOVs associated with each pixel in the imaging receiver, which minimises the number of rays accepted. Secondly, the use of beam steering helps reduce delay spread. It should be noted that steering light to a receiver, not only increases the received power, it more importantly reduces the delay spread by increasing the power received through the direct ray well beyond the power received through reflections. To further decrease the delay spread, the CDIR system is proposed. The CDIR system has the lowest delay spread compared with the other systems. The results show that the CDIR system reduces the delay spread by a factor of 10 compared with the HDIR system (from 0.3 to 0.03 ns) at the room centre. This is due to the distance

between the IR transmitter and the receiver being at a minimum compared with the other systems.

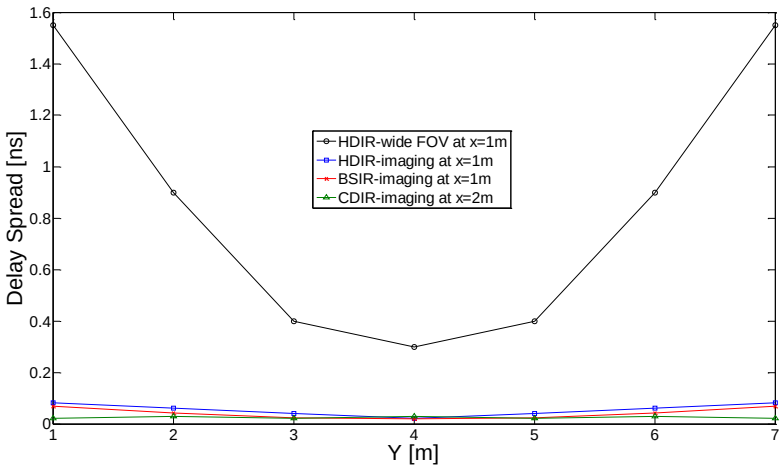

Figure 9.6: Delay spread of proposed systems.

Table 9.1 shows the 3 dB channel bandwidth of the proposed systems. The 3 dB channel bandwidth of the HDIR system is very low and this is due to the number of IR spots seen within the receiver's FOV. However, when the HDIR is combined with the imaging receiver (with narrow FOV) the channel bandwidth increases dramatically, as shown in Table 9.1. It can be clearly seen that when the BSIR system replaces the HDIR (with wide FOV and imaging) system the channel bandwidth increases, and this is due to the effects explained. The results show that the CDIR system has the ability to offer a communication channel with 3 dB bandwidth greater than 5 GHz in the worst case scenario.

Table 9.1: 3 dB channel bandwidth of proposed systems.

System	3 dB Channel Bandwidth [GHz]						
	Receiver Locations along the y-axis, y [m]						
	1	2	3	4	5	6	7
HDIR-wide	0.1	0.1	0.4	0.5	0.4	0.1	0.1
HDIR-image	2	2.7	4	7.9	4	2.7	2
BSIR-image	2.4	3.9	6.9	8.7	6.9	3.9	2.4
CDIR-image	7.8	5.5	7.8	5.5	7.8	5.5	7.8

9.4.2 SNR and BER

The SNR evaluation of the proposed backup VLC systems was performed under the effect of receiver noise, mobility and multipath propagation. The proposed systems were set to operate at 1.25 Gb/s and 2.5 Gb/s. Figure 9.7 shows the SNR of the proposed systems when operated at 1.25 Gb/s. It can be clearly seen that the HDIR system with wide FOV receiver does not have the ability to operate at a high data rate. However, when the imaging receiver is combined with this system it can perform better than when using the wide FOV receiver. This is due to the ability of the imaging receiver to combine the signals from the optimum pixels that monitor the best received signal during mobility. The imaging receiver uses a large number of detectors with a narrow FOV and small detector area. The HDIR system coupled with an imaging receiver provides around 10 dB under the worst case scenario, while the HDIR system with wide FOV can only achieve -14 dB at the same location. It should be noted that the BSIR system has comparable performance with the HDIR imaging system when both used a 100 mW transmission power. To achieve a BER of

10^{-9} in OOK, a SNR of 15.6 dB is required. It can be noted that the CDIR system has the ability to provide SNR values higher than this required value in all the receiver locations. The CDIR system outperforms other systems in terms of SNR, as it achieves about a 22.5 dB SNR gain over the HDIR system (with wide FOV) in the middle of the room. This significant improvement in the SNR level is attributed to the small path loss between the transmitter and the receiver (the IR transmitter is always close to the receiver).

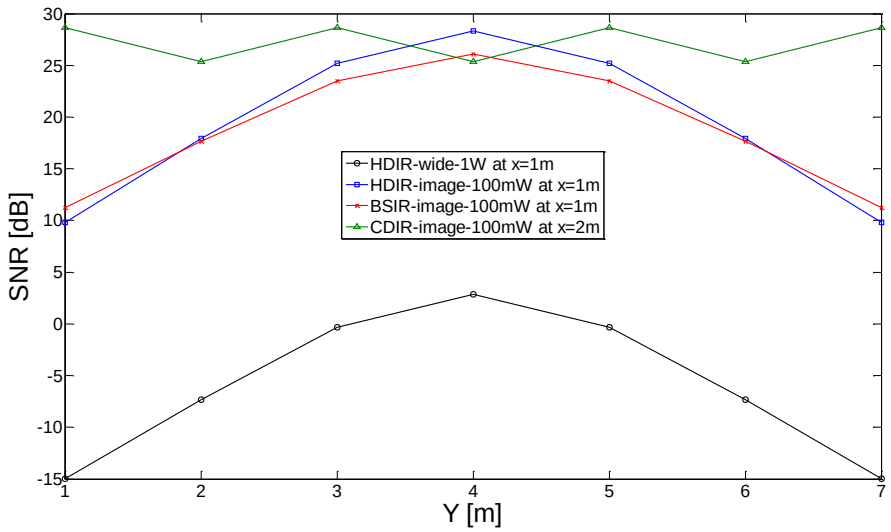

Figure 9.7: SNR of four systems when operated at 1.25 Gb/s.

Figure 9.8 shows the SNR of the VLC backup systems at 2.5 Gb/s. Our simulation findings illustrate a degradation in the SNR of the HDIR system when employing the wide FOV or imaging receiver. This is due to most of the received power coming from the reflections and will be considered as ISI at high data rates (i.e., 2.5 Gb/s). A considerable enhancement can be obtained by using the BSIR system, which offers a 33 dB SNR advantage above the HDIR wide FOV receiver at location x=1m, y=1m, z=1m. This enhancement in the SNR is due to the fact that the SBIR system has the ability to steer the IR beam towards the receiver location and, thus, increase the power received by the pixels. Although improvements were achieved in the BSIR system SNR, a

degradation in the SNR is noted when the receiver is on the move (mobile). Therefore, the effect of receiver mobility can be reduced by employing our CDIR system, which is capable of equally covering its environment through the use of a number of IR transmitters distributed on the ceiling (see Figure 9.4).

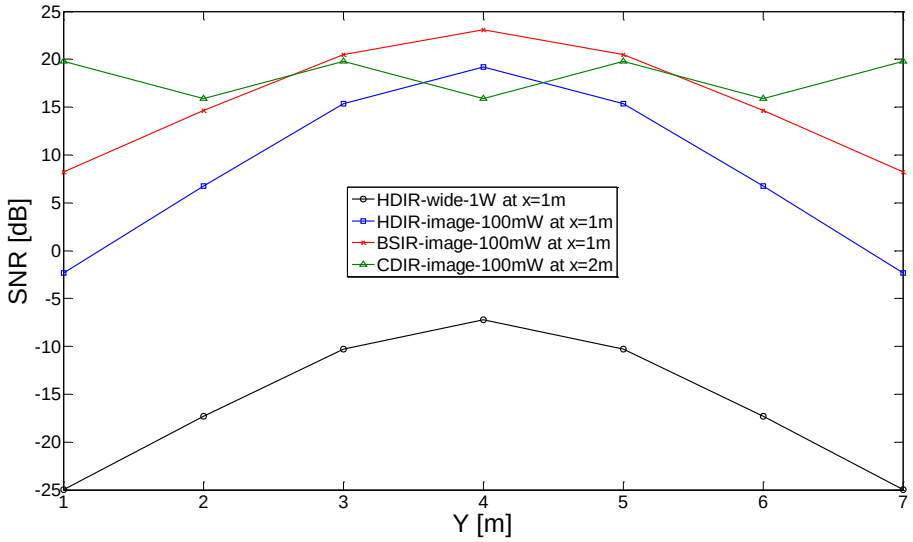

Figure 9.8: SNR of four systems when operated at 2.5 Gb/s.

Table 9.2 shows the BER at 2.5 Gb/s for the proposed systems (HDIR wide FOV, HDIR imaging, BSIR and CDIR). It should be noted that the CDIR system has the best performance compared to the other systems. At certain locations in the room, e.g., at x=2m, y=2, z=1m, the BER of the CDIR system is higher. However, this increase does not severely affect the performance of the system; for example, the maximum value of the BER provided by the CDIR system is equal to 2.3×10^{-10}.

Table 9.2: BER of proposed systems.

System	BER			
	Receiver Locations along the y-axis, y [m]			
	1	2	3	4
HDIR-wide	Error	Error	Error	8×10^{-1}
HDIR-image	3×10^{-1}	1.6×10^{-2}	2.2×10^{-9}	Error free
BSIR-image	5.5×10^{-3}	3.6×10^{-8}	Error free	Error free
CDIR-image	8.3×10^{-23}	2.3×10^{-10}	Error free	2.3×10^{-10}

9.5 Summary

In this chapter, we addressed a key problem related to the implementation of dimming in VLC systems. We introduced four backup systems to support a VLC system in the case of full dimming (lights off). We proposed new systems that use diffuse IR, beam steering and clustering distribution coupled with imaging receivers to improve the system performance at high transmission rates (1.25 Gb/s and 2.5 Gb/s) to provide alternative high data rate wireless communication during the dimming time.

The proposed HDIR system is coupled with a wide FOV and imaging receiver to improve the received optical signal SNR in the presence of multipath dispersion, receiver noise and mobility. The imaging receiver is shown to be tremendously efficient in reducing the channel delay spread from 1.55 ns to 0.1 ns. A BSIR system is also proposed to further reduce the delay spread and increase the SNR by steering the IR beam nearer to the receiver location at each given receiver location. In addition, our CDIR system has the ability to decrease the delay spread of the HDIR wide FOV system by 90% from 0.3 to

0.03 ns at the room centre (x=2m, y=4m), which leads to an increase in the channel bandwidth by a factor of 10 from 550 MHz to 5.5 GHz.

Simulation results show that the HDIR and the BSIR systems coupled with an imaging receiver achieved around -2 dB and 8.2 dB SNR at 2.5 Gb/s, respectively. Further improvement of the SNR can be achieved by introducing a new CDIR system and employing more than one IR source distributed on the ceiling (attached to the VLC sources). The simulation results show that the CDIR system can significantly improve the SNR, as well as reduce the delay spread, compared to other systems. The BER provided by the CDIR system is better than 10^{-9} at 2.5 Gb/s in the worst case scenario.

One of the key issues in such a backup system is that we require the same device to be operated in the lights ‘‘ON’’ regime (i.e., VLC) and also work in the lights ‘‘OFF’’ regime (i.e., IR). However, to deal with this issue the receiver may employ VLC and IR detectors connected through an electronic switching mechanism to control their functions. The development of control algorithms to switch between VLC and our HDIR, BSIR and CDIR systems is of interest and should be pursued. Additional future work will address methods to enhance the SNR of the CDIR system to achieve data rates higher than 2.5 Gb/s.

10 Collaborative VLC/IROW Systems

10.1 Introduction

The concept of VLC systems is based on the use of light units (LED/LD) for both lighting and communications. Therefore, using light units (i.e., LED or LD) for communications should not interfere with the light units' main function (i.e., illumination). A user may arbitrarily dim the light source in the VLC system to save power, so it is essential to maintain communication in this case.

The received power at the VLC receiver is reduced when the user dims the light to low levels, and this will lead to a degradation in the SNR and affect the data rate achievable. The VLC link needs to collaborate with the IROW connection to provide continuous data transmission. When the VLC link has recovered (i.e., there is no dimming), the VLC and IROW systems can cooperated together to increase the data rate at the receiver side.

The main target of the work presented in this chapter is to provide practical solutions in the case of light dimming, hence to maintain the achievable data rate (5 Gb/s) even when under dimming or the light is totally off. In this chapter we investigate the performance of a VLC system under the impact of different levels of dimming, propose an adaptive rate technique (ART) and produce the concept of cooperation between VLC and IROW systems. The VLC system is able to achieve high data rates (5 Gb/s) when the light units are 'ON'. However, the achieved data rate (i.e., 5 Gb/s) will decrease as a result of light dimming. Therefore, IROW systems are proposed to ensure the continuity of the wireless communication and to maintain the target data rate (5 Gb/s), as the IROW system can be used to compensate for the degradation of the data rate due to

dimming in the VLC system. In addition, the IROW system can be used to increase the data rates so they are higher than the target (5 Gb/s) when the lights are ‘ON’ and the VLC system is operating normally.

Two IROW systems are proposed: CDIR system and a cluster distributed beam steering IR (CDBSIR) system, to collaborate with the VLC system. The data rates achieved by our proposed backup systems are 5 Gb/s when using a very simple modulation format (OOK). In this study we used an imaging receiver that employs 50 pixels. The photocurrents received in each pixel can be amplified separately and can be processed using different methods (SC, EGC or MRC). For simplicity, SC is considered here.

The remainder of this chapter is organised into the following sections: Section 10.2 presents the proposed systems’ configurations. Section 10.3 introduces the ART and the impact of dimming on the VLC system performance. Section 10.4 introduces the simulation results and discussion of the IROW systems. Section 10.5 provides the simulation results and discussion of the collaborative VLC/IROW system in an empty room. Finally, a summary is provided at the end of the chapter.

10.2 Proposed Systems’ Configurations

In this section, four OW systems are presented, analysed and compared to identify a reliable and high data rate wireless communication system for an indoor user.

10.2.1 Imaging LD-VLC system

The imaging LD-VLC system employed eight RGB-LD transmitters (lighting fixtures) on the ceiling connected by fibre interconnect and controlled by a central controller and an imaging receiver with 50 pixels. The imaging LD-VLC system was proposed in Chapter 4 and it is considered here to investigate its

performance under the impact of different levels of dimming. In addition, it will be integrated with an IROW system to provide reliable and high data rate services for an indoor user. Figure 10.1 shows the architecture of the imaging LD-VLC system.

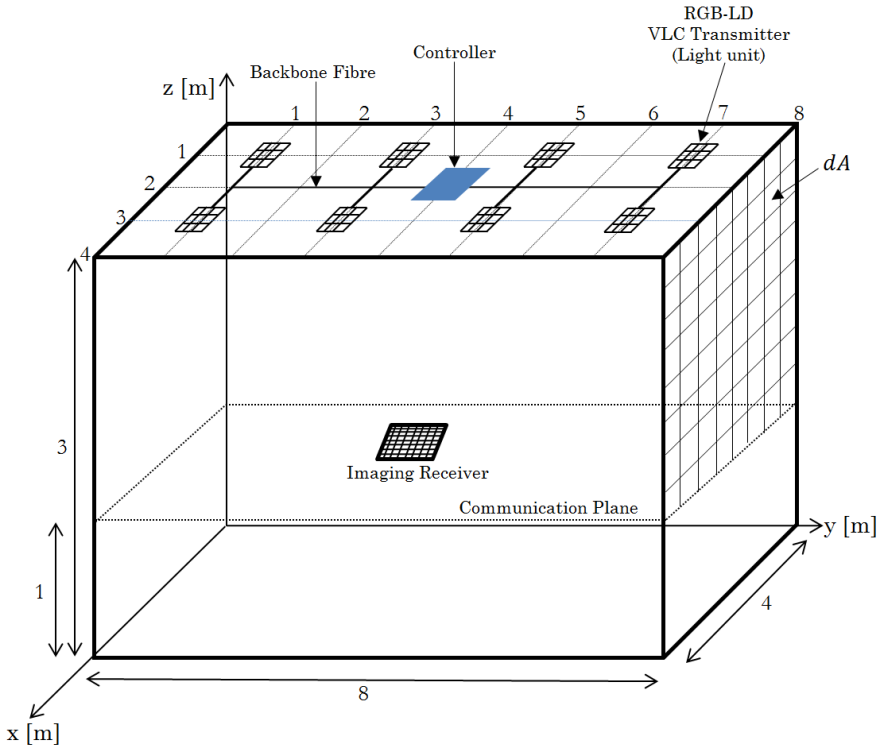

Figure 10.1: Architecture of imaging LD-VLC system with imaging receiver on communication plane.

10.2.2 IROW systems

Two IROW systems are presented, analysed and compared to identify the most appropriate system for use to collaborate with the VLC system (imaging LD-VLC).

10.2.2.1 Cluster distributed IR (CDIR) system

The CDIR system employed eight IR transmitters attached to the light units (VLC transmitters), and each IR transmitter can provide a direct LOS link to the receiver on the CP. All IR sources are connected via fibre and a control unit is

used to perform the cluster mechanism. Figure 10.2 shows the CDIR communication architecture. The CDIR system was proposed in Chapter 9 and it is considered here to compare it with CDBSIR system**.**

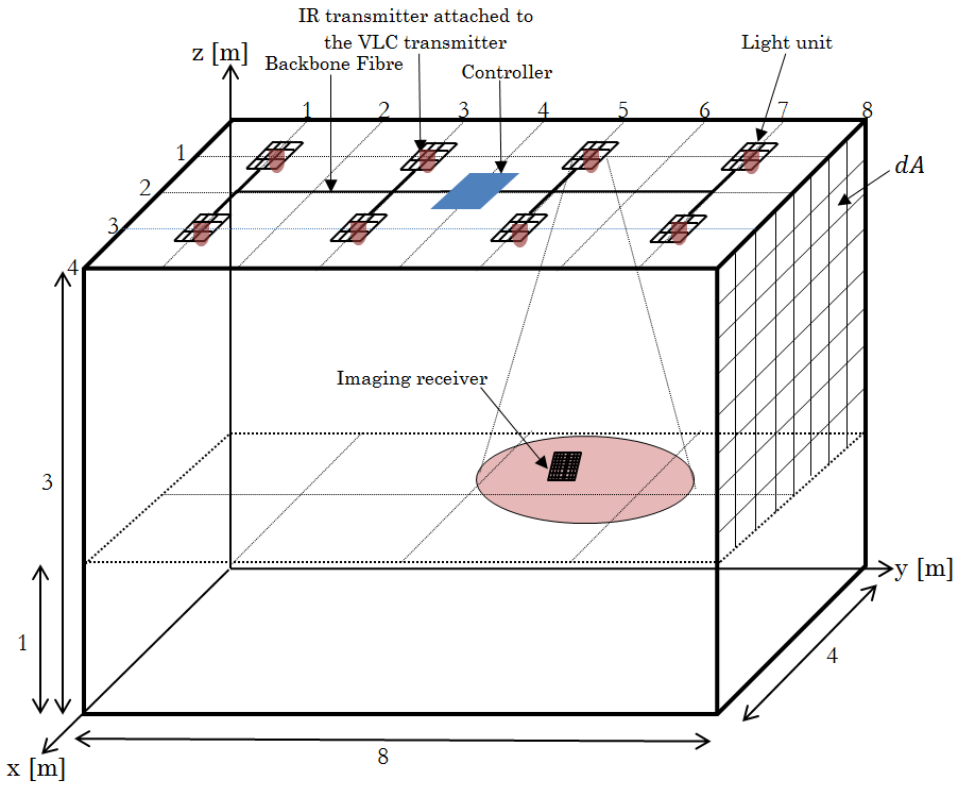

Figure 10.2: Architecture of CDIR system with imaging receiver on communication plane.

10.2.2.2 Cluster distributed beam steering IR (CDBSIR) system

In contrast to the CDIR, in the CDBSIR system the IR transmitter uses the beam steering to steer the IR beam toward the receiver location. Like, CDIR, the CDBSIR system employs a STB algorithm to select the closest IR transmitter to the receiver. Then selected IR transmitter in the STB algorithm will then apply fast beam steering technique similar to the ones used in Chapter 8.

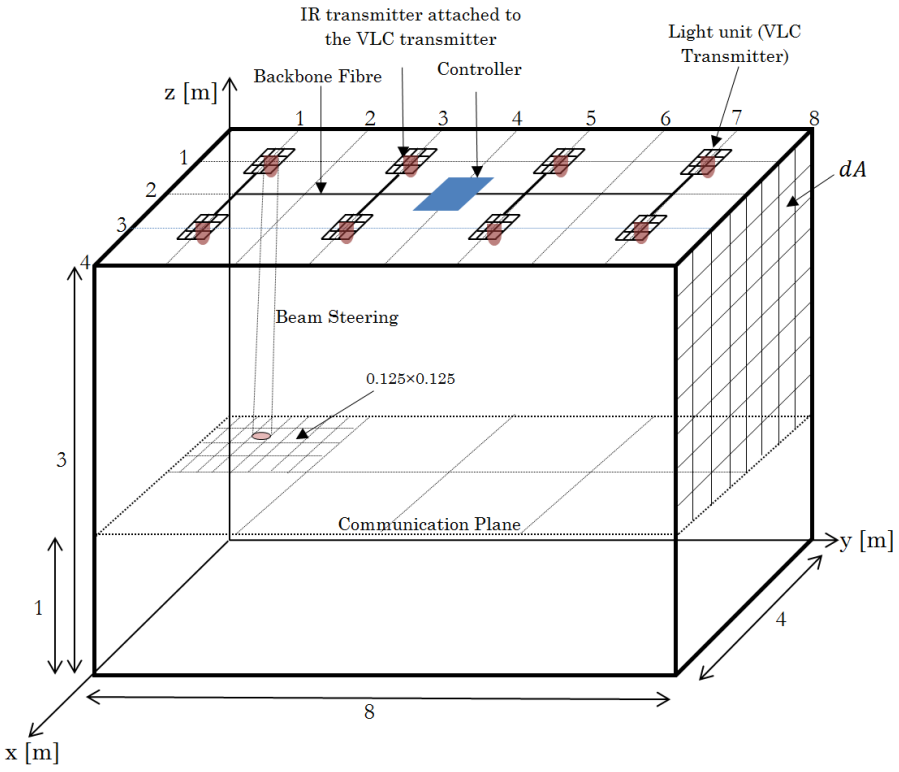

Figure 10.3: Architecture of CDBSIR system.

10.2.3 Collaborative VLC/IROW system

It is desirable to continue to provide a high data rate service while a user dims the light source to any level. However, the received power at the VLC receiver is reduced when the user dims the light to low levels, and this leads to a degradation in the SNR and affects the achievable data rate. Therefore, a collaborative VLC/IROW system is introduced to address this issue, and when the VLC has partial dimming, such as 75% or 50%, both the IROW and VLC systems can collaborate to maintain the target data rate (5 Gb/s). The IROW system can be used to compensate for the degradation of the data rate due to dimming in the VLC system. It should be noted that the IROW system sends information at a fixed rate of 5 Gb/s. In the case of no dimming, the VLC and IROW can be used to increase the data rate higher than the maximum VLC data rate (i.e., higher than 5 Gb/s); hence, the achieved data rate will be 10

Gb/s instead of 5 Gb/s. Figure 10.4 shows the architecture of the VLC/IROW system. The proposed system consists of eight IR sources (similar to those used in the CDBSIR system) and eight VLC transmitters (similar to those used in the imaging LD-VLC system) and employs an imaging receiver with 50 pixels.

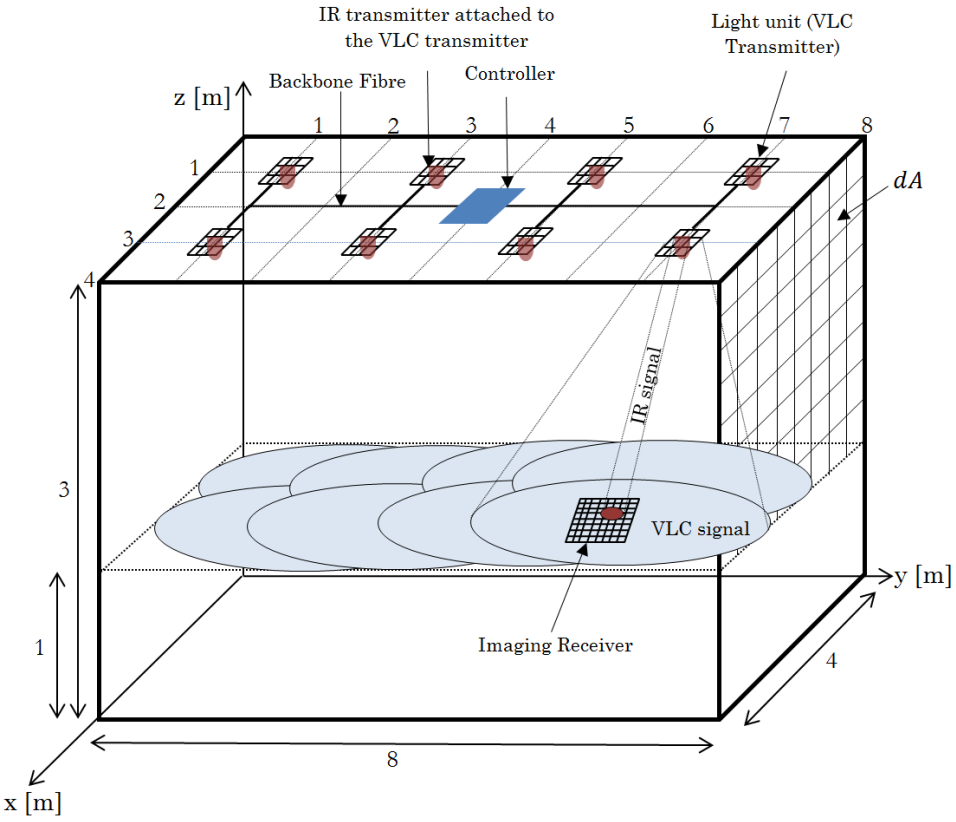

Figure 10.4: Architecture of collaborative system.

10.3 Adaptive Rate Technique

In this section, we introduce the ART and evaluate the performance of the imaging LD-VLC system under the impact of multiple levels of light dimming (25%, 50% and 75%). The results are presented in terms of the SNR at different operating data rates (5 Gb/s, 2.5 Gb/s and 1.25 Gb/s).

It should be noted that an SNR equal to 13.5 dB is needed for a 10^{-6} BER. Therefore, we have chosen BER=10^{-6} as the threshold in the imaging LD-VLC

and we employ an ART to ensure that we have an acceptable quality communication link under different levels of dimming. ART is carried out at the receiver and the controller. First, the receiver monitors BER continuously, and when it becomes higher than 10^{-6}, the receiver send a feedback signal called the channel quality indicator (CQI) to inform the controller to move to the next transmission rate (lower transmission rate when the BER becomes higher than 10^{-6}).

In our VLC system we provide three data rates (5 Gb/s, 2.5 Gb/s and 1.25 Gb/s). For example, when the receiver is operating at 5 Gb/s and the BER becomes higher than 10^{-6} (i.e., the SNR decrease below 13.5 dB), the receiver will send CQI_1 to inform the controller to reduce the transmission rate to 2.5 Gb/s. Then the receiver measures the SNR and if the BER is still higher than 10^{-6}, then the receiver will send CQI_2 to inform the controller to further reduce the data rate (i.e., from 2.5 Gb/s to 1.25 Gb/s). Again, if the BER is still higher than 10^{-6}, then the receiver will send CQI_3 to inform the controller to stop transmission and the communication link is disconnected. However, it is desirable to maintain communication while a user arbitrarily dims the light source. Therefore, we have introduced a collaborative VLC/IROW system to address this issue (i.e., degradation in the SNR due to dimming will lead to a disconnect in the communication link). It should be noted that the ART has two procedures: down convert and up convert. Down convert is when the controller reduces the data rate due to degradation in the BER (when dimming occurs). Up convert is when the controller increases the data rate (e.g., from 1.25 Gb/s to 2.5 Gb/s) due to maintaining a very low BER at the receiver side (i.e., 10^{-9}). The CQI_4 and CQI_5 signals can be used to inform the controller to increase the data rate from 1.25 Gb/s to 2.5 Gb/s and from 2.5 Gb/s to 5 Gb/s, respectively.

ART is carried out at the start of a one second frame, and if the BER has changed compared to the previous frame's values then the receiver uses the

feedback channel to update the controller. The ART (down convert) can be applied according to the following steps:

1- The receiver sends (using an infrared beam) a low data rate control feedback signal (CQI) to inform the controller that the BER has become lower than 10^{-6}.
2- The controller decreases the current data rate to the lower service (e.g., 5 Gb/s to 2.5 Gb/s).
3- The receiver estimates the BER, and if it is still below 10^{-6}, it will send another CQI to inform the controller.
4- The controller further decreases the data rates (e.g., from 2.5 Gb/s to 1.25 Gb/s), and if it receives another CQI from the receiver, the controller will stop the transmission.

A flow chart of the down convert ART is shown in Figure 10.5. To evaluate the performance of the imaging LD-VLC system at different levels of light dimming, the SNR was calculated at 5 Gb/s, 2.5 Gb/s and 1.25 Gb/s. Figure 10.6 illustrates the SNR of the VLC system when it was operated at 5 Gb/s; the imaging LD-VLC system achieved about a 15.6 dB SNR at the room centre (worst case scenario) when dimming did not exist. However, it can be clearly seen that when the user dims the light by more than 25% the SNR is decreased and the BER becomes higher than 10^{-6}. This means that the VLC system cannot operate at this data rate (5 Gb/s) when the light is dimmed by more than 25%. Figures 10.7 and 10.8 show the SNR of the imaging LD-VLC system when operating at 2.5 Gb/s and 1.25 Gb/s, respectively. When the imaging LD-VLC is operated at 2.5 Gb/s it is able to maintain a BER of 10^{-6} at a dimming level of up to 50%. On the other hand, the VLC system has the ability to achieve 1.25 Gb/s with a BER lower than 10^{-6} at deferent levels of dimming (25%, 50% and 75%), as shown in Figure 10.8. It should be noted that the receiver bandwidth has to be changed (reduced) when the data rate is decreased.

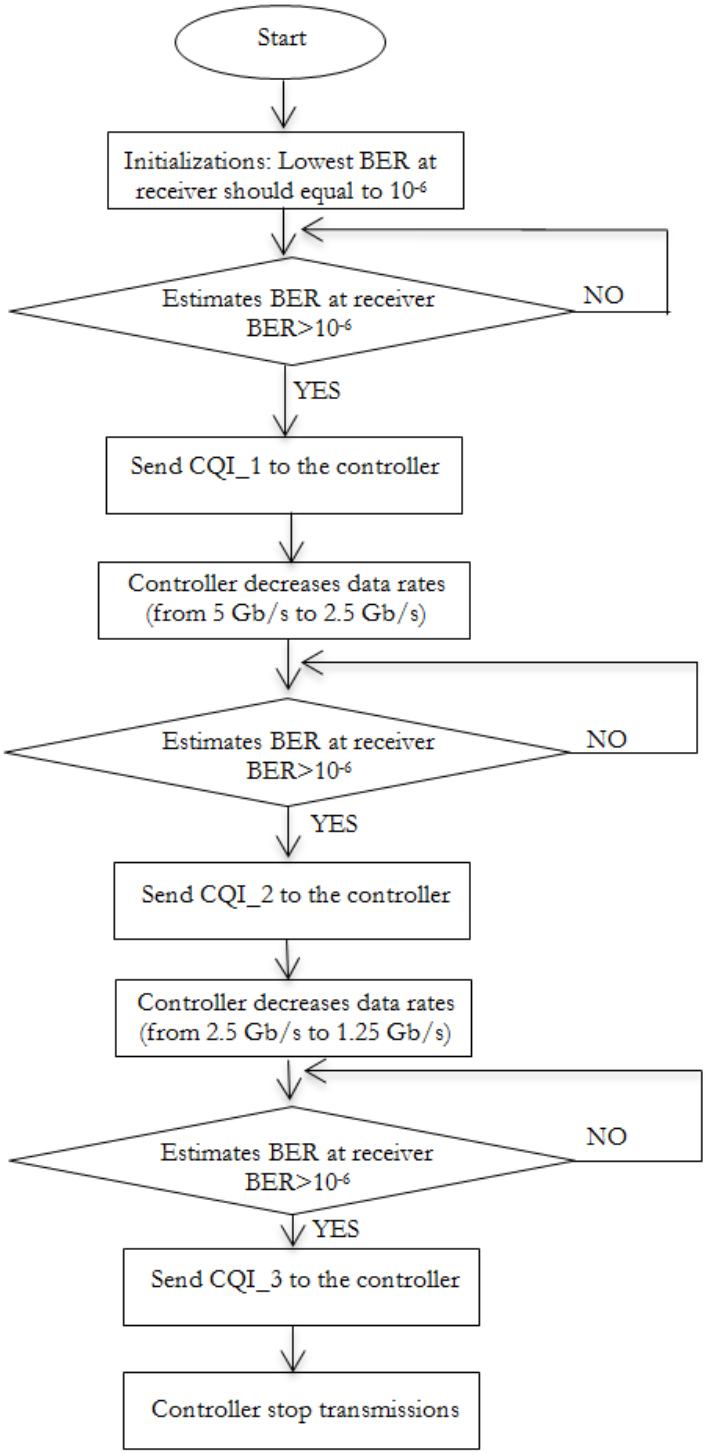

Figure 10.5: Flow chart of ART (down convert case).

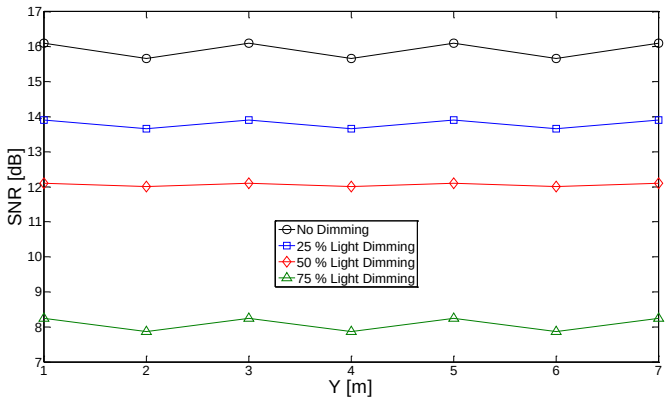

Figure 10.6: SNR of imaging LD-VLC system operating at 5 Gb/s with different levels of dimming (25%, 50% and 75%) when receiver moves at x=2m along y-axis.

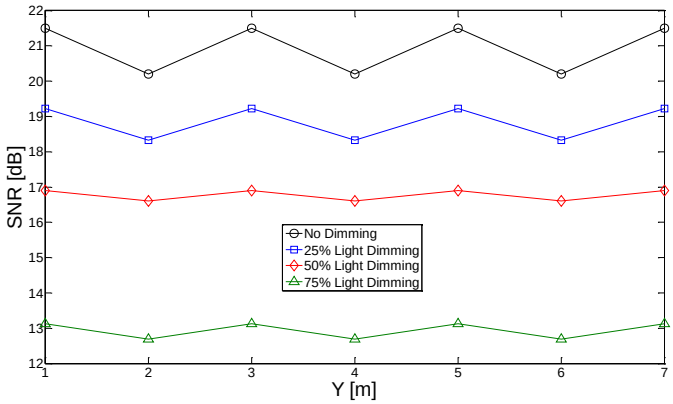

Figure 10.7: SNR of imaging LD-VLC system operating at 2.5 Gb/s with different levels of dimming (25%, 50% and 75%) when receiver moves at x=2m along y-axis.

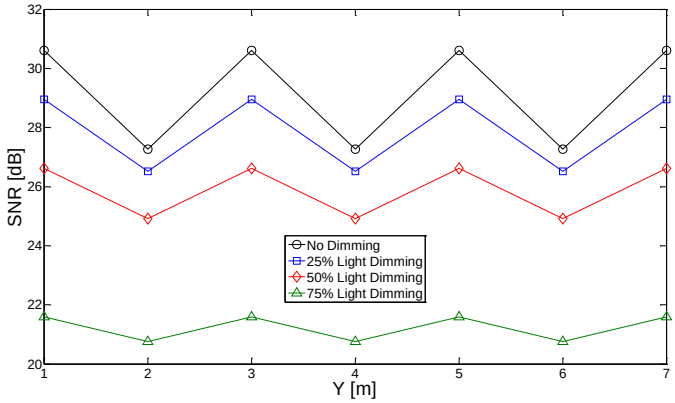

Figure 10.8: SNR of imaging LD-VLC system operating at 1.25 Gb/s with different levels of dimming (25%, 50% and 75%) when receiver moves at x=2m along y-axis.

10.4 Simulation Results and Discussions of IROW Systems

In this section, we evaluate the performance of the proposed support systems in an empty room in the presence of multipath dispersion, receiver noise, back ground noise (light units) and mobility. The results are presented in terms of delay spread, 3 dB channel bandwidth, SNR and BER.

10.4.1 Delay spread and 3 dB channel bandwidth

Figure 10.9 presents the communication system delay spread associated with the CDIR and CDBSIR systems. The results show that the CDBSIR system has a lower delay spread than the CDIR system at all the receiver locations considered. The delay spread for the CDIR system is relatively low (0.03 ns in the worst case), and this is attributed to two reasons: firstly, due to the narrow FOVs associated with each pixel in the imaging receiver, and this limitation in the FOV minimises the number of rays accepted. Secondly, the IR transmitter is very close to the receiver (IR sources distributed on the ceiling see Figure 10.2). However, the delay spread can be further reduced (i.e., less than 0.03 ns) by employing beam steering. The CDBSIR system outperforms the CDIR system, as it dramatically decreases the delay spread from 0.03 ns to 0.003 ns (by a factor of 10) at the room centre. The minimum communication channel bandwidth of the CDBSIR was 29 GHz (where the delay spread is 0.003 ns at points x=2m, y=2m, 4m, 6m) as shown in Table 10.1.

10.4.2 SNR and BER

Since the IROW systems operate when the VLC system is also present, we therefore considered the background noise component coming from the light units (VLC transmitters). Figure 10.10 shows the SNR of the proposed systems when operated at 5 Gb/s. It can be clearly seen that the CDIR system with

imaging receiver does not have the ability to operate at a high data rate. However, when the beam steering technique is combined with this system it can perform better. The significant improvement in the SNR level is attributed to the ability of the beam steering technique to steer the IR beam towards the receiver location and, thus, increase the power received by the pixels.

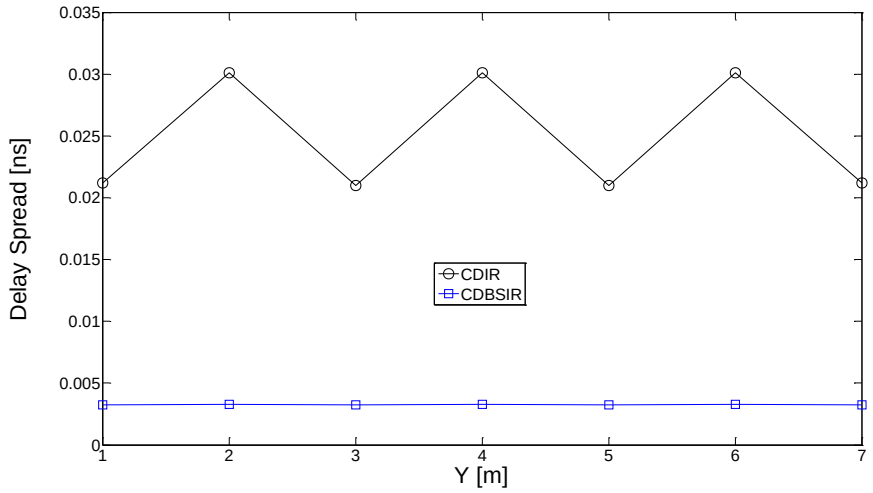

Figure 10.9: Delay spread of two systems at x=2m and along y-axis.

Table 10.1: Channel bandwidth of proposed systems at x=2m.

System	3 dB Channel Bandwidth [GHz]						
	Receiver Locations along the y-axis, y [m]						
	1	2	3	4	5	6	7
CDIR	7.89	5.5	7.89	5.5	7.89	5.5	7.89
CDBSIR	29.3	29	29.3	29	29.3	29	29.3

Table 10.2 shows the BER at 5 Gb/s for the proposed systems (CDIR and CDBSIR). It can be noted that the CDBSIR system has a better performance compared to the CDIR. At certain locations in the room, e.g., at x=2m, y=2m and z=1m, the BER of the CDIR system was increased. This is due to increasing path loss. However, this increase in BER does not severely affect the performance of the system; for example, the maximum value of the BER provided by the CDBSIR system is equal to 8.8×10^{-7}.

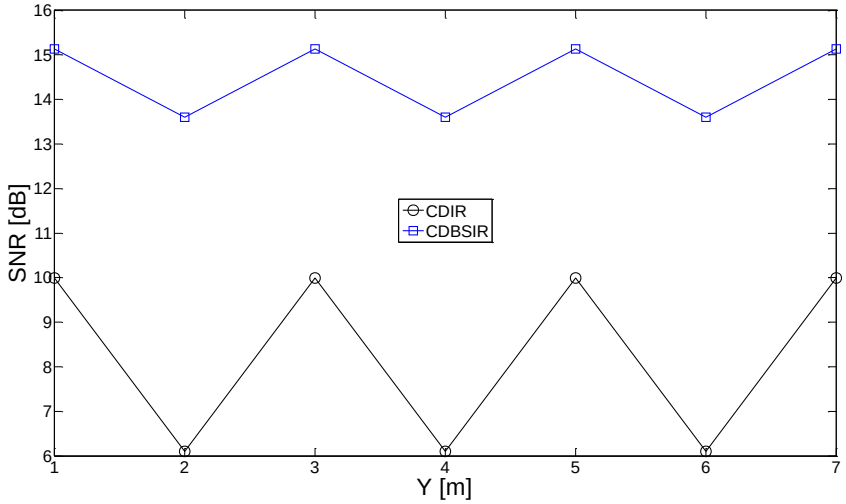

Figure 10.10: SNR of two systems operating at 5 Gb/s when receiver moves at x=2m along y-axis.

Table 10.2: BER of proposed systems at x=2m.

System	BER			
	Receiver Locations along the y-axis, y [m]			
	1	2	3	4
CDIR	8.7×10^{-4}	2.5×10^{-2}	8.7×10^{-4}	2.5×10^{-2}
CDBSIR	6.5×10^{-9}	8.8×10^{-7}	6.5×10^{-9}	8.8×10^{-7}

10.5 Simulation Results and Discussions for Collaborative VLC/IROW System

Dimming is an important feature of an indoor lighting system where the illumination level can be controlled by the user. One of the main issues in VLC systems is that the light unit should be ‘‘ON’’ all the time to ensure continuous communication. However, the user may dim the light at any time and this will severally degrade the performance of the VLC system. In this section, a collaboration between VLC and IROW systems (CDBSIR) is proposed to support the VLC system when the light is dimmed at different levels (25%, 50% and 75%). An ART can be used with the VLC system to manage the reduction in the SNR due to the light dimming and to establish a high quality communication link under the impact of dimming. To provide a high data rate service for an indoor user under different conditions (with\without dimming), an IROW (CDBSIR) system can be used to support the VLC system. Figure 10.11 shows the SNR of the VLC system when the ART is carried out. It can be clearly seen that the data rate diminishes in a very graceful manner when the light is dimmed beyond 50%. However, when employing the CDBSIR system the achieved data rates at the receiver will be 5 Gb/s even though the VLC system is off. It means that the user can dim the lights and maintain a high quality communication service (5 Gb/s and beyond). In the case of partial dimming (50% and 75%) in the VLC system, it can achieve 2.5 Gb/s and 1.25 Gb/s, respectively. Therefore, the collaborating system (VLC/IROW) can always achieve higher than the target data rate (5 Gb/s). For example, 7.5 Gb/s (2.5 Gb/s from the VLC system and 5 Gb/s from the CDBSIR) can be achieved when the light is dimmed by 50%. In the case of no dimming, 10 Gb/s can be achieved by using both systems (VLC and IROW).

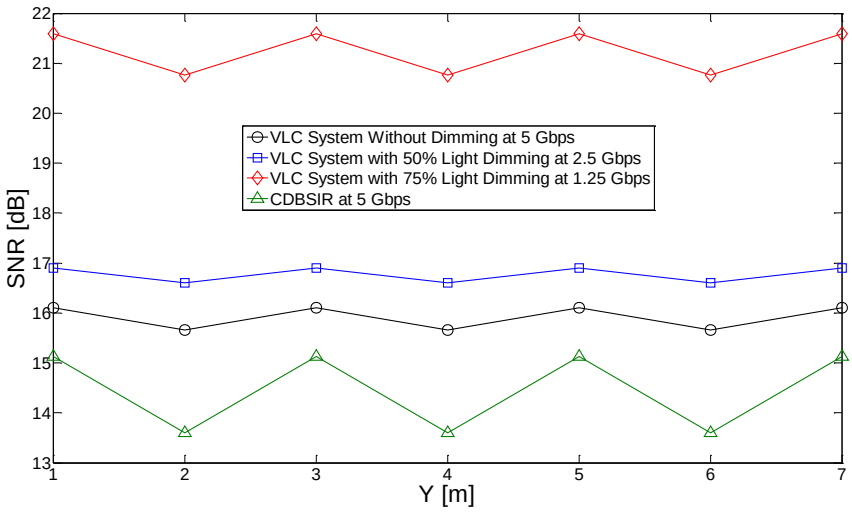

Figure 10.11: SNR of collaborative systems when receiver moves at x=2m along y-axis.

10.6 Summary

In this chapter we proposed, designed and investigated the concept of a collaborative VLC/IROW system. In addition, we investigated the impact of partial dimming (25%, 50% and 75%) on the performance of the VLC system. Moreover, we introduced a novel ART to reduce the effect of the dimming and to create an optimum communication link under the impact of partial dimming.

Two novel IROW systems (CDIR and CDBSIR) were introduced to support and collaborate with the VLC system in the case of partial dimming. These IROW systems used an imaging receiver with 50 pixels.

The proposed CDIR system is coupled with the imaging receiver to improve the received optical signal SNR in the presence of back ground noise, multipath dispersion, receiver noise and mobility. A beam steering technique is also proposed to further reduce the delay spread and increase the SNR by steering the IR beam nearer to the receiver at each given location. Simulation results show that the CDBSIR system has the ability to decrease the delay spread of the CDIR system by 90% from 0.03 to 0.003 ns at the room centre (x=2m and

y=4m), which leads to an increase in the channel bandwidth by a factor of 5.5 from 5.5 GHz to 29 GHz. In addition, a notable enhancement in the SNR can be achieved by introducing beam steering to the CDIR system. The simulation results show that the CDBSIR system can significantly improve the SNR. The BER provided by the CDBSIR system is better than 10^{-6} at 5 Gb/s in the worst case scenario. Therefore, we used the CDBSIR to collaborate with a VLC system.

Simulation results show that the collaborative VLC/IROW system has the ability to achieve 10 Gb/s when dimming does not exist and 6.25 Gb/s (5 Gb/s from the IROW and 1.25 Gb/s from the VLC) in the case of 75% light dimming (worst case scenario).

11 Summary of Contributions and Future Directions

11.1 Introduction

This chapter summarises the work that has been achieved and presented in this thesis as well as its findings and original contributions. In addition, it suggests possible directions for future research in the area. Next section presents the contributions of the thesis. Section 11.3 introduces the potential areas that deserve further investigations.

11.2 Summary of Contributions

VLC systems have become promising candidates to complement conventional radio frequency systems due to the increasingly saturated RF band and the potential high data rates that can be achieved by VLC systems. A major interest in VLC systems is to understand and tackle the design challenges to achieve multi gigabits per second. These challenges include the low modulation bandwidth of the LEDs, ISI due to multipath propagation and CCI due to multiple transmitters. This thesis has presented a range of tools and mathematical models and simulation methods to model the VLC channel link in different indoor environments. This thesis has concentrated on VLC system design, with emphasis on approaches that can tackle the impairments discussed as well as shadowing effect and user mobility. In addition, it has designed high speed VLC systems that can operate at high data rates (5 Gb/s, 10 Gb/s, 20 Gb/s and 25 Gb/s). Most of the proposed systems were evaluated in a typical rectangular room with dimensions of 4m × 8m × 3m (width × length × height). The simulation results were carried out through the use of a light ray

tracing algorithm where the transmitted VLC signal travels through various paths (LOS, first and second reflections) of different lengths before it reaches to the receiver. The simulations and calculations reported in this thesis were carried out using MATLAB. The performance evaluation of the VLC systems concentrated on the impulse response, delay spread, 3 dB channel bandwidth, SNR and BER.

In this thesis, we proposed, designed and investigated a novel LD-VLC system that uses LD instead of LEDs as the transmitters in conjunction with different receivers (wide-FOV receiver, an ADR with three and seven branches and an imaging receiver with 50 pixels) to deal with the main constraints of the traditional VLC system, namely the low modulation bandwidth of the LEDs and ISI caused by multipath dispersion.

The ADR with three branches is introduced for VLC system. The AZs, ELs and FOVs were chosen through an optimisation process to achieve high SNR and low delay spread. The ADR LD-VLC system has the ability to decrease the delay spread of the wide FOV LD-VLC system by 91% from 0.65 ns to 0.053 ns at the room centre (x=2m and y=4m), which leads to an increase in the channel bandwidth by a factor of 32 from 114 MHz to 3.7 GHz. Our ADR LD-VLC system provides full mobility within the test area in the presence of multipath propagation and achieves a BER better than 10^{-6} at 5 Gb/s when using a simple modulation format (OOK).

A custom design imaging receiver was introduced for VLC system. In addition, the LD-VLC system was studied with an imaging receiver (50 pixels) to enhance the mobile VLC system performance. Imaging reception can significantly help to reduce the delay spread and improve 3 dB channel bandwidth. The imaging LD-VLC has the ability to decrease the delay spread of the wide FOV LD-VLC system by 94% from 0.7 ns to 0.04 ns at the room centre, which leads to an increase in the channel bandwidth by a factor of 36

from 116 MHz to 4.2 GHz. Furthermore, at a low data rate (30 Mb/s) imaging LD-VLC was obtained 8 dB SNR gain over the wide FOV LD-VLC system, and the lowest SNR achieved was 19.2 dB at a high data rate (5 Gb/s) at the room centre.

A novel DAT was introduced for a VLC system to improve the SNR and channel bandwidth as well as to reduce the effect of multipath dispersion. The DAT was combined with seven branched ADR (DAT ADR) and an imaging receiver (DAT imaging LD-VLC). The DAT ADR system achieved 5 Gb/s and a BER of 10^{-5} at the least successful point in the empty room. However, there was degradation in the performance (BER increase) when the DAT ADR system operated in the realistic environment considered. On the other hand, the DAT imaging LD-VLC system has the ability to decrease the delay spread of the imaging LD-VLC system by 83% from 0.04 ns to 0.007 ns at the room centre, which leads to an increase in the channel bandwidth by a factor of 5.4 from 4.2 GHz to 23 GHz, and this channel bandwidth has the ability to provide data rates of up to 33 Gb/s. Moreover, at low data rates (30 Mb/s), the proposed algorithm does not offer SNR improvements, which is due to the low ISI at these data rates. The BER provided by our DAT imaging LD-VLC system is better than 10^{-5} at 10 Gb/s, in the worst case scenarios. The DAT imaging system in a realistic room has lower delay spread (higher 3 dB channel bandwidth) but also lower received power and overall has slightly lower SNR.

The concept of relays in a VLC system has been proposed to improve performance of VLC system. Two novel algorithms were introduced (CS and SB) to create optimum transmitter-relay and relay-receiver communication links. Three novel VLC systems (ADRR-LD, IMGR-LD and SBIMGR-LD) are proposed. These VLC systems use LD instead of LEDs as transmitters, and they use two different types of receiver: an ADR with 7 branches and an imaging receiver with 50 pixels. Different room sizes were also considered to examine the performance of the proposed systems. The performance of the proposed

systems was better in the small office than the large office and this is due to the distance between the transmitter and receiver, which was smaller and led to reduced path loss, delay spread and increased SNR. The proposed systems were evaluated under diverse situations including an empty room and a room with very strong shadowing effects resulting from mini cubicle offices.

This thesis also introduces beam steering and location estimation algorithms for VLC system. It is combined these algorithms with the concept of delay adaptation to produce a fully adaptive VLC system that has the ability to achieve 20 Gb/s with full receiver mobility in a realistic indoor environment. The effect of beam steering on the illumination was investigated and it was observed that up to 20% of the light from the RGB-LD can be beam steered towards the receiver position to improve SNR without affecting the illumination. In addition, at a low data rate (30 Mb/s) fully adaptive system offers an SNR improvement of 10 dB over the imaging LD-VLC system when using the MRC approach. At a high data rate (20 Gb/s) a 29 dB SNR gain is achieved when the fully adaptive system replaces the imaging LD-VLC system under the worst case scenario, and these improvements in the SNR enable our fully adaptive system to provide a BER of better than 10^{-9} at all receiver locations when operated at 20 Gb/s in a harsh room environment. The delay adaptation adjusts the switching times of the signals in a fashion that allows the signals to reach the receiver at the same time. The significant enhancements in channel bandwidth and SNR enable our proposed system to operate at higher data rates (20 Gb/s and beyond). Moreover, the fully adaptive VLC system can achieve 100% of the data rate (20 Gb/s) when it is stationary and 70.4% (14 Gb/s) in the case of user movement, and this is due to the time needed (296 ms) for the adaptation process.

We introduced a FCGHs VLC system and introduced a new fully adaptive ADR VLC system that has ability to achieve 25 Gb/s. The proposed system is coupled with three branched ADR and an imaging receiver to improve the received VLC signal in the presence of multipath dispersion, mobility, and

shadowing. The proposed FCGHs can effectively steer the VLC beam nearer to the receiver location at each given receiver location. It should be noted that the time required to find the optimum location to steer the beam to, was reduced from 224 ms to 32 ms. Moreover, the proposed system can also adapt to environmental changes, offering a link that is robust against signal blockage and shadowing. The BER provided by our proposed system in realistic indoor environment is about 10^{-6} at 25 Gb/s in the worst case scenario. Further enhancement can be achieved when our fully adaptive system is used in conjunction with imaging receiver instead of ADR. The highest value of BER in the fully adaptive imaging system is equal to 4×10^{-12}.

We proposed four IROW systems (hybrid diffuse IR with wide field of view receiver, hybrid diffuse IR with imaging receiver, beam steering IR with imaging receiver and cluster distributed IR with imaging receiver) to support VLC systems when the light is totally turned off. The ultimate goal of our proposed systems is to maintain a high data rate service when the VLC system is disabled. The simulation results show that the proposed systems have the ability to achieve high data rates (1.25 Gb/s and 2.5 Gb/s) with a BER of 10^{-9} in the presence of multipath dispersion, receiver noise and mobility.

Finally, we introduced and implemented the concept of a collaborative VLC/IROW system. In addition, we investigated the impact of partial dimming on the VLC system's performance and we proposed an ART to mitigate the impact of light dimming. Furthermore, we proposed new IROW systems (CDIR and CDBSIR) to collaborate with the VLC system to maintain the target data rate in the case of partial dimming. We have achieved 10 Gb/s in an indoor environment, which is a 2× increase in the data rate compared with a pure VLC system.

11.3 Future Directions

The following is a list of potential areas that deserve further investigation and research:

1- Investigate WDM scheme with LD, the use of colour-mixed laser light would enable to send different data sources on different wavelengths on a single channel. WDM promise great flexibility and bandwidth efficiency as it did in the case of fibre optic communication system and VLC system using LEDs. This scheme will ensure an efficient use of available spectrum and abundant data rate (up to 75 Gb/s).
2- A MIMO VLC system employing LD can be demonstrated. The transmission capacity of VLC system can be significantly increased by space division de-multiplexing scheme. Such a MIMO LD-VLC system would be attractive for providing high data rate service.
3- Multicarrier code division multiple access (MC-CDMA) is a transmission scheme that combines the robustness of orthogonal modulation with the flexibility of CDMA schemes. MC-CDMA can be used to provide high data rates for multi user scenarios.
4- To further reduce the BER in the proposed VLC systems FEC codes can be used when the VLC systems operate at high data rates.
5- LEA, BSR and delay adaptation technique have been investigated for a single user scenario where the VLC beam is assigned to one receiver location. In the case of a multiple users scenario, opportunistic scheduling can be used where LEA, BSR and delay adaptation algorithms are implemented opportunistically (or randomly between users/regions) to maximise the 3 dB channel bandwidth and the SNR in a given region for a given time period.
6- Due to the energy efficiency, scalability and flexibility of VLC systems, they can be used in the next generation of data centres replacing a hundred metres of UTP cable or optical fibre. Investigations in this area

are required to examine the benefits of applying VLC systems in data centres.

7- VLC transmitter mapping, each transmitter can be allocated to one user or more according to the numbers of active users and their locations on the CP. This technique can be used to further reduce delay spread, increase 3 dB channel bandwidth and enable multi users' scenario.

References

[1] R. W. Burns, “Communications: An international history of the formative years,” IET Publication, vol. 32, no.1, pp.192-196, 2004.

[2] A. G. Bell, "On the production and reproduction of sound by light," American Journal of Science, vol.1, no.118, pp.305-324, 1880.

[3] S. Arnon, J. Barry, G. Karagiannidis, R. Schober, and M. Uysal, "Advanced optical wireless communication systems, " Cambridge University Press, 2012.

[4] A. T. Hussein, and J. M. H. Elmirghani, "A Survey of Optical and Terahertz (THz) Wireless Communication Systems," IEEE Communications Surveys & Tutorials, (to be submitted), 2016.

[5] GreenTouch, “Green Meter Research Study: Reducing the Net Energy Consumption in Communications Networks by up to 90% by 2020,” A GreenTouch White Paper, Version 1, 2013, [online]: http// www.greentouch.org / uploads / documents /GreenTouch_Green_Meter_ Research_Study_26_June_2013.pdf.

[6] F. R. Gfeller, and U. Bapst, "Wireless in-house data communication via diffuse infrared radiation," Proceedings of the IEEE, vol. 67, no.11, pp.1474-1486, 1979.

[7] M. Kavehrad, "Sustainable energy-efficient wireless applications using light," IEEE Communications Magazine, vol.48, issue 12, pp.66-73, 2010.

[8] D. J. T. Heatley, D. R. Wisely, I. Neild, and P. Cochrane, "Optical wireless: the story so far," IEEE Communications Magazine, vol.36, issue 12, pp.72-74, 1998.

[9] G. R. Aiello, and G. D. Rogerson, "Ultra-wideband wireless systems," IEEE Microwave Magazine, vol.4, issue 2, pp. 36-47, 2003.

[10] P. Smulders, "Exploiting the 60 GHz band for local wireless multimedia access: prospects and future directions," IEEE Communications Magazine, vol.40, issue 1, pp.140-147, 2002.

[11] M. Tonouchi, "Cutting-edge terahertz technology," Nature photonics, vol.1, no.1, pp. 97-105, 2007.

[12] R. Piesiewicz, T. Kleine-Ostmann, N. Krumbholz, D. Mittleman, M. Koch, and J. Schoebel, "Short-Range Ultra-Broadband Terahertz Communications: Concepts and Perspectives," IEEE Antennas and Propagation Magazine, vol. 49, issue 6, pp.24-39, 2007.

[13] J. Federici, and L. Moeller, "Review of terahertz and subterahertz wireless communications," Journal of Applied Physics, vol.107, no.1, pp. 111101-111101-22, 2010.

[14] T. Kleine-Ostmann, and T. Nagatsuma, "A review on terahertz communications research," Journal of Infrared, Millimeter, and Terahertz Waves, vol.32, issue 2 pp.143-171, 2011.

[15] T. H. Maiman, "Stimulated optical radiation in ruby," Nature letters, vol.187, no.1, 1960.

[16] K. L. Sterckx, J. M. H. Elmirghani, and R. A. Cryan, "Pyramidal fly-eye detection antenna for optical wireless systems," IEE Colloquium on Optical Wireless Communications, pp.5/1-5/6, 1999.

[17] Cisco Visual Networking Index: Global Mobile Data Traffic Forecast Update, 2015–2020 White Paper, [online]: http://www.cisco.com/c/en/us/solutions/collateral/service-provider/visual-networking-index-vni/white_paper_c11-520862.html.

[18] WiGig and Wi-Fi Alliance, [online]: http://www.wi-fi.org/discover-wi-fi/wigig-certified.

[19] D. O'Brien, G. Parry, and P. Stavrinou, "Optical hotspots speed up wireless communication," Nature Photonics, vol.1, no.5, pp.245-247, 2007.

[20] G. Yun and M. Kavehrad, "Spot-diffusing and fly-eye receivers for indoor infrared wireless communications," IEEE International Conference on Selected Topics in Wireless Communications, pp.262-265, 1992.
[21] M. D. Audeh and J. M. Kahn, "Performance evaluation of baseband OOK for wireless indoor infrared LAN's operating at 100 Mb/s," IEEE Transactions on Communications, vol. 43, issue 6, pp.2085-2094, 1995.
[22] A. G. Al-Ghamdi, and J. M. H. Elmirghani, "Performance evaluation of a triangular pyramidal fly-eye diversity detector for optical wireless communications," IEEE Communications Magazine, vol. 41, issue 3, pp.80-86, 2003.
[23] M. Kavehrad, and S. Jivkova, "Indoor broadband optical wireless communications: optical subsystems designs and their impact on channel characteristics," IEEE Wireless Communications, vol.10, issue 2, pp.30-35, 2003.
[24] O. Gonzalez, R. Perez-Jimenez, S. Rodriguez, J. Rabadan, and A. Ayala, "OFDM over indoor wireless optical channel," IEE Proceedings Optoelectronics, vol. 52, issue 4, pp.199-204, 2005.
[25] Z. Ghassemlooy, W. Popoola, and S. Rajbhandari, "Optical wireless communications: system and channel modelling with MATLAB," CRC Press, 2012.
[26] J. M. Kahn, and J. R. Barry, "Wireless infrared communications," Proceedings of the IEEE, vol.85, issue 2, pp.265-298, 1997.
[27] J. M. Kahn, J. Barry, W. Krause, M. Audeh, J. Carruthers, and G. Marsh, "High-speed non-directional infrared communication for wireless local-area networks," Twenty-Sixth Asilomar Conference on Signals, Systems and Computers, pp. 83-87, 1992.
[28] T. Komine and M. Nakagawa, "Fundamental analysis for visible-light communication system using LED lights," IEEE Transactions on Consumer Electronics, vol. 50, issue 1, pp.100-107, 2004.
[29] Energy Efficiency of White LEDs, [online]: http://www.fcgov.com/utilities/img/site_specific/uploads/led-efficiency.pdf
[30] LED Basics, [online]: http://energy.gov/eere/ssl/led-basics.
[31] G. Cossu, A. Khalid, P. Choudhury, R. Corsini, and E. Ciaramella, "3.4 Gbit/s visible optical wireless transmission based on RGB LED," Optic Express, vol.20 no.26, pp.501–506, 2012.
[32] A. M. Khalid, G. Cossu, R. Corsini, P. Choudhury, and E. Ciaramella, "1-Gb/s Transmission Over a Phosphorescent White LED by Using Rate-Adaptive Discrete Multitone Modulation," IEEE Photonics Journal, vol.4, issue5, pp.1465-1473, 2012.
[33] A. Street, P. Stavrinou, D. O'brien, and D. Edwards, "Indoor optical wireless systems–a review," Optical and Quantum Electronics, vol.29, issue 3, pp.349-378, 1997.
[34] K. Lee, H. Park, and J. R. Barry, "Indoor channel characteristics for visible light communications," IEEE Communications Letters, vol.15, issue 2, pp.217-219, 2011.
[35] A. Boucouvalas, "Indoor ambient light noise and its effect on wireless optical links," IEE Proceedings Optoelectronics, vol.143, issue 6, pp.334-338, 1996.
[36] A. J. C. Moreira, R. T. Valadas, and A. M. de Oliveira Duarte, "Performance of infrared transmission systems under ambient light interference," IEE Proceedings Optoelectronics, vol.143, issue 6, pp.339-346, 1996.
[37] J. M. H. Elmirghani, H. H. Chan, and R. A. Cryan, "Sensitivity evaluation of optical wireless PPM systems utilising PIN-BJT receivers," IEE Proceedings Optoelectronics, vol.143, issue 6, pp.355-359, 1996.
[38] S. Arnon, "Visible light communication, " Cambridge University Press, 2015.
[39] Getting to Know LEDs and Solutions, [online]: http://www.dialight.com/Assets%5CApplication_Notes%5CIndication%5CGetting%20To%20Know%20LEDs.PDF.
[40] K. Asatani, and T. Kimura, "Analyses of LED nonlinear distortions," IEEE Journal of Solid-State Circuits, vol.13, issue 1, pp.125-133, 1978.
[41] J. R. Barry and J. M. Kahn, "Link design for nondirected wireless infrared communications," Applied optics, vol.34, no.19, pp.3764-3776, 1995.

[42] E. Sarbazi, M. Uysal, M. Abdallah, and K. Qaraqe, "Indoor channel modelling and characterization for visible light communications," International Conference in Transparent Optical Networks (ICTON 2014), pp.1-4, 2014.

[43] D. Tronghop, J. Hwang, S. Jung, Y. Shin, and M. Yoo, "Modeling and analysis of the wireless channel formed by LED angle in visible light communication," International Conference in Information Networking (ICOIN), pp.354-357, 2012.

[44] K. D. Langer and J. Grubor, "Recent Developments in Optical Wireless Communications using Infrared and Visible Light," International Conference in Transparent Optical Networks (ICTON 2007), pp.146-151, 2007.

[45] X. Ning, R. Winston, and J. O'Gallagher, "Dielectric totally internally reflecting concentrators," Applied Optics, vol. 26, no.1, pp.300-305, 1987.

[46] J. P. Savicki and S. P. Morgan, "Hemispherical concentrators and spectral filters for planar sensors in diffuse radiation fields," Applied optics, vol.33, no.1, pp.8057-8061, 1994.

[47] K. P. Ho and J. M. Kahn, "Compound parabolic concentrators for narrowband wireless infrared receivers," Optical Engineering, vol.34, issue 5, pp.1385-1395, 1995.

[48] J. Fadlullah and M. Kavehrad, "Indoor high-bandwidth optical wireless links for sensor networks," Journal of lightwave technology, vol.28, issue 21, pp.3086-3094, 2010.

[49] A. J. Moreira, R. T. Valadas, and A. de Oliveira Duarte, "Optical interference produced by artificial light," Wireless Networks, vol.3, issue 6, pp.131-140, 1997.

[50] A. J. Moreira, R. T. Valadas, and A. de Oliveira Duarte, "Characterisation and modelling of artificial light interference in optical wireless communication systems," IEEE International Symposium in Personal, Indoor and Mobile Radio Communications, pp.326-331, 1995.

[51] A. J. Moreira, R. T. Valadas, and A. de Oliveira Duarte, "Reducing the effects of artificial light interference in wireless infrared transmission systems," IEE Colloquium Optical Free Space Communication Links, pp.1-5, 1996.

[52] L.-M. Hoa, D. O'Brien, G. Faulkner, Z. Lubin, L. Kyungwoo, and J. Daekwang, "100-Mb/s NRZ Visible Light Communications Using a Postequalized White LED," IEEE Photonics Technology Letters, vol.21, issue 15, pp.1063-1065, 2009.

[53] D. O'Brien, L. Zeng, L.-M. Hoa, G. Faulkner, J. W. Walewski, and S. Randel, "Visible light communications: Challenges and possibilities," IEEE 19th International Symposium in Personal, Indoor and Mobile Radio Communications, pp.1-5, 2008.

[54] S. Dimitrov, and H. Haas, "Principles of LED Light Communications: Towards Networked Li-Fi," Cambridge University Press, 2015.

[55] K. Cui, G. Chen, Z. Xu, and R. D. Roberts, "Line-of-sight visible light communication system design and demonstration," International Symposium in Communication Systems Networks and Digital Signal Processing, pp. 621-625, 2010.

[56] T. Komine, S. Haruyama, and M. Nakagawa, "A study of shadowing on indoor visible-light wireless communication utilizing plural white LED lightings," IEEE International Symposium in Wireless Personal Communications, pp.211-225, 2005.

[57] W. T. Welford, "High collection nonimaging optics," Elsevier, 1989.

[58] L. Zeng, D. C. O'Brien, H. Minh, G. E. Faulkner, K. Lee, and D. Jung, "High data rate multiple input multiple output (MIMO) optical wireless communications using white LED lighting," IEEE Journal on Selected Areas in Communications, vol.27, issue 9, pp.1654-1662, 2009.

[59] C. Singh, J. John, Y. Singh, and K. Tripathi, "A review of indoor optical wireless systems," IETE Technical review, vol.19, no.1, pp.3-18, 2002.

[60] D. O'Brien, H. Le Minh, G. Faulkner, M. Wolf, L. Grobe, and J. Li, "High data-rate infra-red optical wireless communications: implementation challenges," IEEE in GLOBECOM Workshops, pp.1047-1051,2010.

[61] H. Le Minh, D. O'Brien, G. Faulkner, O. Bouchet, M. Wolf, and L. Grobe, "A 1.25-Gb/s indoor cellular optical wireless communications demonstrator," IEEE Photonics Technology Letters, vol. 22, issue 21, pp.1598-1600, 2010.

[62] M. Khatib, "Advanced Trends in Wireless Communications, ", 2011.
[63] J. M. Senior and M. Y. Jamro, "Optical fiber communications: principles and practice, " Pearson Education, 2009.
[64] P. A. Haigh, T. T. Son, E. Bentley, Z. Ghassemlooy, H. Le Minh, and L. Chao, "Development of a Visible Light Communications system for optical wireless local area networks," Computing, Communications and Applications Conference, pp. 351-355, 2012.
[65] H. Chun, S. Rajbhandari, G. Faulkner, and D. O'Brien, "Effectiveness of blue-filtering in WLED based indoor Visible light communication," 3rd International Workshop in Optical Wireless Communications, pp.60-64, 2014.
[66] J.-Y. Sung, C.-W. Chow, and C.-H. Yeh, "Is blue optical filter necessary in high speed phosphor-based white light LED visible light communications?," Optics express, vol. 22, issue 17, pp. 20646-20651, 2014.
[67] B. G. Streetman and S. Banerjee, "Solid state electronic devices, " Prentice Hall New Jersey, 2000.
[68] S. Hranilovic, "Wireless optical communication systems", Springer Science and Business Media, 2006.
[69] Y.-G. Wey, K. S. Giboney, J. E. Bowers, and M. JW, "108-GHz GaInAs/InP pin Photodiodes with Integrated Bias Tees and Matched Resistors," IEEE Photonic Technology Letters, vol. 5, no.11, pp.1310-1312, 1993.
[70] "IEEE Standard for Local and Metropolitan Area Networks--Part 15.7: Short-Range Wireless Optical Communication Using Visible Light," IEEE Std 802.15.7-2011, pp.1-309, 2011.
[71] J. B. Carruther and J. M. Kahn, "Angle diversity for nondirected wireless infrared communication," IEEE Transactions on Communications, vol.48, issue 6, pp.960-969, 2000.
[72] H. Le Minh, D. O'Brien, G. Faulkner, L. Zeng, K. Lee, and D. Jung, "High-speed visible light communications using multiple-resonant equalization," IEEE Photonics Technology Letters, vol.20, issue 14, pp.1243-1245, 2008.
[73] H. Le Minh, D. O'Brien, G. Faulkner, L. Zeng, K. Lee, and D. Jung, "80 Mbit/s visible light communications using pre-equalized white LED," 34th European Conference in Optical Communication, pp.1-2, 2008.
[74] Z. Lubin, L.-M. Hoa, D. O'Brien, G. Faulkner, L. Kyungwoo, and J. Daekwang, "Equalisation for high-speed Visible Light Communications using white-LEDs," 6th International Symposium in Communication Systems, Networks and Digital Signal Processing, pp.170-173, 2008.
[75] K. D. Langer, J. Vucic, C. Kottke, L. Fernandez, K. Habe, and A. Paraskevopoulos, "Exploring the potentials of optical-wireless communication using white LEDs," 13th International Conference in Transparent Optical Networks (ICTON 2011), pp. 1-5, 2011.
[76] Z. Xie, C. Kaiyun, Z. Hongming, and X. Zhengyuan, "Capacity of MIMO visible light communication channels," IEEE in Photonics Society Summer Topical Meeting Series, pp.159-160, 2012.
[77] C. Kottke, J. Hilt, K. Habel, J. Vucic, and K. D. Langer, "1.25 Gbit/s visible light WDM link based on DMT modulation of a single RGB LED luminary," European Conference and Exhibition in Optical Communications, pp.1-3, 2012.
[78] Z. Shuailong, S. Watson, J. J. D. McKendry, D. Massoubre, A. Cogman, and G. Erdan, "1.5 Gbit/s Multi-Channel Visible Light Communications Using CMOS-Controlled GaN-Based LEDs," Journal of Lightwave Technology, vol.31, issue 8, pp.1211-1216, 2013.
[79] N. Fujimoto, and H. Mochizuki, "477 Mbit/s visible light transmission based on OOK-NRZ modulation using a single commercially available visible LED and a practical LED driver with a pre-emphasis circuit," in Optical Fiber Communication Conference and Exposition and the National Fiber Optic Engineers Conference, pp.1-3, 2013.

[80] D. Tsonev, C. Hyunchae, S. Rajbhandari, J. J. D. McKendry, S. Videv, E. Gu, and H. Hass, "A 3-Gb/s Single-LED OFDM-Based Wireless VLC Link Using a Gallium Nitride," IEEE Photonics Technology Letters, vol.26, issue 7, pp.637-640, 2014.

[81] Y. Wang, X. Huang, L. Tao, J. Shi, and N. Chi, "4.5-Gb/s RGB-LED based WDM visible light communication system employing CAP modulation and RLS based adaptive equalization," Optics Express, vol. 23, no.18, pp.13626-13633, 2015.

[82] T. Komine, S. Haruyama, and M. Nakagawa, "Bidirectional visible-light communication using corner cube modulator," Wireless and Optical Communications, pp.41-46, 2003.

[83] S. Shao, A. Khreishah, M. B. Rahaim, H. Elgala, M. Ayyash, and T. D. Little, "An indoor hybrid WiFi-VLC internet access system," IEEE 11th International Conference in Mobile Ad Hoc and Sensor Systems, pp.569-574, 2014.

[84] F. H. Fitzek, and M. D. Katz, "Cognitive wireless networks: concepts, methodologies and visions inspiring the age of enlightenment of wireless communications", Springer Science and Business Media, 2007.

[85] W. Yuanquan, and C. Nan, "A high-speed bi-directional visible light communication system based on RGB-LED," Communications, China, vol.11, issue 3, pp.40-44, 2014.

[86] M. T. Alresheedi, and J. M. H. Elmirghani, "Performance evaluation of 5 Gbit/s and 10 Gbit/s mobile optical wireless systems employing beam angle and power adaptation with diversity receivers," IEEE Journal on Selected Areas in Communications, vol. 29, issue 6, pp.1328-1340, 2011.

[87] M. T. Alresheedi, and J. M. H. Elmirghani, "10 Gb/s Indoor Optical Wireless Systems Employing Beam Delay, Power, and Angle Adaptation Methods With Imaging Detection," Journal of Lightwave Technology, vol.30, issue 12, pp.1843-1856, 2012.

[88] F. E. Alsaadi, M. A. Alhartomi, and J. M. H. Elmirghani, "Fast and Efficient Adaptation Algorithms for Multi-Gigabit Wireless Infrared Systems," Journal of Lightwave Technology, vol. 31, issue 23, pp.3735-3751, 2013.

[89] M. T. Alresheedi, A. T. Hussein and J. M. H. Elmirghani, "Uplink Design in VLC Systems with IR Sources and Beam Steering,", IET Communications, accepted, 2016.

[90] Y. Tanaka, T. Komine, S. Haruyama, and M. Nakagawa, "Indoor visible communication utilizing plural white LEDs as lighting," IEEE International Symposium in Personal, Indoor and Mobile Radio Communications, pp. F-81-F-85, 2001.

[91] K. K. Wong, and T. O'Farrell, "Spread spectrum techniques for indoor wireless IR communications," IEEE Wireless Communications, vol.10, issue 2, pp.54-63, 2003.

[92] Z. Wang, C. Yu, W.-D. Zhong, J. Chen, and W. Chen, "Performance of a novel LED lamp arrangement to reduce SNR fluctuation for multi-user visible light communication systems," Optics Express, vol.20, issue 4, pp.4564-4573, 2012.

[93] J. Tan, K. Yang, and M. Xia, "Adaptive equalization for high speed optical MIMO wireless communications using white LED," Frontiers of Optoelectronics in China, vol.4, issue 4, pp. 454-461, 2011.

[94] T. Komine, J. H. Lee, S. Haruyama, and M. Nakagawa, "Adaptive equalization system for visible light wireless communication utilizing multiple white LED lighting equipment," IEEE Transactions on Wireless Communications, vol.8, issue 6, pp. 2892-2900, 2009.

[95] A. G. Al-Ghamdi, and J. M. H. Elmirghani, "Analysis of diffuse optical wireless channels employing spot-diffusing techniques, diversity receivers, and combining schemes," IEEE Transactions on Communications, vol.52, issue 10, pp.1622-1631, 2004.

[96] A. G. Al-Ghamdi, and J. M. H. Elmirghani, "Characterization of mobile spot diffusing optical wireless systems with diversity receiver," IEEE International Conference in Communications, pp.133-138, 2004.

[97] T. Q. Wang, R. J. Green, and J. Armstrong, "Prism array-based receiver with application in MIMO indoor optical wireless communications," International Conference in Transparent Optical Networks (ICTON 2014), pp. 1-4, 2014.

[98] S. D. Dissanayake, J. Armstrong, and S. Hranilovic, "Performance analysis of noise cancellation in a diversity combined ACO-OFDM system," International Conference in Transparent Optical Networks (ICTON 2012), pp.1-4, 2012.

[99] J. Armstrong, "OFDM for Optical Communications," Journal of Lightwave Technology, vol. 27, issue 3, pp.189-204, 2009.

[100] A. T. Hussein, and J.M.H. Elmirghani, “High-Speed Indoor Visible Light Communication System Employing Laser Diodes and Angle Diversity Receivers,” 17th International Conference in Transparent Optical Networks (ICTON 2015), pp.1-6, 2015.

[101] A. T. Hussein, and J.M.H. Elmirghani, “10 Gbps Mobile Visible Light Communication System Employing Angle Diversity, Imaging Receivers and Relay Nodes,” Journal of Optical Communications and Networking, vol.7, issue 8, pp.718–735, 2015.

[102] A. T. Hussein, and J.M.H. Elmirghani, “Performance Evaluation of Multi-gigabit Indoor Visible Light Communication System,” The 20th European Conference on Network and Optical Communications, (NOC 2015), pp.1-6, 2015.

[103] A. T. Hussein, and J.M.H. Elmirghani, “Mobile Multi-gigabit Visible Light Communication System Employing Laser Diodes, Imaging Receivers and Delay Adaptation Technique in Realistic Indoor Environment,” Journal of Lightwave Technology, vol.33, no.15, pp.3293-3307 2015.

[104] A. T. Hussein, M. T. Alresheedi and J. M. H. Elmirghani, “20 Gb/s Mobile Indoor Visible Light Communication System Employing Beam Steering and Computer Generated Holograms,” Journal of Lightwave Technology, vol.33, issue 24, pp. 5242 - 5260, 2015.

[105] A. T. Hussein, M. T. Alresheedi and J. M. H. Elmirghani, "Fast and Efficient Adaptation Techniques for Visible Light Communication Systems," Journal of Optical Communications and Networking, vol.8, issue 6, pp.382-397, 2016.

[106] J. R. Barry, J. M. Kahn, E. A. Lee, and D. G. Messerschmitt, "High-speed nondirective optical communication for wireless networks," IEEE Network, vol. 5, issue 6, pp.44-54, 1991.

[107] H. Le Minh, Z. Ghassemlooy, D. O'Brien, and G. Faulkner, "Indoor gigabit optical wireless communications: challenges and possibilities," International Conference in Transparent Optical Networks (ICTON2010), pp.1-6, 2010.

[108] A. Street, P. Stavrinou, D. Edwards, and G. Parry, "Optical preamplifier designs for IR-LAN applications," IEE Colloquium on Optical Free Space Communication Links, pp. 8/1-8/6, 1996.

[109] M. Biagi, T. Borogovac, and T. D. C. Little, "Adaptive Receiver for Indoor Visible Light Communications," Lightwave Technology, Journal of, vol. 31, issue 23, pp. 3676-3686, 2013.

[110] S. Rajagopal, R. D. Roberts, and S.-K. Lim, "IEEE 802.15. 7 visible light communication: modulation schemes and dimming support," IEEE Communications Magazine, vol. 50, issue 3, pp.72-82, 2012.

[111] K. Lee and H. Park, "Modulations for visible light communications with dimming control," IEEE Photonics Technology Letters, vol.23, issue 16, pp.1136-1138, 2011.

[112] D. Shiu, and J. M. Kahn, "Differential pulse-position modulation for power-efficient optical communication," IEEE Transactions on Communications, vol. 47, issue 8, pp.1201-1210, 1999.

[113] J. B. Carruthers and J. M. Kahn, "Multiple-subcarrier modulation for non-directed wireless infrared communication," IEEE in Global Telecommunications Conference, pp.1055-1059, 1994.

[114] R. You, and J. M. Kahn, "Average-power reduction techniques for multiple-subcarrier optical intensity modulation," IEE Colloquium on Optical Wireless Communications, pp. 6/1-6/6, 1999.

[115] K. Wong, T. O'Farrell, and M. Kiatweerasakul, "The performance of optical wireless OOK, 2PPM and spread spectrum under the effects of multipath dispersion and artificial light interference," International Journal of Communication Systems, vol.13, issue 7-8, pp.551-576, 2000.

[116] R. Cryan, R. Unwin, and J. M. H. Elmirghani, "Optical fibre digital pulse position modulation," Analogue Optical Fibre Communications, pp.138-139, 1995.

[117] H. Park, and J. Barry, "Performance of multiple pulse position modulation on multipath channels," IEE Proceedings in Optoelectronics, vol.143, issue 4, pp. 60-364, 1996.
[118] J. Garcia, M. A. Dalla-Costa, J. Cardesin, J. M. Alonso, and M. Rico-Secades, "Dimming of high-brightness LEDs by means of luminous flux thermal estimation," IEEE Transactions on Power Electronics, vol.24, issue 4, pp.1107-1114, 2009.
[119] J. h. Choi, E.-b. Cho, T.-G. Kang, and C. G. Lee, "Pulse width modulation based signal format for visible light communications," in OptoeElectronics and Communications Conference, pp.276-277, 2010.
[120] Z. Wang, W.-D. Zhong, C. Yu, J. Chen, C. P. S. Francois, and W. Chen, "Performance of dimming control scheme in visible light communication system," Optics Express, vol. 20, issue 17, pp.18861-18868, 2012.
[121] W. Howell, "An overview of the electronic drive techniques for intensity control and colour mixing of low voltage light sources such as LEDs and LEPs," ed: Berlin: Artistic Licence Ltd., Application Note, 2002.
[122] Visible Light Communication Consortium, [online]: http://www.vlcc.net/modules/xpage1/
[123] JEITA, "CP-1221 Visible Light Communications System,", 2007.
[124] JEITA, "CP-1222 Visible Light ID System,", 2007.
[125] OMEGA Project, [online]: http://www.ict-omega.eu/home.html.
[126] Smart Lighting, [online]: http://smartlighting.rpi.edu/index.shtml.
[127] Li-Fi Consortium, [online]: http://www.lificonsortium.org/.
[128] S. Haruyama, "Visible light communications: Recent activities in Japan," A Smart Lighting ERC Industry—Academia Day at BU Photonics Center, Boston University, 2011.
[129] Visible light communication system: Nakagawa Group, [online]: http://www.youtube.com/watch?v=QEh5f49LsB4
[130] M. Nakajima, and S. Haruyama, "New indoor navigation system for visually impaired people using visible light communication," EURASIP Journal on Wireless Communications and Networking, vol.1, no.1, pp.1-10, 2013.
[131] K. Panta, and J. Armstrong, "Indoor localisation using white LEDs," Electronics letters, vol.48, issue 4, pp.228-230, 2012.
[132] S. Y. Jung, S. Hann, and C.-S. Park, "TDOA-based optical wireless indoor localization using LED ceiling lamps," IEEE Transactions on Consumer Electronics, vol.57, issue 4, pp.1592-1597, 2011.
[133] W. Zhang, and M. Kavehrad, "Comparison of VLC-based indoor positioning techniques," SPIE Proceedings, vol.8645, no.1, pp.86450M-86450M-6, 2013.
[134] H. Binti Che Wook, T. Komine, S. Haruyama, and M. Nakagawa, "Visible light communication with LED-based traffic lights using 2-dimensional image sensor," 3rd IEEE in Consumer Communications and Networking Conference, pp.243-247, 2006.
[135] A. G. Al-Ghamdi, and J. M. H. Elmirghani, "Line strip spot-diffusing transmitter configuration for optical wireless systems influenced by background noise and multipath dispersion," IEEE Transactions on Communications, vol. 52, issue 1, pp. 37-45, 2004.
[136] J. R. Barry, J. M. Kahn, W. J. Krause, E. A. Lee, and D. G. Messerschmitt, "Simulation of multipath impulse response for indoor wireless optical channels," IEEE Journal on Selected Areas in Communications, vol.11, issue 3, pp.367-379, 1993.
[137] A. G. Al-Ghamdi, and J. M. H. Elmirghani, "Optimization of a triangular PFDR antenna in a fully diffuse OW system influenced by background noise and multipath propagation," IEEE Transactions on Communications, vol.51, issue 12, pp.2103-2114, 2003.
[138] A. G. Al-Ghamdi, and J. M. H. Elmirghani, "Triangular PFDR antenna optimisation under the restriction of background noise and multipath propagation in an optical wireless system," IEEE International Conference Communications, pp. 2013-2019, 2003.
[139] J. B. Carruthers and J. M. Kahn, "Modeling of nondirected wireless infrared channels," IEEE Transactions on Communications, vol.45, issue 10, pp.1260-1268, 1997.

[140] S. Jivkova and M. Kavehrad, "Indoor wireless infrared local access, multi-spot diffusing with computer generated holographic beam-splitters," IEEE International Conference in Communications, pp.604-608, 1999.
[141] S. Jovkova and M. Kavehard, "Multispot diffusing configuration for wireless infrared access," IEEE Transactions on Communications, vol.48, issue 6, pp. 970-978, 2000.
[142] S. D. Personick, "Receiver design for digital fiber optic communication systems, I," Bell system technical journal, vol. 52, issue 6, pp.843 - 874, 1973.
[143] S. D. Personick, "Receiver design for digital fiber optic communication systems, I & II," Bell system technical journal, vol. 52, issue 6, pp.875 - 886, 1973.
[144] E. Desurvire, D. Bayart, B. Desthieux, and S. Bigo, "Erbium-doped fiber amplifiers", John Wiley, 2002.
[145] E. Desurvire and M. N. Zervas, "Erbium-doped fiber amplifiers: principles and applications," Physics Today, John Wiley, 1995.
[146] F. E. Alsaadi, and J. M. H. Elmirghani, "Performance evaluation of 2.5 Gbit/s and 5 Gbit/s optical wireless systems employing a two dimensional adaptive beam clustering method and imaging diversity detection," IEEE Journal on Selected Areas in Communications, vol. 27, issue 8, pp.1507-1519, 2009.
[147] T. Komine, "Visible Light Wireless Communication and Its Fundamental," PhD Dissertation, Department of Information & Computer Science, Keio University, 2005.
[148] A. G. Al-Ghamdi, and J. M. H. Elmirghani, "Performance analysis of mobile optical wireless systems employing a novel beam clustering method and diversity detection," IEE Proceedings Optoelectronics, vol.151, issue 4, pp. 223-231, 2004.
[149] J. M. Kahn, J. R. Barry, M. D. Audeh, J. B. Carruthers, W. J. Krause, and G. W. Marsh, "Non-directed infrared links for high-capacity wireless LANs," IEEE Personal Communications, vol.1, issue 2, pp.12-16, 1994.
[150] Laser Light Leading the way to the future, [online]: http://46.4.5.252/en_au/bmw-i8/laser-light-leading-the-way-to-the-future/94/#laser-light-leading-the-way-to-the-future
[151] A. Neumann, J. Wierer, W. Davis, Y. Ohno, S. R. Brueck, and J. Tsao, "Four-color laser white illuminant demonstrating high color-rendering quality," Optic Express, vol.19, issue s4, pp. A982-A990, 2011.
[152] R. Gatdula, J. Murray, A. Heizler, and M. Shah, "Solid State Lighting with Blue Laser Diodes,", [online]: http://www.winlab.rutgers.edu/~crose/capstone12/entries/SolidStateLightingwBlueLaser Diodes-Revised.pdf
[153] C. Basu, M. Meinhardt-Wollweber, and B. Roth, "Lighting with laser diodes," Advanced Optical Technologies, vol.2, no.4, pp.313-321, 2013.
[154] LD Lighting Engine is a new type of light source from Toshiba, [online]: http://reefbuilders.com/2012/07/23/ld-lighting-engine-toshiba/.
[155] K. A. Denault, M. Cantore, S. Nakamura, S. P. DenBaars, and R. Seshadri, "Efficient and stable laser-driven white lighting," AIP Advances, vol.3, no.1, pp. 072107, 2013.
[156] European standard EN 12464-1: Lighting of indoor work places, 2003.
[157] W. R. McCluney, "Introduction to radiometry and photometry," Artech House, 1994.
[158] A. Ryer, and V. Light, "Light measurement handbook,", 1997.
[159] S. Soltic, and A. Chalmers, "Optimization of laser-based white light illuminants," Optics express, vol. 21, issue 7, pp. 8964-8971, 2013.
[160] A. Stimson, "Photometry and radiometry for engineers," New York, Wiley-Interscience, 1974.
[161] B. Leskovar, "Optical receivers for wide band data transmission systems," IEEE Transactions on Nuclear Science, vol.36, issue 1, pp. 787-793, 1989.
[162] P. Djahani and J. M. Kahn, "Analysis of infrared wireless links employing multibeam transmitters and imaging diversity receivers," IEEE Transactions on Communications, vol. 48, issue 12, pp. 2077-2088, 2000.

[163] F. E. Alsaadi and J. M. H. Elmirghani, "High-Speed Spot Diffusing Mobile Optical Wireless System Employing Beam Angle and Power Adaptation and Imaging Receivers," Journal of Lightwave Technology, vol.28, issue 16, pp. 2191-2206, 2010.

[164] J. M. Kahn, R. You, P. Djahani, A. G. Weisbin, B. K. Teik, and A. Tang, "Imaging diversity receivers for high-speed infrared wireless communication," IEEE Communications Magazine, vol.36, issue 12, pp. 88-94, 1998.

[165] F. E. Alsaadi and J. M. H. Elmirghani, "Mobile Multigigabit Indoor Optical Wireless Systems Employing Multibeam Power Adaptation and Imaging Diversity Receivers," IEEE/OSA Journal of Optical Communications and Networking, vol.3, issue 1, pp.27-39, 2011.

[166] M. Tolstrup, "Indoor Radio Planning: A Practical Guide for Gsm, Dcs, Umts, Hspa and Lte, " John Wiley and Sons., 2011.

[167] P. Viswanath, D. N. C. Tse, and R. Laroia, "Opportunistic beamforming using dumb antennas," IEEE International Symposium in Information Theory, pp.449-452, 2002.

[168] E. Kimber, B. Patel, I. Hardcastle, and A. Hadjifotiou, "High performance 10 Gbit/s pin-FET optical receiver," Electronics Letters, vol.28, issue 2, pp.120-122, 1992.

[169] A. G. Al-Ghamdi, and J. M. H. Elmirghani, "Performance comparison of LSMS and conventional diffuse and hybrid optical wireless techniques in a real indoor environment," IEE Proceedings Optoelectronics, vol.152, issue 4, pp.230-238, 2005.

[170] F. E. Alsaadi, and J. M. H. Elmirghani, "Adaptive mobile line strip multibeam MC-CDMA optical wireless system employing imaging detection in a real indoor environment," IEEE Journal on Selected Areas in Communications, vol.27, issue 9, pp.1663-1675, 2009.

[171] T. J. Harrold and A. R. Nix, "Capacity enhancement using intelligent relaying for future personal communication systems," IEEE Vehicular Technology Conference, pp.2115-2120, 2000.

[172] J. N. Laneman, D. N. Tse, and G. W. Wornell, "Cooperative diversity in wireless networks: Efficient protocols and outage behavior," IEEE Transactions on Information Theory, vol.50, issue 12, pp.3062-3080, 2004.

[173] E. C. Van Der Meulen, "Three-terminal communication channels," Advances in applied Probability, 1971.

[174] M. Safari, and M. Uysal, "Relay-assisted free-space optical communication," IEEE Transactions on Wireless Communications, vol.7, issue 12, pp.5441-5449, 2008.

[175] M. Karimi, and M. Nasiri-kenari, "Free Space Optical Communications via Optical Amplify-and-Forward Relaying," Journal of Lightwave Technology, vol.29, issue 2, pp.242-248, 2011.

[176] G. Corbellini, S. Schmid, S. Mangold, T. R. Gross, and A. Mkrtchyan, "Demo: LED-to-LED Visible Light Communication for Mobile Applications,", Disney Research, 2012.

[177] F. E. Alsaadi, M. Nikkar, and J. M. H. Elmirghani, "Adaptive mobile optical wireless systems employing a beam clustering method, diversity detection, and relay nodes," IEEE Transactions on Communications, vol.58, issue 3, pp.869-879, 2010.

[178] Microchip, [online]: http://www.microchip.com/wwwproducts/Devices.aspx?product=PIC32MX110F016B.

[179] K. Wang, A. Nirmalathas, C. Lim, and E. Skafidas, "High-speed indoor optical wireless communication system with single channel imaging receiver," Optics express, vol. 20, issue 8, pp.8442-8456, 2012.

[180] D. Resler, D. Hobbs, R. Sharp, L. Friedman, and T. Dorschner, "High-efficiency liquid-crystal optical phased-array beam steering," Optics letters, vol.21, issue 9, pp.689-691, 1996.

[181] L. Wu, Z. Zhang, and H. Liu, "Transmit Beamforming for MIMO Optical Wireless Communication Systems," Wireless Personal Communications, vol.78, issue 1, pp.1-14, 2014.

[182] S. M. Kim and S. M. Kim, "Wireless optical energy transmission using optical beamforming," Optical Engineering, vol.52, no.4, pp.205-210, 2013.

[183] M. T. Alresheedi, and J.M.H. Elmirghani, "High-Speed Indoor Optical Wireless Links Employing Fast Angle and Power Adaptive Computer-Generated Holograms with Imaging Receivers," IEEE Transactions on Communications, 2016.

[184] M. T. Alresheedi, and J.M.H. Elmirghani, "Hologram Selection in Realistic Indoor Optical Wireless Systems with Angle Diversity Receivers," IEEE Journal of Optical Communications and Networking, vol.7, no.8, pp.797-813, 2015.

[185] M. Biagi, S. Pergoloni, and A. M. Vegni, "LAST: A Framework to Localize, Access, Schedule, and Transmit in Indoor VLC Systems," Journal of Lightwave Technology, vol.33, issue 9, pp.1872-1887, 2015.

[186] J. A. Davis, D. E. McNamara, D. M. Cottrell, and T. Sonehara, "Two-dimensional polarization encoding with a phase-only liquid-crystal spatial light modulator," Applied Optics, vol.39, issue 10, pp.1549-1554, 2000.

[187] Spatial Light Modulators', [online], Available: http://holoeye.com/wp-content/uploads/Spatial_Light_Modulators.pdf.

[188] P. Carnevali, L. Coletti, and S. Patarnello, "Image processing by simulated annealing," IBM Journal of Research and Development, vol.29, no.6, pp.569-579, 1985.

[189] M. A. Seldowitz, J. P. Allebach, and D. W. Sweeney, "Synthesis of digital holograms by direct binary search," Applied Optics, vol.26, pp.2788-2798, 1987.

[190] J. Gimlett, "A new low noise 16 GHz PIN/HEMT optical receiver," Fourteenth European Conference in Optical Communication, pp.13-16, 1988.

[191] A. P. Tang, J. M. Kahn, and H. Keang-Po, "Wireless infrared communication links using multi-beam transmitters and imaging receivers," IEEE International Conference in Communications, pp.180-186, 1996.

[192] 40 GB/s optical transponder, [Online]: http://media.digikey.com/pdf/Data%20Sheets/Finisar/40Gb_s_Smal_Form_Facto_NRZ_Br.pdf.

[193] G. W. Marsh, and J. M. Kahn, "50-Mb/s diffuse infrared free-space link using on-off keying with decision-feedback equalization," IEEE Photonics Technology Letters, vol.6, issue 10, pp.1268-1270, 1994.

[194] F. Haider, X. Gao, X.-H. You, Y. Yang, D. Yuan, H. M. Aggoune, "Cellular architecture and key technologies for 5G wireless communication networks," IEEE Communications Magazine, vol.52, issue 2, pp.122-130, 2014.

[195] J. Kleinberg, and É. Tardos, "Algorithm design," Pearson Education India, 2006.

[196] B. U. H. Klepser, J. Spicher, C. Bergamaschi, W. Patrick, and W. Bachtold, "High speed, monolithically integrated pin-HEMT photoreceiver fabricated on InP with a tunable bandwidth up to 22 GHz using a novel circuit design," The 8th International Conference in Indium Phosphide and Related Materials, pp.443-446, 1996.

[197] M. B. Rahaim, A. M. Vegni, and T. D. C. Little, "A hybrid Radio Frequency and broadcast Visible Light Communication system," IEEE GLOBECOM Workshops (GC Wkshps), pp. 792-796, 2011.

[198] W. Yunlu and H. Haas, "Dynamic Load Balancing With Handover in Hybrid Li-Fi and Wi-Fi Networks," Journal of Lightwave Technology, vol. 33, no.22, pp. 4671-4682, 2015.

[199] D. O'Brien, "Cooperation in Optical Wireless Communications," in Cognitive Wireless Networks: Concepts, Methodologies and Visions Inspiring the Age of Enlightenment of Wireless Communications, F. H. P. Fitzek and M. D. Katz, Eds., ed Dordrecht: Springer Netherlands, pp. 623-634, 2007.

[200] A. Gomez, K. Shi, C. Quintana, M. Sato, G. Faulkner, and B. C. Thomsen, "Beyond 100-Gb/s Indoor Wide Field-of-View Optical Wireless Communications," IEEE Photonics Technology Letters, vol. 27, issue 4, pp. 367-370, 2015.

[201] V. Pohl, V. Jungnickel, and C. Von Helmolt, "Integrating-sphere diffuser for wireless infrared communication," IEE Proceedings in Optoelectronics, vol.174, issue 4, pp. 281-285, 2000.

Appendix A

Results of Traditional VLC System

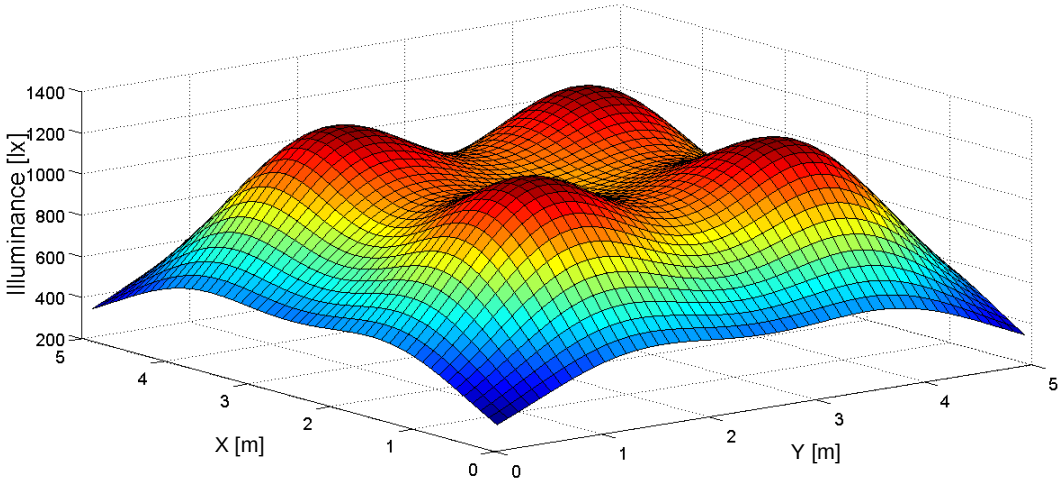

Figure A1.1: Distribution of horizontal illumination at the communication plane (0.85m) in room with dimensions of 5 m × 5 m × 3 m.

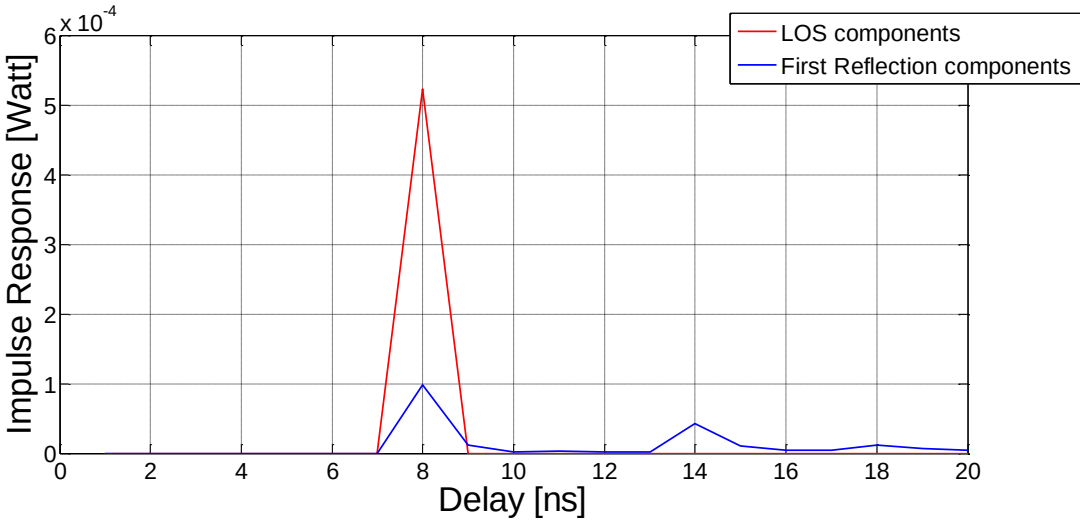

Figure A1.2: Impulse response at 0.01m, 0.01m, 0.85m in room with dimensions of 5 m × 5 m × 3 m.

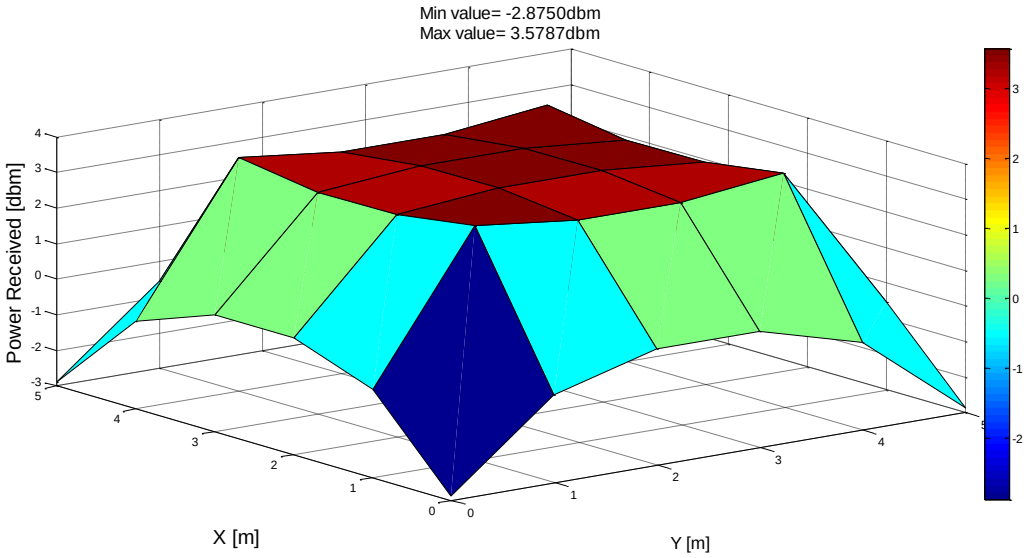

Figure A1.3: The distribution of the received power from LOS component. Min. -2.8 dBm, Max. 3.5 dBm.

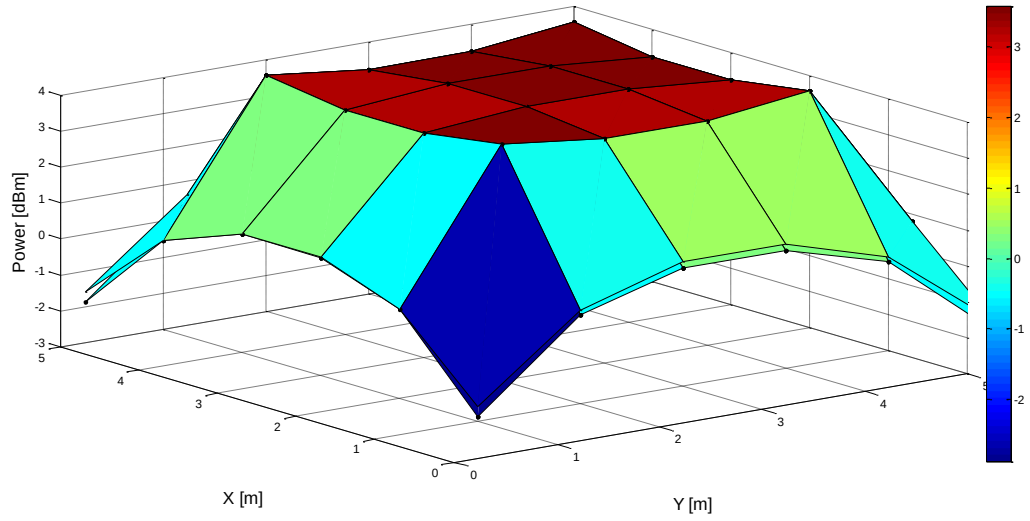

Figure A1.4: The distribution of the received power from LOS and first reflection component. Min. -2.8 dBm, Max. 3.8 dBm.

Appendix B

Results of Traditional IROW Systems

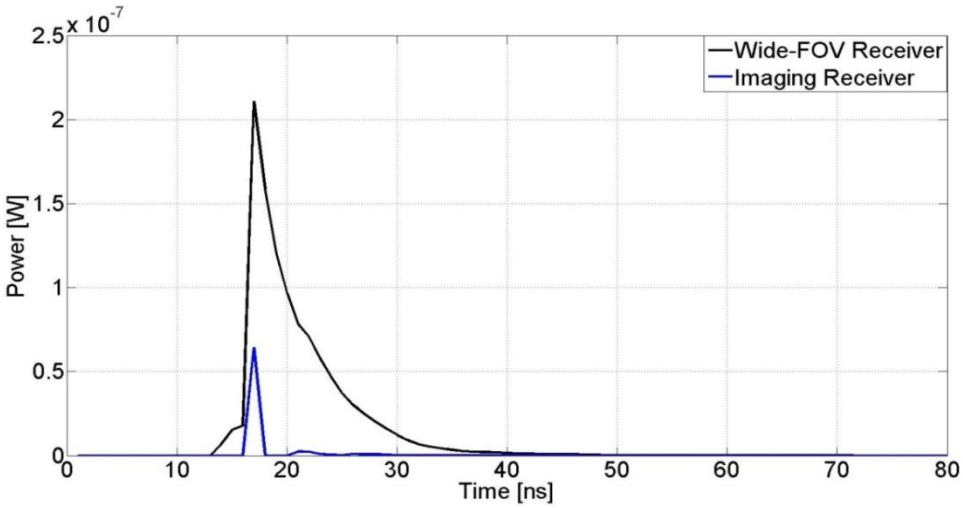

Figure A2.1: Impulse response of CDS system with wide FOV receiver and an imaging receiver with 200 pixels.

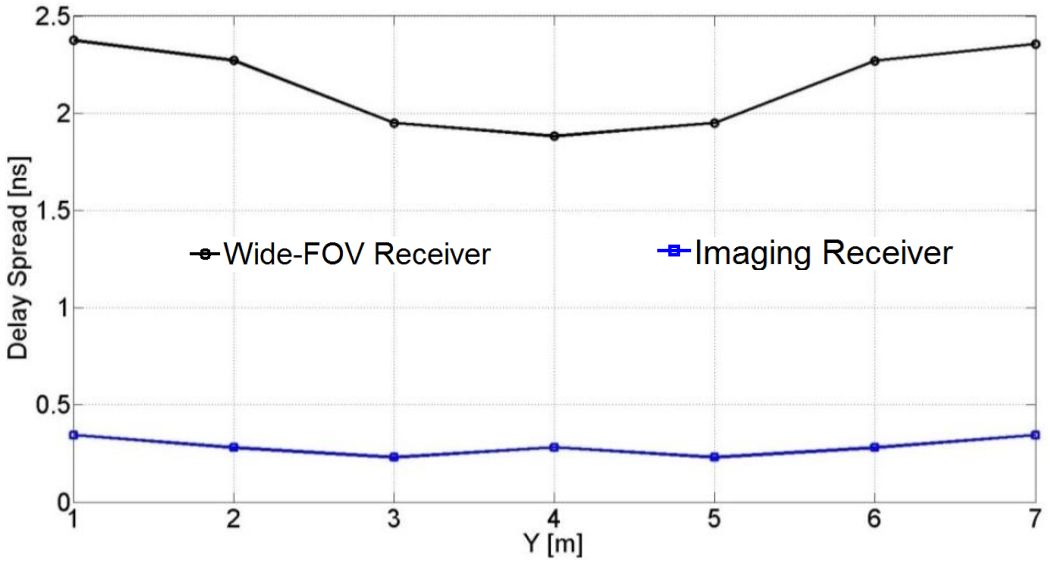

(a)

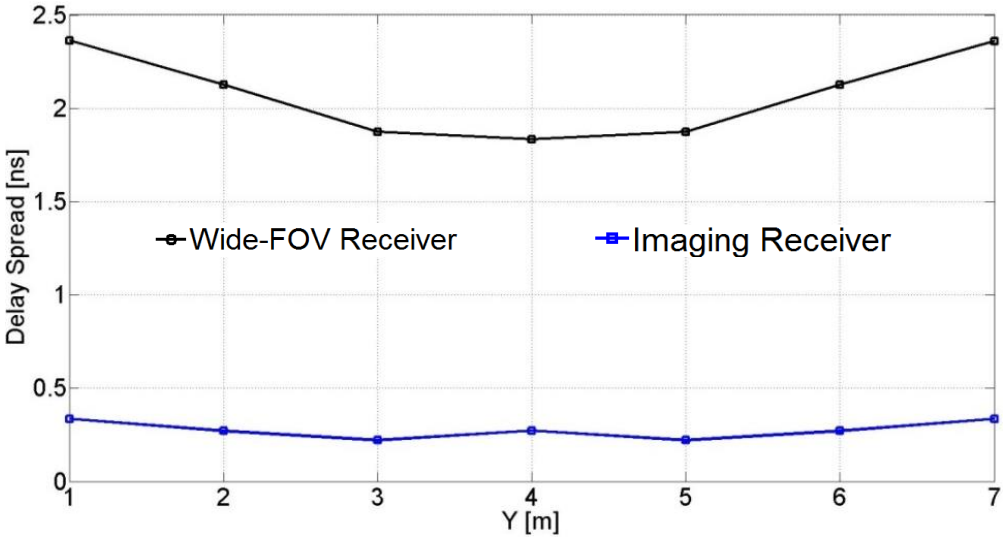

(b)

Figure A2:2: The delay spread of CDS system with two receivers (a) at x=1m, (b) at x=2m over communication plane.

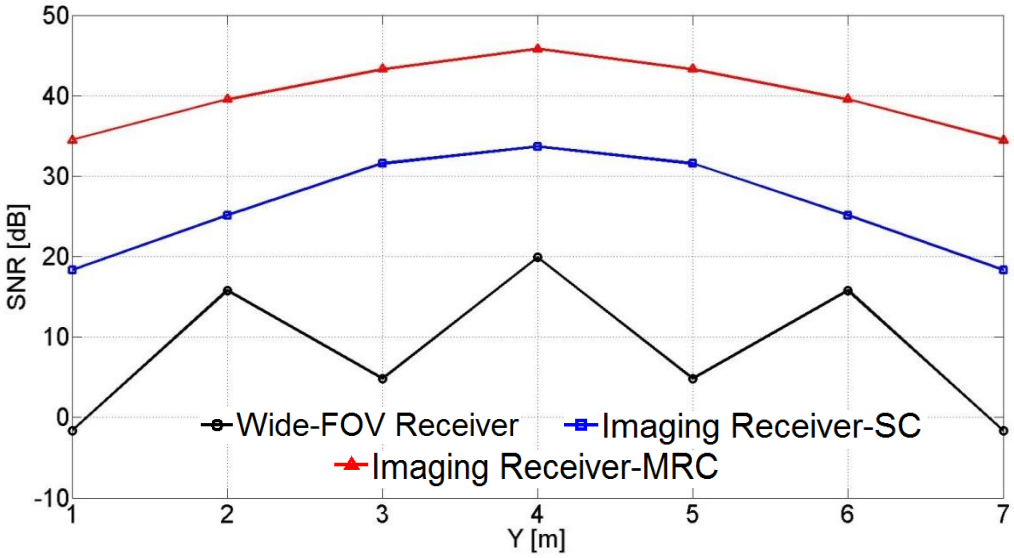

(a)

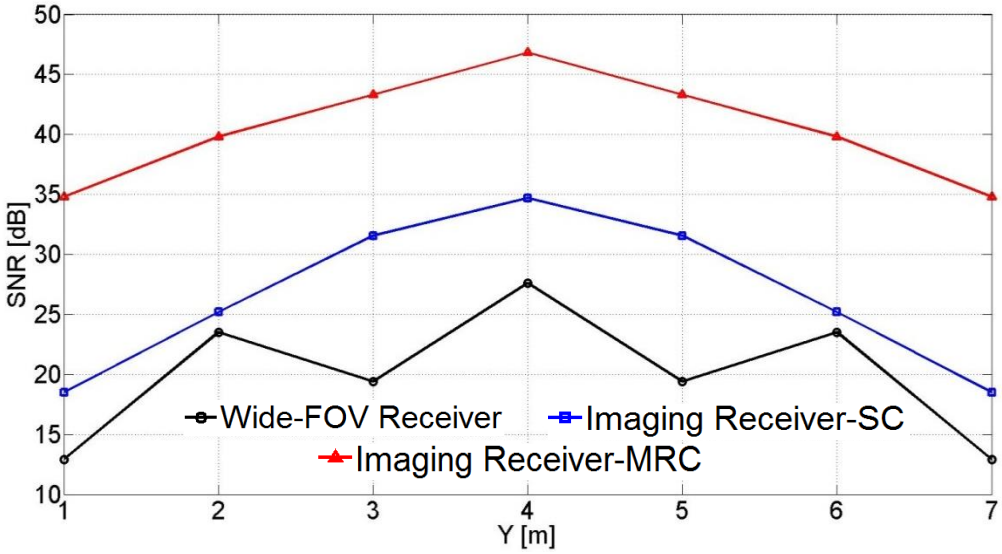

(b)

Figure A2.3: The SNR of CDS system with wide-FOV receiver and imaging receiver (a) at x=1m, (b) at x=2m over CP.

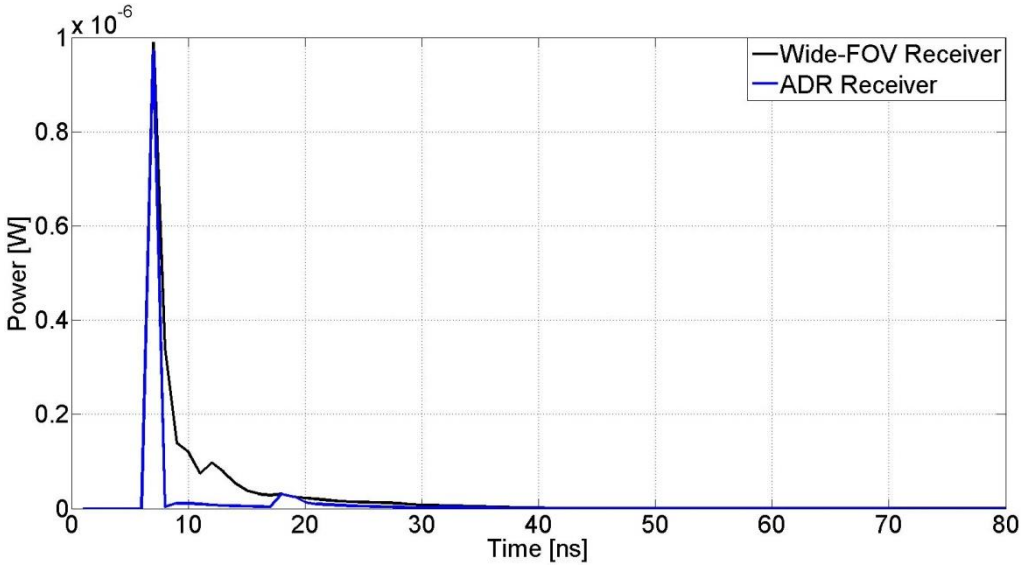

Figure A2.4: Impulse response of LSMS system with wide-FOV receiver and ADR receiver.

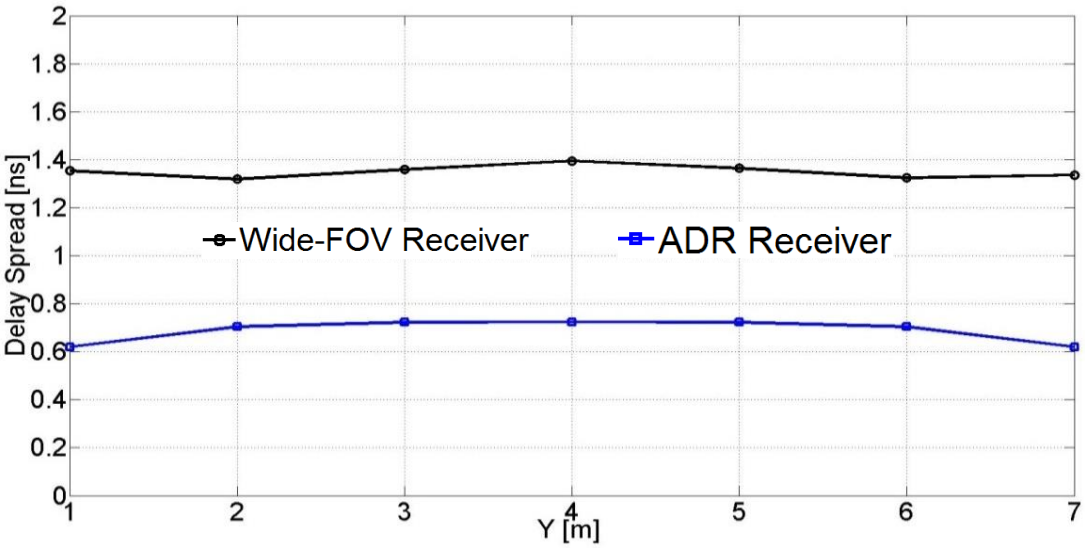

(a)

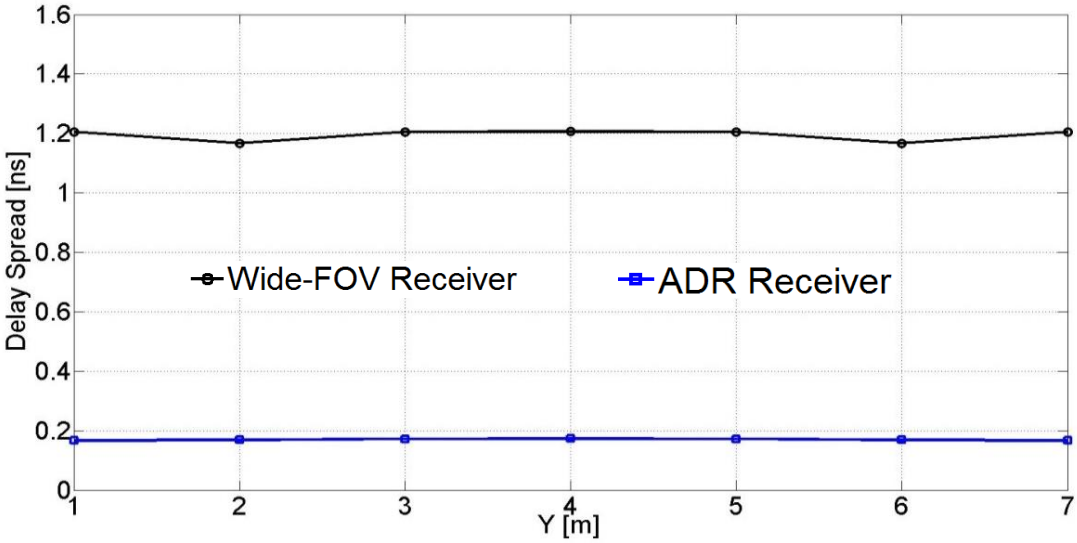

(b)

Figure A2.5: Delay spread distribution of LSMS system using wide-FOV and ADR receiver (a) at x=1m, (b) at x=2m over communication plane.

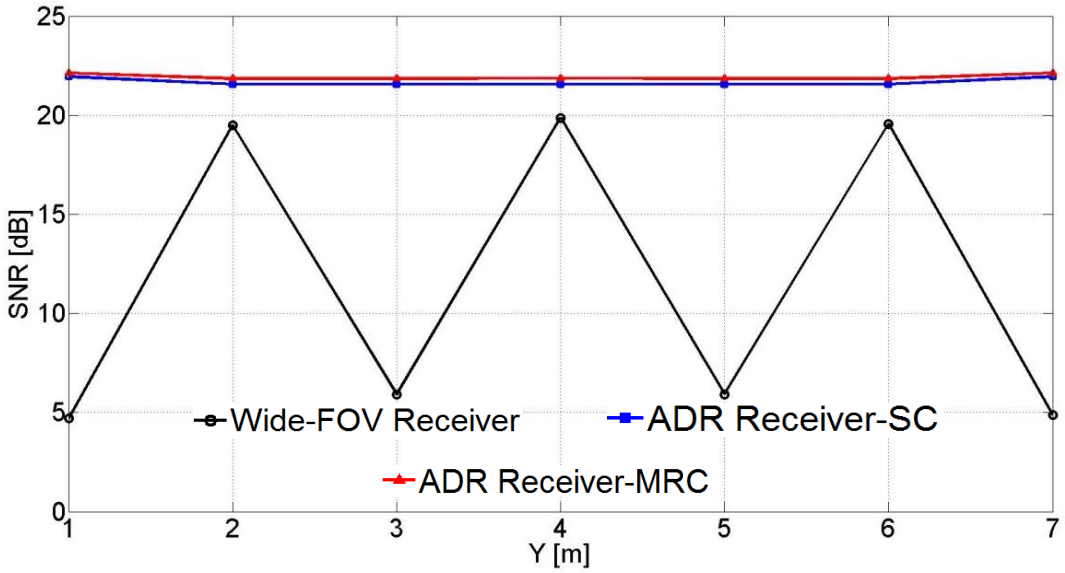

(a)

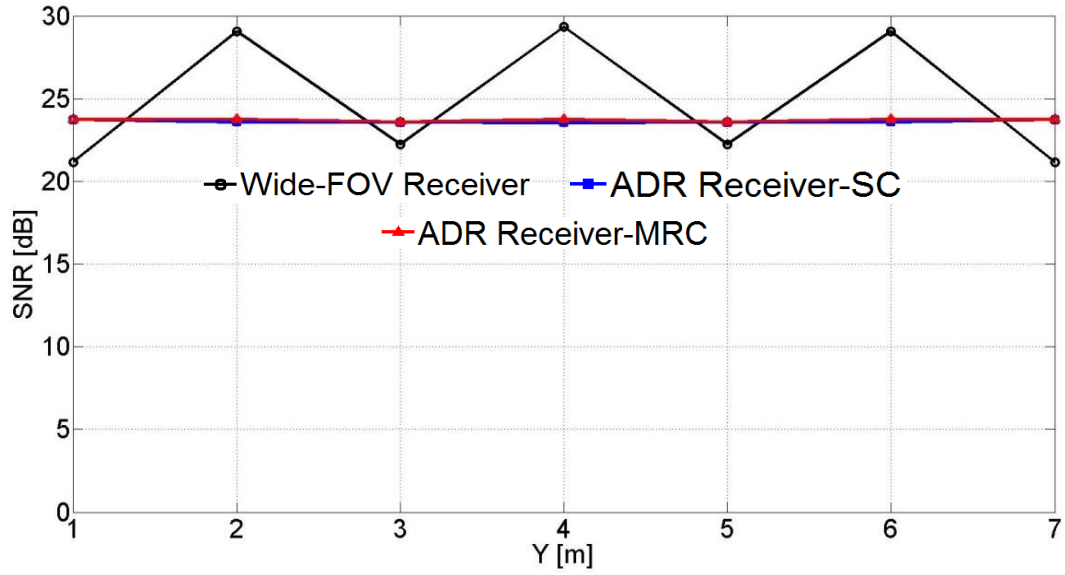

(b)

Figure A2.6: SNR of LSMS system using wide-FOV receiver and ADR receiver (a) at x=1m, (b) at x=2m over communication plane.

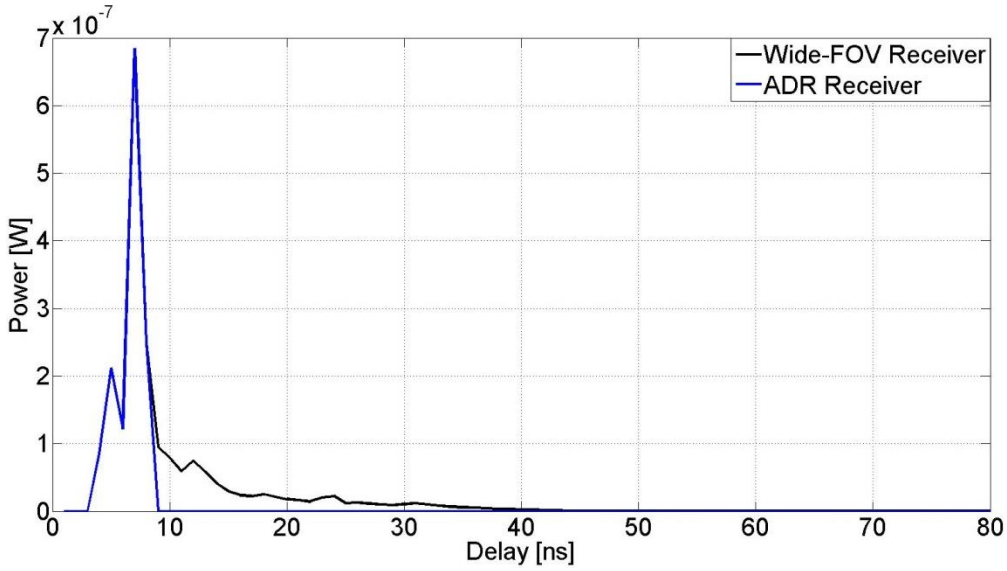

Figure A2.7: Impulse response of BCM system with wide-FOV receiver and ADR receiver.

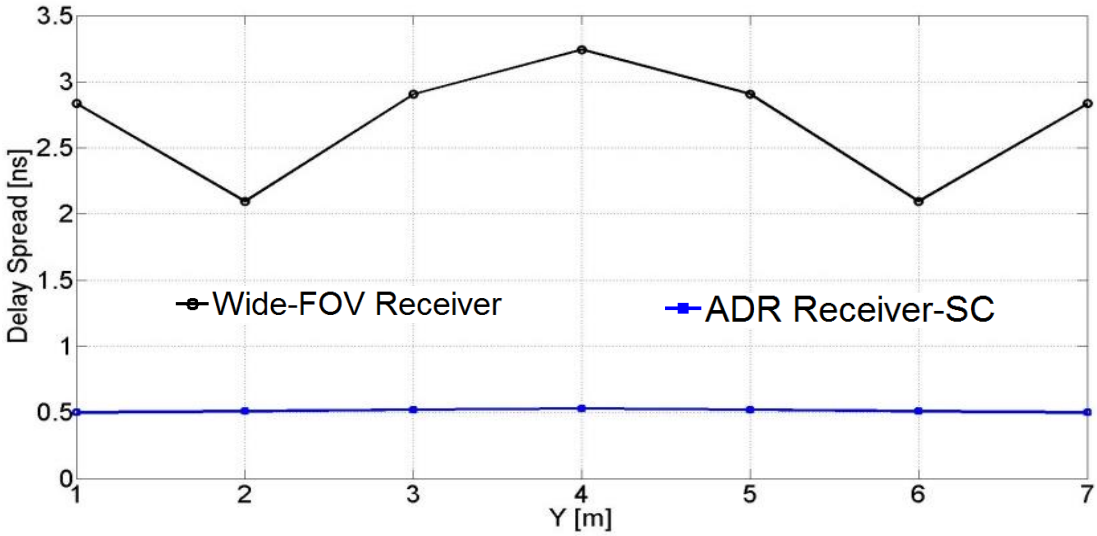

(a)

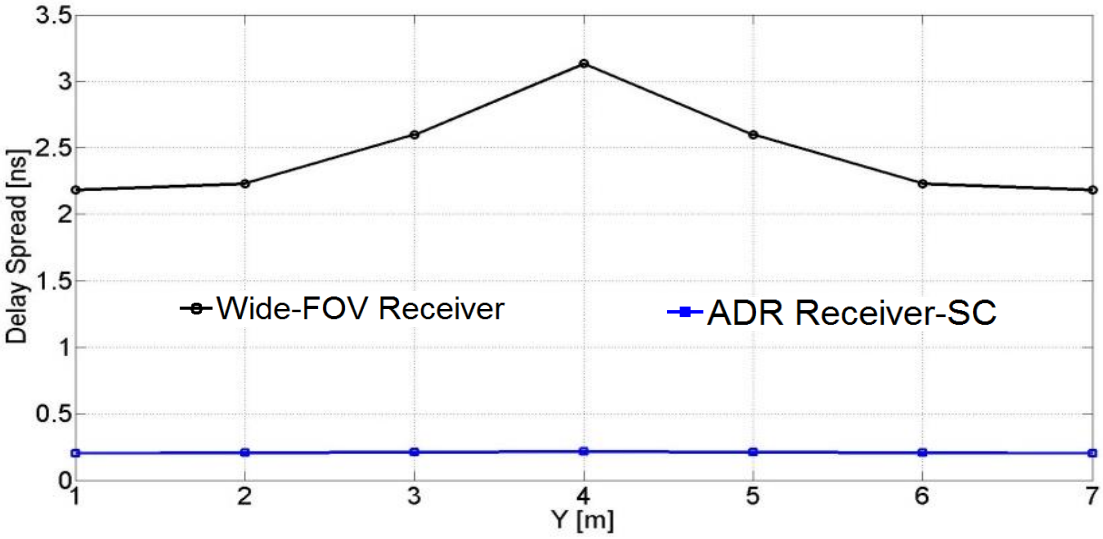

(b)

Figure A2.8: Delay spread distribution of BCM system using wide-FOV receiver and ADR receiver (a) at x=1m, (b) at x=2m over communication plane.

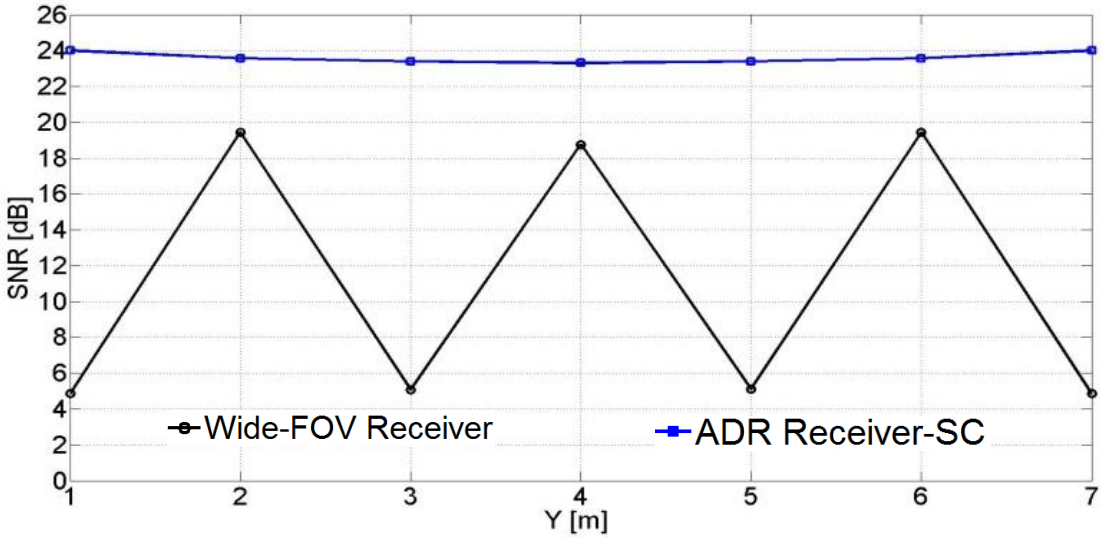

(a)

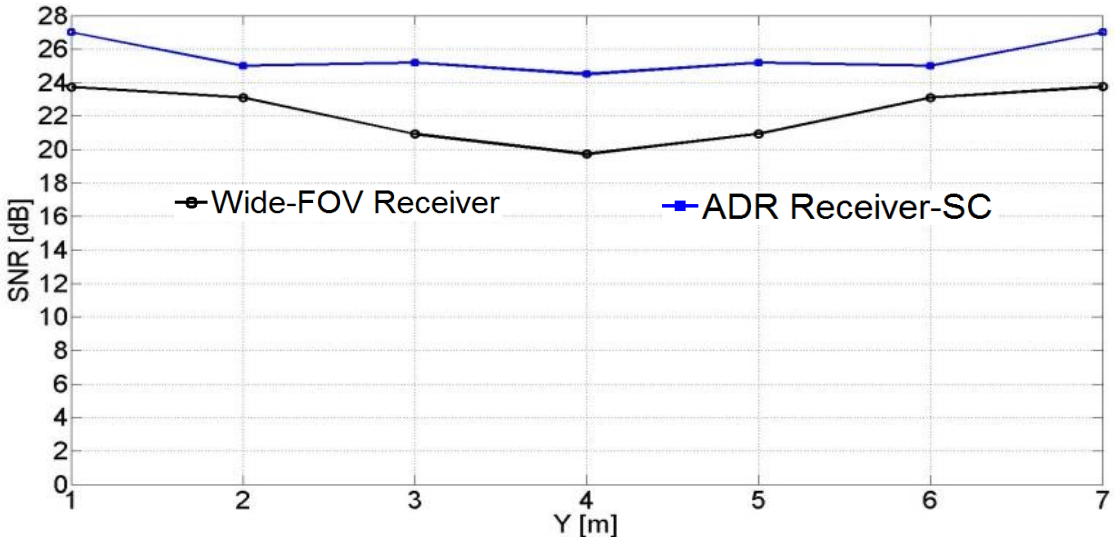

(b)

Figure A2.9: SNR of BCM system using wide-FOV and ADR receiver (a) at x=1m, (b) at x=2m over communication plane.